

Studies on Poly(caprolactone-co-dimethyl siloxane) Copolymers for Thermoresponsive Shape Memory Applications

Thesis Submitted to Delhi Technological University
for the Award of the Degree of

DOCTOR OF PHILOSOPHY

by

Radha Sachan

(2K18/PhD/AC/14)

Under the Supervision of

Prof. Roli Purwar

and

Prof. Sudhir G. Warkar



DEPARTMENT OF APPLIED CHEMISTRY

DELHI TECHNOLOGICAL UNIVERSITY

DELHI-110042 (INDIA)

April 2024

© DELHI TECHNOLOGICAL UNIVERSITY-2024

All rights reserved

Dedicated

To my Parents

Smt. Girja Devi and Kailash Phandra Sachan

To my sibling

Ritu Sachan

To my Husband

Vikramajeet Singh

To my lovely daughters

Aashvi and Aanya

Thanks for your endless encouragement, support,

Love and prayers



DELHI TECHNOLOGICAL UNIVERSITY

Formerly Delhi College of Engineering

(Under Delhi act 6 of 2009, Govt. of NCT Delhi)

hahabad Daulatpur, Main Bawana Road, Delhi-110042

DECLARATION

This is to certify that the work, embodied in the thesis entitled “**Studies on Poly(caprolactone-co-dimethyl siloxane) Copolymers for Thermoresponsive Shape Memory Applications**” is an original work carried out by me for the degree of **Doctor of Philosophy** under the supervision of Dr. Roli Purwar, Professor, Department of Applied Chemistry and Dr. Sudhir Warkar, Professor, Department of Applied Chemistry. This thesis is a contribution of my original research work. Wherever research contributions of others are involved, every effort has been made to clearly indicate the same. To the best of my knowledge, this research work has not been submitted in part or full for the award of any degree or diploma of Delhi Technological University or any other University/Institutions.

Radha Sachan

Research Scholar

(Reg. No. 2K18/Ph.D./AC/14)

Date: .04.2024



DELHI TECHNOLOGICAL UNIVERSITY

Formerly Delhi College of Engineering

(Under Delhi act 6 of 2009, Govt. of NCT Delhi)

Shahabad Daulatpur, Main Bawana Road, Delhi-110042

CERTIFICATE

This is to certify that the work, embodied in the thesis entitled “**Studies on Poly(caprolactone-co-dimethyl siloxane) Copolymers for Thermoresponsive Shape Memory Applications**” by **Ms. Radha Sachan** (Roll No.: **2K18/PhD/AC/14**) in the partial fulfillment of the requirements for the award of degree of **Doctor of Philosophy**, is an authentic record of student’s own work carried by her.

This work is based on original research and the matter embodied in this thesis has not been submitted earlier for the award of any degree or diploma to the best of our knowledge and belief.

Prof. Roli Purwar

Department of Applied Chemistry
Delhi Technological University
Delhi-110042

Prof. Sudir G. Warkar

Department of Applied Chemistry
Delhi Technological University
Delhi-110042

Prof. Anil Kumar

Head of Department
Applied Chemistry, DTU
Delhi-110042

ACKNOWLEDGEMENTS

The journey of Ph.D., full of challenges, ups & down and excitement is different for each one but it can only be completed when support, guidance and motivation of every individual and institution is added. First and foremost, I would like to extend my heartfelt appreciation to my supervisors **Prof. Roli Purwar** and **Prof. Sudhir G. Warkar**. Your guidance, expertise, and unwavering support have been instrumental in shaping this research. Your encouragement and insightful feedback have consistently pushed me to excel and have made this journey both intellectually stimulating and rewarding. I'd want to warmly thank **my parents**, my **husband** and **kids** for their love, understanding, and patience during this journey.

I am extremely grateful to **Prof. Yogesh Singh**, former Honourable Vice-Chancellor and **Prof. Prateek Sharma**, Honourable Vice-Chancellor, Delhi Technological University for the kind permission for doing Ph.D. from DTU. Also, my gratitude extends to **Prof. Sudhir G. Warkar**, former Head, Department of Applied Chemistry and **Prof. Anil Kumar**, Head, Department of Applied Chemistry, DTU for providing me the necessary facilities to carry out this research work. I wish to express my sincere thanks to whole faculty members of Department of Applied Chemistry, DTU for their help and support during this research work. I would like to thank **SRC and DRC members** along with other faculty members of the Department of Applied Chemistry, Delhi Technological University for their expertise and constructive feedback which immensely contributed to the quality of this thesis.

I am obliged for the help of all the non-teaching as well as technical staff of the department for their endless help and resource management whenever required which made my PhD journey as easy as possible. I would especially like to thank **Mr. Ankesh Kumar**, **Mr. Raju Kumar**, **Ms. Sharmila Jas** for their constant support.

I would like to thank my friends and colleagues who have supported me throughout this journey. Your encouragement, intellectual discussions, and camaraderie have been invaluable. I would especially like to mention **Mr. Jitendra Kumar, Ms. Priti, Dr. Priya Bansal, Dr. Reetu Yadav, Dr. Radhika Batra, Dr. Surya Tanwar, Ms. Daan Kaur, Dr. Deepali Ahluwalia, Mr. Ram Mangeram** and **Dr. Babita Veer** for their help and keeping the moral high throughout Ph.D. tenure.

Lastly, I would like to express my gratitude and acknowledge to the TEQIP-III for providing me with funding for my research project.

Radha Sachan

2K18/PhD/AC/14

Table of Content

<i>Declaration</i>	<i>i</i>
<i>Certificate</i>	<i>ii</i>
<i>Acknowledgements</i>	<i>iii</i>
<i>Table of Content</i>	<i>v</i>
<i>List of Figures</i>	<i>ix</i>
<i>List of Schemes</i>	<i>xiii</i>
<i>List of Tables</i>	<i>xiv</i>
<i>List of abbreviation</i>	<i>xv</i>
<i>Abstract</i>	<i>xvii</i>
<i>Overview of thesis</i>	<i>xix</i>
Chapter 1. Introduction and Objectives	1
1.1 Introduction	1
1.2 Research Gap	5
1.3 Motivation of research	5
1.4 Objective of the research work	5
1.4.1 Specific objectives	5
Chapter 2: Literature review	7
2.1 Introduction to PCL copolymers, blends and composite	7
2.2 Synthesis of polycaprolactone copolymers, blends and composites	9
2.3 Properties of polycaprolactone copolymers, blends and composites	18
2.3.1 Thermal properties	19
2.3.2 Mechanical properties	27
2.3.3 Electrical properties	30
2.3.4 Structural properties	31
2.3.5 Rheological properties	33
2.3.6 Shape memory properties	35

2.3.7 Biodegradation	38
2.4 Applications	41
2.4.1 Biomedical applications	41
2.4.2 Non-biomedical applications	45
2.4.2.1 Packaging	45
2.4.2.2 Self-healing	46
2.4.2.3 Coatings	47
2.4.2.4 Purification	49
2.4.2.5 Plant grafting	49
2.4.2.6 Photothermal absorption	49
2.5 Commercial products	50
2.6 Conclusion	51
Chapter 3: Materials and Methodology	53
3.1 Materials	53
3.2 Methods	53
3.2.1 Synthesis of PCL-PDMS-PCL triblock photocrosslinked copolymer	53
3.2.2 Fourier Transform Infrared (FTIR) Spectroscopy	60
3.2.3 Nuclear Magnetic resonance (NMR) Spectroscopy	60
3.2.4 Gel permeation chromatography (GPC)	61
3.2.5 Rheology	61
3.2.6 Mechanical Properties	62
3.2.7 Thermogravimetry Analysis (TGA)	62
3.2.8 Differential Scanning Calorimetry (DSC)	63
3.2.10 Wide Angle X-Ray diffraction (WAXRD)	64
3.2.11 Dynamic Mechanical Analysis (DMA)	65
3.2.12 Optical microscopy	65
3.2.13 Scanning Electron Microscope (SEM)	66
3.2.14 Soil burial test	67
3.2.15 Shape memory properties	67

Chapter 4: Synthesis of PCL-PDMS-PCL triblock copolymers and its structural characterization	69
4.1 Attenuated Total Reflection-Fourier Transform Infrared (ATR-FTIR)	69
4.2 Nuclear Magnetic resonance (NMR)	71
4.3 X-Ray diffraction (XRD)	77
4.4 Conclusion	79
Chapter 5: Rheological characterization of PCL-PDMS-PCL triblock copolymer	
Films	80
5.1 Linear viscoelastic region	80
5.2 Frequency Sweep	82
5.3 Creep and Creep recovery behaviour	86
5.4 Structure Recovery	91
5.5 Tensile Properties and Dynamic Mechanical Analysis	92
5.6 Conclusion	94
Chapter 6: Thermal characterization of PCL-PDMS-PCL triblock copolymer films	96
6.1 Optical Microscope	96
6.2 Thermal Gravimetric Analysis	98
6.3 Differential Scanning Calorimetry	100
6.3.1 Non-Isothermal	100
6.3.2 Isothermal	102
6.4 Conclusion	114
Chapter 7: Shape memory properties of PCL-PDMS-PCL triblock copolymer films	113
7.1 Qualitative Analysis of Shape Memory Properties	113
7.2 Quantitative Analysis of Shape Memory Properties	116
7.3 Correlation of isothermal crystallization kinetics and shape memory properties	118
7.4 Conclusion	118
Chapter 8: Biodegradation behaviour of PCL-PDMS-PCL triblock copolymer films	119
8.1 Morphological Changes	119
8.1.1 Macroscopic view	119
8.1.2 Microscopic view	121

8.2 Macrolevel changes	125
8.2.1 Weight loss in soil burial	125
8.2.2 Thermal Properties	126
8.3 Structural changes	129
8.4 Mechanism of degradation	132
8.4 Conclusion	133
Chapter 9: Conclusion and Future Scope	135
9.1 Conclusion and future scope of the research work	135
9.2 Future scope	137
Chapter 10: References	138
Publications from the proposed research work	170
Book chapter (s)	170
Conference Publications.	170
Other publications during research tenure	171
Brief bio-data of the author	173

List of Figures

Figure No.	Title	Page No.
2.1	Synthesis routes of copolymerization of polycaprolactone	10
2.2	Synthesis methods of blends of Polycaprolactone	13
2.3	Synthesis methods of composites of polycaprolactone	15
2.4	Different factors which influence the properties of copolymers, blends, and composites of polycaprolactone	19
2.5	Thermal gravimetric analysis of PCL	19
2.6	Melting 1(a) and cooling 1(b) DSC curves of PCL-co- ω -pentadecalactone; TGA curves 2(a); DSC curves melting 2(b) and cooling 2(c) of PCL/pine resin blends; TGA curves 3(a), DSC curves melting 3(b) and cooling 3(c) of PCL/MWCNT nanocomposite	23
2.7	POM of crystals growth in PCL/PLLA copolymers (1); PCL/PLLA blends (2)	25
2.8	Structural analysis by XRD of PEG-PCL copolymer (1); PCL/PMMA blend (2); PCL/SiC nanocomposite (3)	33
2.9	Non-biomedical applications include packaging reproduced with permission; self-healing coatings corrosion resistance coatings; flame retardant coatings; oil-water separation; plant grafting; photo-thermal absorption of PCL copolymers, blends and composites	48
3.1	Preparation of hydroxyl terminated macromer	54
3.2	Preparation of acrylic terminated PCL-PDMS macromer	54
3.3	UV curing of acrylic terminated macromer	55
3.4	Fourier Transform Infrared (FTIR) Spectrophotometer (Perkin Elemer)	60
3.5	Nuclear Magnetic Resonance (Bruker - Advance Core 400 MHz)	60
3.6	Gel permeation chromatography (Perkin Elmer series 200)	61
3.7	MCR 302 Rotational Rheometer (Anton Paar GmbH, Graz, Austria)	62

3.8	Thermal Gravimetry Analyser (TGA 4000 - Perkin Elemer)	63
3.9	Differential Scanning Calorimetry (DSC 8000- Perkin Elmer)	64
3.10	Panalytical's X'Pert Pro X-Ray diffractometer	64
3.11	Dynamic Mechanical Analyser (DMA 4000-Perkin Elemer)	65
3.12	Optical Microscope (Motic BA410E) with Moticam Pro 285A camera	66
3.13	Scanning Electron Microscope (SEM CARL ZEISS EVO 50)	66
3.14	Pictorial representation of shape memory properties analysis in quantitative mode	68
4.1	ATR-FTIR of photocrosslinked pure PCL and PCL-PDMS-PCL triblock copolymer films	70
4.2	400 MHz ¹ H NMR spectroscopy of (a) 40-40 OH, (b) 40-40 OAc, (c) 30-30 OH (d) 30-30 OAc (e) 20-20 OH (f) 20-20 OAc (g) 10-10 OH (h) 10-10 OAc (i) 5-5 OH (j) 5-5 OAc (k) PCL OH (l) PCL OAc	75
4.3	X-ray diffraction plot of PCL and PCL-PDMS-PCL triblock copolymer films	78
5.1	Amplitude sweep showing linear viscoelastic region (LVER) of PCL and PCL-PDMS-PCL triblock polymer at 80°C	80
5.2	Storage modulus and loss modulus verses angular frequency plots of PCL and PCL-PDMS-PCL triblock polymer at 80°C	83
5.3	Loss factor and phase shift angle against angular frequency of PCL and PCL-PDMS-PCL triblock polymer at 80°C	84
5.4	Complex viscosity of PCL and PCL-PDMS-PCL triblock polymer at 80°C	85
5.5	Pictorial presentation of PCL-PDMS-PCL photo-crosslinked copolymer, with increase in PCL chain length, crosslink points decreases and overall crosslink density decreases	85
5.6(a)	Creep and creep recovery of PCL and PCL-PDMS-PCL triblock polymer at 80°C	87
5.6(b)	Creep compliance of PCL and PCL-PDMS-PCL triblock polymer at 80°C	87
5.6(c)	Burgers model fitting on the creep strain responses for PCL and PCL-PDMS-PCL triblock polymer	89
5.7	Structure recovery of PCL and PCL-PDMS-PCL triblock polymer	91

	at 80°C	
5.8	Dynamic mechanic analyses profiles of PCL, PDPCL40, PDPCL30 and PDPCL20 (a) Storage modulus and (b) $\tan \delta$ vs. temperature	94
6.1	Optical images of crystallized films at time (a) $t = 45$ sec to 1 min 30 sec for PCL (b) $t = 45$ sec to 2 min 10 sec for 40-40 (c) $t = 50$ sec to 2 min 20 sec for 30-30 (d) $t = 50$ sec to 2 min 30 sec for 20-20 (e) 10-10 and (f) 5-5	98
6.2	TGA curves of PCL and PCL-PDMS-PCL photo-crosslinked films	99
6.3	DSC thermograms of PCL and PCL-PDMS-PCL triblock copolymer films	101
6.4	Plot of relative crystallinity for (a) PCL, (b) 40-40, (c) 30-30 and (d) 20-20 PCL-PDMS-PCL triblock copolymer films	103
6.5	Plot of crystallization half-time $t_{1/2}$ against crystallization temperature T_c for PCL and PCL-PDMS-PCL triblock copolymeric films	104
6.6	Isothermal crystallization tests and Avrami fit for (a) PCL, (b) 40-40, (c) 30-30 and (d) 20-20	105
6.7	Plots of T'_{cm} verses T_c for PCL and PCL-PDMS-PCL triblock copolymeric films	108
6.8	Plot of $\ln G + U^*/R (T_c - T_{\infty})$ against $1/T_c(\Delta T) f$ for PCL and PCL-PDMS-PCL triblock copolymeric films	110
7.1	Shape memory behaviour of from rectangular to ring with recovery time of PCL(a), 40-40(b), 30-30(c), 20-20(d)	115
7.2	Shape memory behaviour from cross-shaped to cube with recovery time of PCL(a), 40-40(b), 30-30(c), 20-20(d)	116
8.1	Macroscopic view of PCL and PCL-PDMS-PCL triblock copolymer films at different intervals	120
8.2	Microscopic view by optical microscope of PCL and PCL-PDMS-PCL triblock copolymer films	121
8.3	SEM images of PCL and PCL-PDMS-PCL triblock copolymer films before degradation and after 180 days of degradation. PCL (a) before soil burial, PCL (b) after 180 days of soil burial, 40-40 (c) before soil burial, 40-40 (d) after 180 days soil burial, 30-30 (e)	122

	before soil burial, 30-30 (f) after 180 days soil burial, 20-20 (g)	
	before soil burial, 20-20 (h) after 180 days soil burial, 10-10 (i)	
	before soil burial, 10-10 (j) after 180 days soil burial, 5-5 (k)	
	before soil burial, 5-5 (l) after 180 days soil burial	
8.4	Percentage weight loss of PCL-PDMS copolymer films with time in soil burial	126
8.5	TGA curves of a pure PCL and PCL-PDMS-PCL triblock copolymer films at different degradation time	137
8.6	FTIR of PCL and PCL-PDMS-PCL triblock films before degradation and after degradation of 180 days	130
8.7	DSC percentage crystallinity of PCL and PCL-PDMS-PCL triblock films before degradation and degradation at different time of interval	132
8.8	Mechanism of degradation of PCL-PDMS-PCL photo-crosslinked triblock copolymer films	133

List of Scheme

Scheme No.	Title	Page No.
3.1	Schematic representation of chemical reaction involved in PCL film Preparation	58
3.2	Schematic representation of chemical reaction involved in PCL-PDMS-PCL film preparation	59

List of Table

Table No.	Title	Page No.
2.1	Copolymers of polycaprolactone	10
2.2	Blends of Polycaprolactone	13
2.3	Composites of Polycaprolactone	16
2.4	Thermal and mechanical properties of copolymers, blends, and composite of PCL	25
2.5	Shape memory properties of copolymers, blends, composites of PCL	38
2.6	Scaffold types of PCL copolymer, blends, and composites for bio-medical applications	43
2.7	Commercial products based on polycaprolactone	50
4.1	Molecular weights by NMR, GPC, PDI by GPC and percentage conversion of PCL and PCL-PDMS-PCL macromers	74
4.2	Crystallinity of PCL-PDMS-PCL triblock copolymer	79
5.1	Parameters of the fittings of Burgers model on the creep behaviour of PCL/PCL-PDMS-PCL triblock photocrosslinked copolymers	90
5.2	Mechanical properties of PCL-PDMS-PCL triblock copolymer films	93
6.1	Avrami equation's isothermal crystallization parameter at various T_{cm}	106
6.2	Equilibrium crystal melting temperature T_{0cm} , stability parameter ϕ , nucleation parameter K_g , pre-exponential factor G_0 and fold surface free energy σ_e values for PCL and PCL-PDMS-PCL triblock copolymeric films	110
7.1	Thermomechanical cycles of shape memory properties for PCL-PDMS-PCL triblock copolymers	117
8.1	TGA data from Figure 8.5 and degradation analysis by SEM images of after degradation with hole diameter calculation	128
8.2	Percentage crystallinity, crystal melting point and crystallization temperature of PCL and PCL-PDMS-PCL triblock copolymer films at before degradation and different time of interval of degradation	131

List of Abbreviations

PCL	:	Polycaprolactone
ROP	:	Ring opening polymerization
RROP	:	Radical ring opening polymerization
RAFT	:	Reversible Addition Fragmentation Chain-Transfer
MDO	:	2-Methylene-1,3dioxepane
IPN	:	Interpenetrating polymer network
PLA	:	Poly lactic acid
PLLA	:	Poly L-lactide acid
HCA	:	Hydroxycinnamic acid
CNT	:	Carbon nano-tubes
MWCNT	:	Multi walled carbon nano-tubes
T _m	:	Melting temperature
T _c	:	Crystallization temperature
T _g	:	Glass transition temperature
TSMP	:	Thermoresponsive shape memory polymers
HNT	:	Halloysite nanotubes
M _n	:	Number average molecular weight
E	:	Young's modulus
TS	:	Tensile strength
h-MoO ₃	:	Hexagonal molybdenum oxide
T _{cm}	:	Crystalline melting temperature
HA	:	Hydroxyapatite
SiC	:	Silicon carbide
PVB	:	Polyvinyl butyrate
PVAC	:	Polyvinyl acetaldehyde
PGA	:	Polyglycolic acid
CO ₂	:	Carbon dioxide
PDS	:	Pamidronate

ZnO	:	Zinc Oxide
ZnO-CA	:	Citric acid modified ZnO
NIR	:	Near infrared
FDA	:	Food and Drug Administration
POEGMA	:	Poly[oligo(ethylene glycol) methyl ether methacrylate]
PmCbA	:	Carborane
ADH	:	Adult Human Dermal
TiO ₂	:	Titanium dioxide
PGA	:	Polyglycolic acid
TPU	:	Thermoplastic polyurethane
MMT	:	Montmorillonite
PHB	:	Polyhydroxybutyrate
IBOA	:	Isobornyl acrylate
FGO	:	Functionalised graphene oxide
OWPU	:	Waterborne polyurethane nanocomposite
HTPB	:	hydroxyl-terminated polybutadiene
PTHF	:	Polytetrahydrofuran
NaCl	:	Sodium Chloride

Abstract

Polycaprolactone – polydimethylsiloxane – polycaprolactone (PCL-PDMS-PCL) triblock copolymer is a type of polymer that consists of three distinct polymer segments arranged in a linear structure. Polycaprolactone is biodegradable polyester that has gained attention due to its unique properties such as low melting point, good mechanical strength, and biocompatibility. It has found various applications in fields such as biomedical engineering, drug delivery, tissue engineering and 3D printing. PDMS is a type of silicone polymer with unique characteristics, including low surface energy, excellent thermal stability, and high hydrophobicity. PDMS exhibits good biocompatibility, chemical resistance, and low toxicity, making it suitable for various applications such as biomedical devices, microfluidic systems, and coatings. The PCL segments act as "end blocks" as well as "hard blocks" due to their relatively higher glass transition temperature (T_g) and more rigid nature. On the other hand, the PDMS segment acts as a "soft block" due to its lower T_g and more flexible nature. The arrangement of PCL-PDMS-PCL triblock copolymer results in a unique material with tunable properties. By adjusting the length of each polymer block, the mechanical, thermal, and surface properties of the copolymer can be tailored.

The shape memory triblock photocrosslinked copolymeric films of varying poly(ϵ -caprolactone) (PCL) chain length and constant polydimethylsiloxane (PDMS) content are synthesized. The effect of PCL chain length on structural, rheological, mechanical, thermal and shape memory properties of triblock copolymeric films is studied. The structural properties are analysed by X-ray diffraction (XRD) and optical microscope. Discrete crystal morphology is observed with increase in PCL chain length. Viscoelastic and mechanical properties are evaluated for the films of PCL and copolymers. Thermal properties are evaluated by differential scanning calorimetry (DSC) using non-isothermal and isothermal

modes. The crystallinity and crystal melting point of triblock polymer increases with increase in PCL chain length. The crystallization kinetics of triblock PCL-PDMS-PCL copolymeric films is studied with the help of Avrami model and Lauritzen-Hoffman (LH) model. The three-dimensional growth of PCL crystals is observed in triblock copolymers. Inclusion of PDMS block resulted in longer crystallization time, higher energy barrier and affects the crystal growth rate of PCL block, which further affect the shape fixity and shape recovery ratio accordingly.

The soil burial degradation behavior of PCL-PDMS-PCL triblock copolymer films is studied to understand its landfill effect and degradation mechanism. The microlevel, macrolevel and structural changes in the samples of homopolymer and triblock copolymer are analyzed before and after soil burial test. Microlevel changes are determined by evaluation of morphological properties with digital camera, optical microscope (OM) and scanning electron microscope (SEM) images and found that degradation of copolymer films enhanced with increase in PCL chain length. A Macrolevel structural changes are examined by Fourier transform infra-red spectroscopy (FTIR) and DSC crystallinity. The soil burial degradation mechanism is proposed for PCL-PDMS-PCL tri-block copolymer films on the basis of results obtained.

Overview of the Thesis

The entire research work has been divided into ten chapters. Chapter **one** provides past and current information related to this work. It insights the significance of the work along with the motivation to conduct this research study. This chapter gives a brief overview of the research gap, main objectives, and sub-objectives of the thesis work. In chapter **two** the extensive scientific literature is discussed on the synthesis routes of PCL copolymers, blends and composites, their properties such as structural, thermal, mechanical, rheological, shape memory and degradation behaviour and their application in biomedical and non-biomedical fields. Chapter **three** provides information related to experimental techniques, synthesis of PCL and PCL-PDMS-PCL triblock photocrosslinked films, methodology and tools which had been utilised to achieve the objectives are mentioned in this chapter. This chapter includes a description of the source of materials used during the study along with a brief outline of the adopted methodology, scheme of experiment done and details of the parameters of several characterization techniques employed to fulfil the research objectives. The chapter **four** discusses about structural evaluation which includes determination of molecular weight by Gel permeation chromatography and Nuclear Magnetic resonance, while chemical structure analysis carried out with the help of FTIR and NMR along with percentage crystallinity calculated by X-ray diffraction. Chapter **five** is designed to give a detailed analysis of rheological characteristics of PCL-PDMS-PCL triblock copolymer films. Oscillatory shear rheology tests are performed to measure the dynamics of the viscoelastic behaviour of photocrosslinked films above their crystal melting temperature (T_{cm}). Time dependent effect on the copolymer films has been analysed by creep recovery behaviour. Their structure recovery is also evaluated. Dynamic Mechanical Analysis (DMA) is carried at varying temperature. The mechanical properties are evaluated at ambient conditions only.

Chapter **six** gives an insight about thermal properties of PCL-PDMS-PCL triblock copolymer films. To evaluate thermal properties Thermal Gravimetry Analysis (TGA) and Differential Scanning Calorimetry (DSC) in non-isothermal and isothermal mode has been carried out. The non-isothermal mode is used to study about crystal melting temperature (T_{cm}) range and crystallization temperature (T_c) range. The percentage crystallinity is also evaluated with DSC results. The T_{cm} and T_c range is used to study the thermal properties in isothermal mode. In isothermal mode, crystallization kinetics has been studied with the help of Avrami model and Lauritzen-Hoffman (LH) model to quantify energy barrier associated with nucleation and crystal growth. The crystal formation after melting point is observed by optical microscope as well. The shape memory properties are evaluated in chapter **seven** via qualitative and quantitate modes. Chapter **eight** give a brief about soil burial degradation behaviour of PCL-PDMS-PCL triblock films with different PCL chain length. The structural, thermal morphological changes, weight loss are evaluated and mechanism of soil burial degradation has been proposed. The chapter **nine** summarises the entire research work accomplished based on the study. Chapter **ten** contains the literature that was reviewed and referred to conduct the entire research study as well as to evaluate the findings of the experiments and characterizations.

Chapter 1

Introduction and Objectives

1.1 Introduction

Copolymer materials are of great interest because they combine the intrinsic properties of different homopolymers at the nanometre scale[1]. Block copolymers offer unique opportunities for tailoring the microstructures in polymeric materials under various thermodynamic and mechanical environments. The covalent bonding of chemically incompatible polymer chains in block copolymers produces the microphase separations on the length scale of a few nanometres to a few hundred nanometres that may self-organize into long-range-ordered mesoscale crystalline orders[2]. Furthermore, judicious design of the chain architecture of block copolymers enhances desired mechanical properties.

Thermoresponsive shape memory (TSM) polymers exhibit changes in shape from a deformed position to their original shape induced by temperature. TSM polymers changes into another shape or temporary shape when heated above transition temperature, deformed under load and cooling conditions. The polymer maintains this temporary shape until it is heated again without any load and regains its original shape. Strain fixity describes the ability to switch segments to fix/hold the temporary mechanical deformation and can be calculated with equation (1.1).

$$R_f = \frac{\varepsilon_u - \varepsilon_o}{\varepsilon_m - \varepsilon_o} \times 100 \quad (1.1)$$

The strain recovery describes the ability of the shape memory material to recover its permanent shape and can be calculated with equation (1.2).

$$R_r = \frac{\varepsilon_u - \varepsilon_p}{\varepsilon_u - \varepsilon_o} \times 100 \quad (1.2)$$

Where ε_o is initial length, ε_m length after stretching, ε_u length after removal of load and ε_p recovered length.

Polycaprolactone (PCL) is aliphatic polyester, composed of hexanoate repeat units. It is hydrophobic, semi-crystalline, soluble at room temperature in organic solvents, easily processible due to its low melting temperature (54-71°C). PCL was first synthesized by ring-opening polymerization technique by Natta et al. in 1934. PCL is widely explored for thermoresponsive shape memory (TSM) behaviour. The first TSM polyurethane based on PCL was synthesized by Kim *et al.* in 1996 using the ring opening polymerisation (ROP) method. TSM behaviour of PCL near-normal human body temperature makes it an interesting material for biomedical applications. The TSM behaviour increases its application exponentially, including robotics, textiles, self-healing coatings, corrosion-resistant coatings, and anti-counterfeit materials. Polydimethylsiloxane (PDMS) is commonly referred as silicones. PDMS is inert, non-toxic, completely amorphous, hydrophobic and stable under high temperature. Low-molecular weight PDMS is a liquid used in lubricants, antifoaming agents, and hydraulic fluids. At higher molecular weights, PDMS is a soft, compliant rubber or resin. It is used in caulks, sealants, contact lenses and medical devices. In this study PDMS is taken as comonomer with PCL which serves as soft segment and PCL as switching segment. The glass transition temperature of PDMS ($T_g = -125^\circ\text{C}$) is much lower than PCL ($T_g = -60^\circ\text{C}$) which help to modulate its mechanical properties and thermo-responsive shape memory behaviour.

In the past two decades, PCL-PDMS-PCL triblock copolymers have been synthesized and are found its applications in biomedical, self-replenishing,[3] antifouling[4] and water erodible[5] coatings and oxygen sensors.[6] The properties such as thermal, mechanical, structural, morphological, shape memory and degradation of PCL-PDMS-PCL triblock copolymers are studied by various research groups[7–10] Ekin and Webster first synthesized

a series of PCL-PDMS-PCL triblock copolymer in 2006 by using terminal hydroxyl modified PDMS to form block copolymer and studied its molecular structural and thermal properties.[9] Poojari and Clarson have synthesized PCL-PDMS-PCL block copolymer using lipase as a catalyst and studied the structure and thermal properties by varying the ratio of monomers.[11] Schoener *et al.* synthesized triblock copolymer with constant PDMS block and studied structural and shape memory properties.[12] Zhang *et al.* reported structural and shape memory properties by varying PDMS in triblock copolymer.[13] Addition of PDMS changed the hydration property of PCL however, it has not affected degradation mechanism of PCL in triblock copolymer.[14] Yilgor *et al.* have synthesized PCL-PDMS-PCL block copolymer and studied morphology, microphase separation, crystallization of PCL and surface properties.[10] The inclusion of PDMS in PCL improved the hydrophobicity of copolymer surface.

Although structural, thermal, morphological properties of PCL-PDMS-PCL triblock copolymer are well documented; isothermal crystallization and its correlation with shape memory properties are less explored. Understanding the structure, morphology and crystallization of block copolymers is important since it has a direct relationship with the shape memory properties and performance in desired applications. Crystallization of PDMS/PCL block copolymer with amorphous and crystallizable block is not only of theoretical interest to understand polymer morphology but also provide process parameters for shape memory behaviour. Composition, molecular design and molecular weight of individual block affect the crystallization behaviour of block copolymers.

The rheological properties of PCL homopolymer[15–19], blends[20–25] and composites[26–33] are reported by researchers in the temperature range of 70 - 230°C. The solution and melt rheology of PCL based material have been done to analyse processing parameter while rheological study on polymer films have been carried out to determine viscoelastic behaviour

of sample. The copolymer comprised of polystyrene/polyisoprene[34], polystyrene/poly(*n*-butylacrylate)[1], Poly(ethylenepropylene-*b*-dimethylsiloxane)[35], multiblock olefins[36–38] are studied to investigate self-assembling capacity and mesophase/microphase separation. The rheology of various block copolymers of PCL-PDMS-PCL is never studied.

On the basis of medical application, degradation studies on PCL and its copolymer are majorly focused on simulated body fluids. These simulated environments are enzymes, buffer solution and water. Degradation of polycaprolactone is bulk process proceeded in two steps: 1) erosion of surface 2) cleavage of C-O bond or degradation of macromolecules. The copolymers of PCL with lactic acids[39], glycolide[40] and δ -valerolactone[41] increased the *in-vitro* degradation rate of copolymer due to change in chemical structure, crystallinity and hydrophilicity. The copolymer of PCL exhibit two separate polymer degradation fractions formed throughout the study[40]. PDMS are exceptionally resistant to hydrolytic or oxidative breakdown under ordinary ambient conditions. Thermoresponsive shape memory behavior of polycaprolactone widens its application area such as self-knotting sutures, active packaging, self-healing coating, robotics and anticounterfeit material. These extended application products ended in landfill which make it essential to study soil burial degradation. In soil, PDMS hydrolyses to yield the monomeric dimethylsilanediol. The hydrolysis reaction is much faster as the soil dries and PDMS undergoes extensive degradation when exposed to dry soils. The clay constituents of the soils are found to promote this rearrangement process. PCL [42, 43], graft copolymer with poly (ethylene -co -vinyl alcohol)[44], blend with corn starch[45] and composites with organoclays[46–48] are studied for soil burial degradation. PCL-PDMS-PCL triblock copolymer degradation studies are limited to simulated environment as of now.

1.2 Research gap

PCL-PDMS-PCL triblock films have been studied by researchers and reported broad range of crystal melting temperature by changing the PCL chain length alongwith optimum mechanical properties and excellent shape memory properties. The correlation between thermal properties and shape memory properties has not been studied yet. The rheological properties are also not reported till now. PCL-PDMS-PCL triblock films are examined for simulated environment but not studied for soil burial degradation.

1.3 Motivation of research

The shape memory polymers become interesting material due to their non-conventional application. Medical as well as non-medical field are getting well explored for shape memory polymers for the ease of work and betterment of living beings. The widening horizons of application area are meant to have in-depth study about its structural, thermal, rheological and degradation behaviour and to examine their co-relation with each other. White pollution is also a major concern to focus upon as this ends up in the form of landfill for years. This motivated to carry out the thesis work on unexplored area of PCL-PDMS-PCL triblock copolymer.

1.4 Objectives of the research work

The broad objective of this research work was to study the multifunctional properties like structural, thermal, rheological, mechanical, soil burial and shape memory properties of PCL-PDMS-PCL triblock copolymer films by synthesizing it via ring opening polymerisation.

1.4.1 Specific objectives

To achieve this objective, the specific objectives of the thesis were as follows:

1. Synthesis of PCL-PDMS-PCL triblock copolymers with varying PCL chain length and their structural characterization.
2. Rheological properties of PCL-PDMS-PCL triblock copolymers.

3. Isothermal crystallization kinetics study and its correlation with shape memory properties.
4. Soil Burial biodegradation behaviour of PCL-PDMS-PCL triblock copolymers.

Chapter 2

Literature Review

Overview

This chapter summarises the extensive scientific literature on the synthesis routes of PCL copolymers, blends and composites, their properties such as structural, thermal, mechanical, rheological, shape memory and degradation behaviour and application in various fields. The chapter included the discussion about studies carried out on PCL-PDMS-PCL triblock copolymers and their application. The commercial products based on polycaprolactone are also listed.

2.1 Introduction to PCL copolymers, blends, and composite

Polycaprolactone (PCL) is a semi-crystalline, hydrophobic, synthetic aliphatic polyester consisting of hexanoate repeat units. It shows high solubility at the ambient conditions in organic solvents and is easily processible due to its low melting temperature (54-71°C). PCL's biodegradable and biocompatible properties make it highly researched material for tissue engineering, controlled drug delivery systems, wound dressing, contraceptive, dentistry, and bone engineering.[49–51] PCL has a low degradation rate in combination with high ductility and plasticity. It is certified by Food and Drug Administration, USA and CE registered mark by European Community for application in numerous biomedical devices.[52] Molecular weight and degree of crystallinity affect its physical, thermal, mechanical, and rheological properties. The superior viscoelastic and mechanical properties make it suitable for food packaging, coating, adhesive, and textiles.

Natta *et al.* in 1934, first synthesized PCL by ring-opening polymerization technique.[52] Three well-known synthesis routes of polycaprolactone are : (i) ionic and metal-catalysed

ring-opening polymerization (ROP) of ϵ -caprolactone, (ii) radical ring-opening polymerization (RROP) of 2-methylene -1,3 dioxepane (MDO), and (iii) condensation of 6-hydroxycaproic acid.[53] A good comprehensive study about the synthesis of polycaprolactone is given by Thielemans *et al.*[54]

A decent number of review articles are published on PCL and its applications, limited to biomedical and tissue engineering.[49, 50, 61–65, 51, 52, 55–60] A review on PCL is published by Woodruff *et al.* in 2010, which gives a detailed analysis of biodegradability, biocompatibility, and application in the biomedical field.[52] In 2019, Janmohanmmadi *et al.* published a review paper on biomedical applications of polycaprolactone scaffolds prepared using electrospinning technique.[51] Bartnikowski *et al.* have published a comprehensive review on degradation mechanism of polycaprolactone, its copolymer and composite.[66] Recently, reviews have been published on polycaprolactone-triol,[59] *in-vivo* studies of 3D model of polycaprolactone,[49] bone scaffolds [50] and biodegradable conducting polymers[67].

More recently, PCL has been widely explored for thermo-responsive shape memory (TSM) behaviour. Using the ROP method, the first TSM polyurethane based on PCL synthesized by Kim *et al.* in 1996.[68] The polymer exhibits temperature responsive shape memory behaviour due to its semi-crystalline nature and low melting range. PCL shows exceptional blend compatibility.[59] TSM behaviour of PCL copolymers and blends near-normal human body temperature makes it an interesting material for biomedical applications. The TSM behaviour increases its application exponentially, including robotics, textiles, self-healing coatings, corrosion-resistant coatings, and anti-counterfeit materials.

Major published review papers focus on synthesis, biomedical application, and degradability of PCL. Since 2010, a plethora of research has been reported on PCL copolymers, blends, and composites in different fields. Copolymers of PCL are synthesized to tune the properties

on molecular level. PCL blends and composites have been synthesized in single & multi-phase with easier fabrication methods than copolymerization to modify their properties and broaden their applicability. Here, fabrication of PCL's copolymers, blends and composites with their correlation on thermal, mechanical, structural, rheological, electrical, degradation and shape memory properties and applications are discussed in below sections.

2.2 Synthesis of polycaprolactone copolymers, blends, and composites

Copolymers are composed of more than one monomer repeat unit provides an additional degree of freedom over homopolymers. Polymer properties can easily be tuned by adjusting the ratio of the monomers. PCL copolymers are synthesized by ROP and RROP methods, as shown in Figure 2.1. ROP is the most preferred route for the synthesis of PCL block copolymers, graft copolymers or random copolymers due to high yield (above 90%). For di-block, tri-block, or multi-block copolymers, in the presence of catalyst stannous octoate ROP method is used where other monomers are L-lactide,[69, 70] dimethyl siloxane,[12, 71] polyethylene glycol[72] and *N*-2-hydroxypropyl methacrylamide.[73] ROP is used to functionalize monomers and further condensation[74] or crosslinking[75–77] is carried out to get block copolymer. Bulk polymerization of ϵ -CL with other monomers with different weight percent gives random copolymer [78–80] by ROP mechanism. The graft copolymers with cellulose[81], hydroxyethyl methyl acrylate[82], ethyl vinyl acetate[83] is synthesized by ROP followed by grafting from[82] grafting through[82] and transesterification method[83]. Vinyl monomers are copolymerized with MDO(2-methylene-1,3dioxepane) for the cognizance of functional biodegradable polyesters, include vinyl bromobutanoate[84], methyl methacrylate[85], hydroxyethylacrylate[86], vinylcyclopropane[87], vinyl ethers[67] and glycidyl methacrylate[88, 89] by radical ring-opening polymerization(RROP). Another outstanding feature is that PCL's structure obtained with RROP method changes when compared to ionic or metal-catalysed ROP of ϵ -caprolactone. These copolymers have been

suggested to comprehend materials integrating the elasticity of PCL, shape memory behaviour, and alter degradation times. Table 2.1 represents the copolymers of polycaprolactone with different monomers and their synthesis conditions.

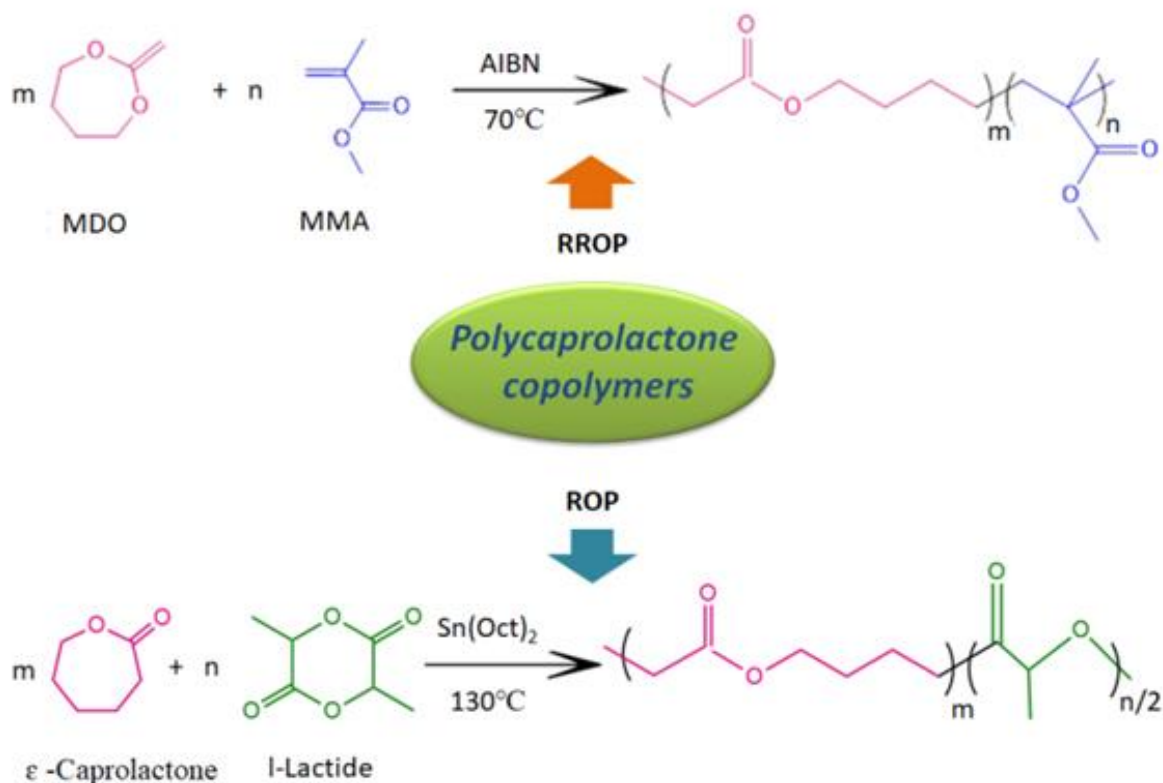


Figure 2.1. Synthesis routes of copolymerization of polycaprolactone

Table 2.1. Copolymers of polycaprolactone

S. No.	Co-monomer	Method	Copolymer type	Catalyst/ Initiator	Reaction Condition	Ref
1.	L-lactide	ROP	Block	Stannous Octoate	140°C , 3 hrs	[69, 70]
2.	Dimethyl Siloxane	ROP	Block	Stannous 2-ethylhexanoate	145°C , 24 hrs and 120°C , 48 hrs	[12, 71]
3.	Polyethylene glycol	ROP	Block	Stannous 2-ethylhexanoate	140°C , 24 hrs	[72]
4.	N-2-hydroxypropyl methacrylamide	ROP	Block	Stannous 2-ethylhexanoate	65°C , 24 hrs	[73]
5.	ω -pentadecalactone	ROP	Block	Ethylene glycol	Condensation of diols and reaction with 4-methylhexamethylene	[90]

					diisocyanate at 83°C	
6.	4-hydroxycinnamic acid	ROP	Block	Stannous 2-ethylhexanoate	Thermal polycondensation of diols at 200°C	[74]
7.	<i>p</i> -dioxanone	ROP	Random	Stannous 2-ethylhexanoate	130°C, 48 hrs	[31]
8.	D.L-lactide	ROP	Random	Stannous 2-ethylhexanoate	110°C, 24 hrs	[32]
9.	Butyl acrylate	ROP	Random	Stannous 2-ethylhexanoate	Melt mixing of oligo caprolcatone diol with butyl acrylate at 80°C	[78–80]
10.	Cellulose	ROP	Graft	Stannous 2-ethylhexanoate	120°C, 24 hours, grafting from	[81]
11.	Hydroxyethyl methyl acrylate	ROP	Graft		Grafting though and grafting from	[82]
12.	Ethyl vinyl acetate	ROP	Graft	Titanium propoxide	Transesterfication	[83]
13.	Vinyl bromobutanoate	RROP	Random	azobis(isobutyronitrile) (AIBN)	60°C, 9 hrs	[84]
14.	Methyl methacrylate	RROP	Partial random	AIBN	75°C, 24 hrs	[85]
15.	Hydroxyethyl acrylate	RROP	Graft	2,20-azobis (4-methoxy-2,4-dimethylvaleronitrile) (V-70)	30°C, 24hrs	[86]
16.	2-vinylcyclopropane 1,1-dicarboxylate	RROP	Random	di-tert-butyl peroxide	120°C, 48 hrs	[87]
17.	Functional vinyl ethers	RROP	Graft	Diethylazobisisobutyrate	70°C, 8hrs	[67]
18.	Glycidyl methacrylate	RROP	Random	AIBN	60°C, 3 hrs	[88, 89]

Polymer blends and composite are easier method than copolymerization to improve properties of polymeric system by incorporating other polymer, copolymer, or filler. There are number of method available for blending of polymers such as melt mixing, solution mixing, latex mixing, and preparation of interpenetrating polymer networks (IPN). Synthesis of PCL blends is mostly carried out by melt blending, solution blending method due to low melting temperature and solubility in organic solvents as shown in Figure 2.2. Several polymers such as poly(L-lactide)/poly(lactic acid),[91–95] pine resin,[96] poly(glycolic acid),[97] lignosulfate,[98] chitosan[99] and hydroxybutyrate[100, 101] are melt blended by mixing at different temperature. Table 2.2 represents different polymer used to prepare blend with PCL along with their blending conditions. The melting temperature is chosen on the basis of polymer of higher melting point and crystallinity. To improve the compatibility of blends, free radicals like benzoyl peroxide are used for PCL/poly(3-hydroxybutyrate) in melt blending method by Przybysz *et al.*[101] and Woodard *et al.* have chosen different method i.e. semi-IPN network for PCL/PLLA blend.[102] Solution blend of PCL and PLA/PLLA,[23, 103, 104] poly(glycolic acid),[105] poly(3-hydroxybutyrate-co-3-hydroxyhexanoate),[106] poly(hexylene adipate)[107] and poly(methylmethacrylate)[108] are prepared either by chloroform or mixture of chloroform with dimethylformamide, 1-4, dioxane, acetone or ethanol because of ease of solubility at ambient conditions.

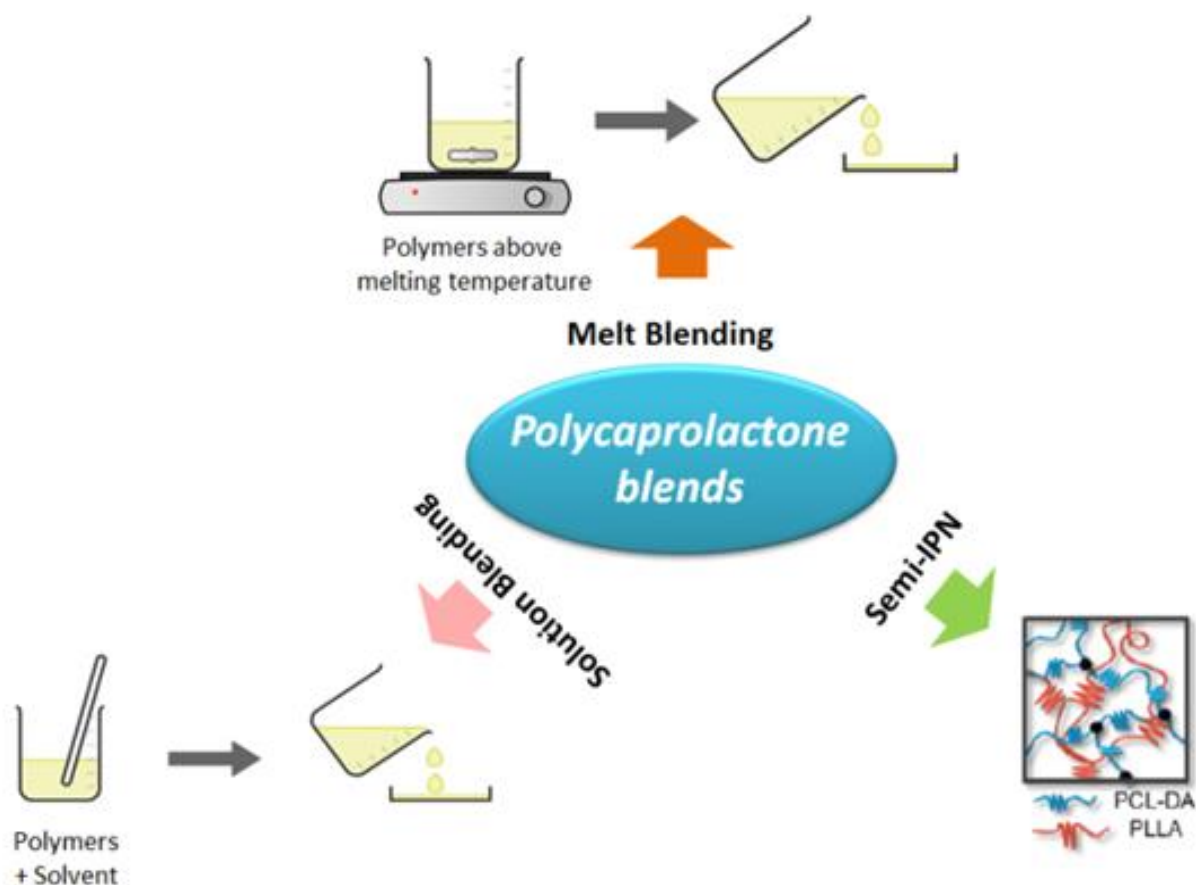


Figure 2.2. Synthesis methods of blends of Polycaprolactone

Table 2.2. Blends of Polycaprolactone

S. No.	Polymers	Method	Blending conditions	Ref
1.	Poly (L-lactide)	Melt blended	Twin screw extruder, 150 rpm, 180°C or Haake polylab rheometer, 50 rpm, 170°C, 6 mins. or Brabender Plasticorder, 60 rpm, 10 min at 180°C	[91–95]
2.	Pine resin	Melt blended	Mini max molder, 50 rpm, 15 min at 80°C.	[96]
3.	Poly (glycolic acid)	Melt blended		[97]
4.	Lignosulphate	Melt blended	Rheomix 600 OS, 60 rpm, 10 min at 120°C	[98]
5.	Chitosan	Melt blended	HAPRO RM-200A, 20 rpm, 20 min at 110°C	[99]

6.	poly(3-hydroxybutyrate)	Melt blended	Brabender mixer, 100 rpm, 8 min at 170°C	[100, 101]
7.	Poly(L-lactide)	IPN	Photo-crosslinking of acrylate terminated PCL and PLLA mixture	[102]
8.	Poly(L-lactide)	Solution blended	Chloroform or Chloroform/ <i>N, N</i> -dimethylformamide mixture or Chloroform/1,4-dioxane mixture	[23, 103, 104]
9.	Poly(glycolic acid)	Solution blended	1,1,1,3,3,3,-hexafluoroisopropanol	[105]
10.	Poly(3- hydroxybutyrate-co-3-hydroxyhexanoate)	Solution blended	Chloroform	[106]
11.	Poly(hexylene adipate)	Solution blended	Chloroform	[107]
12.	Poly(methylmethacrylate)	Solution blended	Chloroform	[108]

Composites are synthesized by various methods such as intercalation, in-situ polymerization, and direct mixing of polymer and fillers. The preparation of PCL composite is reported by all the above techniques as shown in Figure 2.3. Different fillers used to prepare composite of PCL are shown in Table 2.3. PCL easily melts above 60°C and becomes soluble in chloroform or its mixture; that is why melt mixing is the preferred route to synthesize composite followed by the solvent method. Composite of PCL with alumina,[27] niobium pentoxide,[27] multi wall carbon nano tube (MWCNT),[109] leaf sheath date palm fibre,[110] hydroxyapatite,[111] silica carbide,[112] soy protein isolate,[113] halloysite,[114] babassu,[115] rice straw fibre,[116] clam shell powder[117] and calcium phosphate[118] are processed by melt compounding/mixing method. A significant hurdle in the production of PCL composites with natural waste by products' fillers is that PCL is relatively hydrophobic, in contrast most natural fillers are hydrophilic, which leads to poor compatibility between the two phases of the composites. To overcome this problem, compatibilizers in the form of reactive functional groups are incorporated to PCL polymer backbone for miscibility. Melt intercalation method is used for clay composites.[46, 119] The solvent method is used for

films, nano-fibrous and 3D printed composites of PCL with fillers such as magnetite,[120] casein,[120] cellulose nano-whiskers,[121] hexagonal molybdenum oxide,[122] CNT,[123] MWCNT,[124] carbonyl iron powder[125] chitosan [126] and gold nanoparticles (AuNPs)[90]. In-situ method is used for carbon nano tubes (CNT)[127] and graphene oxide[128] where nanofillers are added in ϵ -caprolactone before polymerization. On a different approach, nanocomposites of PCL/ gold nanoparticles are prepared by solution casting of AuNPs over PCL nanofibers.[129] The sandwich-type of composite is fabricated by compression moulding method, where reinforcement layers of electrospun cellulose nanofibers [130] and gelatine [131] are placed between PCL matrix layers.

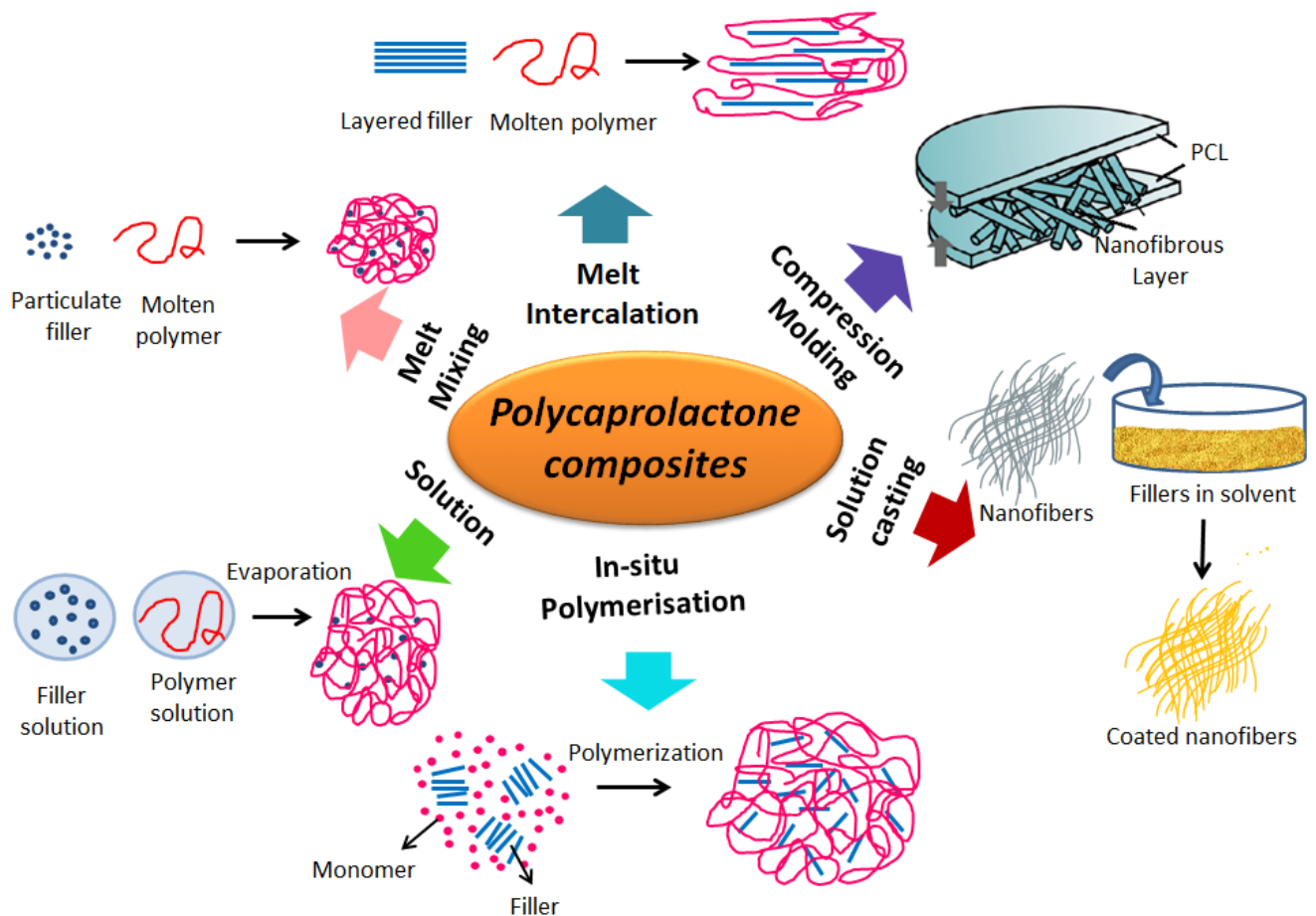


Figure 2.3. Synthesis methods of composites of polycaprolactone

Table 2.3. Composites of Polycaprolactone

S. No.	Fillers	Method	Conditions	Ref
1.	Alumina	Melt mixing	Haake Rheomix 3000 laboratory internal mixer, 150°C	[27]
2.	Niobium pentoxide	Melt mixing	Haake Rheomix 3000 laboratory internal mixer, 150°C	[27]
3.	MWCNT	Melt mixing	Twin-screw Extruder, 400 rpm, 90 °C, 2 min	[109]
4.	Leaf sheath date palm fibre	Melt mixing	Twin-screw co-rotating extruder, feed rate 3.5 kg/h, screw speed 100 and 400 rpm, 120 °C,	[110]
5.	Hydroxyapatite	Melt mixing	Twin screw Compounder, 100°C, 100 rpm, 6 mins.	[111]
6.	Silicon carbide	Melt mixing	Twin screw Thermo Scientific Haake Rheomixer, 100°C, 50 rpm, 10 min.	[112]
7.	Soy protein isolate	Melt mixing	Intensive mixer, 100°C, 30 rpm, 10 min	[113]
8.	Halloysite	Melt mixing	Haake Rheocorder, 100°C, 60 rpm, 10 min	[114]
9.	Babassu	Melt mixing	Haake Rheomix laboratory internal mixer, 150°C, 60 rpm, 15 min	[115]
10.	Rice straw fiber	Melt mixing	Plastograph 200-Nm mixer W50EHT 70-80 °C, 20 min, 50 rpm	[116]
11.	Clam shell powder	Melt mixing	Intensive mixer, 100°C 30 rpm, 10 min	[117]
12.	Calcium Phosphate	Melt mixing	Extruder, room tempera- ture	[118]

			to 160°C	
13.	Clay (Na ⁺ MMT, Cloisite 30B, Cloisite 20A, bentonite)	Melt Intercalation	Double-screw mini-extruder DSM Xplore 5&15 microcompounder 60–90–120 °C, 150 rpm, 1 min.	[46, 119]
14.	Magnetite	Solution method	THF, dispersed for 8 minutes, 15000 rpm	[120]
15.	Casein	Solution method	THF, dispersed for 8 minutes, 15000 rpm	[120]
16.	Cellulose nanowhiskers	Solution method	DMF, 70°C	[121]
17.	Hexagonal molybdenum oxide	Solution method	Chloroform, 27°C	[122]
18.	CNT	Solution method	Chloroform, sonication for 5 min.	[123]
19.	MWCNT	Solution method	MWCNT in DMF & PCL in THF	[124]
20.	Carbonyl iron powder	Solution method		[125]
21.	Chitosan	Solution method	DMF, Chloroform, Ultrasonication	[126]
22.	CNT	In-situ polymerization	Addition before polymerization	[90]
23.	Graphene oxide	In-situ polymerization, solvent mixing. Covalent attachment	Addition before polymerization, DMF dispersed GO mixed with PCL, Addition of filler in the presence of N,N'-dicyclohexylcarbodiimide as coupling agent and 4-dimethylaminopyridine as catalyst	[128, 132]
24.	Gold Nanoparticles	Solution casting	Electrospun PCL nanofiber dipped in AuNPs methanol mixture	[129]
25.	Cellulose nanofiber	Compression moulding	Hydraulic press at 80°C	[130]
26.	Gelatine	Compression moulding	Hydraulic press at 80°C	[131]

All copolymers are reported by ROP and RROP methods with a good number of synthetic polymers and cellulose as natural polymer. Here natural polymers like polysaccharides (e.g. natural gums) and proteins (e.g. silk) still need to work upon. Copolymers of polycaprolactone can also be synthesized by condensation of 6-hexanoic acid. PCL blends are prepared by melt, solution and IPN methods, but latex mixing method is untouched. Latex mixing is used for blending two latexes. This method can lead to preparing an emulsion of polycaprolactone and blend it with water-based polymers. Such emulsions can be used for low volatile organic content (VOC) systems. A large number of PCL composites are reported with natural and synthetic fillers. Composites based on nanoparticles of copper and silver are not reported, yet their antibacterial properties make a mark in biomedical field.

2.3 Properties of polycaprolactone copolymers, blends, and composites

PCL has melting temperature between 54-71°C and a glass transition temperature (T_g) of -60°C.[133] It is a well-known semi-crystalline polymer having a maximum degree of crystallinity of 69%.[134] The physical, thermal and mechanical properties of PCL are influenced by its molecular weight and degree of crystallinity. Extensive research has been carried out to improve or modify the chemical, mechanical, and thermal properties of PCL by copolymerization, blending, and formation of composites. They also modify degradation time and rheological properties, which changes its processing parameters. Different factors which influence the properties of polycaprolactone copolymers, blends and composites are summarized in Figure 2.4. The Following sections summarize the thermal, mechanical, electrical, structural, rheological, shape memory and degradation properties of PCL copolymers, blends and composites.

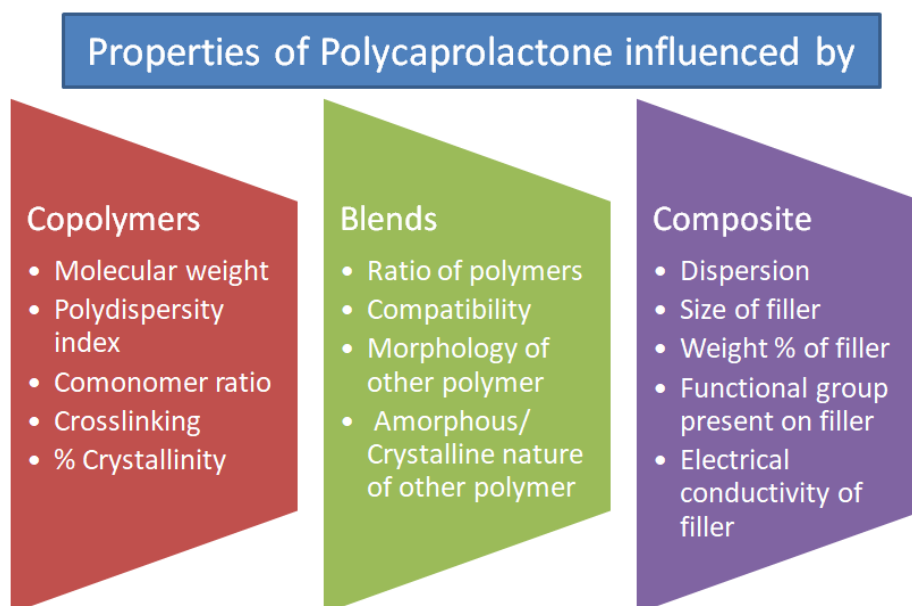


Figure 2.4. Different factors which influence the properties of copolymers, blends, and composites of polycaprolactone

2.3.1 Thermal properties

The thermal properties of PCL are highly reliant on molecular weight and degree of crystallinity[135]. The thermal degradation of PCL is reported as a single step in the range of 358-400°C, as shown in Figure 2.5. Copolymerization, blending and formation of composites influence the T_g , degradation temperature, crystallization behaviour and percentage crystallinity of PCL.

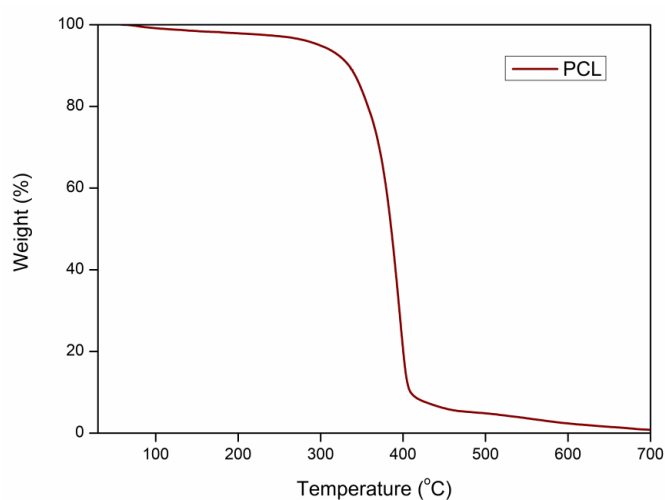


Figure 2.5. Thermal gravimetric analysis of PCL

The thermal properties of PCL copolymers with other monomer like ω -pentadecalactone,[136] L-lactide,[69, 76, 79] dimethyl siloxane,[12] butyl acrylate,[80] p-dioxanone,[78] ethyl vinyl acetate,[83] hydroxymethyl acrylate,[82, 137] glycidyl methacrylate,[138] hydroxycinnamic acid[74] and ethylene glycol[77] are studied by researchers. Block copolymer of PCL with ω -pentadecalactone (PDL) shows two distinct peaks of melting and crystallization owing to PCL and PDL since both have their own melting and crystallization temperature range. There is an increase in melting temperature (T_m) and crystalline temperature (T_c) of PCL with a rise in PCL content due to bigger block formation of PCL, as shown in Figure 2.6.1[136]. Similar observations are found in the case of PCL/L-Lactide block copolymer[69]. With increasing content of hydroxycinnamic acid (HCA) in copolymer[74] thermal stability, T_m and crystallinity are decreased because the HCA chain disturbed the crystal growth of PCL content. Copolymers based on completely amorphous dimethylsiloxane ($T_g = -125^\circ\text{C}$) and n-butyl acrylate($T_g = -60^\circ\text{C}$) are showing a decrease in T_m , T_c and crystallinity with decreasing PCL content due to shorter chain length of crystalline polymer[12, 80]. PCL and p-dioxane copolymer showed no significant change in thermal stability. Still, there is a huge decrement in melting & crystallization peak and percentage crystallinity with an increase in dioxane content due to increased disorder along the polymer chains and imperfect packing of the polymeric segment in the crystalline lattice[78]. The graft copolymer of EVA/PCL showed improved thermal stability, melting temperature, and crystallinity dependent on the molar mass of both and structural differences between the two[83].

Thermal properties of PCL blends with Poly(L-lactide) acid[91, 92], polyglycolic acid (PGA)[97], thermoplastic starch (TPS)[97], chitosan[97, 139], PMMA[108], polyhydroxy butyrate (PHB)[100, 101, 106], lignosulphonate[98] are reported. Blends of PCL with PLLA, PHB, lignosulphonate and PGA are immiscible and miscible blends are with pine resin, TPS,

chitosan, PHA and PMMA. The miscibility is reported by single T_m and T_g peaks mostly. PLLA has a higher melting point than PCL and blends showed a gradual increase in melting point with a higher content of PLLA[91, 92]. The ternary blend of TPS/PGA with PCL showed a decrease in melting peak and multi-melting peak because these blends are not able to co-crystallize. A blend of PCL with pine resin becomes thermally unstable because pine resin itself is thermally unstable(onset temperature $\sim 130^\circ\text{C}$)[96]. PCL/pine resin blends are showed a single T_m and T_c peaks indicating their miscibility and reduction in both with increased content of pine resin, as shown in Figure 2.6.2. Though, an improvement in thermal properties is reported with chitosan. An immiscible blend of PLA with PCL increases its crystallization temperature by 10°C due to discrete PLA solid phase having a strong nucleating effect[23, 93]. The immiscible blends of PCL/PHB showed two distinct peaks in DSC thermogram; however, the addition of compatibilizer i.e. di-(2-tert-butylperoxyisopropyl)-benzene (BIB) has shown improvement in blend miscibility due to partial crosslinking [100, 101].

The thermal properties of PCL composites with a variety of filler are studied extensively. Some of them include montmorillonite nanoclays,[46] bentonite,[119] carbon nanotubes,[109, 123, 124, 127, 140] alumina,[27] niobium pentoxide,[27] natural filler,[110, 115, 121, 130] halloysite,[114] hydroxyapatite(HA),[111] silicon carbide,[112] zinc oxide nanoparticles[141] and graphene[128, 132]. CNT/MWCNT based nanocomposite showed improvement in thermal stability, melting & crystallization peaks, and crystallinity, as shown in Figure 2.6.3.[124] Functionalization of CNT showed an improvement in interfacial interaction between polymer and CNT[109, 123, 124, 127] which resulted in improved thermal properties significantly. Chemically modified graphene, i.e. reduced graphene oxide showed better improvement in thermal properties of PCL as compared to graphene oxide [128, 132]. Natural fillers like babassu fibre[115], leaf sheath date palm fibre waste

biomass[110], cellulose nanofiber[130] & whiskers[121] and gelatine films[131] are incorporated in PCL to tailor thermal properties. There is a common observation that thermal stability, melting peak, crystallization peak, and crystallinity improved with natural fibre nanocomposite due to their good compatibility and they behave as a nucleating agent. Nanocomposite prepared with silicon carbide doesn't affect thermal stability and melting point in a significant way, but there is an improvement in crystallization temperature and crystallinity due to heterogeneous nucleation and an increase in the lamellar thickness of the crystallite formed[112]. When citric acid modified ZnO (ZnO-CA) nanoparticles are added to the PCL matrix, with increase in ZnO-CA content, the crystallization temperature (T_c) increases because, here, ZnO-CA acts as a nucleating point[141]. Thermal stability of PCL/clay nanocomposites is decreased with addition of clay due to its hydrophilicity and organically modified ions.[46, 119, 142] Addition of halloysite nanotubes increases the T_g because of the restricted segmental motion of polymeric chains.[114] A very good study by Sousa *et al.* demonstrated that thermal properties are not only affected by filler percentage and type but also depend on the rate of heat flow[27]. The thermal properties of PCL copolymers, blends and composites are reported in Table 2.4.

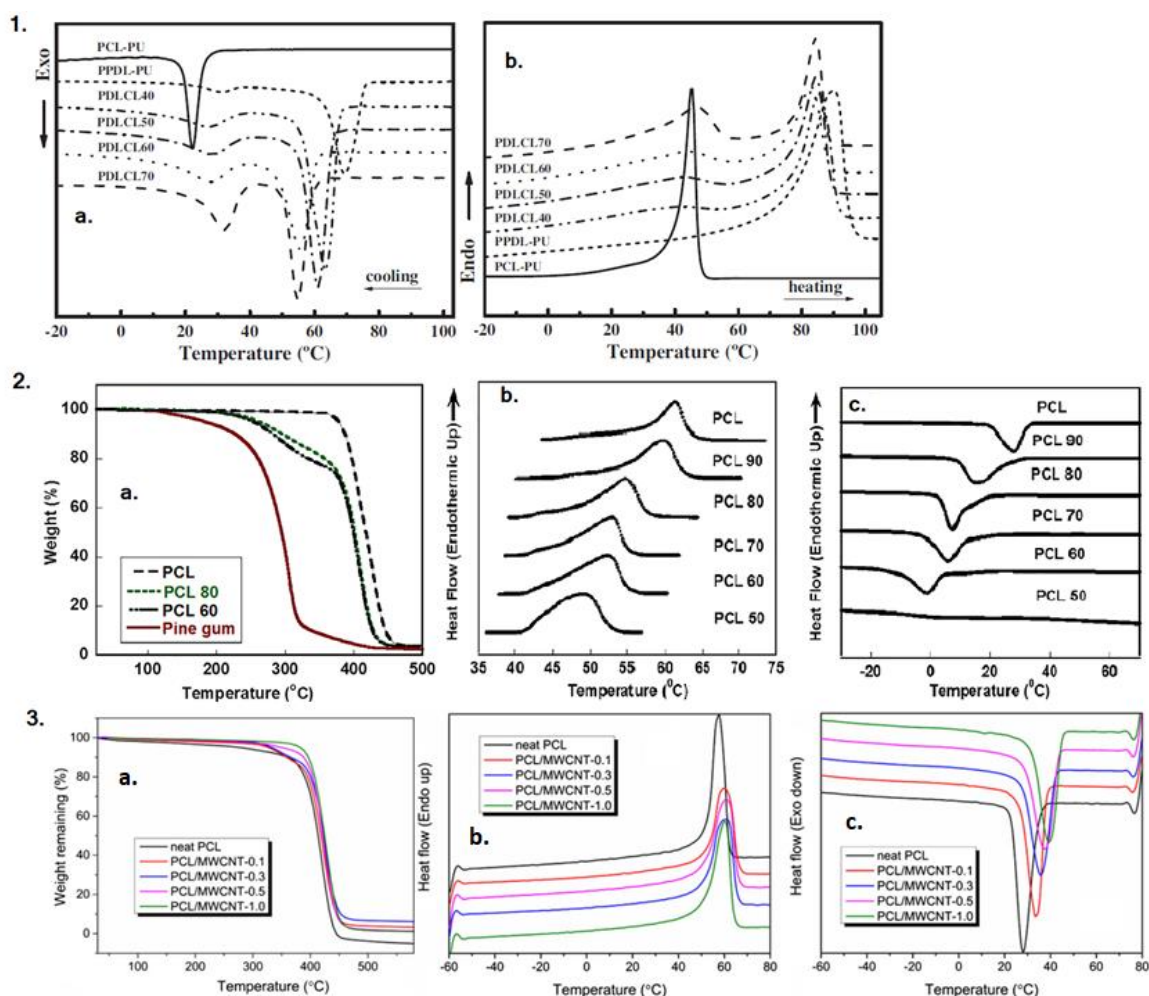


Figure 2.6. Melting 1(a) and cooling 1(b) DSC curves of PCL-co- ω -pentadecalactone reproduced with permission [91] 2019, Wiley; TGA curves 2(a); DSC curves melting 2(b) and cooling 2(c) of PCL/pine resin blends reproduced with permission [48] 2014, Wiley; TGA curves 3(a), DSC curves melting 3(b) and cooling 3(c) of PCL/MWCNT nanocomposite reproduced with permission [79] 2019, TnF.

Two different approaches are used to describe PCL copolymers' thermal properties. In the first approach, comonomer content is kept constant and varied the PCL chain length. The other approach is constant PCL chain length and varied comonomer content. The T_m , T_c and percentage crystallinity increase when PCL chain length increases in copolymers. Whereas, for copolymers of fixed PCL length and varying comonomer content, thermal properties are

shifting to lower degrees with increasing comonomer ratio. The blends exhibit their properties based on their miscibility. In general, miscibility or immiscibility is reported by single peak of T_g and T_m , while in case of PCL blends, only T_m and T_c are discussed. In some studies, compatibility of blends is not even examined. Some immiscible blends, which are studied by researchers, are not explored for the methods to improve the miscibility. Almost negligible data is available on effect on T_g for PCL copolymers, blends, and composites.

Formation of crystals in PCL is reported via optical microscope or polarized optical microscope (POM).[69, 143, 152–155, 144–151] Copolymers of PCL with L-lactide acid[69] poly(2-hydroxyethylmethacrylate)[151] are used to study the effect of chain length in crystallization. In double crystalline PCL-co-PLLA copolymers, PCL segments are trapped in PLLA spherulites. As PCL chain length increases, a non-banded structure is formed, as shown in Figure 2.7.1.[69] Grafting of poly(2-hydroxyethyl methyl acrylate) branches on PCL decreases the overall crystallization growth of crystals.[151] Blends of PCL/PLLA[150, 152] and PCL/polyvinyl butyrate (PVB)[149] and PCL/polyvinyl acetaldehyde (PVAC)[149] are studied for crystallization behaviour. The immiscible blends of PCL/PLLA showed an exceptional morphology when heated above T_m of PLLA and quenched to T_c of PCL. PCL is inserted into concentric ring band of PLLA during melting and a wrinkle pattern, along with a small concentric ring band, is induced in blends as shown in Figure 2.7.2.[150] PVB and PVAC are functioned as nucleating agents in blends with PCL. Their addition increases the spherulite size and reduces the crystallization temperature of PCL.[149] PCL composites with ZnO,[145] Oleic acid,[145] glycerol monooleate(GMO),[145] hydroxy apatite,[144] clays,[144, 153] and babassu[143] are reported for crystallization kinetics. In small amounts, organic additives, oleic acid, and GMO are acted as nucleating agents and increase the crystallinity, while higher amounts work as plasticizer. Inorganic additives such as ZnO, hydroxyapatite and clay increases the crystallinity and crystal growth rate due to nucleating

effect.[144] In PCL/babassu composite system, significant effect on crystallization parameters is not observed with addition of filler.[143]

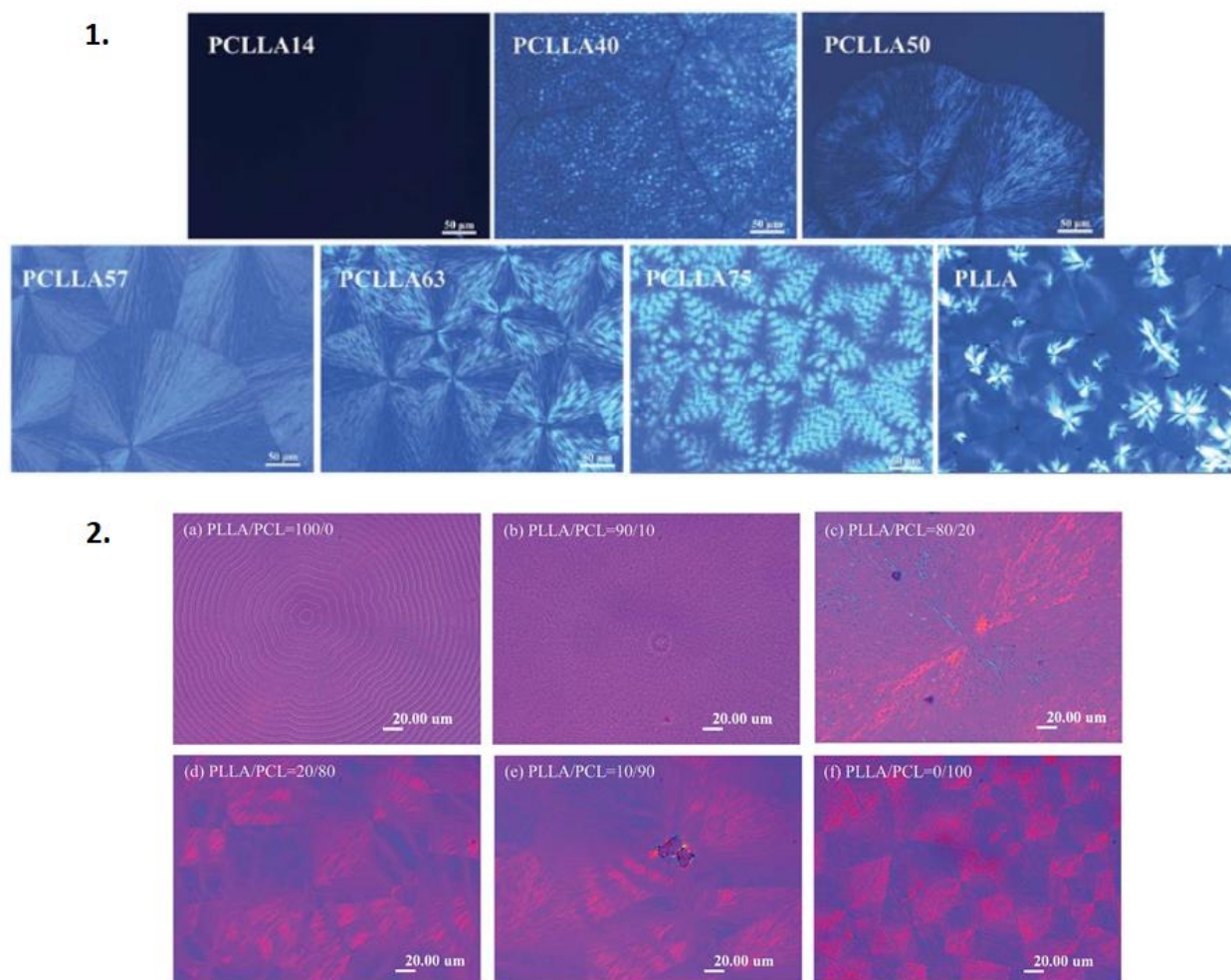


Figure 2.7. Polarized Optical Microscope of crystals growth in PCL/PLLA copolymers (1) reproduced with permission [21] 2017, RSC; PCL/PLLA blends (2) reproduced with permission [106] 2014, RSC.

Table 2.4. Thermal and mechanical properties of copolymers, blends, and composite of PCL

S. no.	Polymers	Synthesis mode	Composition	T _m [°C]	%X _c	Young's Modulus [Mpa]	Tensile strength [Mpa]	Elonga tion [%]	Ref
1	PCL-PDMS-PCL	Triblock copolymer	PCL ₅₀ -PDMS ₃₇ -PCL ₅₀	51.0	30.0	60.5	15.9	1197.0	[23]
2	<i>n</i> BA-PCL	Block Copolymer	PCL-BA (75:25)	28.0	—	—	38.0	55.0	[33]

3	PCL-PLLA	Block Copolymer	PCL-PLLA (50:50)	49.9 & 159.9	27.5 & 55.1	–	–	–	[28]
4	CL- <i>p</i> dioxanone	Random copolymer	CL-DA (87:13)	43.5	29.5	325.0	–	450.0	[31]
5	PCL-EVA	Graft copolymer	PCL-EVA (59.5/38.6)	50.6	–	–	2.9	409.0	[83]
6	PCL-HCA	Block copolymer	PCL-HCA (87:33)	56.6	28.0	–	–	–	[74]
7	PCL-PEG	Random copolymer	PCL-PEG (50:50)	40.0	45.2	0.023	–	–	[72]
8	PCL-PLLA	Block Copolymer	PCL-PLLA (80:20)	35.0	8.1	3.6	2.9	3200.0	[32]
9	PCL/PHB	Melt blending	75/25	61.2 & 154.0	39.1	–	11.4	125.0	[53]
10	PCL/PLLA	Semi IPN	75/25	49.1 & 157.9	25.4 & 15.4	93.3	18.8	593.0	[102]
11	PCL/ Pine resin	Melt blending	70/30	53		–	15.2	2600.0	[96]
12	PCL/PLA	Melt blending	70/30	56.7	38.3	732.5	25.3	–	[47]
13	PCL/lignosu lpahte	Melt blending	70/30	56.0	36.1	410.8	14.7	110.9	[98]
14	PCL/Chitosa n	Melt blending	80/20	–	–	–	15.6	151.8	[97]
15	PCL/poly(3- hydroxybuty rate-co-3- hydroxyhexa noate)	Solution blending	20/80 P(3HB- co-7mol% 3HH)	59.9	38.9	477.0	11.3	–	[106]
16	PCL/PHA	Solution blending	60/40	56.9	55.2		–	–	[107]
17	PCL/PLA	Solution blending (Electrospun)	20/80	54.0 & 153.0	18.9 & 2.9		1.7	94.4	[57]
18	PCL/cellulos e nanofiber	Compression composite	100/17	59.4	56	744.7	32.8	9.0	[130]
19	PCL/gelatin	Compression composite	90/10	58.2	50.3	535.7	13.2	175.3	[131]

20	PCL/CNT	In-situ composite	100/1	58.0	54.0	126.7	–	3.5	[90]
21	PCL/Graphene oxide	In-situ composite	100/0.5	–	–	199.0	13	788.0	[84]
22	PCL/Alumina	Melt composite	100/3	–	–	239.8	21.9	413.0	[27]
23	PCL/Niobium pentaoxide	Melt composite	100/5	–	–	243.9	23.5	485.0	[27]
24	PCL/Leaf sheath date palm fibre waste	Melt composite	100/20	–	–	284.0	24	21.0	[110]
25	PCL/SiC	Melt composite	96/4	56.5	35.2	102.8	26.8	3063.0	[112]
26	PCL/HNT	Melt composite	90/10	53.1	42.1	919.0	84.7	743.0	[27]
27	PCL/Rice straw fibre	Melt composite	90/10	59.9	41.7	–	36.1	655.0	[116]
28	PCL/Na ⁺ MMT	Melt intercalation	100/5	–	68.0	240.0	15.8	1345.0	[73]
29	PCL/C30B	Melt intercalation	100/5	–	72.0	303.0	14	1212.0	[73]
30	PCL/C20A	Melt intercalation	100/5	–	71.0	331.0	14.1	1430.0	[73]
31	PCL/cellulose nanowhiskers	Solution composite (electrospun)	100/1	64.1	25.4	5.0	1.1	115.0	[121]
32	PCL/MWCNT	Solution composite	100/1	60.0	45.3	–	30.4	1286.0	[124]
33	PCL/chitosan	Solution composite (electrospun)	100/50	–	–	26.5	4.4	133.0	[126]

2.3.2 Mechanical properties

PCL having number average molecular weight (M_n) of 80,000 g/mol, showed extremely ductile behaviour with an average elongation of 450%[98]. The ultimate tensile strength, Young's modulus and yield strength of PCL is reported as 20 MPa, 374 MPa and 16 MPa, respectively[133]. The copolymers, blends and composites of PCL in the form of films,

porous structures, 3D structures and electrospun fibres are widely studied for mechanical properties. Table 2.4 represents data of mechanical properties with the addition of comonomers, polymers, and fillers in PCL.

Crosslink density and crystallinity are the major factors that affect mechanical properties of copolymers. Crystalline PCL is served as physical cross-linked points, which contribute to mechanical strength, thus, higher crystallinity results in higher tensile strength. Covalently crosslinked networks of PCL-co-BA[80] and PCL-EVA graft copolymers[83] showed a decrement in mechanical properties. Copolymers with LLA[75, 76, 79], dimethyl siloxane[12, 13], cellulose fibre[156] and dioxanone[78] are reported with improved mechanical properties. The copolymers with *p*-dioxanone are showed peculiar behaviour, its E and TS are reduced with increased content of dioxanone, but elongation initially decreased then suddenly increased drastically from 930% for pure PCL to 450% for 87:13 ratio and 1690% for 80:20 ratio copolymers[78].

The mechanical properties of polymer blends are dependent on the miscibility or compatibility between components along with crystallinity. Good impact properties of PCL make it a favourite polymer to be blended with other polymers to enhance their mechanical properties. PCL blends with PLA showed an improvement in mechanical properties despite their incompatibility due to the ductility of PCL, whereas PLA is very brittle (impact energy $< 2.5 \text{ kJ m}^{-2}$)[94]. Crystallinity has a great impact on mechanical properties that is studied by Bai *et al.* in PLA/PCL blend[91]. An improvement in mechanical properties are observed when compatibility is improved by functionalization or addition of compatibilizer for incompatible blends like Lignosulphate[98], PLA[95], PHB. A compatible blend of PCL/pine resin showed improved mechanical properties with increased content of PCL[96]. The mechanical properties of porous scaffolds prepared by PLLA/PCL blend are highly dependent on pore size. The scaffolds with larger pore sizes showed lower mechanical

properties due to reduced polymer content[103]. Gelatine/PCL blend films showed compatibility and improved mechanical properties[131].

Polymer composite is a renowned method for enhancing the mechanical property of any polymeric system. Factors like dispersion, morphology and aspect ratio of fillers play a major role in mechanical properties. Composites of PCL with different types of carbon base fillers[124, 127, 128, 132], silica base fillers[46, 112, 114], natural waste byproduct[110, 113, 115, 116, 121, 130], minerals[97, 117], alumina and niobium pentoxide[27] are studied for their mechanical behaviour. Carbon filler in the form of MWCNT/CNT and graphene is incorporated in PCL matrix. The carbon base fillers have improved the mechanical strength of composites due to reinforcing effect of nanofillers. The addition of different types of clays such as Cloisite Na⁺, Cloisite 30B and Cloisite 20B in PCL matrix improved Young's modulus (E) while the tensile strength (TS) remained almost constant and the elongation at break decreased in the range of 25–36%. PCL/Silica Carbide composite showed increased E, yield stress, TS, and elongation when added up to 4%[112]. Incorporation of alumina and niobium pentoxide is not able to enhance any mechanical properties. Tensile strength, elongation at break and impact strength decreased with filler addition due to agglomeration, while Young's modulus is unaffected due to inefficient chemical interaction at the filler-matrix interface[27]. Composites based on natural waste by products and minerals showed reduced mechanical properties, including TS, % elongation and impact strength due to poor interaction with PCL matrix. Whereas palm fibre showed reinforcement effects due to fibre-matrix interfacial compatibility[110]. The naturally occurring clay mineral halloysite nanotube (HNT) is, improved the TS and E of the PCL/HNT composite due to uniform dispersion of HNT, its hollow tubular structure, low hydroxyl group density on the surface, high aspect ratio and good compatibility of the HNT with PCL. Increased elongation at break results is uncommon behaviour for PCL/HNT composite than pure PCL due to strong strain

hardening of the PCL matrix endorsed by stiff HNTs[114]. A good study is available for micro and nanocomposite of hydroxyapatite indicates that mechanical properties are improved and identical for both nano and micro composite till they are dispersed well in the matrix.[111]

The incorporation of PCL grafted cellulose, even in small amounts, has increased the mechanical properties of PCL nanofiber mats. The improvements in mechanical behaviour are attributed to the higher molecular weight (longer chains) of the grafted PCL chains and respective decrease in the diameter of the fibre.[81] Improved mechanical properties are observed for electrospun PLA/PCL blends.[104] Enhancement in E and TS of electrospun PCL mats after adding natural filler nanofibrillate chitosan is due to the reinforcing effect of embedded chitosan nanofibrils oriented along the fibre axis, uniform dispersion and potential inter-molecular interactions. Lower elasticity of the nanocomposite is in correlation with stiffening of chitosan[126]. When electrospun regenerated cellulose nanofibers are used in composite, E and TS increase with addition of nanofiber up to 17%, due to good compatibility[130].

The copolymers, blends, and composites of PCL in the form of films, porous structures, 3D structures and electrospun fibres are widely studied for mechanical properties.

2.3.3 Electrical properties

PCL is considered an insulating polymer having an electrical conductivity of 4.96×10^{-13} S/cm. A copolymer of PCL with aniline induce the conductivity of 0.62 S/cm and its nanofiber showed conductivity of 0.03 S/cm[157]. Electrical conductivity data for blends are not available because blends of PCL are not intended to have an application area of electrical conductivity. Incorporation of some conductive filler improved the conductivity of PCL composites. When MWCNT contents added up to 0.3 wt.%, the electrical conductivity of composites dramatically increased to 1.67×10^{-5} S/m. The fine spherulite and decreased

crystallinity of PCL caused by MWCNT-induced effect favoured the conductive properties of composites[124]. The conductivity of PCL is elevated by around 12-fold magnitude by inclusion of 5 wt. % chemically modified graphene in matrix[132]. Saravanamoorthy *et al.* have studied electrical properties of PCL/ hexagonal molybdenum oxide (h-MoO₃) nanocomposite and reported that the conductivity of the nanocomposites increased with addition of h-MoO₃ [122]. No change in the dielectric constant value is observed at low frequency as well as on the high frequency for pure PCL, whereas dielectric loss of the PCL/h-MoO₃ nanocomposites decreases with the increase in frequency (100 Hz to 1 MHz) and is showed better dielectric loss than pure PCL.

2.3.4 Structural properties

A well-defined semi-crystalline PCL crystal structure is studied by the X-ray diffraction method. PCL shows three strong peaks at the 2θ angles of about 21.4°, 22.0° and 23.7°, corresponding to the of diffraction planes (110), (111) and (200) of the orthorhombic unit cell, whereas lattice constants are $a= 7.45 \text{ \AA}$, $b=4.98\text{\AA}$, and $c=17.05\text{\AA}$ [133]. Copolymers of PCL-co-PEG[158] showed a combined peak of both. Similarly, PCL-co-PLLA showed peaks of both PCL and PLLA[159]. With the increased content of PCL, its peak dominated other polymers' peaks, as shown in Figure 2.8.1.[158] When analysis is carried out at 60°C, its peaks get diminished due to loss of crystallinity above melting point[159]. The characteristics peaks are diminished with increasing content of PDMS in PCL-PDMS-PCL triblock copolymer[10].

The XRD scans of the polymer blend are used to determine its homogeneity and overlap. Mixing PCL with miscible amorphous polymer doesn't influence its crystalline structure. If two crystalline polymers have low compatibility, then each polymer would have its individual crystal region in the blend. In this case, XRD showed distinct peaks of individual polymers with different lattice constants. In other cases, if crystalline polymers are

compatible or miscible, they will show enhanced degree of crystallinity of blend than pure polymers. XRD patterns of PCL/PMMA showed miscibility by merging the amorphous hump of PMMA and distinct crystalline peaks of PCL, as shown in Figure 2.8.2. The incorporation of PMMA did not influence crystalline structure of PCL.[108] A similar peak pattern is observed in PCL/TPU blend, where broad diffraction peaks ranging from 18° to 24° are replaced by sharper peaks with addition of PCL[160].

Degree of crystallinity of PCL is increased by addition of silica carbide as observed in wide-angle XRD diffractogram as shown in Figure 2.8.3.[112] Incorporation of citric acid modified zinc oxide (ZnO-CA) nanoparticle reduces the intensity of PCL diffraction peaks due to weak hydrogen bond interaction. This weak interaction restricted the movement of PCL chain to some extent, making it difficult for PCL to crystallize.[141] Seyrek *et al.* have claimed that PCL/MMT composites exhibit diminishing peaks with inclusion of clay, indicating exfoliation of filler in polymeric system due to absence of characteristic peak of MMT around 5.00° with distinct crystal structure of PCL.[142]

There is a limited study available for structural properties of copolymers, blends, and composites of PCL. The change in structural properties of PCL can be easily studied by an XRD diffractogram. Although researchers have prepared copolymers of PCL with amorphous monomers such as acrylates, acetates, and semicrystalline monomers such as PDL, p-dioxanone, HCA and cellulose, their structural properties have not been evaluated. XRD is method to evaluate compatibility in blends along with thermal properties. XRD will provide better insight of PCL blends with pine resin, PGA, lignosulphonate and PHBA for their compatibility and structural stability. XRD, along with TEM, is a renowned method to analyse dispersion of filler in composites. To attain a better understanding of PCL composites with natural waste by-products, minerals, carbon fillers need to analyse for structural properties as well.

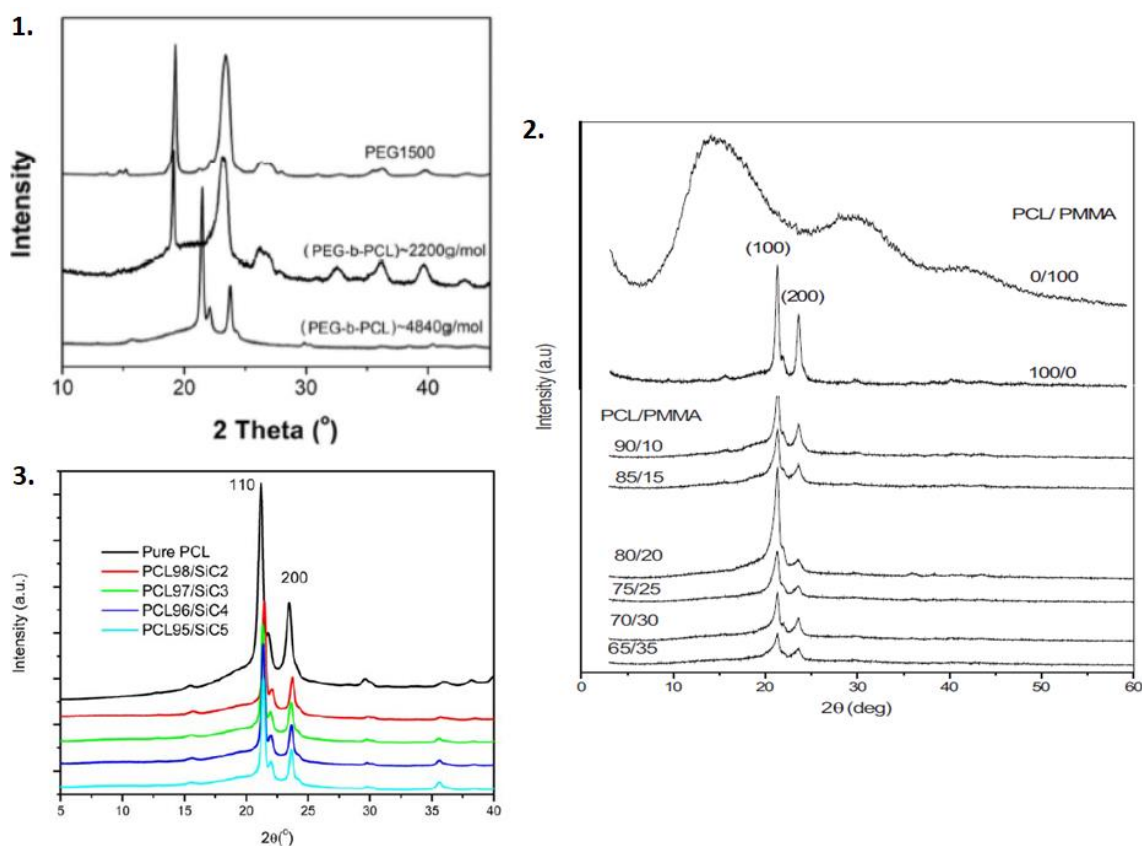


Figure 2.8. Structural analysis by XRD of PEG-PCL copolymer (1) reproduced with permission [115] 2015, RSC; PCL/PMMA blend (2) reproduced with permission [61] 2016, Elsevier; PCL/SiC nanocomposite (3) reproduced with permission [66], 2015, Wiley.

2.3.5 Rheological properties

Rheological studies give an idea about processing parameters, mechanical and thermal behaviour, and degradation conditions. Rheological properties of polycaprolactone are completely dependent on molecular weight, molecular weight distribution, molecular structure (linear/cyclic/star/branched)[15, 17, 18]. Pure PCL shows Newtonian behaviour at lower frequency (less than 10Hz) and shear thinning at higher frequency range (above 10 Hz). A very beautiful analysis of stress relaxation behaviour on different molecular weight based films and scaffolds of PCL was carried out by Sethuraman *et al.*[161]. The higher molecular weight samples exhibit higher elasticity than lower ones. Films showed higher stress relaxation than scaffolds. The viscoelastic properties of scaffolds depend on pore size,

structure and type of processing used. Copolymers of PCL and HPMA showed Newtonian behaviour with complex viscosity of 130-140 Pa.s at 160°C.[83] Copolymer of PCL and EVA showed intermediate values of complex viscosity with respect to their neat counterparts.[83] Aqueous solution of PCL- co-*N*-2-Hydroxypropyl methacrylamide showed shear thinning behaviour as studied by Rani *et al.*[73] Melt rheology of PCL-r-PLLA copolymer showed zero shear viscosity and relaxation time in between the neat polymers.[75] The blends of PCL with M_n 84000 g/mol with PLA of different molecular weights ranging from 55350, 92500, and 106,900 g/mol showed interesting results for rheology. In the high molecular weight PLA (106900 g/mol) system, storage modulus (G') and loss modulus (G'') decreased with higher PCL content, as PCL is a less viscous component. In contrast, for the low molecular weight PLA (55350) system, it is noticed that G' and G'' of blends increased with an increase of PCL phase.[23]

The sandwich composite of gelatine film with PCL matrix shows higher storage modulus as compared with pure PCL throughout investigated temperature range. This is primarily attributed to an increase in stiffness of the matrix due to their enforcing effect imparted by PCL-gelatine films composite that permitted a higher degree of stress transfer from the matrix to the gelatine.[131] The sandwich structure of PCL and cellulose nanofiber showed that storage modulus is increased throughout all temperatures between -110 and 55°C in respect of pristine PCL, compensating for decrease in storage moduli at glass transition temperature and melting temperature in respect of PCL.[130]

The PCL/HNT nanocomposites are studied for melt rheological behaviour to get an idea of microstructure in the melted state and its behaviour at the processing time.[114] The storage modulus and loss modulus values of nanocomposites showed an increment when compared with neat PCL due to the homogeneous dispersion of HNT and good interphase attraction between PCL matrix and HNT. Viscoelastic properties of hydroxyapatite micro and

nanoparticle-based PCL composite are examined at dry and wet conditions at 37°C. The stiffness of materials is increased under a dynamic load with HA concentration.[111] Melt rheology of nanocomposites with graphene[28, 31], nanoclays[28] is suggested that with increase in size and percentage of filler, viscosity increases until size of nanofiller (graphene) is less than radius of gyration of PCL molecule. Detailed analysis of PCL/cellulose nanocrystal is carried out by Wang *et al.* for linear rheology, non-linear rheology, creep behaviour and transient rheology. Here particle-particle interaction of cellulose nanocrystals in PCL matrix affects the viscosity, creep behaviour and network formation.[30]

The processing parameters are perceived by flow properties like flow curve and complex viscosity. Detailed rheological analysis such as linear viscoelastic region, frequency sweep, creep recovery, structure recovery, stress relaxation, time-temperature superposition is a tool to understand behaviour of materials during application and utilization. There are very few and limited studies available for rheological properties. A huge gap needs to fill by study of detailed rheological properties of all PCL copolymers, blends and composites which are synthesized.

2.3.6 Shape memory properties

Shape memory polymers (SMP) have ability to memorize a permanent shape and fixed to temporary shape under specific triggers. These triggers include temperature, pH, electric and magnetic field, and light. Thermoresponsive shape memory polymers (TSMP) exhibit changes in shape from a deformed position to their original shape induced by temperature. TSMP changes into another shape or temporary shape when heated above transition temperature, deformed under load and cooling conditions. The polymer maintains this temporary shape until it is heated again without any load and regains its original shape. Strain fixity rate describes the ability to switch segments to fix/hold the temporary mechanical deformation.

$$R_f(N) = \frac{\varepsilon_u(N)}{\varepsilon_m} \quad \dots \text{eq.1.}$$

The strain recovery rate describes the ability of the shape memory material to recover its permanent shape.

$$R_r(N) = \frac{\varepsilon_m - \varepsilon_p(N)}{\varepsilon_m - \varepsilon_p(N-1)} \quad \dots \text{eq.2.}$$

Where N is cycle number, $\varepsilon_u(N)$ is strain in the stress-free state after the withdrawal of tensile stress in the Nth cycle, ε_m is the maximum strain executed on the polymer and $\varepsilon_p(N)$ and $\varepsilon_p(N-1)$ are the strains of the sample in two successive cycles in the stress -free state before yield stress is applied.

The semi-crystalline nature of PCL makes it a promising candidate for thermoresponsive shape memory applications. Along with crystallinity, the crosslinking network in PCL helps to store elastic energy and provides driving force to recover shape when heated above crystalline melting temperature (T_{cm}). The shape fixing ability of shape memory polycaprolactone is found to be influenced by the PCL-diol molecular weight. At the same time, the R_r reaches 99% when heated above melting point irrespective of the length of PCL diol[162]. It is due to the stored energy in crystalline region, which is released faster than stimulated in their T_{cm} range and allows the chains to recover their original shape with less time.

Shape fixity and shape recovery properties of copolymers, blends and composites are listed in Table 2.5. The shape memory behaviour of PCL is tailored by copolymerizing it with L-lactides[163] butyl acrylates[80], PDMS[12, 13], cellulose and its derivatives[156, 164, 165]. PCL-PDMS-PCL[12] and PCL-BA[80] copolymers showed increased shape fixity with an increased chain length of PCL. Copolymers composed of PCL with a molecular weight of 3000 g/mol or lower are exhibited no transition temperature, no crystallinity and act as amorphous phase. In this case, T_g and crosslinking of copolymer help in shape recovery and shape fixity[13, 156, 165]. A 4D printed drug-loaded vascular stent prepared by grafting PCL

on β -cyclodextrin showed good shape memory properties, which made it self-expandable[166].

The blends of PCL for change in thermoresponsive behaviour include thermoplastic polyurethanes[160], diglycidyl ether of bisphenol A (DGEBA)[167], polyvinyl chloride[168], olefin block copolymers[169], polymethylvinylsiloxane, and natural rubber[170]. The shape memory properties of blends depend on PCL content, its crystallinity and compatibility. The strain recovery ratios of the natural rubber (NR)/PCL blends are high, nearly 100% regardless of PCL content, due to stress release after sample moulding, though shape fixity increased with increased PCL content.[170] DGEBA/PCL blend showed a different pattern. Shape fixity decreases with increase in PCL content with each consecutive cycle.[167] In PCL/Thermoplastic Poly Urethane (TPU) blend high recovery ratio with increase in TPU content is observed. TPU domain stored the deformation energy and contributed to the strain recovery, while the ductile and crystalline PCL contributed to the strain fixing.[160] A physically crosslinked olefin block copolymer (OBC)/PCL blend compatibilized with dicumyl oxide showed two distinct peaks of T_m ($\sim 55^\circ\text{C}$ and $\sim 120^\circ\text{C}$) and T_c ($\sim 27^\circ\text{C}$ and $\sim 96^\circ\text{C}$). The blend showed good shape memory properties at 65°C .[169]

Shape memory properties of the composite of PCL studied for hydroxyapatite,[171] titanium nitride,[172] nanocrystalline cellulose,[173] calcium carbonate,[163] MWCNT[174] and Polyhedral Oligomeric Silsesquioxane (POSS) [175]. A common observation is obtained from strain fixity and strain recovery values of composites that they are independent of filler content and dependent on PCL chain length. Qu *et al.* coated MWCNT over PCL/TPU wet spun fibre. The composite fibres showed a self-healable thermo-electrical double response shape memory effect.[176]

The copolymers or blends with sharp transition temperature (T_{trans}) peaks are desirable for good shape memory properties. Broad T_{trans} peak affects the SMP properties negatively, as

seen in case of cellulose-g-PCL, which showed inferior strain fixity and strain recovery.[156]

The structural and thermal properties are altered while copolymerization, blending or composite preparation of PCL. This further affects the transition temperature and crystallinity of the material, accordingly shape memory properties and its testing parameters vary.

Table 2.5. Shape memory properties of copolymers, blends, composites of PCL

S.no.	Polymers	Synthesis mode	Composition	Shape fixity	Shape recovery	Ref
1	PCL-PDMS-PCL	Triblock copolymer	PCL ₅₀ -PDMS ₃₇ -PCL ₅₀	99.7	98.3	[12, 13]
2	PCL-PDMS-PCL	Triblock copolymer	PCL ₄₀ -PDMS ₂₀ -PCL ₄₀	99.9	98.6	[12, 13]
3	EC-PCL	Graft copolymer	EC M70-PCL1400 mixed with EC M70-PCL 7600	97.3	94.8	[13, 156, 165]
4	MC-PCL	Graft copolymer	MC30K - PCL3K	91.8	92.6	[13, 156, 165]
5	<i>n</i> BA-PCL	Block Copolymer	PCL-BA (75:25)	77.0	-	[80]
6	PCL / OBC	Melt blend	40/60/ 1 phr DCP	89.0	99.8	[169]
7	PCL/NR	Melt blend	50/50/ 0.5 phr	98.9	100.0	[170]
8	PCL/TPU	Melt blend	75/25	90.0	100.0	[160]
9	PCL / DGEBA	Solution blend	50/50	88.0	99.2	[167]
10	PCL/PVC	Solution blend	30/70	98.0	92.0	[168]
11	PCL/MWCNT	Solution composite	99.4/0.6	-	98.0	[174]
12	PCL/HA	Solution composite	100/5	90.0	90.0	[171]
13	PCL / cellulose	Solution composite	100/3	90.0	93.3	[173]

2.3.7 Biodegradation

Biodegradation of aliphatic polyesters is associated to their physical and chemical properties, e.g. hydrophilicity, molar mass, T_g , T_m , degree of crystallinity, chemical structure and surface area.[83] In biodegradability, degree of crystallinity plays a significant role, as amorphous domains of a polymer are mainly attacked by enzymes. The enzymatic degradation takes

place on surface of the PCL. Hydrophobic nature of PCL makes its hydrolytic degradation very slow.[177] Feng *et al.* have carried out enzymatic depolymerization of polycaprolactone involving two elementary steps: triad assisted nucleophilic attack and C-O bond cleavage.[178] The C-O bond cleavage is considered as the rate determining step of degradation with an average energy barrier of 15 kcal/mol. Almeida *et al.* have studied quantum mechanics and molecular mechanics molecular dynamics (QM/MM MD) for enzymatic hydrolysis of PCL by thermophilic esterase.[179] The degradation of PCL copolymers, blends and composites can be divided into two parts: 1) soil burial and 2) simulated environment.

Soil burial degradation of PCL composites with silicon carbide,[112] clay,[46] gelatin[131] are studied. It is observed that cloisite Na⁺ and cloisite 20A based nanocomposites showed higher weight loss in comparison to pure PCL though incorporation of cloisite 30B slowed down the rate of degradation of the polymer attributing the fact that the presence of reinforcement hindered the access of the microorganisms' attack on ester groups of PCL.[46] Presence of SiC nanoparticles in PCL matrix increases the crystallinity hence biodegradation process becomes slow.[112] PCL/gelatin sandwich composite degrades faster than pure PCL due to high water affinity of gelatin.[131]

Hydrolytic biodegradation of PCL copolymers with *p*-dioxanone,[78] 4-hydroxycinnamic,[74] EVA,[83] aniline,[157] blends with PLLA[102, 180] and composites with bioactive glass,[181] cellulose nano-whiskers[121] are studied. As hydrophilicity is an effective factor in biodegradability, it is observed that CL-co-dioxanone copolymer showed higher mass loss and reduced molecular weight with increase in content of *p*-dioxanone.[78] The crosslinked structure induces hydrophobicity, resulting in a slower degradation rate as seen in poly(ϵ -caprolactone)-co-poly(4-hydroxycinnamic acid).[74] PCL-co-polyaniline nanofibers underwent rapid mass loss of almost 45% in 35 days in phosphate buffer solution (PBS).[157] Degradation rate is much higher in alkaline conditions than normal PBS of pH

7.4, as observed in semi-IPN blends of PCL with PLLA. Increased content of PLLA is responsible for more water uptake and showed more hydrolytic degradation.[102] PCL blend with EVA, a conventional non-biodegradable polymer showed decreased biodegradability.[83] The biodegradation rate of PCL composites with natural filler cellulose whiskers is increased because of higher hydrophilicity of the latter than pure PCL.[121] The PCL/bioactive glass nanocomposite coating on magnesium substrate showed more degradation than pure PCL due to dissolution of bioactive glass in simulated body fluid [181].

In-vivo degradation of P(CL-r-LLA) copolymer is investigated with varying content of LLA. These copolymers are hypodermically implanted in the backs of rats. The degradation of P(CL-r-LLA) is determined as a function of the implantation time and monitored by weight loss, changes in molecular weight and macroscopic observation. The results showed the degradation and absorption of copolymers eliminate the necessity for removal of the materials implanted *in vivo* when used as a drug matrix.[79] Enzymatic degradation of PCL blends with pine resin,[96] epoxidized soyabean oil (ESO)[182] and poly(β -hydroxybutyrate)[100] are studied. The pine resin mainly consists of triglycerides that is easily degraded by lipase. High enzymatic hydrolysis rate of pine resin is enhanced by the overall hydrolysis of blend in the presence of lipase from *porcine pancreatic*. [96] PCL/ESO blends are immersed in the mixture of lipase from *Pseudomonas cepasia* and buffer solution of PBS. Almost 40% weight loss is observed due to degradation of PCL content only and no mass change is observed for ESO in 5 days.

High Ductility and plasticity of PCL with a slow degradation rate help to counterbalance the expeditious degradation of natural polymers.[66] Addition of hydrophilic polymers/fillers via copolymerization or blending increases the degradation rate. The addition of crystalline filler

of semicrystalline polymers increases the overall crystallinity of material and reduces the weight loss during degradation.

2.4 Applications

2.4.1 Biomedical applications

PCL is one of the most preferred and well-explored thermoplastics, which received much attention because of its adaptability, biodegradability with outstanding biocompatibility *in vitro* and *in vivo* for biomedical applications. This includes skin tissue engineering, bone tissue engineering and drug delivery. Scaffolds are integral to their regenerative process, assist adhesion and spreading of cells, support their growth, and successively activate their development in specific tissues.[183] Review articles emphasizing PCL-based scaffolds prepared by electrospinning for tissue engineering, drug delivery and wound dressing materials have been reported recently.[51, 56, 60] Suwantong has discussed about factors affecting electrospinning, such as polymer concentration, molecular weight of polymer, solution conductivity, solvent volatility, applied voltage, flow rate and ambient parameters.[56] The major scaffold fabrication techniques for PCL are summarized by Dwivedi *et al.* including solvent casting, porogen leaching, phase separation, 3D printing and electrospinning for bone scaffolds.[50] Prasad *et al.* have discussed about fused deposition technique used in fabrication of scaffolds for PCL composites using 3D printing.[58] Hajiali *et al.* have focused only on PCL/ calcium phosphate-based ceramic and PCL/ bioactive glasses composites for bone tissue engineering.[57] Chan *et al.* have provided a systematic review about tracheal stents and splints patches to be used in tracheal surgeries.[49] Salehi *et al.* have provided an insight in the use of PCL in corneal tissue engineering.[64] In this review, they discussed PCL-based scaffolds prepared by different techniques to be used in epithelium, stroma and endothelium of cornea. Different techniques used for scaffolds fabrication such as salt leaching,[183] rotary jet spinning,[184] electrospinning,[185] aligned

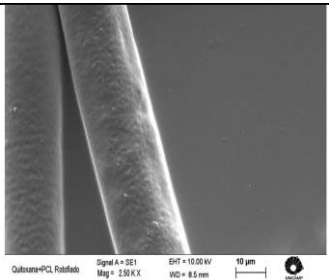
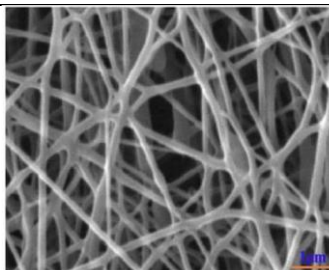
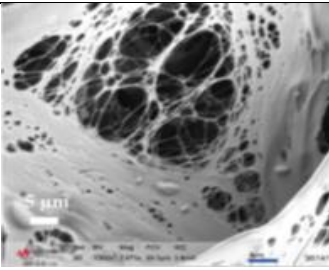
electrospinning,[186] supercritical CO₂ batch foaming,[187] porogen leaching,[188] sol-gel method,[189] 3D printing,[190] controlled humidity,[191] unidirectional freeze drying[192] and hot embossing[193] are presented in Table 2.6.

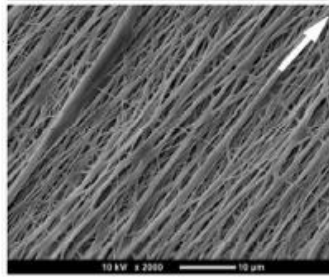

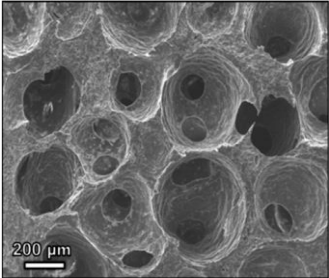
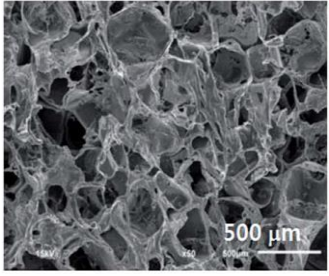
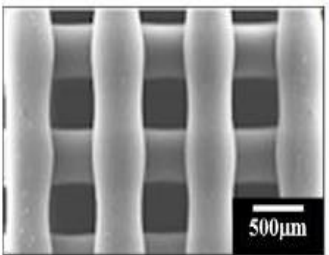
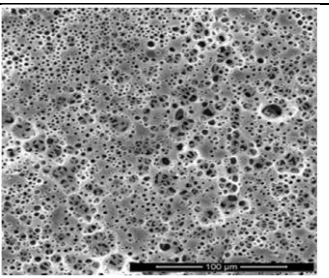
Apart from tissue engineering, drug delivery and wound healing, other bio-medical applications of PCL copolymers, blends and composites are bio-imaging and coatings for bio-implants. Bio-imaging is a useful tool to detect cancer and tumour. Various nanoparticles of PCL copolymers are synthesized to act as a carrier for bio-imaging. PCL-copolyamidoamine linear dendritic block copolymer nanoparticles as a small molecule carrier for Rhodamine B, curcumin and indolizine cyanine dye in NIR imaging and photothermal therapy are synthesized by Chandrasiri *et al.*[194]. Block copolymers of PEG and PCL[195–197] and four-arm PEG-PCL copolymers[198] are synthesized and fabricated with dyes,[195] cyclo(Arg-Gly-Asp),[196] polythiophene[197] and porphyrin[198] for bio-imaging applications. Organic fluorophore synthesized by incorporating di(thiophene-2-yl)-diketopyrrolopyrrole in the middle of polymer chain of PCL by Huang *et al.*[199] A fluorescence backbone, macroinitiator conjugated polymer poly(fluorene-alt-(4,7-bis(hexylthien)-2,1,3- benzothiadiazole)) (PFTB) grafted with PCL, poly oligo(ethylene glycol) methyl ether methacrylate] (POEGMA) blocks[200] and carborane (PmCbA) containing triblock copolymer POEGMA-PmCbA-PCL conjugated with a NIR fluorescence probe[201] are fabricated to be used in bio-imaging for effective treatment of cancer cells.

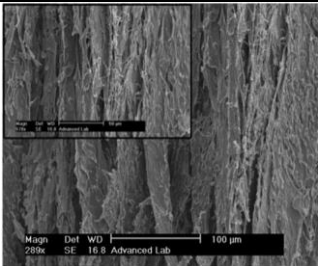
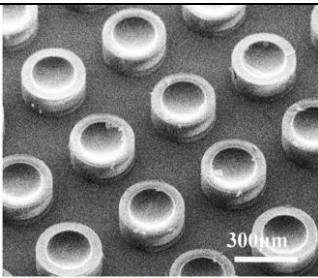
Nowadays nanocomposite coatings based on PCL are preferred to overcome inferior abrasion and wear resistance of bioimplants made-up of metal alloys and stainless steel. PCL/Laponite nanocomposite coating by electrophoretic deposition method showed great improvement in corrosion resistance than uncoated stainless steel and makes it applicable for bone implant[202]. Jokar *et al.*[203] and Shafiee *et al.*[204] have used the dip-coating method to coat stainless steel with PCL/gelatine and PCL/forsterite (Mg₂SiO₄) nanocomposites for

improved bioactivity and corrosion resistance. Titanium alloy coated with PCL nanofibers using electrospinning. Further, it is treated with TiO₂ nanotubes to give cell biocompatibility to orthopaedic and dental implants.[205] PCL/ HA,[206] PCL/bioactive glass[181] nanocomposite coating and PCL coating on MgCO₃ coated Mg[207] by dip-coating showed a decreased rate of degradation and improved bioactivity of Mg and Mg alloys substrate. Electrospinning is also used for coating PCL/zinc oxide[208] and PCL/MgO-Ag[209] nanocomposite on Mg substrate to improve biocompatibility and corrosion resistance. Huang *et al.* have coated Mg alloy with PCL/amino acid to enhance cytocompatibility using electrografting and dip coating method.[210]

Table 2.6. Scaffold types of PCL copolymer, blends, and composites for bio-medical applications.

S. No.	Polymers	Synthesis mode	Fabrication method	Scaffold	Ref
1.	PCL / chitosan	Hybrid membrane, Chitosan coatings over PCL mesh.	Rotary jet spinning		[184]
2.	PCL / Curcumin	Composite	Electrospinning		[185]
3.	PCL / PLA	Blend	Supercritical CO ₂ batch foaming		[187]

4.	PCL-PTHF-PCL	Triblock copolymer	Aligned electro-spinning		[186]
5.	PCL / CNT/ TiO ₂	Composite	Porogen leaching		[188]
6.	PCL / Bioglass	Composite	Sol-gel method		[189]
7.	PCL / Magnetite nanoparticles	Nanocomposite	Salt (NaCl) leaching		[183]
8.	PCL / silanted silica nanoparticles	Nanocomposite	3D printing		[190]
9.	PCL / calcium silicate	Composite	Controlled humidity		[191]

10.	PCL / Zein	Composite	Unidirectional freeze drying		[192]
11.	PCL / Furosemide	Composite	Hot embossing		[193]

2.4.2 Non-biomedical applications

Copolymers, blends, and composites of PCL are entering into non-biomedical applications, which includes packaging, self-healing & corrosion resistance coatings, flame retardant coatings, oil-water separation, plant grafting and photothermal absorption. Figure 2.9 shows different non-medical applications of PCL copolymers, blends, and composites.

2.4.2.1 Packaging

Hydrophobicity of PCL is an advantage in packaging because it reduces water vapor transmission rate, however, it shows weak oxygen barrier properties.[211] This limitation is overcome by inclusion of other polymers or nanoparticles. Blend and copolymers of PCL/PLA improved the oxygen barrier and mechanical properties. Further, addition of zinc oxide, clove oil, cinnamaldehyde and impregnation of supercritical CO₂ enhances antimicrobial properties and makes it suitable for the packaging of button mushroom and scrambled egg[212–214]. Blends of PCL with Polyhydroxybutyrate (PHB),[215] PVC[216] and starch[217, 218] showed improvement in oxygen barrier properties for food packaging. PCL mixed with other material such as pomegranate rind,[219] chitosan/grapefruit seed extract[220], sodium metabisulphate,[221] silver-kaolinite,[222] hydroxytyrosol/cloisite

30b,[215] titanium dioxide nanoparticles[223] and organically modified montmorillonite[142] to form active packaging material. These materials added not only antimicrobial properties but also enhanced mechanical, thermal, and biodegradation properties. Cai *et al.* have developed novel PCL composite films by mixing curcumin loaded zeolitic imidazolate framework, which showed pH and light responsive antibacterial activity.[224] Electrospinning, electrospraying[225] and microfluidic spinning technology (MST) are recent methods to fabricate improved active packaging material. It is found that CS/ OEO/PCL blended electrospun nanofibers have lower water vapor permeability than cast film and exhibit distinctive antibacterial activity toward Gram-positive/Gram-negative bacteria.[226] Mathiazhagan *et al.* have fabricated a food packaging film by soaking PCL nanofibrous mat in leaf extract of *Acalypha indica*[227]. These antibacterial nanofibrous mats show good microbial inhibition as compared to commercial polyethylene for carrot piece packaging. Films composed of fibres of nano-sized functional particles of silver loaded konjac glucomannan (KGM) and PCL blend prepared by MST exhibit excellent antibacterial properties for active packaging material.[228]

2.4.2.2 Self-healing

PCL is a well-known polymer for its shape memory properties which makes it capable of self-healing.[229] Excellent shape memory and self-healing are achieved when linear PCL is incorporated in crosslinked PCL network and forms a simultaneous IPN network. Partial fractures generated in the film can heal up by this IPN network.[230] Blends of natural rubber and PCL are used for the application of shape memory-assisted self-healing properties.[231] A high-performance and self-healable PCL/polydopamine nanocomposites are fabricated. The photothermal conversion nature of polydopamine provides self-healing functionality to the nanocomposite. On exposure to near-infrared (NIR) light, the temperature of nanocomposites swiftly goes above the polymer T_{cm} . This allows rapid NIR light-induced

self-healing properties.[128] The nanocomposites comprised of PCL/polydopamine-capped reduced graphene oxide nanofiller[128] and TPU/PCL blend with multi-walled carbon nanotubes (MWCNTs) exhibit excellent self-healing properties in the presence of near-infrared (NIR) irradiation compared with the traditional heat-induced self-healing shape memory composites. NIR irradiation not only reduces the healing time (3 min.) but also selectively repairs the exposed damaged regions without distinct interference to the performance of surrounding parts.[232]

2.4.2.3 Coatings

A self-healing UV curable corrosion-resistant coating is prepared by acrylated polycaprolactone polyurethane, where soft segment is comprised of PCL and the hard segment is comprised of isobornyl acrylate (IBOA). Partial self-healing, corrosion protection and barrier properties are achieved at the melting temperature of PCL (at 60°C) and complete healing is observed at the T_g of IBOA (115°C).[233] Microsphere of PCL and 8-hydroxyquinoline corrosion inhibitor are added to the epoxy matrix to improve self-healing and corrosion resistance.[234] Ranjitha *et al.* have studied PCL/functionalized graphene oxide (FGO) nanocomposite coating and found superior barrier and anti-corrosion properties by improving the dispersion and exfoliation of FGO in the PCL matrix.[235]

An elastomeric coating of hyperbranched-PCL/siloxane is applied on stainless steel panels and showed good antifouling property. The PCL segment inhibits marine biofouling and siloxane provides fouling release property due to good surface elasticity and low surface energy.[236] Low gloss organic montmorillonite/waterborne polyurethane nanocomposite (OWPU) coatings with polycaprolactone (PCL) and hydroxyl-terminated polybutadiene (HTPB) are prepared by Ding *et al.* and applied to polyvinyl chloride leather. Nanosheets of MMT have increased thermal stability of hard segments and soft segments derived from PCL and promoted cross-linking. Further, cyclization of HTPB at high temperature imparted flame

retardant and anti-dripping properties to OWPU coatings [237]. For coating application Arya *et al.* have studied the effects of solvents, methyl chloride and toluene on the basis of morphological properties, drying properties and cost of system[238]. They have reported that methyl chloride provides a smooth, dense and cheaper coating system in comparison to toluene. In case of PCL, methyl chloride and toluene are the most used solvents. So here, a detailed analysis made remarkable addition for the recommendation of solvent.

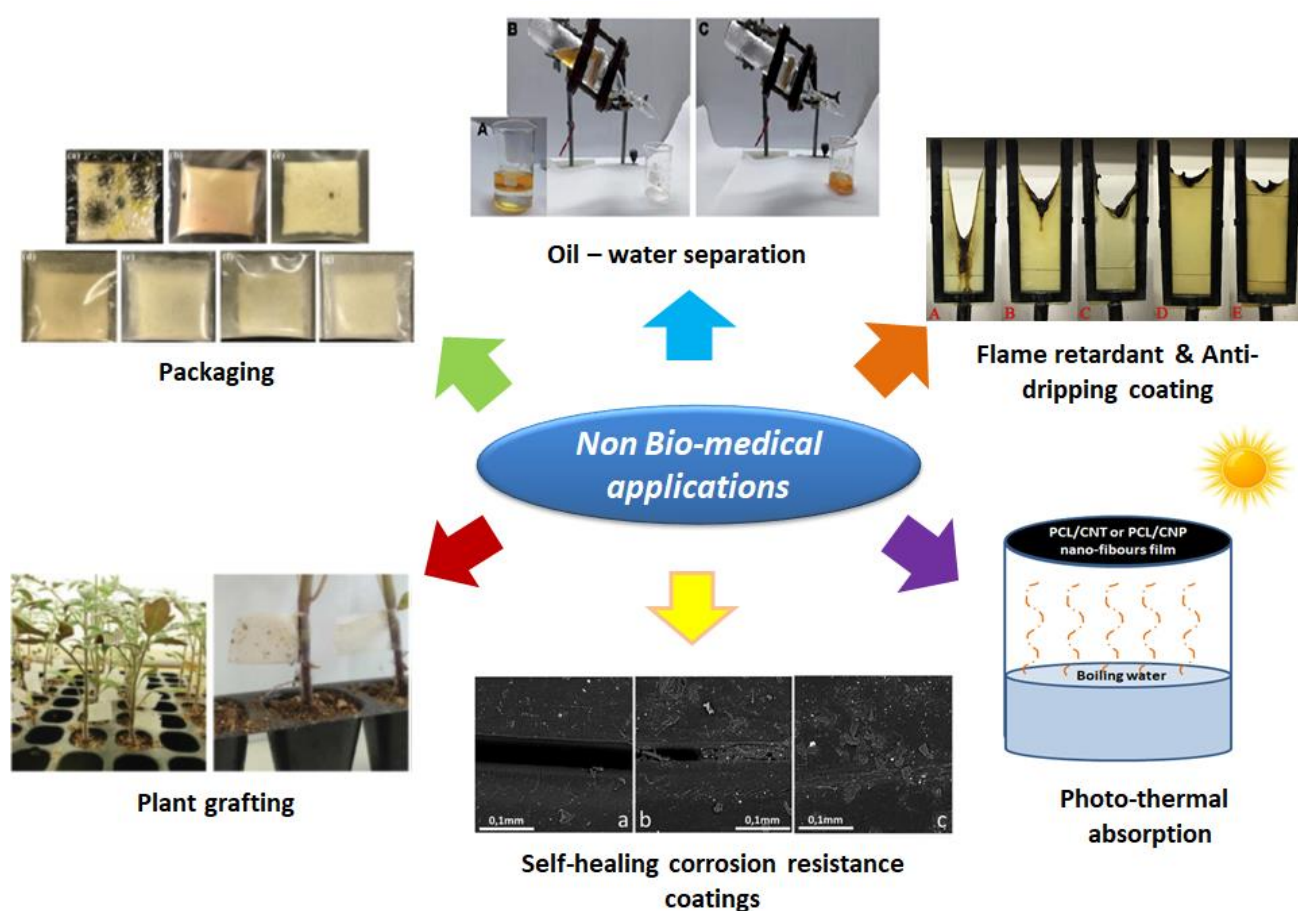


Figure 2.9. Non-biomedical applications include packaging reproduced with permission [185] 2020, Elsevier; self-healing coatings corrosion resistance coatings reproduced with permission [198] 2018, ACS; flame retardant coatings reproduced with permission [201] 2019, Elsevier; oil-water separation reproduced with permission [204] 2016, RSC; plant grafting reproduced with permission [207] 2017, TnF; photo-thermal absorption reproduced with permission [208] 2021, ACS of PCL copolymers, blends and composites.

2.4.2.4 Purification

For purification/filtration of water, PCL becomes a favourite polymer due to environmental concerns. A thiol-ended polycaprolactone is synthesized by Korpinar *et al.* to remove lead Pb(II) and cadmium Cd(II) ions.[239] Reshmi *et al.* fabricated a superhydrophobic, superoleophilic electrospun nanofibrous membrane of PCL/beeswax blend to separate oil from polluted water with great separation efficiency and good recyclability.[240] In another approach, Zhang, He and coworkers have developed composites based on superhydrophobic and superoleophilic membrane with a hierarchical microsphere structure by alternate electrospinning and electrospraying technology. This PCL/SiO₂ composite membrane showed superhydrophobicity, extreme oil-water separation efficiency (>99.8%), oil flux, stability and excellent oil adsorption performance.[241, 242]

2.4.2.5 Plant grafting

Eksiler *et al.* have developed films made of PCL/cis-1,4-polyisoprene blend as a biodegradable joining tool for plant grafting on fresh tomato plants. Soybean lecithin and acrylated-epoxidized soybean oil are used as a non-reactive compatibilizer due to poor compatibility of PCL/PI blend. These compatibilizers also accelerated the weight loss of the films in soil and increased the microorganism growth on the film. It is observed that all the spliced plants are grown without any defect at the end of two weeks.[243]

2.4.2.6 Photothermal absorption

Chen *et al.* have fabricated PCL nanofiber composite thin films with carbon nanotubes and carbon nanoparticles to use it as photothermal absorbers. From neat PCL nanofiber thin films to composite thin films, the solar absorbance is recorded from 0.04 to 0.94 along with its good salt rejection properties while working in high salinity conditions.[244]

2.5 Commercial products

PCL is manufactured mainly by BASF, Perstrop, Daicel, Haihang, Foster and Innovate chemicals with brand names Capromer, CAPA, PLACCEL, Polycaprolactone and INV, respectively with various molecular weight and functionality. Biogeneral and Durect provide PCL-co-PDLL copolymer with different monomer compositions. These products have suggested areas of application for dental adhesive, control release drug carrier, cell and tissue culture, surgical sutures, orthopaedic splint, radiation board, resin bandage, plastic modifier & plasticizer, textiles and leather coating and ink. They are available in the form of powder, films, fibres and tubes. Table 2.7 summarizes some of the commercial products based on PCL. The commercial PCL-co-PEG copolymers are reported by Dabbaghi *et al.*[62]

Table 2.7 Commercial products based on polycaprolactone

S. No.	Manufacturer	Polymer	Product name	Application
1.	BASF, Germany	PCL	Capromer PD1-10 Capromer PD1-20 Capromer PD1-20A Capromer PD4-05 Capromer PT1-05	Textile and leather coatings.
2.	Perstorp, Sweden	PCL / PCL copolymers	CAPA 1301 CAPA 2043-2803 CAPA 2077A- 2403D CAPA 3022- 3301 CAPA 4101- 4801 CAPA 6100-6800 CAPA 7201A-7203	Coating, adhesive, foam, orthopaedic splints, dental impressions, oncology immobilization, food packaging, laminates, colour master batch
3.	Daicel Corporation, Tokyo, Japan	PCL	PLACCEL 200 series PLACCEL 300 series PLACCEL 400 series	Resins

			PLACCEL CD series PLACCEL F series PLACCEL H1P	
4.	Haihang Industry co. Ltd, Jinan City, China	PCL	Polycaprolactone	Controlled release drug carrier, cell and tissue culture medium, fully degradable plastic surgical suture line, High strength film filamentous moulding, plastics modifier and plasticizer, medical modelling materials, industrial, art modelling materials, toys, organic colorants, thermal carbon ink adhesives, hot melt adhesive
5.	Biogeneral, San Diego, USA	PCL/PCL-co-PDLL	PLC 70	
6.	Durect, Birmingham, USA	PCL-co-PDLL		Fiber, films and tubing
7.	Foster, Putnam USA	PCL	Polymedex	drug delivery, orthopaedic, dental, and maxillofacial applications
8.	Innovate Chemicals, Guangdong, China	PCL	INV PCL 6500 INV PCL 6800	Surgical sutures, orthopaedic splints radiation board, resin bandage, dental model, Hot melt adhesive, coating, ink, non-woven adhesive, shoes material, structural adhesive, blown films, laminated material, manual models, organic colorants, powder coating

2.6 Conclusion

PCL polyester is easily available and relatively inexpensive. It can be modified to adjust its chemical and biological properties, physiochemical state, degradability, and mechanical properties by copolymerization, blending and composite formation. The synthesis methods of

PCL copolymers, blends and composites are discussed in this review of literature. PCL copolymers with natural polymers except cellulose are not reported yet. Blends prepared by latex mixing and composites with filler like copper and silver are not visible in the literature. PCL based materials are profoundly characterized for thermal, mechanical, structural, and biodegradable properties. Though mechanical and thermal properties are studied in length, however, less attention has been paid to crystallization kinetics/behavior and structural properties. The detailed analysis of rheological behavior of PCL copolymers, blends and composites is also required consideration by researchers. The shape memory properties of PCL make it a promising material for robotics and anti-counterfeit application, which can further investigate for copolymers, blends and composites. The data analyzed and discussed in this review about fabrication and properties allowed us to conclude that PCL copolymers, blends, and composites collectively provide an encouraging polymer platform to produce different materials.

Numerous researches available on applications have shown that PCL widens its horizon from biomedical to packaging, self-healing, coatings, separation membrane and plant grafting, still need to investigate more. Scientists try to develop films for photothermal absorption though their sorbent capacity is quite lower than previously reported adsorbents. Quite a good number of PCL copolymers and blends and composites are synthesized for various applications still, these are not commercialized much. Very few commercial products are reported for PCL homopolymers and copolymers, though commercialization of these extensively researched copolymers, blends and composites is desirable.

Chapter 3

Materials and Methodology

Overview

The information related to experimental techniques, synthesis of PCL-PDMS-PCL triblock copolymer films, methodology and tools which had been utilised to achieve the objectives are mentioned in this chapter. This chapter includes a description of the source of materials used during the study along with a brief outline of the adopted methodology, scheme of experiment done and details of the parameters of several characterization techniques employed to fulfil the research objectives.

3.1 Materials

ϵ -Caprolactone, Poly dimethyl siloxane bis (3-amino) terminated ($\text{NH}_2\text{-PDMS}_{30}\text{-NH}_2$; $M_n=2500$ g/mol), Stannous (II) ethyl hexanoate are obtained from Sigma Aldrich. Acryloyl chloride is procured from Alfa Aesar. Triethyl amine, 1-Vinyl-2-pyrrolidone (NVP) and Dimethoxy-2-phenylacetophenone (DMAP) is supplied by Avra. Reagent grade sodium carbonate, anhydrous sodium sulphate from CDH, Chloroform from Thermo Scientific, Ethanol from CSC, dry Dichloromethane and Methanol from Merck are purchased.

3.2 Methods

3.2.1 Synthesis of PCL-PDMS-PCL triblock photocrosslinked copolymer

The PCL-PDMS-PCL triblock polymers are synthesized in three steps to obtain photocrosslinked polymeric films. Ring opening polymerization of ϵ -caprolactone in the presence of bis-(3-aminopropyl) terminated poly dimethyl siloxane ($\text{NH}_2\text{-PDMS}_{30}\text{-NH}_2$) and tin catalyst yields the diol macromer. The proportion of ϵ -caprolactone to PDMS determines the length of PCL segments. $\text{AcO-PCL}_n\text{-PDMS}_{30}\text{-PCL}_n$ ($n=5,10,20,30,40$) is obtained by reacting the terminal hydroxyl group with acryloyl chloride. Under UV illuminance a flexible

film is obtained. As per PCL chain length the samples nomenclature is given as PCL, 40-40, 30-30, 20-20, 10-10 and 5-5 for PCL homopolymer, PCL₄₀-PDMS₃₀-PCL₄₀, PCL₃₀-PDMS₃₀-PCL₃₀, PCL₂₀-PDMS₃₀-PCL₂₀, PCL₁₀-PDMS₃₀-PCL₁₀, and PCL₅-PDMS₃₀-PCL₅ respectively. A pictorial representation of these three steps is shown in Figure 3.1, 3.2 and 3.3. The reaction scheme involved in synthesis and fabrication of PCL homopolymer and PCL-PDMS-PCL triblock copolymer film is shown in scheme 3.1 and 3.2, respectively.

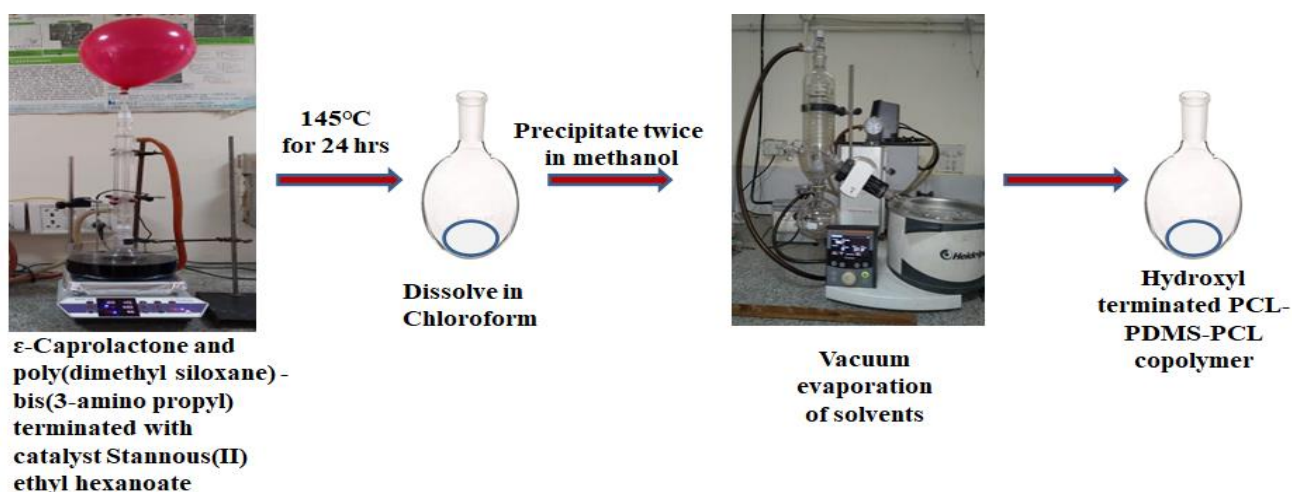


Figure 3.1. Preparation of hydroxyl terminated macromer

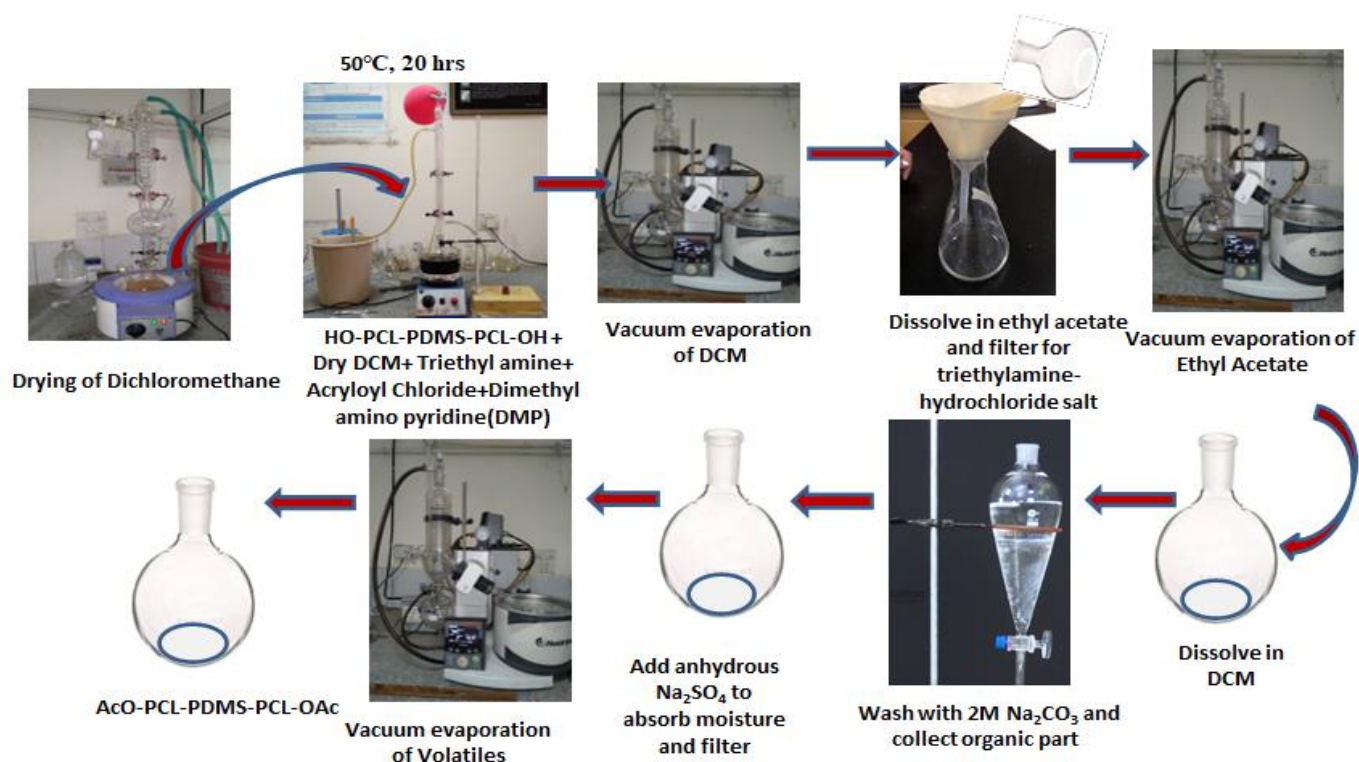


Figure 3.2. Preparation of acrylic terminated PCL-PDMS macromer

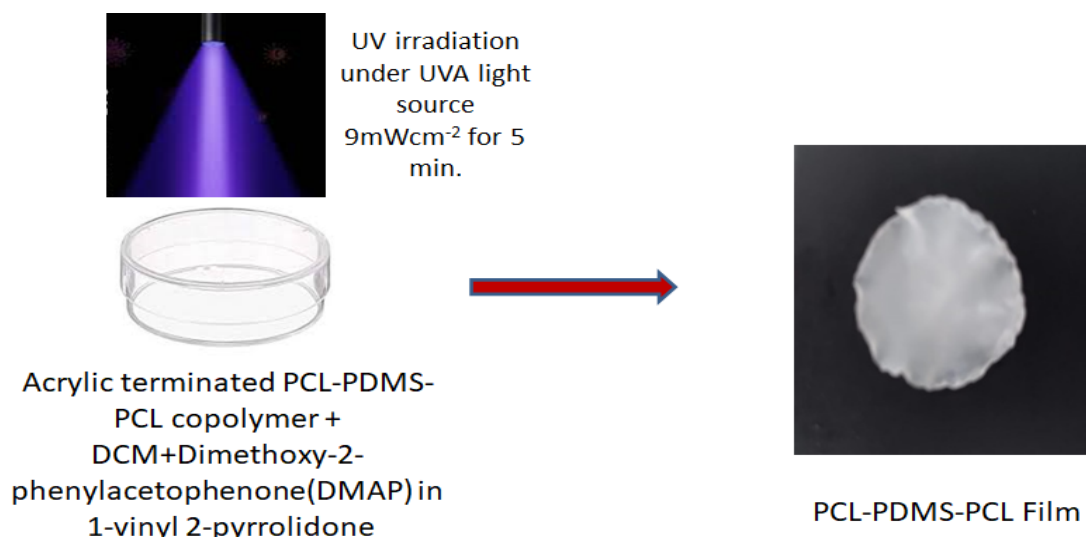


Figure 3.3. UV curing of acrylic terminated macromer

3.2.1.1 Synthesis of Hydroxyl group terminated PCL_{40} -PDMS₃₀- PCL_{40} macromer

NH_2 -PDMS₃₀- NH_2 (4.00 gm, 1.6 mmol), ϵ -caprolactone (14.61 gm, 128mmol) and stannous octoate (0.016 gm, 0.039mmol) are poured into a 250 ml round bottom flask with magnetic Teflon bead. The reaction is carried out for 24 hrs. at 145°C in nitrogen atmosphere and cool down to room temperature. The crude product is dissolved in least required amount of chloroform and precipitated in an excess of methanol. A rotatory evaporator is used to dry the separated product. A solid wax type material is obtained.

3.2.1.2 Synthesis of Hydroxyl group terminated PCL_{30} -PDMS₃₀- PCL_{30} macromer

NH_2 -PDMS₃₀- NH_2 (4.00 gm, 1.6 mmol), ϵ -caprolactone (10.96 gm, 96 mmol) and stannous octoate (0.016 gm, 0.039mmol) are reacted as above. A solid wax type material is obtained.

3.2.1.3 Synthesis of Hydroxyl group terminated PCL_{20} -PDMS₃₀- PCL_{20} macromer

NH_2 -PDMS₃₀- NH_2 (4.00 gm, 1.6 mmol), ϵ -caprolactone (7.30gm, 64mmol) and stannous octoate (0.016 gm, 0.039mmol) are reacted as above. A soft-solid type material is obtained.

3.2.1.4 Synthesis of Hydroxyl group terminated PCL_{10} -PDMS₃₀- PCL_{10} macromer

NH_2 -PDMS₃₀- NH_2 (4.00 gm, 1.6 mmol), ϵ -caprolactone (3.60 gm, 32 mmol) and stannous octoate (0.016 gm, 0.039mmol) are reacted as above. A semi-solid type material is obtained.

3.2.1.5 Synthesis of Hydroxyl group terminated PCL₅-PDMS₃₀-PCL₅ macromer

NH₂-PDMS₃₀-NH₂(4.00 gm, 1.6 mmol), ε-caprolactone (1.82 gm, 16 mmol) and stannous octoate (0.016 gm, 0.039mmol) are reacted as above. A semi-solid type material is obtained.

3.2.1.5 Synthesis of PCL diol macromer

ε-caprolactone (19.00gm, 166mmol), Ethylene glycol (126mg, 2mmol) and stannous octoate (0.042 gm, 0.039mmol) are reacted as above. A solid white material is obtained.

3.2.1.6 Synthesis of acrylic terminated PCL₄₀-PDMS₃₀-PCL₄₀ macromer

Hydroxyl terminated PCL₄₀-PDMS₃₀-PCL₄₀ macromer (6.20 gm, 0.54 mmol) and 4-(dimethyl amino)-pyridine (DMP)(0.0023 gm, 0.019 mmol) are dissolved in 140ml of anhydrous dichloromethane under nitrogen purge at room temperature. Acryloyl chloride (0.24 gm, 2.60 mmol), and triethyl amine (0.11 gm, 1.09 mmol) and is added dropwise under constant magnetic stirring when RB is sealed with rubber septum and nitrogen atmosphere was maintained. Mixing is carried out for 30 min. at RT. Then RB is transferred to condenser with nitrogen atmosphere setup and reaction is carried out at 50°C for 20 hrs. The solvent is removed by rotatory evaporator. Obtained product is dissolved into ethyl acetate. This solution filtered to remove triethylamine hydrochloride salt. Ethyl acetate withdrawn using rotary evaporator under low pressure. The isolated product dissolved in DCM and washed with 2M Na₂CO₃. This mixture placed in separating funnel to form layers. The organic layer is isolated, dried with anhydrous Na₂SO₄, filtered and compound is extracted by removing solvents in rotatory evaporator. A solid yellowish waxy type material obtained.

3.2.1.7 Synthesis of acrylic terminated PCL₃₀-PDMS₃₀-PCL₃₀ macromer

Hydroxyl terminated PCL₃₀-PDMS₃₀-PCL₃₀ macromer (7.0 gm, 0.75 mmol) and 4-(dimethyl amino)-pyridine (DMP)(0.0023 gm, 0.019 mmol) are dissolved in 140ml of anhydrous dichloromethane under nitrogen purge at room temperature. Acryloyl chloride (0.15 gm, 1.6

mmol), and triethyl amine (0.28 gm, 3.00 mmol) are reacted as above. A solid yellowish waxy type material obtained.

3.2.1.8 Synthesis of acrylic terminated PCL₂₀-PDMS₃₀-PCL₂₀ macromer

Hydroxyl terminated PCL₂₀-PDMS₃₀-PCL₂₀ macromer (5.5 gm, 0.778 mmol) and 4 – (dimethyl amino)-pyridine (DMP)(0.0023 gm, 0.019 mmol) are dissolved in 140ml of anhydrous dichloromethane under nitrogen purge at room temperature. Acryloyl chloride (0.281 gm, 3.11 mmol), and triethyl amine (0.157gm, 1.56 mmol) and reacted as above. A soft-solid yellowish waxy type material obtained.

3.2.1.9 Synthesis of acrylic terminated PCL₁₀-PDMS₃₀-PCL₁₀ macromer

Hydroxyl terminated PCL₁₀-PDMS₃₀-PCL₁₀ macromer (7.1 gm, 1.48 mmol) and 4 – (dimethyl amino)-pyridine (DMP) (0.0023 gm, 0.019 mmol) are dissolved in 140ml of anhydrous dichloromethane under nitrogen purge at room temperature. Acryloyl chloride (0.81 gm, 8.91 mmol), and triethyl amine (0.30gm, 2.97 mmol) are reacted as above. A semi-solid yellowish waxy type material obtained.

3.2.1.10 Synthesis of acrylic terminated PCL₅-PDMS₃₀-PCL₅ macromer

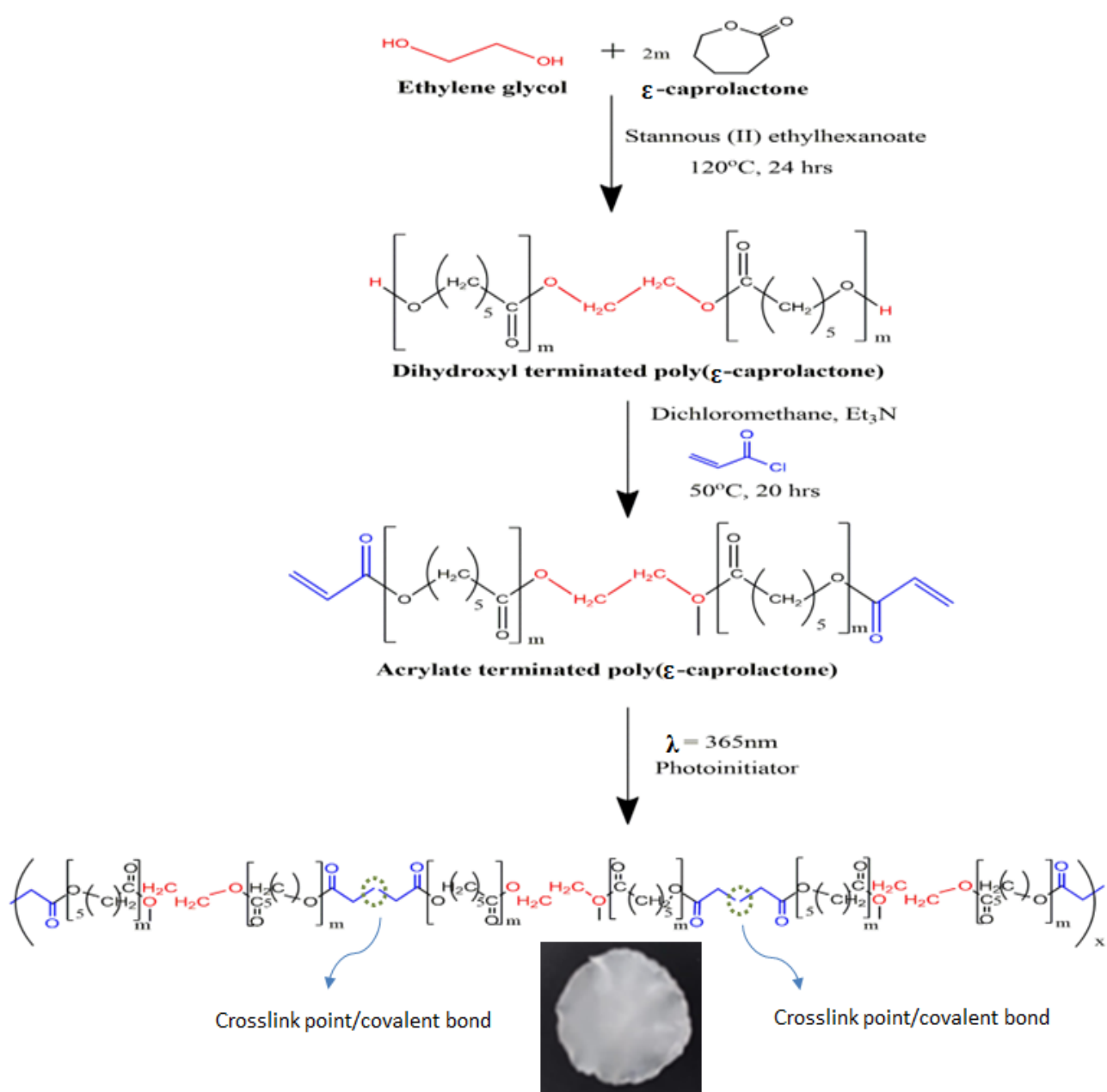
Hydroxyl terminated PCL₅-PDMS₃₀-PCL₅ macromer (5.8 gm, 1.60 mmol) and 4– (dimethyl amino)-pyridine (DMP) (0.0023 gm, 0.019 mmol) are dissolved in 140ml of anhydrous dichloromethane under nitrogen purge at room temperature. Acryloyl chloride (0.60 gm, 6.4 mmol), and triethyl amine (0.32 gm, 3.2 mmol) are reacted as above. A semi-solid yellowish waxy type material obtained.

3.2.1.11 Synthesis of acrylic terminated PCL macromer

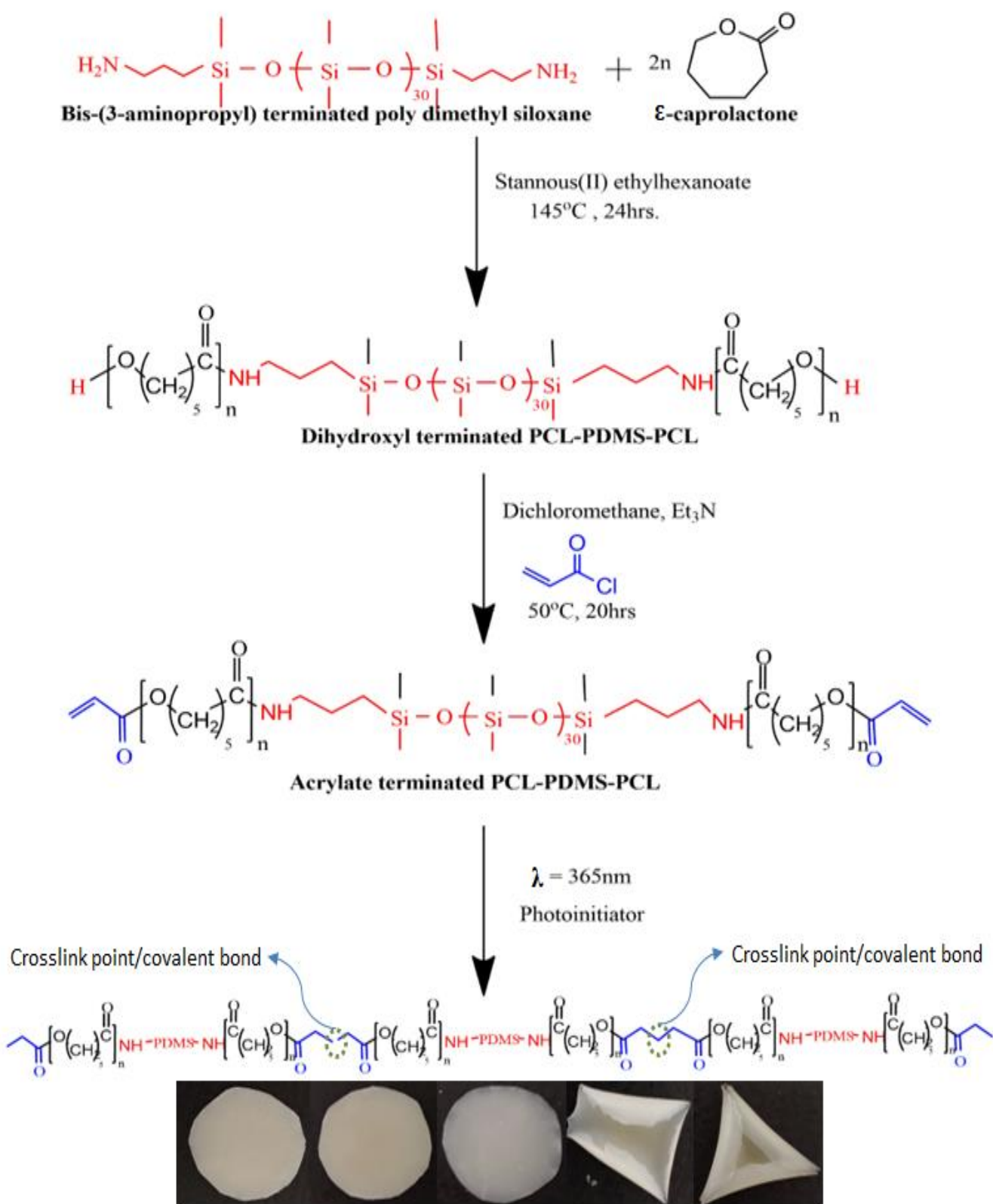
Hydroxyl terminated PCL macromer (19.00 gm, 2mmol) and 4 – (dimethyl amino)-pyridine (DMP)(0.0023 gm, 0.019 mmol) are dissolved in 140ml of anhydrous dichloromethane under nitrogen purge at room temperature. Acryloyl chloride (8.5 gm, 8 mmol), and triethyl amine (0.51gm, 5 mmol) are reacted as above. A solid white waxy type material obtained.

3.2.1.12 Photo-crosslinking of macromers

For crosslinked structure, the acrylated macromers are dissolved in dichloromethane at 25 wt.%. 150 μ L of photocatalyst solution was added to each 1 ml of the prepared macromer solution. The photocatalyst solution prepared by adding 10 wt.% of DMAP in NVP. The mixed solution is added in macromer solution, poured in petri dish with cover and exposed to UV light of intensity 9mW/cm² wavelength 365nm for 4 min. Step-by-step reactions involved in preparation of photo-crosslinked films are shown in Schemes 3.1 and 3.2.



Scheme 3.1. Schematic representation of chemical reaction involved in PCL film preparation



Scheme 3.2. Schematic representation of chemical reaction involved in PCL-PDMS-PCL film preparation

3.2.2 Fourier Transform Infrared (FTIR) Spectroscopy

For the functional group or structural analysis, pure PCL and PCL-PDMS-PCL triblock polymeric films are analysed by ATR- FTIR spectrophotometer (Perkin Elemer) using transmittance mode in the spectral range of 4000 to 500 cm^{-1} in ambient condition. The instrument is shown as Figure 3.4.



Figure 3.4. Fourier Transform Infrared (FTIR) Spectrophotometer (Perkin Elemer)

3.2.3 Nuclear Magnetic resonance (NMR) Spectroscopy

^1H NMR spectrum of the diol and acrylated PCL and PCL-PDMS-PCL macromers are recorded on a Bruker Advance Core 400 MHz spectrometer as shown in Figure 3.5 with an upgraded console using CDCl_3 as a solvent and tetramethyl silane as an internal standard.



Figure 3.5. Nuclear Magnetic Resonance (Bruker - Advance Core 400 MHz)

3.2.4 Gel permeation chromatography (GPC)

GPC analysis is carried out with Perkin Elmer series 200 instrument as shown in Figure 3.6. Chromatographic grade tetrahydrofuran (THF) is used as eluent at a flow rate of 1.0 ml/min at 30°C. Acrylated macromer samples are dissolved at a concentration of 12 mg/mL in THF. Calibration curves made from polystyrene standards are used to calculate molecular weights.



Figure 3.6. Gel permeation chromatography (Perkin Elmer series 200)

3.2.5 Rheology

Rheological characterizations were performed on MCR 302 rotational rheometer (Anton Paar GmbH, Graz, Austria) as shown in Figure 3.7 with the 25 mm parallel plate fixtures. The oscillatory strain sweep was performed to determine a common shear strain region from 0.01 – 100% at 10 rad/sec. The dynamic frequency sweep was then performed at the strain level of 1.0% in angular frequency range of 0.1 rad/s to 100 rad/sec. The creep recovery tests were performed with the stress level of 10 Pa for 300 sec then recovery measured at released stress for 600 sec. The structure recovery test was performed by applying 0.01s^{-1} rotational pre shear to release the residual stress that might have produced at the time of sample preparation. All the samples were passed through three test intervals 1) reference interval (at low shear $=0.01\text{ s}^{-1}$) for 200 sec, 2) high shear interval at 1s^{-1} for 150 sec and 3) regeneration interval at a shear rate of 0.01 s^{-1} for 360 sec to examine structure regeneration from applied

high shear to low shear rates. Stress relaxation test was performed at pre-strain pre strain level (low strain 0.01%) for 100 sec and then relaxation strain level (high strain 1%) for next 2000 sec and shear stress are measured against the time interval. The values of strains to be applied for respective solutions were determined by amplitude sweep in LVER. All the tests were repeated to confirm the results and minimize the error.

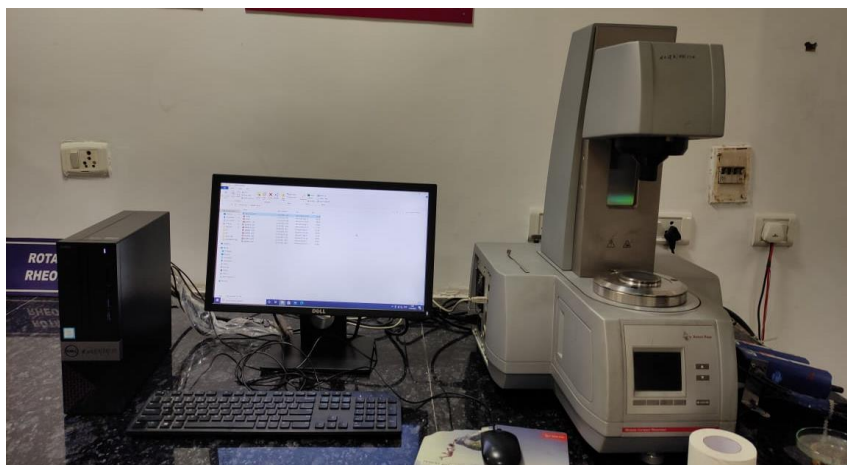


Figure 3.7. MCR 302 Rotational Rheometer (Anton Paar GmbH, Graz, Austria)

3.2.6 Mechanical Properties

Mechanical properties (tensile strength and percentage elongation at break) are measured with a Universal Testing Machine (Instron 3400, USA) at a crosshead speed of 10mm/min with micro tensile specimen having the dimension of length of 80mm, width of 10 mm and thickness of 1 mm.

3.2.7 Thermogravimetry Analysis (TGA)

The thermal degradation behaviour of PCL-PDMS-PCL and PCL photo-crosslinked films is determined from 30 to 700°C at a heating rate of 10°C/min by taking around 0.3 mg of film sample using Perkin Elmer TGA 4000. All tests are carried out under a nitrogen atmosphere. The instrument is shown as Figure 3.8.

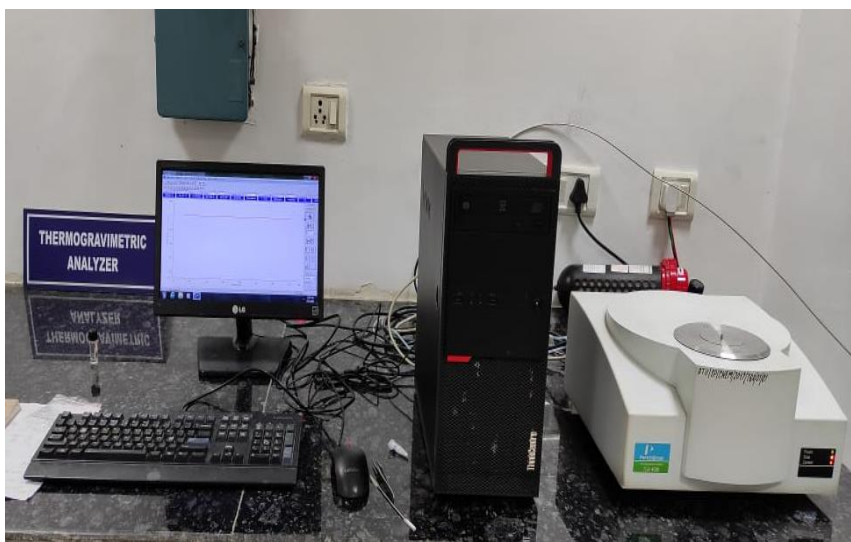


Figure 3.8. Thermal Gravimetry Analyser (TGA 4000 - Perkin Elemer)

3.2.8 Differential Scanning Calorimetry (DSC)

DSC analysis is executed by using Perkin- Elmer DSC 8000 equipment as shown in Figure 3.9. For each test run, five milligrams (5 mg) are measured under nitrogen atmosphere. DSC thermogram for non-isothermal mode are obtained between -20°C and 100°C at $10^{\circ}\text{C}/\text{min}$, melting peak of second run and cooling peak of first run are reported. For isothermal measurements, sample is initially heated from -10 to 100°C at $10^{\circ}\text{C}/\text{min}$. After a hold of 5 min at 100°C , the sample rapidly cools down ($60^{\circ}\text{C}/\text{min}$) to selected crystallization temperatures (T_c). Isothermal essays are followed to isothermal crystallization temperatures for 15 mins., and samples are heated again up to 100°C ($10^{\circ}\text{C}/\text{min}$) to determine heat of fusion(ΔH_f) and crystal melting temperature (T_{cm}). Heat of crystallization(ΔH_c) is recorded at varied isothermal crystallization temperatures (T_c) as a function of time (t) for each cycle in all samples.



Figure 3.9. Differential Scanning Calorimetry (DSC 8000- Perkin Elmer)

3.2.10 Wide Angle X-Ray diffraction (WAXRD)

Wide Angle X-ray diffractograms are recorded by Panalytical's X'Pert Pro X-Ray diffractometer (Figure 3.10) at $\lambda = 1.5406 \text{ \AA}$ using Cu K α as the radiation source. The pure and triblock copolymeric film samples are scanned over the 2θ angle from 10° to 35° at room temperature. WAXS are recorded by Anton – Paar SAXSpace with X-ray source of Primux 3000 sealed tube of Cu. The pure and triblock copolymeric films 40-40, 30-30, 20-20 are measured for q values of 0.2 to 2.0 \AA^{-1} with custom-designed multilayer optics.



Figure 3.10. Panalytical's X'Pert Pro X-Ray diffractometer

3.2.11 Dynamic Mechanical Analysis (DMA)

The quasi-static mechanical evaluation is performed by Dynamic Mechanical Analyser (DMA 4000-Perkin Elemer) (Temperature ramp and frequency sweep) using a with deformation mode of single cantilever bending. Temperature sweeps are performed from 35 to 65°C (ramp rate of 2°C/min), at constant strain of 1% and frequency of 1 Hz. The tests are performed on strip specimens with dimensions of 10×8×0.8 mm³ at tension mode. The instrument is shown as Figure 3.11.



Figure 3.11. Dynamic Mechanical Analyser (DMA 4000-Perkin Elemer)

3.2.12 Optical microscopy

The crystalline morphology is observed with an optical microscope (Motic BA410E) under 40x magnification. Samples are heated to 100°C and kept for 5 minutes to remove thermal history, then cooled to 10°C at the rate of 20°C/min and optical microscope micrographs are recorded using a Moticom Pro 285A camera. The equipment is shown as Figure 3.12.



Figure 3.12. Optical Microscope (Motic BA410E) with Moticam Pro 285A camera

3.2.13 Scanning Electron Microscope (SEM)

Scanning electron microscopy is carried out with CARL ZEISS EVO 50 (Figure 3.13), samples were sputter coated with gold to analysis.



Figure 3.13. Scanning Electron Microscope (SEM CARL ZEISS EVO 50)

3.2.14 Soil burial test

Indoor soil burial experiments are carried out as reported by Luduens *et al.* [46] Natural microflora present in soil (Pinocha type) is used as the degrading medium. Several specimens of rectangular shape (20 mm x 10 mm x 0.6–0.9 mm) of PCL-PDMS-PCL films are buried in soil after placing them in nylon mesh to permit the access of microorganisms and moisture and the easy retrieval of the degraded samples. Total 100 gms of soil used to bury the samples where specimens kept above 60 gms of soil then 40 gms of soil placed above in order to ensure the aerobic degradation. The buried samples are removed at regular intervals (20, 40, 60, 80, 100, 120, 140, 160, 180 days) for different characterisations. The samples are washed carefully with water to remove the soil debris from the surface of the samples after each interval of soil burial. Samples are air dried at ambient temperature until a constant weight. The biodegradability is evaluated by measuring and comparing the weight change (loss) before and after burial. The weight losses of buried samples are calculated using Equation (3.1). The tests are carried out at room temperature of $30 \pm 2^\circ\text{C}$ and relative humidity is kept around 80% by adding distilled water. The specimens are weighed on an analytical balance in order to determine the weight loss ($\%W_L$):

$$\%W_L = \frac{W_0 - W_t}{W_0} \quad (3.1)$$

Here, W_0 is initial weight and W_t is weight at time t of buried samples. The average value of three replicates is reported for all samples.

3.2.15 Shape memory properties

Specimen size of ~ 40 mm (length) \times ~ 10 mm (width) \times ~ 1 mm (thickness) and ~ 40 mm (length) \times ~ 10 mm (width) \times ~ 0.5 mm (thickness) is used to determine shape memory properties quantitatively. The initial length is recorded as ε_o , then specimen is placed at 70°C in hot water bath for few seconds to melt the crystals (sample turns from opaque to translucent), stretched to two-fold of initial length (this length is denoted as ε_m), cool down to

their respective T_c in a cold-water bath with unloading of external forces (after removal of load, length is denoted as ε_u) to obtain temporary shape. The deformed shape is heated again to 70°C in a hot water bath to recover its original shape (this length is denoted as ε_p). A pictorial representation of quantitative analysis is shown in Figure 3.14. The test is repeated three times for all samples and average values with deviation are reported. The shape recovery ratio (R_r) and the shape fixity ratio (R_f) are determined on the basis of the equations (3.2) and (3.3) below:

$$R_r = \frac{\varepsilon_u - \varepsilon_p}{\varepsilon_u - \varepsilon_o} \times 100 \quad (3.2)$$

$$R_f = \frac{\varepsilon_u - \varepsilon_o}{\varepsilon_m - \varepsilon_o} \times 100 \quad (3.3)$$

The qualitative analysis of shape memory property of rectangular shaped and cross shaped samples of PCL and its copolymer is performed by fixing to temporary shape of ring and cube respectively, after cooling at T_c in cold water bath and further shape is recovered by placing them in hot water bath at 70°C. The time required for shape recovery is measured. Experiment is repeated three times and average values are reported.

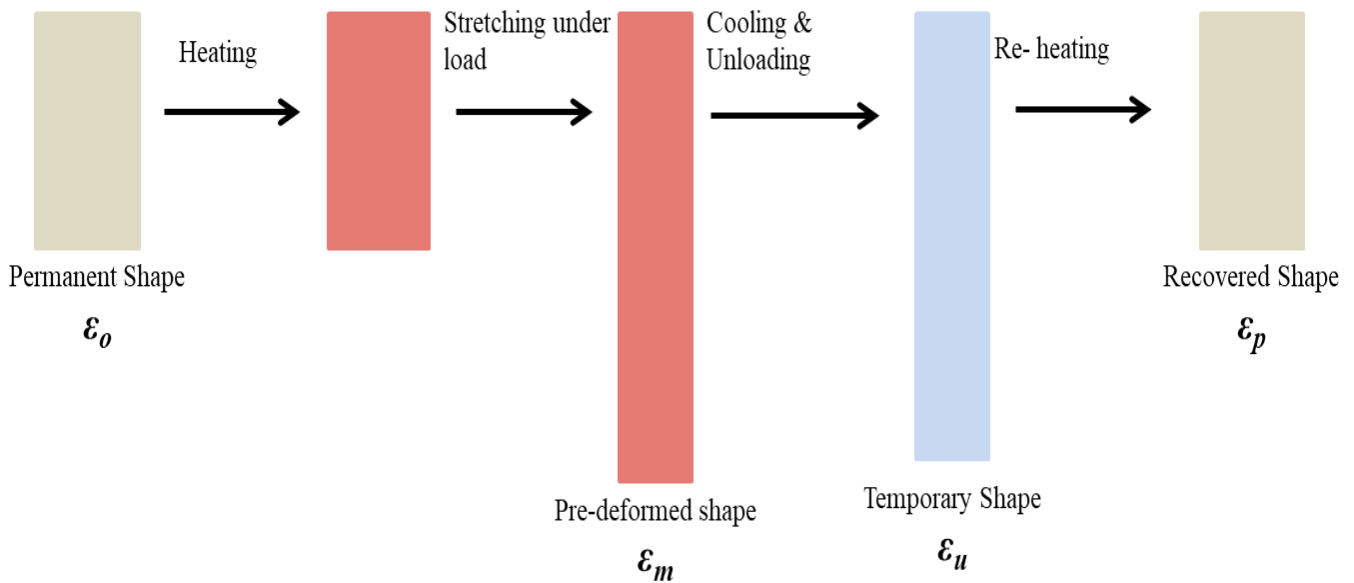


Figure 3.14. Pictorial representation of shape memory properties analysis in quantitative mode

Chapter 4

Synthesis of PCL-PDMS-PCL Triblock Copolymers and its Structural Characterization

Overview

In this chapter, structural characterization of PCL-PDMS-PCL triblock copolymers is discussed. The structural evaluation includes determination of molecular weight by Gel permeation chromatography and Nuclear Magnetic resonance, while chemical structure analysis carried out with the help of FTIR and NMR. The percentage crystallinity is calculated by X-ray diffraction in this chapter. Molecular weight obtained for PCL and its copolymers 40-40, 30-30, 20-20, 10-10 and 5-5 is 9500, 11640, 9348, 4783 and 3641 g/mol and percentage crystallization obtained from XRD is nil, 4.7%, 23.8%, 30.6%, 36.1% and 41.9% respectively.

4.1 Attenuated Total Reflection-Fourier Transform Infrared (ATR-FTIR)

Photocrosslinked PCL-PDMS-PCL films are characterized for attenuated total reflection-fourier transform infrared spectroscopy (ATR-FTIR) as shown in Figure 4.1. The PCL characteristic bands are recorded at 2943 cm^{-1} for asymmetric $-\text{CH}_2$ stretching, 2865 cm^{-1} for symmetric $-\text{CH}_2$ stretching, 1725 cm^{-1} for $\text{C}=\text{O}$ carbonyl stretching, 1294 cm^{-1} for $\text{C}-\text{O}$ and $\text{C}-\text{C}$ stretching, 1239 cm^{-1} for asymmetric $\text{C}-\text{O}-\text{C}$ stretching and 1169 cm^{-1} for symmetric $\text{C}-\text{O}-\text{C}$ stretching. For PCL-PDMS-PCL copolymer films additional peaks are observed at 800 cm^{-1} for $\text{Si}-\text{C}$ (methyl of PDMS), a weak band around 3300 cm^{-1} assigned to amino end groups, a very sharp peak for $-\text{CH}_3$ stretching at 1259 cm^{-1} and doublet at 1090 and 1018 cm^{-1} assigned to $\text{Si}-\text{O}-\text{Si}$ stretching. A non-hydrogen bonded $\text{C}=\text{O}$ peak at 1723 cm^{-1} is observed due to ester group in PCL and there is slight shift observed in $-\text{CH}_2$ stretching at 2961 cm^{-1} in case of triblock copolymer than pure PCL due to additional $-\text{CH}_2$ chain of PDMS. Hydrogen

bonded C=O stretching peak at 1649 cm^{-1} of amide I and H-N-C=O stretching peak at 1531 cm^{-1} of amide II are observed. Similarly, Meikail *et al.* have reported secondary amide and protonated amine stretching at 1648 cm^{-1} and 1555 cm^{-1} . [245] Poojari *et al.* reported absorption band at 1100 cm^{-1} for Si-O-Si and at 1260 cm^{-1} for Si-CH₃ bonds of PDMS. [11] Azemar *et al.* have reported peaks at 800 cm^{-1} for Si-CH₃ bonds and 1097 cm^{-1} for Si-O bond of PDMS while peaks at 2943 cm^{-1} for methylene and at 1725 cm^{-1} for ester of PCL. [4, 14] Chan *et al.* have synthesized poly(PCL/PDMS) urethane and reported similar peaks. [246]

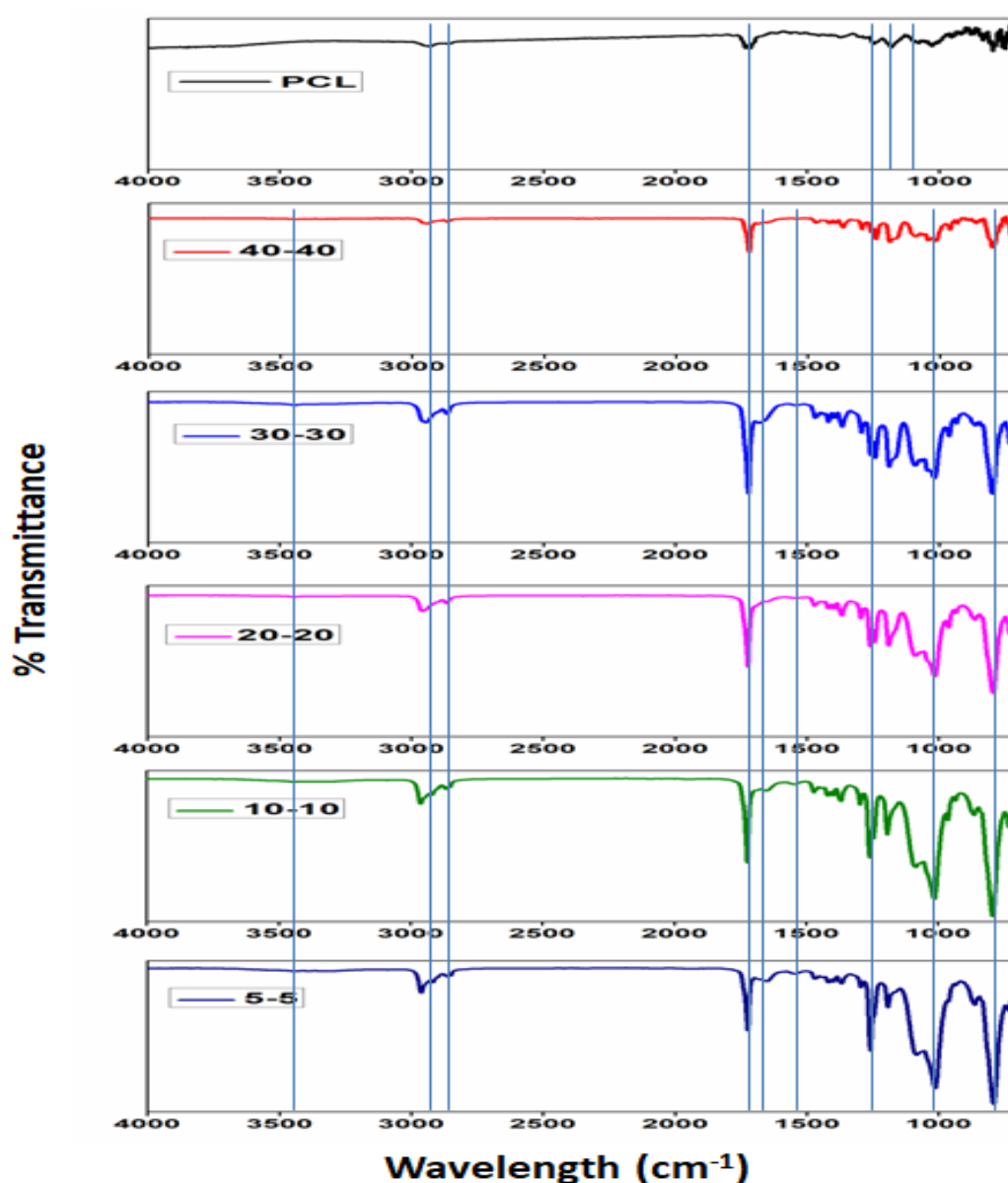


Figure 4.1. ATR-FTIR of photocrosslinked pure PCL and PCL-PDMS-PCL triblock copolymer films

4.2 Nuclear Magnetic resonance (NMR)

Dihydroxy terminated PCL, PCL-PDMS-PCL and acrylated PCL, PCL-PDMS-PCL are characterized for ^1H NMR. ^1H NMR spectrum of PCL diol and PCL-PDMS-PCL diol are presented in Figure 4.2 (a), (b), (c), (d), (e), (f), (g), (h), (k), (l). Number average molecular weight (M_n) and ratio of PCL/PDMS blocks are obtained by NMR spectroscopy results.

4.2.1 NMR shifts of Hydroxyl group terminated $\text{PCL}_{40}\text{-PDMS}_{30}\text{-PCL}_{40}$ macromer

$\delta = 0.01\text{--}0.06$ due to 200H of SiCH_3 , $\delta = 0.52$ due to 4H of $\text{SiCH}_2\text{CH}_2\text{CH}_2\text{-}$, $\delta = 1.38$ due to 160H of $\text{-CH}_2\text{CH}_2\text{CH}_2\text{CH}_2\text{CH}_2\text{OH}$, $\delta = 1.60$ due to 320H of $\text{-CH}_2\text{CH}_2\text{CH}_2\text{CH}_2\text{CH}_2\text{OH}$, $\delta = 2.16$ due to 4H of $\text{-SiCH}_2\text{CH}_2\text{CH}_2\text{NH-}$, $\delta = 2.32$ due to 160H of $\text{-CH}_2\text{CH}_2\text{CH}_2\text{CH}_2\text{CH}_2\text{OH}$, $\delta = 3.20$ due to 4H of $\text{-SiCH}_2\text{CH}_2\text{CH}_2\text{-}$, $\delta = 3.63$ due to 2H of NH and $\delta = 4.05$ due to 160H of $\text{-CH}_2\text{CH}_2\text{CH}_2\text{CH}_2\text{CH}_2\text{OH}$.

4.2.2 NMR shifts of Hydroxyl group terminated $\text{PCL}_{30}\text{-PDMS}_{30}\text{-PCL}_{30}$ macromer

$\delta = 0.01\text{--}0.06$ due to 200H of SiCH_3 , $\delta = 0.52$ due to 4H of $\text{SiCH}_2\text{CH}_2\text{CH}_2\text{-}$, $\delta = 1.39$ due to 120H of $\text{-CH}_2\text{CH}_2\text{CH}_2\text{CH}_2\text{CH}_2\text{OH}$, $\delta = 1.65$ due to 240H of $\text{-CH}_2\text{CH}_2\text{CH}_2\text{CH}_2\text{CH}_2\text{OH}$, $\delta = 2.18$ due to 4H of $\text{-SiCH}_2\text{CH}_2\text{CH}_2\text{NH-}$, $\delta = 2.35$ due to 120H of $\text{-CH}_2\text{CH}_2\text{CH}_2\text{CH}_2\text{CH}_2\text{OH}$, $\delta = 3.25$ due to 4H of $\text{-SiCH}_2\text{CH}_2\text{CH}_2\text{-}$, $\delta = 3.66$ due to 2H of NH and $\delta = 4.08$ due to 120H of $\text{-CH}_2\text{CH}_2\text{CH}_2\text{CH}_2\text{CH}_2\text{OH}$.

4.2.3 NMR shifts of Hydroxyl group terminated $\text{PCL}_{20}\text{-PDMS}_{30}\text{-PCL}_{20}$ macromer

$\delta = 0.03\text{--}0.06$ due to 200H of SiCH_3 , $\delta = 0.50$ due to 4H of $\text{SiCH}_2\text{CH}_2\text{CH}_2\text{-}$, $\delta = 1.39$ due to 80H of $\text{-CH}_2\text{CH}_2\text{CH}_2\text{CH}_2\text{CH}_2\text{OH}$, $\delta = 1.58$ due to 160H of $\text{-CH}_2\text{CH}_2\text{CH}_2\text{CH}_2\text{CH}_2\text{OH}$, $\delta = 2.11$ due to 4H of $\text{-SiCH}_2\text{CH}_2\text{CH}_2\text{NH-}$, $\delta = 2.29$ due to 80H of $\text{-CH}_2\text{CH}_2\text{CH}_2\text{CH}_2\text{CH}_2\text{OH}$, $\delta = 3.22$ due to 4H of $\text{-SiCH}_2\text{CH}_2\text{CH}_2\text{-}$, $\delta = 3.61$ due to 2H of NH and $\delta = 4.00$ due to 80H of $\text{-CH}_2\text{CH}_2\text{CH}_2\text{CH}_2\text{CH}_2\text{OH}$.

4.2.4 NMR shifts of Hydroxyl group terminated PCL₁₀-PDMS₃₀-PCL₁₀ macromer

$\delta = 0.01\text{--}0.06$ due to 200H of SiCH₃, $\delta = 0.50$ due to 4H of SiCH₂CH₂CH₂-, $\delta = 1.39$ due to 40H of -CH₂CH₂CH₂CH₂CH₂OH, $\delta = 1.61$ due to 80H of -CH₂CH₂CH₂CH₂CH₂OH, $\delta = 2.11$ due to 4H of -SiCH₂CH₂CH₂NH-, $\delta = 2.29$ due to 40H of -CH₂CH₂CH₂CH₂CH₂OH, $\delta = 3.20$ due to 4H of -SiCH₂CH₂CH₂-, $\delta = 3.57$ due to 2H of NH and $\delta = 4.00$ due to 40H of -CH₂CH₂CH₂CH₂CH₂OH.

4.2.5 NMR shifts of Hydroxyl group terminated PCL₅-PDMS₃₀-PCL₅ macromer

$\delta = 0.06\text{--}0.12$ due to 200H of SiCH₃, $\delta = 0.54$ due to 4H of SiCH₂CH₂CH₂-, $\delta = 1.38$ due to 20H of -CH₂CH₂CH₂CH₂CH₂OH, $\delta = 1.67$ due to 40H of -CH₂CH₂CH₂CH₂CH₂OH, $\delta = 2.11$ due to 4H of -SiCH₂CH₂CH₂NH-, $\delta = 2.27$ due to 20H of -CH₂CH₂CH₂CH₂CH₂OH, $\delta = 3.23$ due to 4H of -SiCH₂CH₂CH₂-, $\delta = 3.66$ due to 2H of NH and $\delta = 4.07$ due to 20H of -CH₂CH₂CH₂CH₂CH₂OH.

4.2.6 NMR shifts of PCL diol macromer

$\delta = 1.40$ due to 150H of -CH₂CH₂CH₂CH₂CH₂CO-, $\delta = 1.66$ due to 300H of -CH₂CH₂CH₂CH₂CH₂CO-, $\delta = 2.32$ due to 150H of -CH₂CH₂CH₂CH₂CH₂CO-, $\delta = 3.63$ due to 4H of -CH₂OH, $\delta = 4.05$ due to 150H of -CH₂CH₂CH₂CH₂CH₂CO-, $\delta = 4.3$ due to 4H of -CH₂CO-.

4.2.7 NMR shifts of acrylic terminated PCL₄₀-PDMS₃₀-PCL₄₀ macromer

$\delta = 0.04\text{--}0.12$ due to 200H of SiCH₃, $\delta = 0.53$ due to 4H of -SiCH₂CH₂CH₂NH-, $\delta = 1.37$ due to 160H of -CH₂CH₂CH₂CH₂CH₂O-, $\delta = 1.61$ due to 320H of -CH₂CH₂CH₂CH₂CH₂O-, $\delta = 2.09$ due to 4H of -SiCH₂CH₂CH₂NH-, $\delta = 2.30$ due to 160H of -CH₂CH₂CH₂CH₂CH₂O-, $\delta = 3.10$ due to 4H of -SiCH₂CH₂CH₂NH-, $\delta = 3.64$ due to 2H of NH, $\delta = 4.13$ due to 160H of -CH₂CH₂CH₂CH₂CH₂O-, $\delta = 5.82$ due to 2H of -CH=CH₂, $\delta = 6.10$ due to 2H of -CH=CH₂, $\delta = 6.40$ due to 2H of -CH=CH₂.

4.2.8 NMR shifts of acrylic terminated PCL₃₀-PDMS₃₀-PCL₃₀ macromer

$\delta = 0.04\text{--}0.12$ due to 200H of SiCH₃, $\delta = 0.51$ due to 4H of -SiCH₂CH₂CH₂NH-, $\delta = 1.39$ due to 120H of -CH₂CH₂CH₂CH₂CH₂O-, $\delta = 1.62$ due to 240H of -CH₂CH₂CH₂CH₂CH₂O-, $\delta = 2.11$ due to 4H of -SiCH₂CH₂CH₂NH-, $\delta = 2.29$ due to 120H of -CH₂CH₂CH₂CH₂CH₂O-, $\delta = 3.15$ due to 4H of -SiCH₂CH₂CH₂NH-, $\delta = 3.62$ due to 2H of NH, $\delta = 4.13$ due to 120H of -CH₂CH₂CH₂CH₂CH₂O-, $\delta = 5.82$ due to 2H of -CH=CH₂, $\delta = 6.11$ due to 2H of -CH=CH₂, $\delta = 6.40$ due to 2H of -CH=CH₂.

4.2.9 NMR shifts of acrylic terminated PCL₂₀-PDMS₃₀-PCL₂₀ macromer

$\delta = 0.04\text{--}0.12$ due to 200H of SiCH₃, $\delta = 0.51$ due to 4H of -SiCH₂CH₂CH₂NH-, $\delta = 1.39$ due to 80H of -CH₂CH₂CH₂CH₂CH₂O-, $\delta = 1.62$ due to 160H of -CH₂CH₂CH₂CH₂CH₂O-, $\delta = 2.11$ due to 4H of -SiCH₂CH₂CH₂NH-, $\delta = 2.30$ due to 80H of -CH₂CH₂CH₂-CH₂CH₂O-, $\delta = 3.22$ due to 4H of -SiCH₂CH₂CH₂NH-, $\delta = 3.70$ due to 2H of NH, $\delta = 4.13$ due to 80H of -CH₂CH₂CH₂CH₂CH₂O-, $\delta = 5.82$ due to 2H of -CH=CH₂, $\delta = 6.11$ due to 2H of -CH=CH₂, $\delta = 6.40$ due to 2H of -CH=CH₂.

4.2.10 NMR shifts of acrylic terminated PCL₁₀-PDMS₃₀-PCL₁₀ macromer

$\delta = 0.04\text{--}0.12$ due to 200H of SiCH₃, $\delta = 0.51$ due to 4H of -SiCH₂CH₂CH₂NH-, $\delta = 1.39$ due to 40H of -CH₂CH₂CH₂CH₂CH₂O-, $\delta = 1.62$ due to 80H of -CH₂CH₂CH₂CH₂CH₂O-, $\delta = 2.11$ due to 4H of -SiCH₂CH₂CH₂NH-, $\delta = 2.30$ due to 40H of -CH₂CH₂CH₂-CH₂CH₂O-, $\delta = 3.22$ due to 4H of -SiCH₂CH₂CH₂NH-, $\delta = 3.70$ due to 2H of NH, $\delta = 4.13$ due to 40H of -CH₂CH₂CH₂CH₂CH₂O-, $\delta = 5.82$ due to 2H of -CH=CH₂, $\delta = 6.11$ due to 2H of -CH=CH₂, $\delta = 6.40$ due to 2H of -CH=CH₂.

4.2.11 NMR shifts of acrylic terminated PCL₅-PDMS₃₀-PCL₅ macromer

$\delta = 0.01\text{--}0.22$ due to 200H of SiCH₃, $\delta = 0.50$ due to 4H of -SiCH₂CH₂CH₂NH-, $\delta = 1.39$ due to 20H of -CH₂CH₂CH₂CH₂CH₂O-, $\delta = 1.62$ due to 40H of -CH₂CH₂CH₂CH₂CH₂O-, $\delta = 2.11$ due to 4H of -SiCH₂CH₂CH₂NH-, $\delta = 2.27$ due to 20H of -CH₂CH₂CH₂-CH₂CH₂O-, $\delta = 3.23$

due to 4H of $-\text{SiCH}_2\text{CH}_2\text{CH}_2\text{NH}-$, $\delta = 3.61$ due to 2H of NH , $\delta = 4.02$ due to 20H of $-\text{CH}_2\text{CH}_2\text{CH}_2\text{CH}_2\text{CH}_2\text{O}-$, $\delta = 5.82$ due to 2H of $-\text{CH}=\text{CH}_2$, $\delta = 6.11$ due to 2H of $-\text{CH}=\text{CH}_2$, $\delta = 6.40$ due to 2H of $-\text{CH}=\text{CH}_2$.

4.2.12 NMR shifts of acrylic terminated PCL macromer

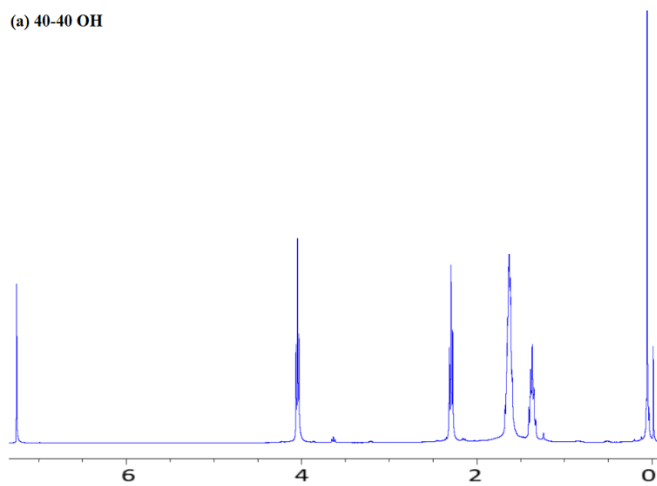
$\delta = 1.40$ due to 140H of $-\text{CH}_2\text{CH}_2\text{CH}_2\text{CH}_2\text{CH}_2\text{CO}-$, $\delta = 1.66$ due to 280H of $-\text{CH}_2\text{CH}_2\text{CH}_2\text{CH}_2\text{CH}_2\text{CH}_2\text{CO}-$, $\delta = 2.32$ due to 140H of $-\text{CH}_2\text{CH}_2\text{CH}_2\text{CH}_2\text{CH}_2\text{CO}-$, $\delta = 4.05$ due to 140H of $-\text{CH}_2\text{CH}_2\text{CH}_2\text{CH}_2\text{CH}_2\text{CO}-$, $\delta = 4.3$ due to 4H of $-\text{CH}_2\text{CO}-$, $\delta = 5.82$ due to 2H of $-\text{CH}=\text{CH}_2$, $\delta = 6.11$ due to 2H of $-\text{CH}=\text{CH}_2$, $\delta = 6.40$ due to 2H of $-\text{CH}=\text{CH}_2$.

Azemar *et al.* have reported similar spectra with peaks at $\delta = 0.06$, 1.35, 1.65, 2.3 and 4.05 ppm of PCL-PDMS-PCL triblock and composition is calculated by ratio of absorbance at 0.06 ppm and 4.05 ppm.[4] Tian *et al.* have reported proton NMR for PCL diol and acrylic terminated PCL similarly.[162] Number average molecular weight (M_n) and PCL:PDMS ratio are determined with help of ^1H NMR. Molecular weights calculated by feed monomer, proton NMR and GPC is presented in Table 4.1.

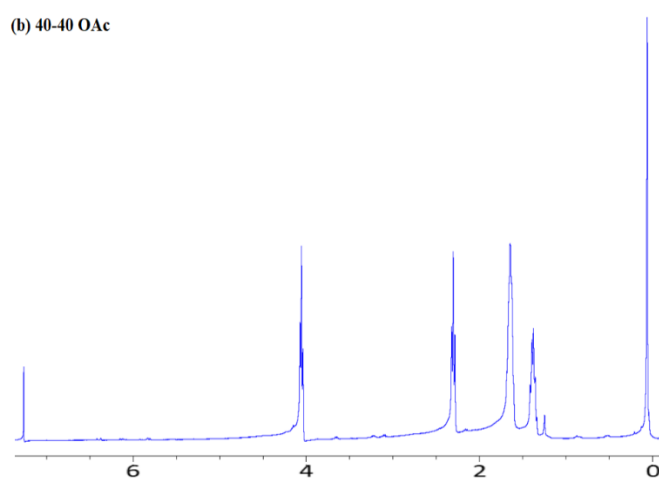
Table 4.1. Molecular weights by NMR, GPC, PDI by GPC and percentage conversion of PCL and PCL-PDMS-PCL macromers.

Sample name	Conversion (%)	M_n (theoretical) (g mol ⁻¹)	M_n (NMR) (g mol ⁻¹)	M_n (GPC) (g mol ⁻¹)	PDI (GPC)
PCL	98.0%	9500	8668	8653	1.8
40-40	98.5%	11630	11220	11138	1.8
30-30	97.3%	9348	9164	9090	1.7
20-20	97.5%	7065	6984	7066	1.6
10-10	96.0%	4783	4406	4643	1.5
5-5	95.0%	3641	3266	3498	1.3

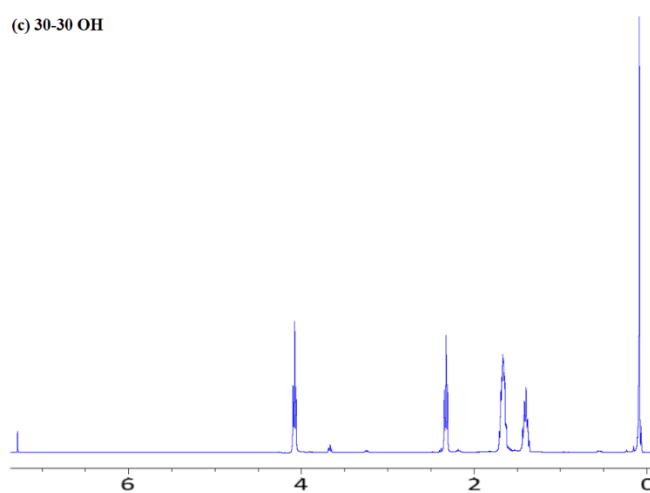
(a) 40-40 OH



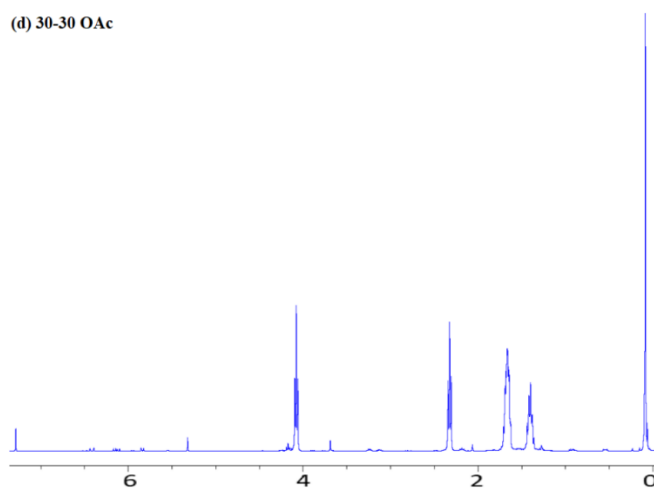
(b) 40-40 OAc



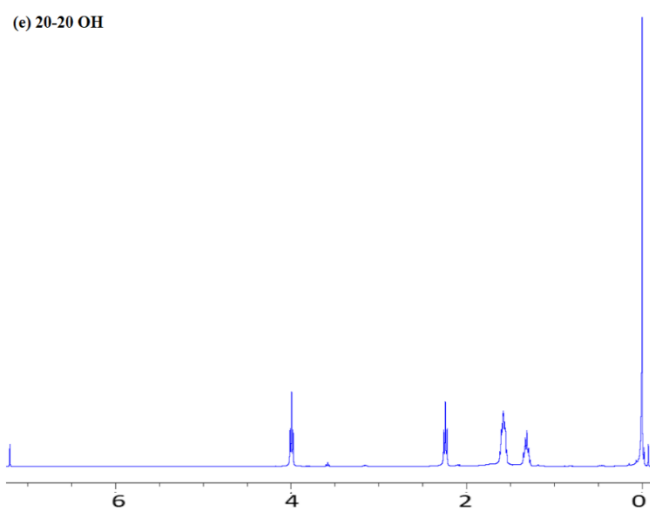
(c) 30-30 OH



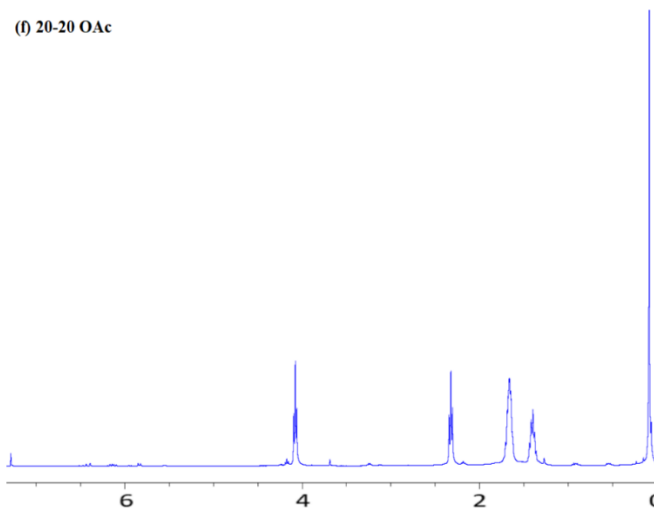
(d) 30-30 OAc



(e) 20-20 OH



(f) 20-20 OAc



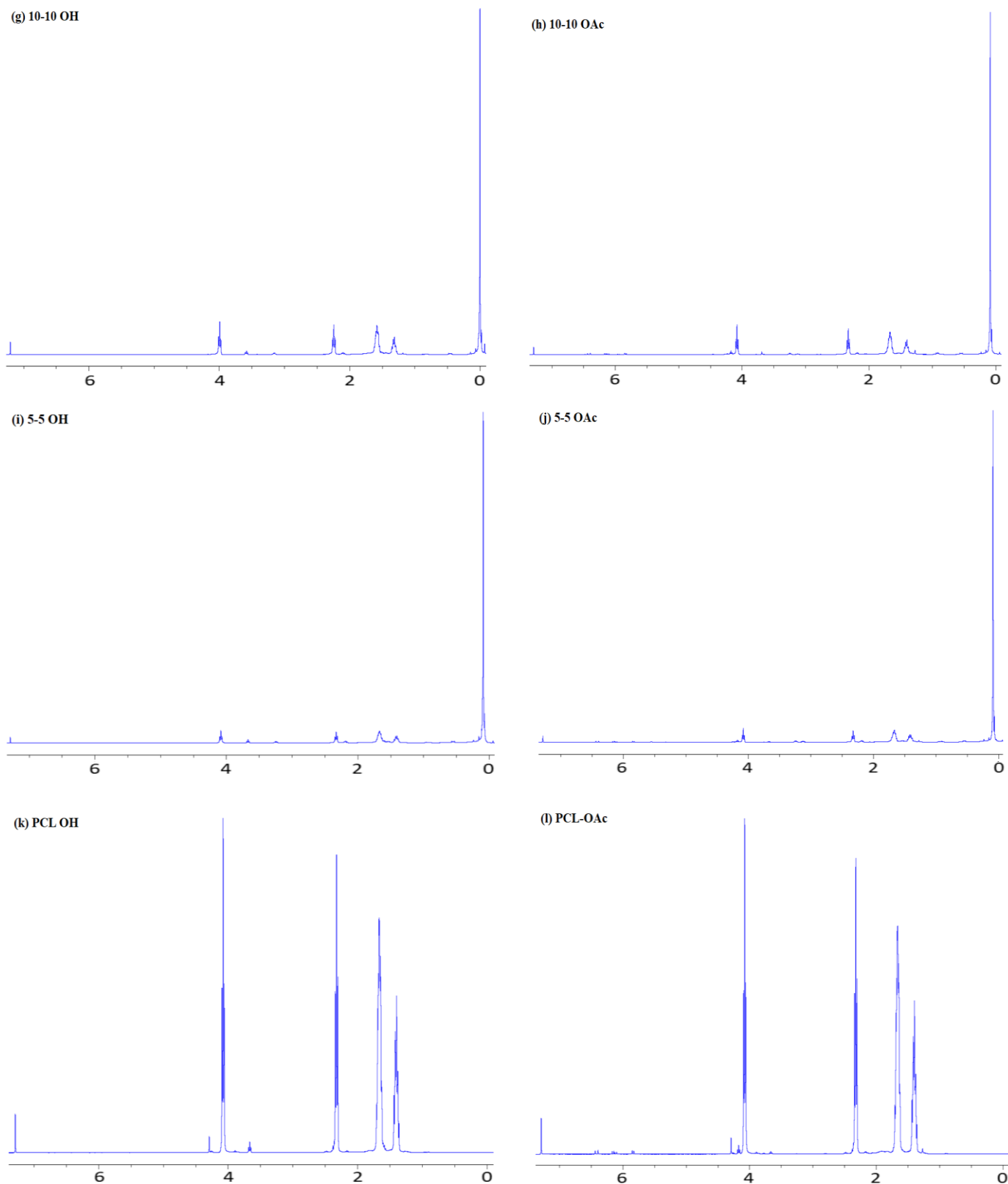


Figure 4.2. 400 MHz ^1H NMR spectroscopy of (a) 40-40 OH, (b) 40-40 OAc, (c) 30-30 OH (d) 30-30 OAc (e) 20-20 OH (f) 20-20 OAc (g) 10-10 OH (h) 10-10 OAc (i) 5-5 OH (j) 5-5 OAc (k) PCL OH (l) PCL OAc

4.3 X-Ray diffraction (XRD)

XRD diffractogram of PCL and PCL-PDMS-PCL triblock copolymeric films with varying PCL chain length and constant PDMS block lengths are presented in Figure 4.3. Three strong peaks marked with (*) observed at 2θ angles 21.4° , 22.0° and 23.6° , represent the (110), (111) and (200) planes, respectively, and a faint peak at 29.5° due to (210) plane of PCL exhibit the orthorhombic crystal structure[10]. Irrespective of chain length of PCL, well-defined crystal structure of PCL at $2\theta = 21.4^\circ$ and 23.6° is visible without any shift upon copolymerization with PDMS. The intensity of peaks is reduced as the PCL content of the copolymer decreases, indicating very good crystallinity in the PCL phase which is well correlated with the crystal growth observed in optical microscope. However, sample of 5-5 does not show any diffraction peak. The degree of crystallinity, $X_c(\%)$, is calculated by integrating the intensity of the diffraction peaks, crystalline region, I_c (which includes the areas corresponding to the (110), (111), (200) and (210) reflections in PCL), and the amorphous region, I_a using the equation (4.3):

$$X_c (\%) = \frac{I_c}{I_c + I_a} \times 100 \quad (4.3)$$

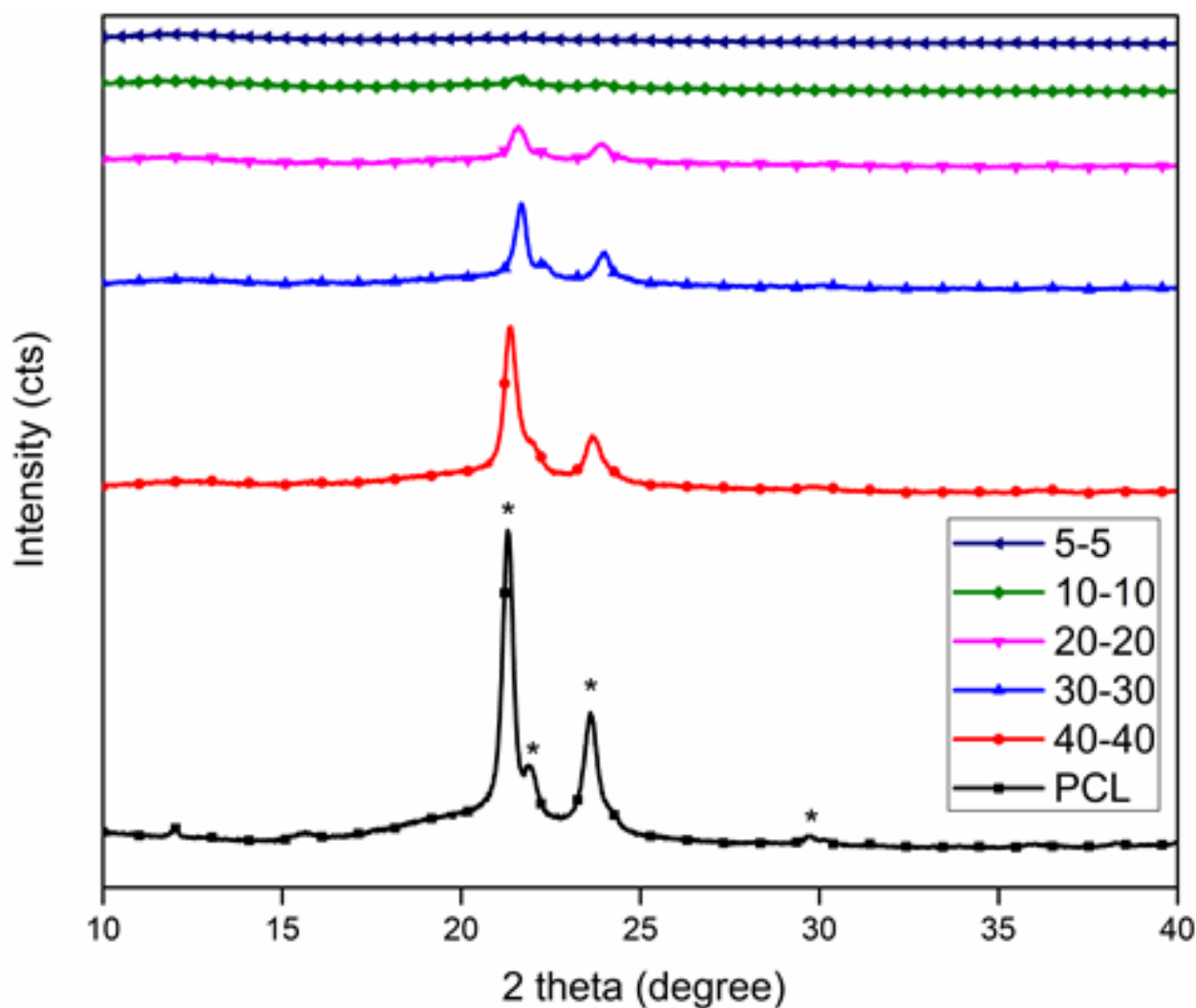


Figure 4.3. X-ray diffraction plot of PCL and PCL-PDMS-PCL triblock copolymer films

The crystallinity of the PCL phase in these copolymers is influenced by the volume fractions and molecular weights of the PCL and PDMS blocks. There is very less crystallinity observed for 10-10 and no crystallinity for 5-5 samples. Table 4.2 shows the degree of crystallinity of the PCL in triblock copolymers using XRD patterns. With increase in PCL chain length, the percentage crystallinity increases from 4.7% to 36.1%. Lipase catalysed PCL-PDMS-PCL triblock copolymer synthesized by Poojari *et al.*[11] having PDMS of M_n 2500 and PCL chain length varying from 50-50 to 5-5 reported 54% to 40% crystallinity by XRD on the basis of PCL content though actual crystallinity is 54% to 9% for complete copolymer corresponds to high molecular weight ranges from 13950 to 4400 g/mol. Yilgor *et*

al.[10] synthesized PCL-PDMS-PCL triblock copolymer with different M_n of PDMS block reported XRD crystallinity from 37% to 65% (on the basis of PCL content in copolymer) with increasing PCL content.

Table 4.2 Crystallinity of PCL-PDMS-PCL triblock copolymer

Samples	Crystallinity (%) by XRD
PCL	41.9
40-40	36.1
30-30	30.6
20-20	23.8
10-10	4.7
5-5	No crystallinity

4.4 Conclusion

The PCL and PCL-PDMS-PCL triblock shape memory films are prepared by ring-opening polymerization followed by photo-crosslinking. Variation in PCL chain length is obtained according to monomer feed ratio and chain length of PCL varies from 40-40 to 5-5 in copolymers. Molecular weight obtained in the range of 11640 g/mol to 3641 g/mol. The percentage crystallinity obtained from X-ray diffraction pattern is between nil to 41.9% and decreasing as the PCL chain length get reduced.

Chapter 5

Rheological Characterization of PCL-PDMS-PCL Triblock Copolymer Films

Copolymer Films

Overview

The chapter is designed to give a detailed analysis of rheological characteristics of PCL-PDMS-PCL triblock copolymer films. Oscillatory shear rheology tests are performed to measure the dynamics of the viscoelastic behaviour of photocrosslinked films above their crystal melting temperature (T_{cm}). Time dependent effect on the copolymer films has been analyzed by creep recovery behaviour. Their structure recovery is also evaluated.

5.1 Linear viscoelastic region

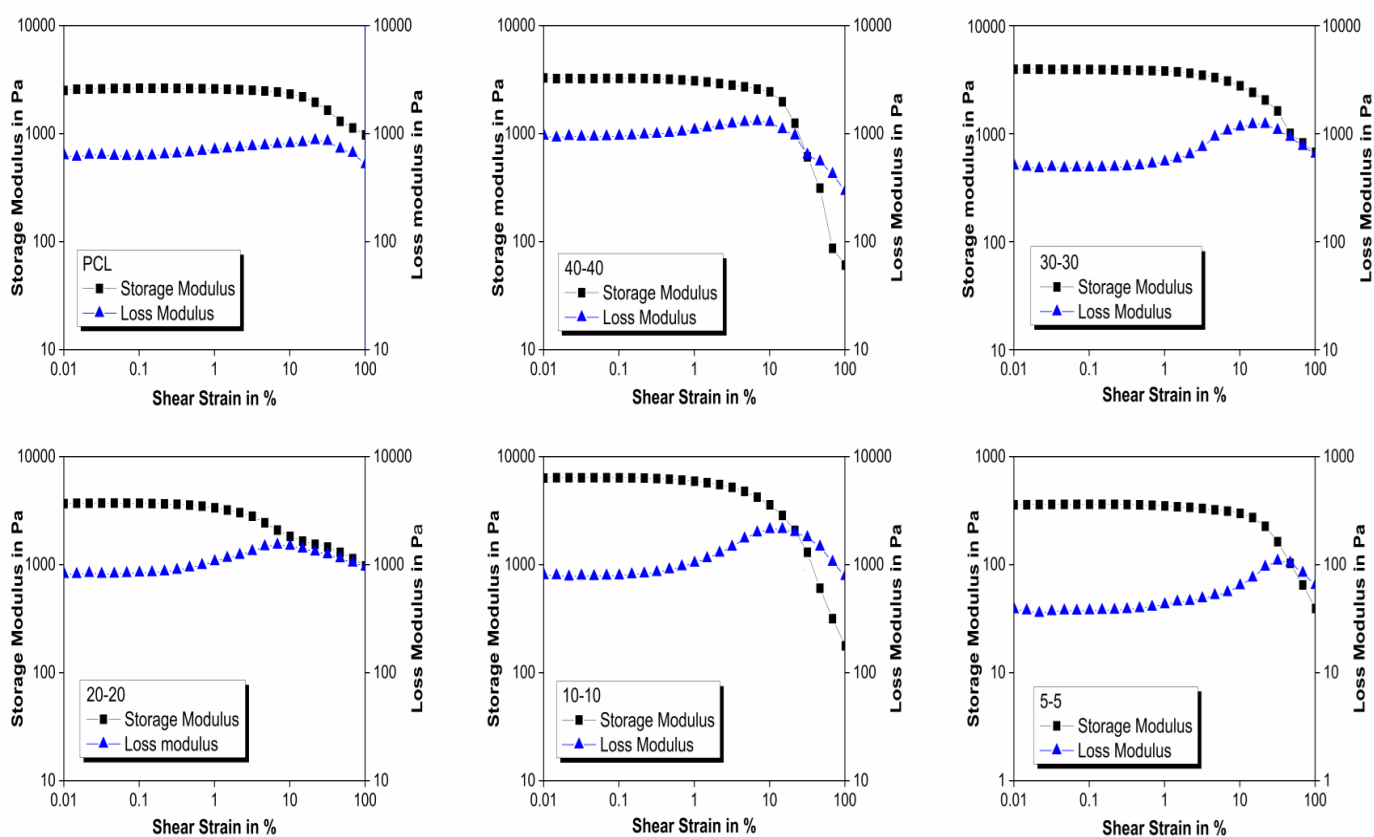


Figure 5.1. Amplitude sweep showing linear viscoelastic region (LVER) of PCL and PCL-PDMS-PCL triblock polymer at 80°C.

The linear viscoelastic properties of the PCL-PDMS-PCL copolymers with different molecular weight or varying PCL chain length were determined at 80°C. During an amplitude sweep, the amplitude of the shear stress was varied at a constant frequency of 10 rad/s. For the analysis, storage modulus G' & loss modulus G'' are plotted against the deformation (shear strain %) and results are shown in Figure 5.1. At low deformation, G' and G'' are found to be constant representing sample structure is undisturbed. This region is called linear-viscoelastic (LVE). As soon as the moduli start to decrease, the structure is disturbed and represents the end of the LVE-region and the strain termed as critical strain value (γ_c). The plateau value of G' in the LVE-region describes the rigidity of the sample at rest; the plateau value G'' is a measure for the viscosity of the unsheared sample. The critical strain value is 14%, 10%, 7%, 3%, 5% and 10% for PCL, 40-40, 30-30, 20-20, 10-10 and 5-5 respectively. Bouakaz *et al.* reported critical strain value from 0.01 to 10% for PCL and its blends with epoxy functionalised graphene and different clays, where PCL shows critical strain value of 10% at 120°C.[28] In different rheological studies of linear polycaprolactone, four armed star polycaprolactone, PCL/polylactide blends and PCL/CNT composites are carried out at strain value of 5% by Chae *et al.*[18], Noroozi *et al.*[23] and Vega *et al.*[32] The ratio of the two moduli (G' and G'') gives information about the characteristic of the sample. If the storage modulus is larger than the loss modulus, the sample behaves more like a viscoelastic solid. In the opposite case ($G'' > G'$) it behaves as viscoelastic fluid[247]. Here, all the composition showed viscoelastic solid behaviour. It can be seen that for pure PCL showed stable structure up to 10% shear strain and no crossover point up to 100%. On addition of PDMS block, all composition showed viscoelastic solid behaviour and stable structure up to 1% but crossover point seen above 10% which represent deformation of structure and viscoelastic fluid behaviour after 10% shear strain. It indicates that addition of PDMS block and decreasing PCL chain length didn't affect stability of structure due to increasing

crosslinking density but viscoelastic fluid behaviour at lower shear strain due to addition of complete amorphous phase as PDMS.

5.2 Frequency Sweep

A dynamic frequency sweep was carried out at LVR range ($\gamma=1\%$) and frequency range in log scale of 0.1 rad/sec to 100 rad/sec at 80°C to study storage modulus, loss modulus, loss factor and complex viscosity. For analysis, the storage modulus loss moduli are plotted against frequency in Figure 5.2. The storage modulus of PCL and PDPCL is increasing with decreasing molecular weight. Loss modulus increases for PCL, 40-40, 30-30 and 20-20 then its decreases for 10-10 and 5-5. With increase in angular frequency the storage modulus and loss modulus both are increasing and there is no cross-over point observed in the graph. Similar trends were observed for PCL by Noroozi *et al.*[23] , Wang *et al.*[30] and Vega *et al.*[32] that storage modulus and loss modulus are increasing with increased angular frequency in the rheology study of PCL/ polylactide blends, PCL/cellulose nanocrystals composite and PCL/ multiwalled carbon nanotubes composites. In the whole range of angular frequency, storage modulus is dominant over loss storage, while the gap between storage and loss modulus is increases with decreasing molar mass of the polymeric films which represents increase in solid like behaviour.

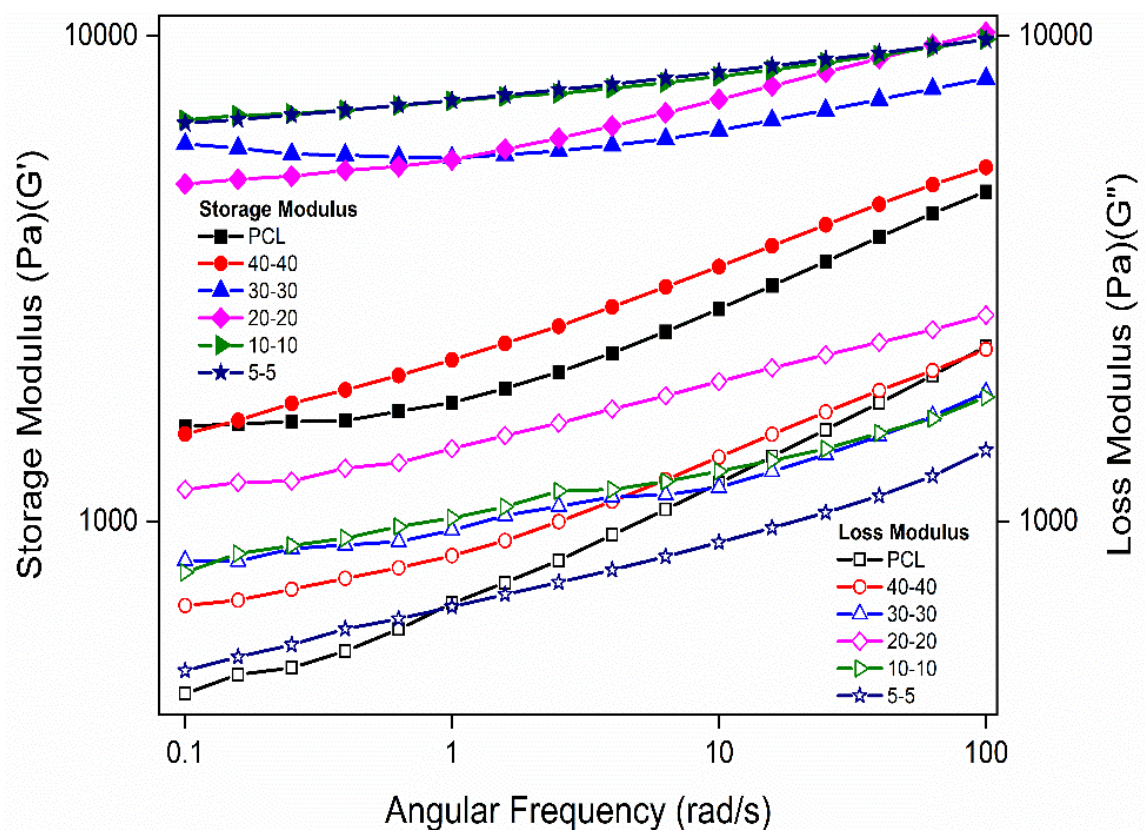


Figure 5.2. Storage modulus and loss modulus versus angular frequency plots of PCL and PCL-PDMS-PCL triblock polymer at 80°C.

To understand damping properties of any viscoelastic material loss factor ($\tan \delta$) is analysed. This is defined as the ratio of energy dissipated in the material during vibration to the maximum potential energy stored in the material i.e. ratio of loss modulus to storage modulus. When the $\tan \delta < 1$, and $G' > G''$, meaning that the sample behaves as the viscoelastic solid, on the contrary, when $\tan \delta > 1$, the sample behaves as the viscoelastic fluid[248]. Here it can be clearly observed in Figure 5.3 that $\tan \delta$ is less than one for each polymer composition and decreases with decreasing molar mass. It indicates solid like behaviour is dominant with decreasing molar mass or decreasing chain length in terpolymer photocrosslinked films. Here the crosslink density plays a major role in these observations. As the molar mass decreases, overall chain length decreased between two crosslink points resulted in increases the crosslink density[12] as depicted in Figure 5.5. Before crosslinking

the sample get melt and flow when heated above T_{cm} . These crosslink points, keep intact the polymer into moulded shape even when the temperature goes above the T_{cm} , though change in opacity is observed after T_{cm} due to melting of crystalline part of PCL. This increased crosslinked density with decreasing molar mass, resulted to increase in storage modulus, decrease in loss factor, and more solid-like behaviour as shown by frequency sweep plot. Winter *et al.*[249] analysed linear viscoelasticity of crosslinked polymer at gel point and reported that storage modulus keeps increasing with increasing crosslink density. The values of loss factor of PCL increase with increasing slope indicating fluid like behaviour at higher frequency. In case of copolymers, loss factor values are almost similar throughout frequency range means there is no significance effect of vibration potential on viscoelastic property of copolymers film above their crystal melting temperature (T_{cm}). Phase shift angle plotted against angular frequency shows that phase angle of PCL shifted from 16° to 26° whereas, no significant change is observed in phase shift angle of copolymers. The phase angle is around 22° for 40-40, 15° for 30-30, 8° - 12° for 20-20, 7° - 10° for 10-10 and 5° - 7° for 5-5.

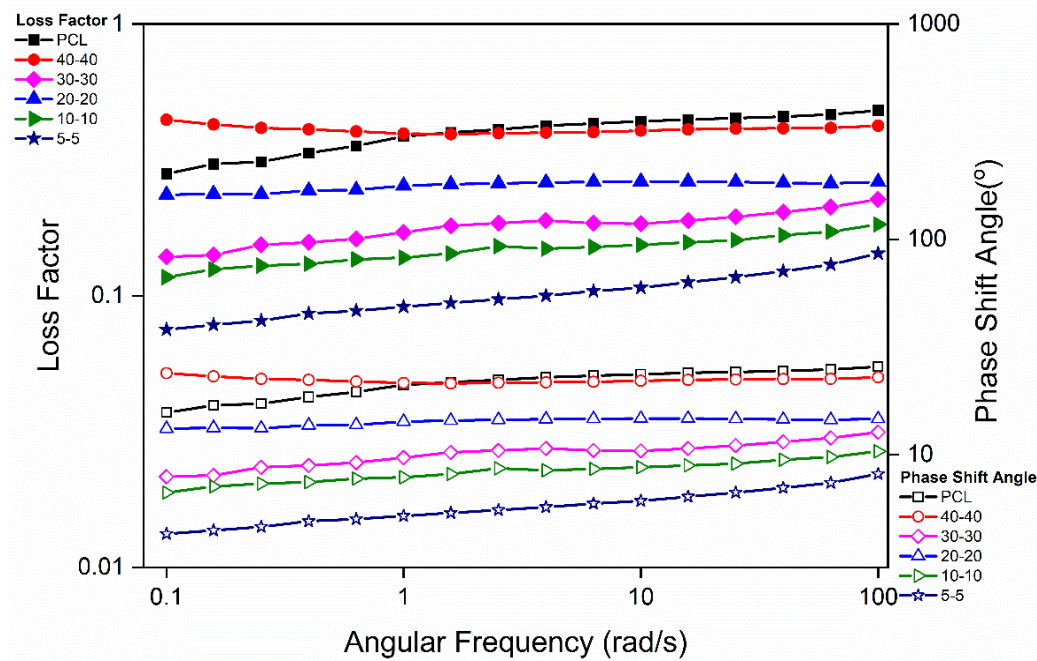


Figure 5.3. Loss factor and phase shift angle against angular frequency of PCL and PCL-PDMS-PCL triblock polymer at 80°C .

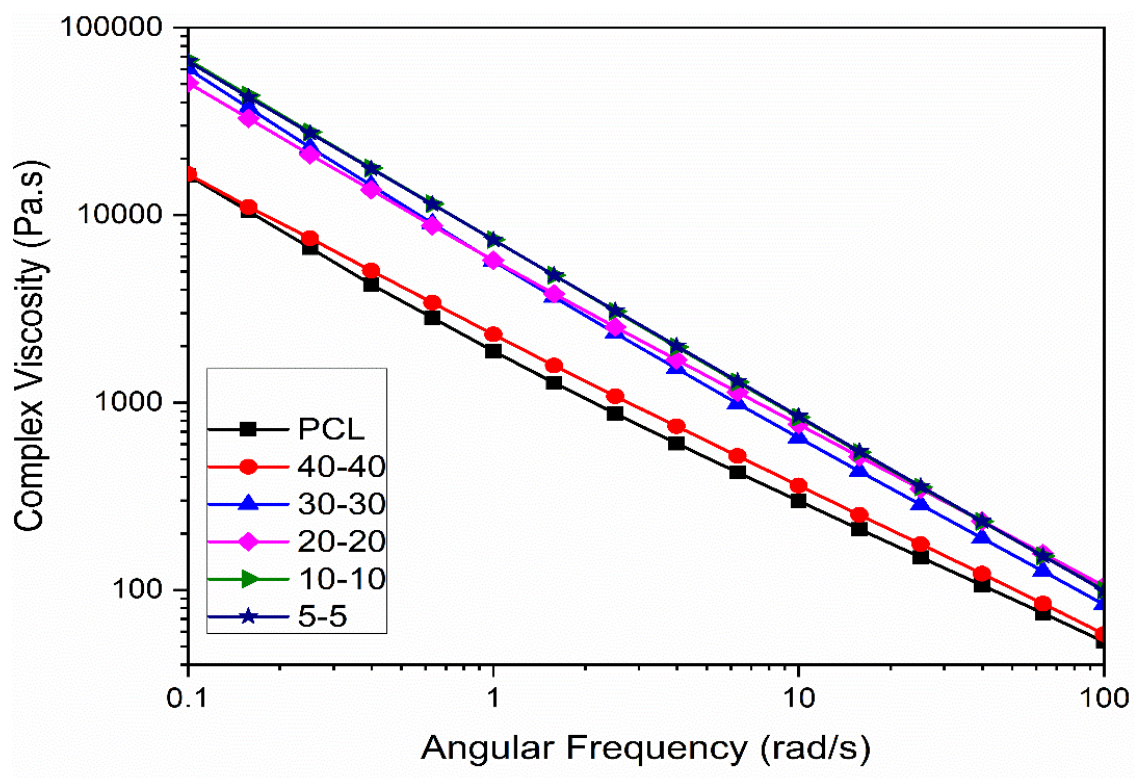


Figure 5.4 Complex viscosity of PCL and PCL-PDMS-PCL triblock polymer at 80°C.

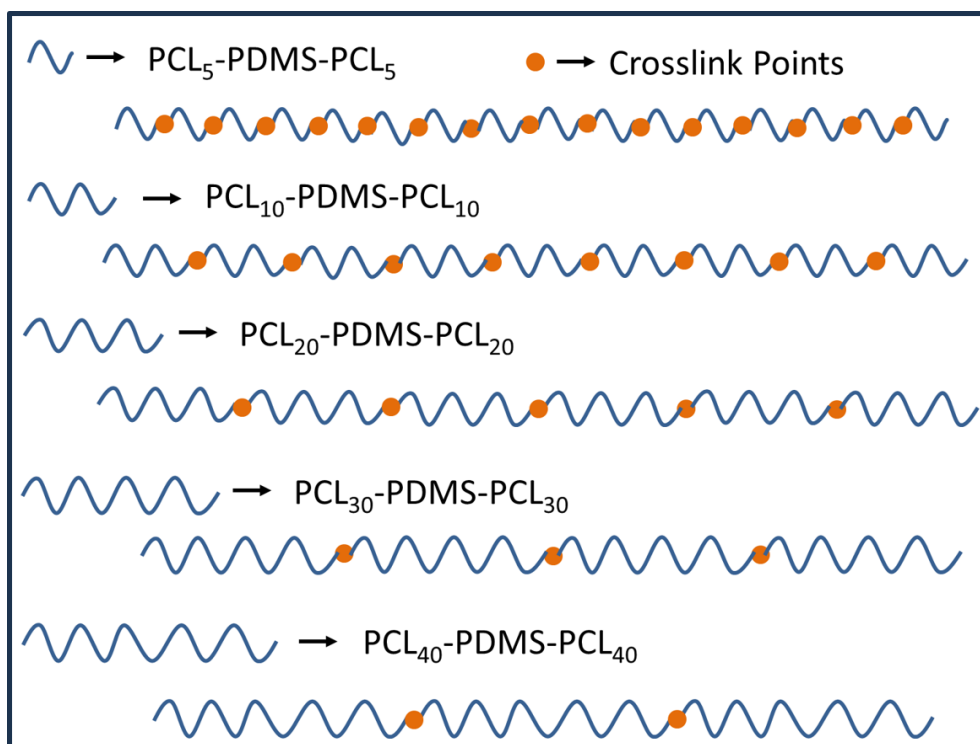


Figure 5.5. Pictorial presentation of PCL-PDMS-PCL photo-crosslinked copolymer, with increase in PCL chain length, crosslink points decreases and overall crosslink density decreases

The frequency dependant viscosity function, also known as complex viscosity was determined in frequency range 0.1 to 100 rad/s. The complex viscosity shows increase in values with increase in crosslink density as shown in Figure 5.4. At lower frequency viscosity is high and keeps decreasing with increasing frequency shows a complete shear thinning behaviour as shown in Figure 4. Shear thinning fluids are non-Newtonian fluids that display decreasing viscosity with increased shear rate and account for the majority of non-Newtonian fluid flows. Because shear-thinning materials are commonly used in everyday activities and in industries, their behaviour has gotten a lot of study in recent decades[250].

5.3 Creep and Creep recovery behaviour

Creep and creep recovery experiments are used to assess the dimensional stability of polymeric material by understanding their time dependent viscoelastic deformation behaviour under constant stress and temperature[251]. The creep recovery test was done by applying a load of 10 Pa for 300 sec and then removed for another 600 sec. The change in strain percentage with time after removal of load used to evaluate creep recovery results as shown in Figure 5.6(a). When a constant load applied, a maximum deformation of 1.2% in PCL, 3.5% in 40-40, 2.0% in 30-30, 0.7% in 20-20, 0.2% in 10-10 and 0.16% in 5-5 was observed. After release of load, films recovered the deformation, and showed permanent deformation of 0.5% in PCL, 2.5% in 40-40, 1.6% in 30-30, 0.2% in 20-20, 0.02% in 10-10 and 0.003% in 5-5. In other words, creep recovery happened of 58% in PCL, 29% in 40-40, 20% in 30-30, 71% in 20-20, 90% in 10-10 and 98% in 5-5. The 40-40, 30-30 and PCL showed high creep due to higher crystalline content because of more semi-crystalline PCL content and lesser creep recovery due to less crosslink density. Whereas, in 20-20, 10-10 and 5-5 very less creep observed due to higher viscous content in the form of PDMS and high recovery because of high crosslink density. Wang *et al.*[30] reported creep and recovery for PCL/cellulose nanocrystal (CNC) nanocomposite. PCL of molecular weight showed creep of around 37%

while lower creep reported for PCL/CNC nanocomposite system due to percolation of filler and no recovery was reported after removal of load.

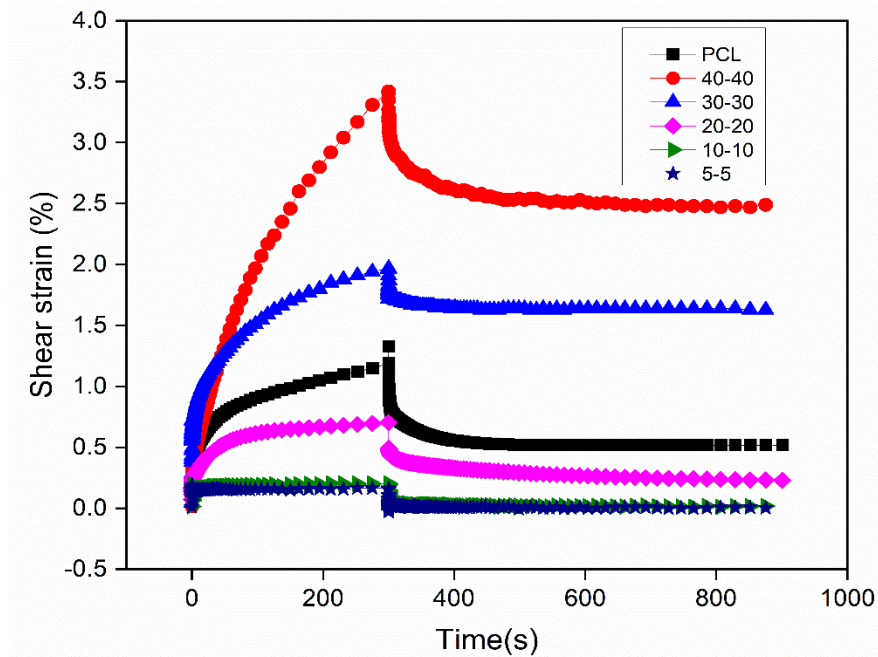


Figure 5.6(a). Creep and creep recovery of PCL and PCL-PDMS-PCL triblock polymer at 80°C.

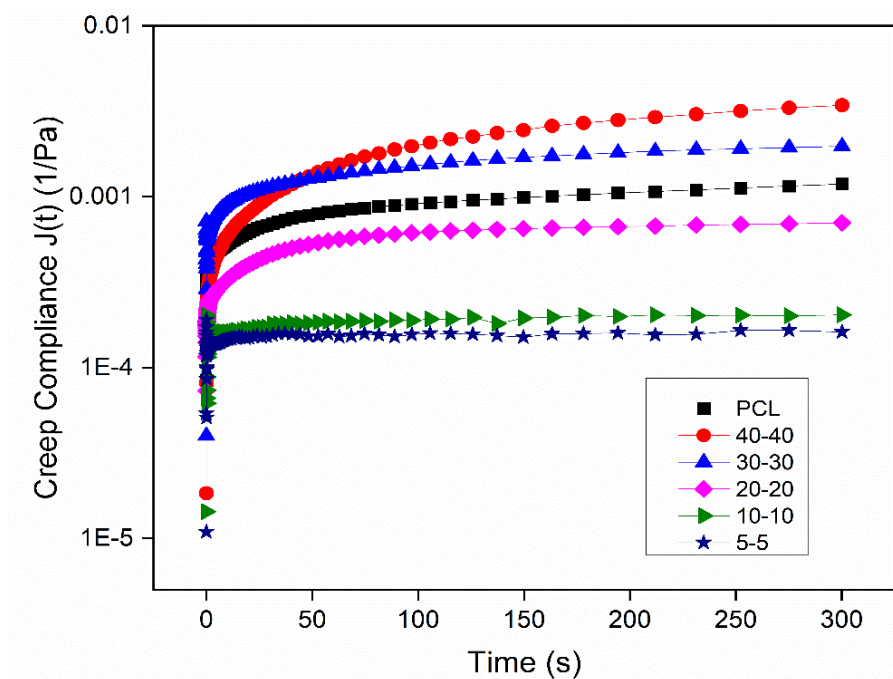


Figure 5.6(b). Creep compliance of PCL and PCL-PDMS-PCL triblock polymer at 80°C

The Creep Compliance, $J(t)$, is defined as change in strain as a function of time under constant load applied instantaneously and provide a method to measure a material's ability to flow under instant load applied. For a linear viscoelastic material, creep compliance doesn't change with applied stress due to linear relationship between stress and strain. All samples show initial increase in $J(t)$ then it became constant with time which implies viscoelastic behaviour of all compositions as shown in Figure 5.6(b). The primary factor affecting rate of creep compliance is weight average molecular weight (M_w) or entanglement distance of the polymer[252]. The creep compliance rate of the copolymers of varying M_w differs noticeably, with the PCL copolymer of bigger M_w indicating the higher rate of contact creep compliance.

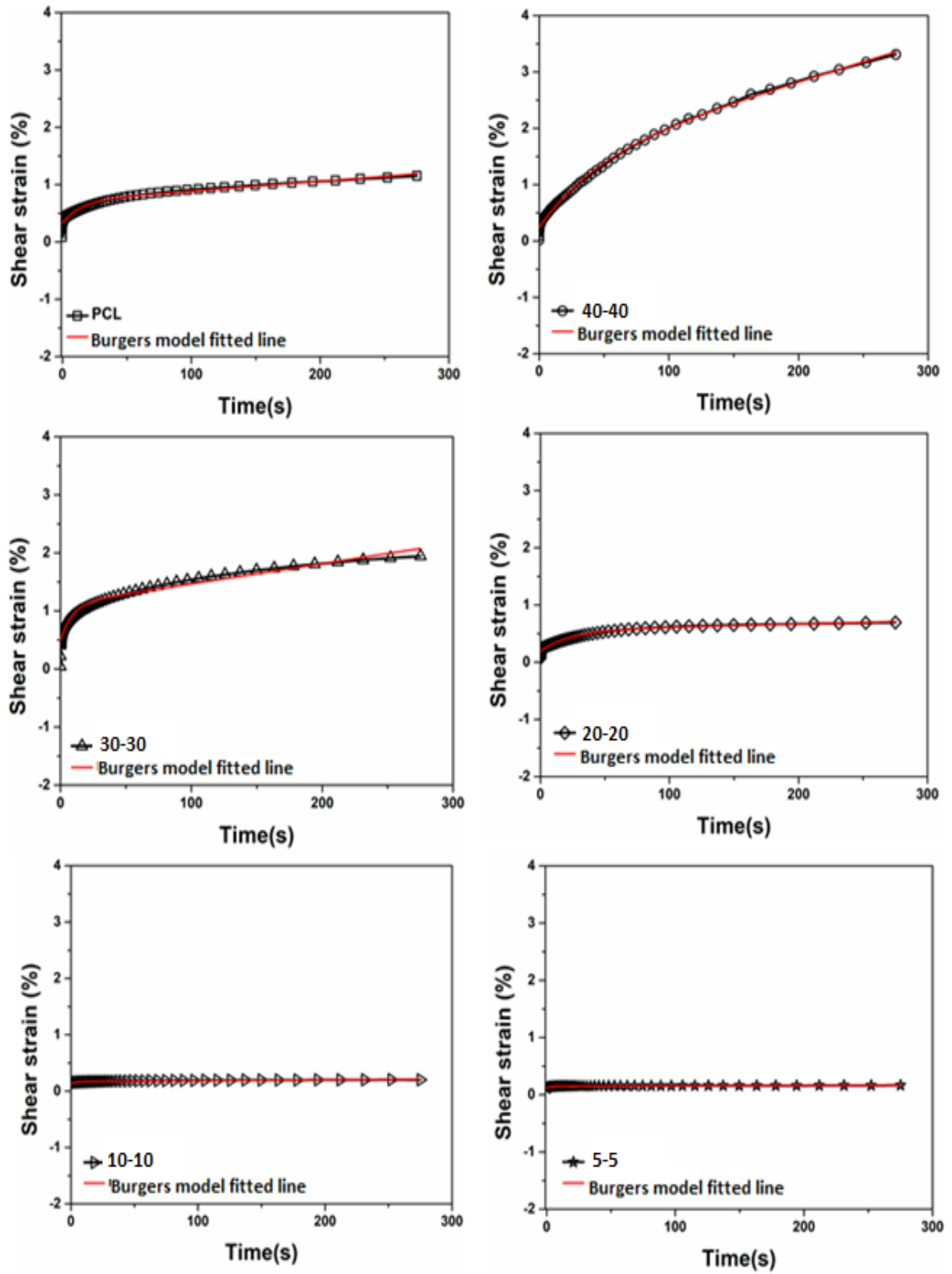


Figure 5.6(c). Burgers model fitting on the creep strain responses for PCL and PCL-PDMS-PCL triblock polymer

Table 5.1. Parameters of the fittings of Burgers model on the creep behaviour of PCL/PCL-PDMS-PCL triblock photocrosslinked copolymers

Samples	E_E (Pa)	E_{Ve} (Pa)	η_{Ve} (Pa.s)	η_{Vv} (Pa.s)	R^2
PCL	38.42	25.93	373.19	1434.72	0.982
40-40	38.58	8.37	386.79	2864.00	0.992
30-30	45.54	16.65	466.47	5828.68	0.919
20-20	50.92	27.78	669.70	17939.28	0.978
10-10	76.24	253.61	749.41	68209.17	0.981
5-5	87.37	300.5	862.84	148283.1	0.976

The theoretical description of the creep responses, on the other hand, can still be used to investigate some relaxation features. In general, three basically distinct components contribute to total strain ($\epsilon(t)$) during creep: elastic (ϵ_E), viscoelastic (ϵ_{Ve}), and viscous (ϵ_{Vv}) as per below equation (5.1):

$$\epsilon(t) = \frac{\sigma}{E_E} + \frac{\sigma}{E_{Ve}} \left[1 - \exp\left(-\frac{tE_{Ve}}{\eta_{Ve}}\right) \right] + \frac{\sigma}{\eta_{Vv}} t \quad (5.1)$$

Where E_E is the instantaneous elastic modulus of the Maxwell region, E_{Ve} is elastic modulus of Kelvin-Voigt unit, η_{Ve} and η_{Vv} are viscosities in viscoelastic and viscous regions, σ is the applied stress and t is the creep time. As the stress is applied, the initial strain (ϵ_E) occurs in the spring with the modulus E_E , and the later strain ($\epsilon_{Ve} + \epsilon_{Vv}$) is generated in parallel from the spring E_{Ve} , dashpot η_{Ve} from Maxwell element representing the residual viscosity and dashpot η_{Vv} from Kelvi-Voigt model stands for internal viscosity. This is known as four-parameter Burgers model which is a combination of Maxwell model and Kelvin-Voigt model used to analyse system deformation as shown in Figure 5.5(c). It is feasible to compare the internal structure of various systems by computing the values of E_E , E_{Ve} , η_{Ve} and η_{Vv} [30, 253]. It can be seen from Table 5.1 that elastic modulus E_E associated with Maxwell model which measure elastic strain that could recovered immediately after elimination of stress keep

increasing with PCL chain length and almost similar for PCL and 40-40. The viscoelastic strain due to molecular rearrangement shows higher relaxation scale than polymeric chain. The viscoelastic modulus of PCL is quite high due to high crystallinity and crosslink structure both and then in copolymers it increases with increasing crosslink density. The increase in residual viscosity and internal viscosity is having the same pattern as seen in complex viscosity results. The PCL/CNC composite system also follows Burgers model, where elastic moduli increases with higher filler content due to formation of percolation network as reported by Wang *et al.*[30]

5.4 Structure Recovery

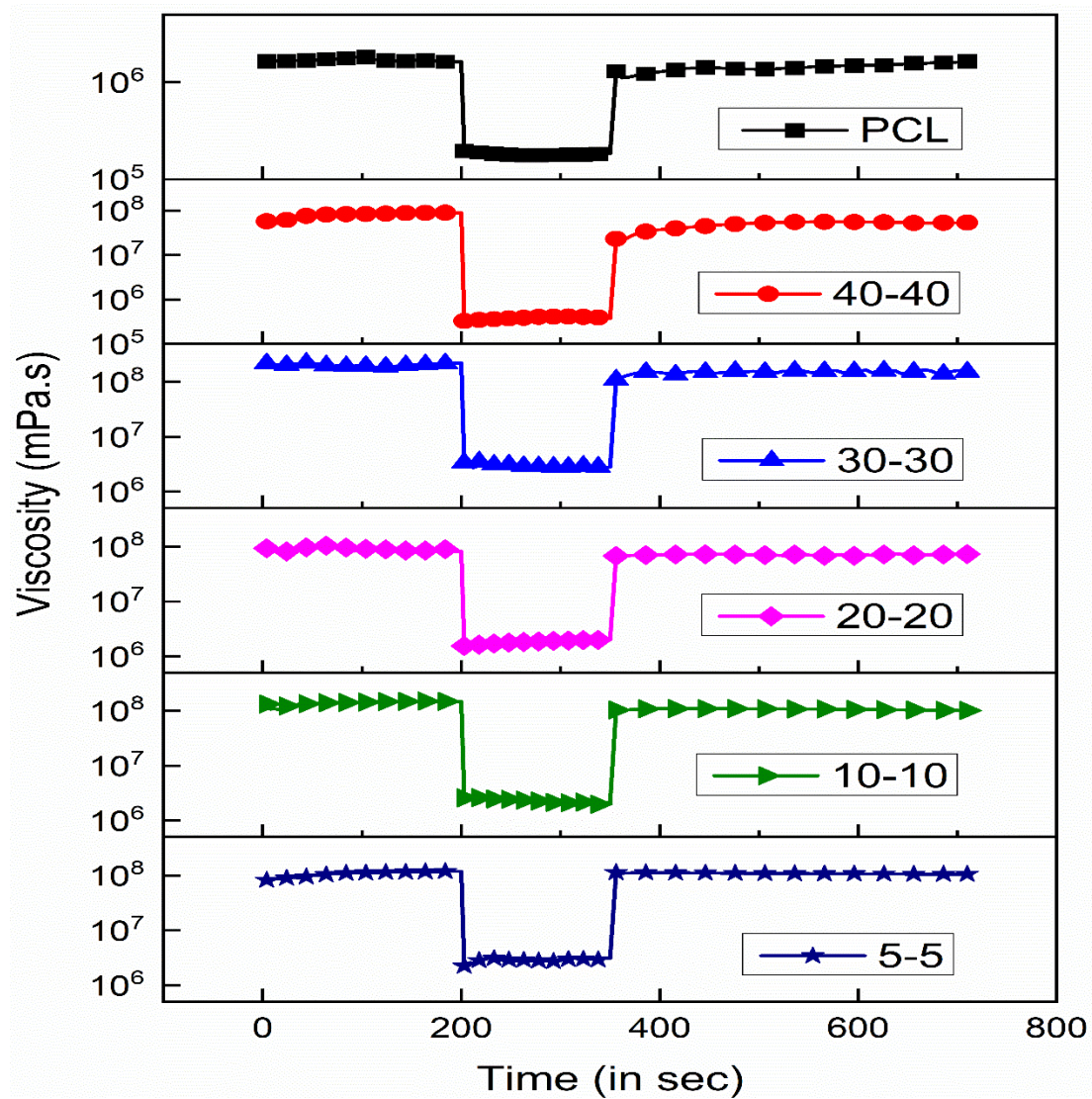


Figure 5.7. Structure recovery of PCL and PCL-PDMS-PCL triblock polymer at 80°C

The structural behaviour of polymer melts is examined by rotational shear test against time which provides time dependent viscosity in three intervals of shear stress applied. For structure recovery study a low shear (rest) applied after being subjected to strong shear, exhibit change in viscosity which represents structure regeneration. Each sample shows high viscosity in first interval (Low shear or rest), then drastic change observed in viscosity under high stress as shown in Figure 5.7. In first interval higher the viscosity indicates, greater the entanglement and viscosity increase with increasing crosslink density as seen in complex viscosity results. When high shear is applied, the viscosity decreases and remains constant throughout the high shear period, and when again low shear is applied, the polymer melt regenerates its structure which resulted in increase in viscosity. Regeneration of structure is found almost 86% in PCL, 72% in 40-40, 81% in 30-30, 93% in 20-20, 98% in 10-10 and 100% in 5-5 which represent high crosslink density helps to regenerate complete structure though samples possess lesser crosslink density which have higher semi-crystalline PCL chain length couldn't reform their structure. As crystalline part become viscous over T_{cm} and cannot contribute in structure recovery in melted form but crosslink point helps to recover the structure in better way as they are intact at processing temperature.

5.5 Tensile Properties and Dynamic Mechanical Analysis

Tensile properties are investigated to assess the impact of PCL chain length on mechanical properties under ambient conditions. Table 5.2 displays the PCL and PDPCL triblock copolymer films' tensile strength and percentage elongation at breakage. There is decrease in percentage crystallinity as the PCL chain length reduces and increase in the crosslink density. Tensile strength (TS) decreases from 11.2 MPa for PCL to 0.4 MPa for PDPCL5 to and percentage elongation decreases from 980% (PCL) to 30% (PDPCL5). Here results are dependent on both percentage crystallinity and crosslink density because these characterizations are carried out ambient temperature ($\sim 25^{\circ}\text{C}$) which is below than T_{cm} of all

samples. So, it can be said that decrease in tensile strength is caused by a reduction in PCL crystalline domains because PCL chain length acts as physical crosslinks to reinforce the network at ambient temperature even when the crosslink density falls. Similar results of tensile study are reported by Schoener *et al.*[12]

Table 5.2. Mechanical properties of PCL-PDMS-PCL triblock copolymer films

Samples	Tensile strength (MPa)	Elongation at break (%)
PCL	11.2 ± 0.6	980 ± 0.1
40-40	10.8 ± 0.4	920 ± 0.1
30-30	7.6 ± 0.5	460 ± 0.1
20-20	4.8 ± 0.4	350 ± 0.1
10-10	1.4 ± 0.3	98 ± 0.1
5-5	0.4 ± 0.1	30 ± 0.1

To evaluate thermomechanical properties at nanoscale, DMA experiments are performed and results are given in Figure 5.8. The storage modulus temperature plot (Figure 5.8(a)) at room temperature of 32°C shows highest modulus for PCL of (1.35×10^9 Pa), then 4.87×10^8 for 40-40, 2.53×10^8 for 30-30 and 1.68×10^8 for 20-20. The storage moduli are high for sample with higher percentage crystallinity as they are tested at well below temperature of their respective transition temperature (T_{trans}). With increase in temperature the storage modulus of each composition starts decreasing and while going above the transition temperature. At above T_{trans} the crystalline region become melt and playing factor for storage modulus is crosslink density. With decrease in molecular weight crosslink density keep increasing and accordingly storage modulus become higher for lower molecular weight composition as seen in Figure 5.8(a). $\tan \delta$ provides valuable information about the dissipation capability of the material when subjected to cyclic loads, with temperature gradients releasing heat rather than storing

them as energy. Figure 5.8(b) shows the $\tan \delta$ vs. temperature plot indicates predominant elastic behaviour of all composition below T_{trans} . As the temperature goes above T_{trans} of individual composition, with increase in temperature the elasticity is increasing in the order of 20-20, 30-30, 40-40 and PCL. This increase in $\tan \delta$ values can thus be attributed to the interlaced polymer chains slipping over each other but kept intact due to crosslink points which helps to maintain elasticity of specimen. PCL/ α -cyclodextrin (CD) based nanofibers examined by Narayanan *et al.* exhibit increase in storage modulus and elasticity with addition of CD.[21]

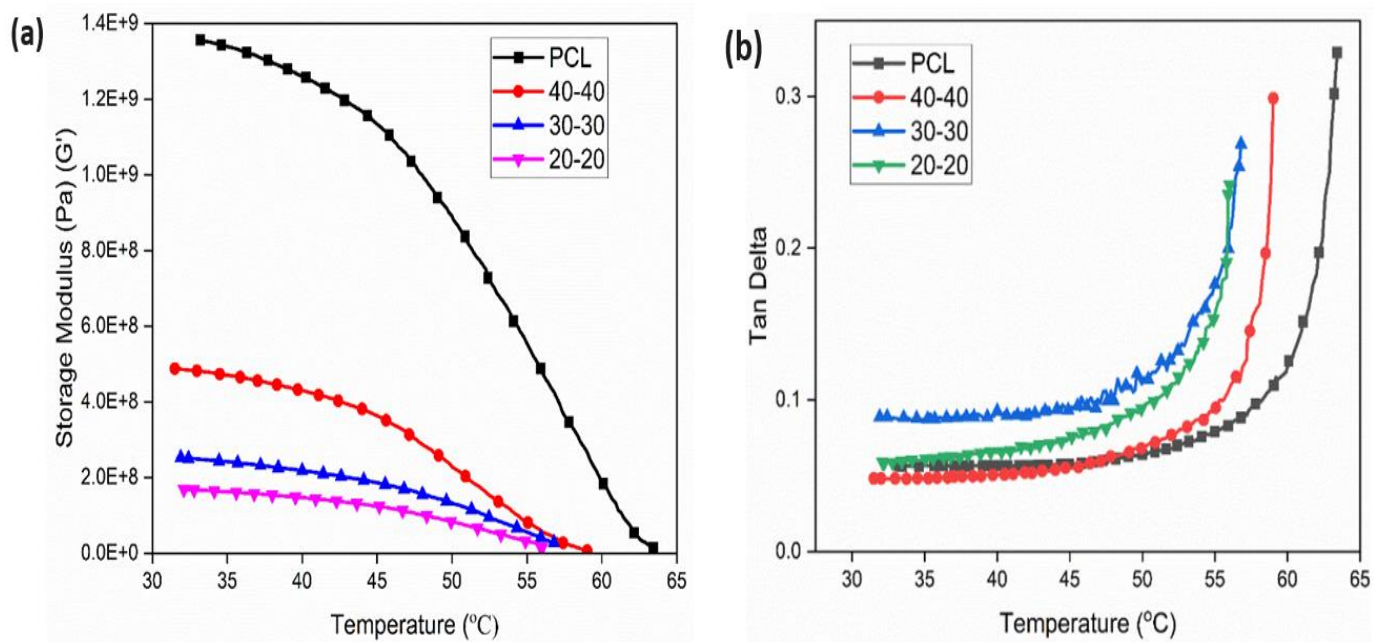


Figure 5.8. Dynamic mechanic analyses profiles of PCL, PDPCL40, PDPCL30 and PDPCL20 (a) Storage modulus and (b) $\tan \delta$ vs. temperature

5.6 Conclusion

The rheological analysis of PCL and PCL-PDMS-PCL triblock copolymer films at 80°C (well above T_{cm} of all samples) is dependent on crosslink density and molecular weight. The linear viscoelastic region of PCL is up to 10% shear strain and for copolymers it is up to 1%. Based on amplitude sweep results, the frequency sweep is carried out at 1% shear strain for all samples. but crossover point seen above 10%. In Frequency sweep, the storage modulus

of PCL and its copolymer is increasing with decreasing molecular weight. Due to increased crosslinked density with decreasing molar mass increase in storage modulus, decrease in loss factor and more solid like behaviour. Creep recovery happened of 58% in PCL, 29% in 40-40, 20% in 30-30, 71% in 20-20, 90% in 10-10 and 98% in 5-5. Regeneration of structure is found almost 86% in PCL, 72% in 40-40, 81% in 30-30, 93% in 20-20, 98% in 10-10 and 100% in 5-5 which represent high crosslink density helps to regenerate the structure of molecular chains. The mechanical strength and dynamic behaviour analysis at ambient temperature shows that tensile strength, elongation, storage modulus is decreasing with decrease in PCL chain length because PCL crystalline domains acts as physical crosslinks to reinforce the network at ambient temperature even when the crosslink density falls

Chapter 6

Thermal Characterization of PCL-PDMS-PCL Triblock

Overview

This chapter gives an insight about thermal properties of PCL-PDMS-PCL triblock copolymer films. The thermal properties are studied by optical microscopy for crystal formation, Thermal gravimetry analyser, Differential Scanning Calorimetry in both non-isothermal as well as isothermal mode. The crystal formation after melting point is observed by optical microscope. The non-isothermal mode of DSC is used to study about crystal melting temperature (T_{cm}) range and crystallization temperature (T_c). The percentage crystallinity is also evaluated with DSC results. The T_{cm} and T_c range is used to study the thermal properties in isothermal mode. In isothermal mode of DSC, crystallization kinetics has been studied with the help of Avrami model and Lauritzen-Hoffman (LH) model to quantify energy barrier associated with nucleation and crystal growth. With decrease in PCL chain length, the supercooling range for crystallization shifted to lower temperature gradually and increased the nucleation factor.

6.1 Optical Microscope

PCL-PDMS-PCL triblock copolymer films made up of crystalline (PCL)-amorphous (PDMS) blocks display interesting morphological behaviour with varying the chain length of PCL. The structure of the crystalline domains formed for PCL, 40-40, 30-30 and 20-20 are analysed by optical microscopy (OM) imaging, as shown in Figure 6.1. No crystal structure is observed for 10-10 and 5-5 films. The crystals of PCL homopolymer are overlapping each other and most of the crystallite cannot be seen in separate domain. To analyse effect on PCL

crystallinity due to copolymerization, the crystal structure of homopolymer is used as a reference.

The inclusion of PDMS strongly affects the nucleation, size of crystallite and rate of crystallization while varying the PCL chain length. For 40-40, 30-30, 20-20 samples, insertion of PDMS shows phase separated micro-regions dispersed between the crystalline domains of PCL. There is a restriction in PCL crystal growth because PCL blocks are restrained between PDMS matrix and therefore are limited in sizes, although there is non-uniform size distribution. It can be seen from optical images that size of crystal becomes slightly smaller and crystal domains are well segregated, decreasing the block length of PCL and keeping the PDMS content constant. Despite the short chain length of PCL and lower content, crystalline PCL domain development is apparent. The difference in solubility parameters and negligible intermolecular interactions between PCL and PDMS create a suitable platform to form microphase-separated crystals of PCL. The length of the PDMS and PCL block chains influences the extent of crystallization. The copolymers samples of 40-40, 30-30 and 20-20 show microphase separated morphologies but are independent of block lengths or compositions.

Wu *et al.* reported polarized optical images of block copolymer of cyclic butylene terephthalate and PCL at different cooling rates of 5°C/min and 1°C/min, where inclusion of PCL decreases the crystallization temperature and mixed type spherulitic morphology is observed.[154] Diblock copolymer of PLLA and PCL morphological studies showed that increasing block length of PCL influenced the twist of PLLA lamellae and formed non-banded spherulitic structure as studied by Han *et al.*[69]

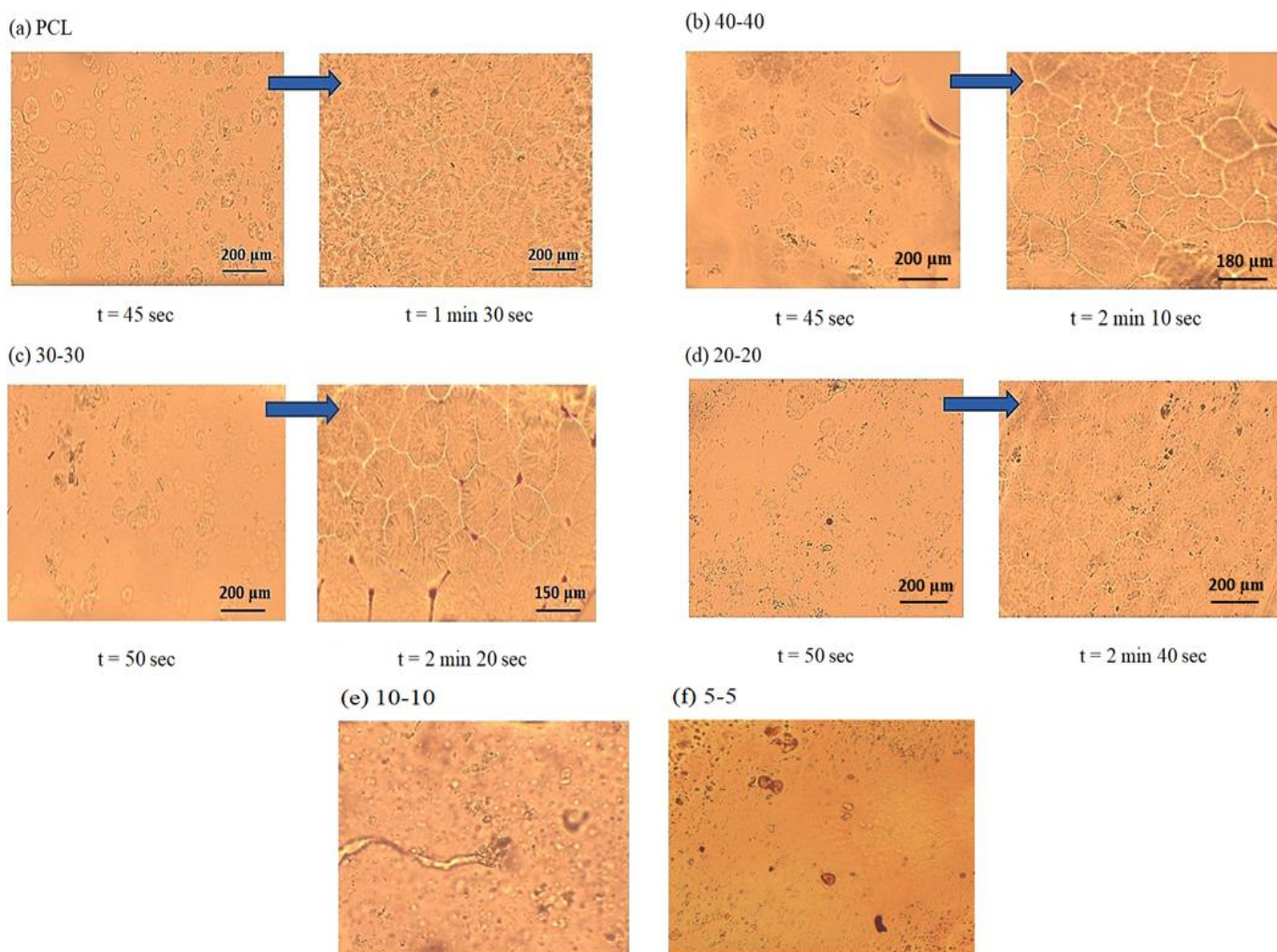


Figure 6.1. Optical images of crystallized films at time (a) $t = 45$ sec to 1 min 30 sec for PCL (b) $t = 45$ sec to 2 min 10 sec for 40-40 (c) $t = 50$ sec to 2 min 20 sec for 30-30 (d) $t = 50$ sec to 2 min 30 sec for 20-20 (e) 10-10 and (f) 5-5

6.2 Thermal Gravimetric Analysis

The thermal degradation behaviour of PCL and PCL-PDMS-PCL photo-crosslinked films is analysed by TGA curves as shown in Figure 6.2. All the samples show single step thermal degradation. Neat PCL, its copolymers and composite[11, 18, 28, 246] shows single degradation curve whereas its blends with polylactic acid[33] and thermoplastic starch[24] shows two steps degradation as reported by earlier researchers. Compared to PCL homopolymer photo-crosslinked films, PCL/PDMS copolymer films are showing significant

increase in thermal stability. This is because of inclusion of PDMS block which is chemically bonded with PCL and increased crosslink density. With increase of PDMS content and photocrosslink density the stability increases. Poojari *et al.* also reported inflation in thermal stability with increase in PDMS content for PCL/PDMS copolymers with assumption of more thermally stable crosslinked product formed due to combination of free radicals[11]. The decomposition temperature (temperature at which 10% mass loss has occurred)[246] for PCL is 334°C and increases for PDPCL40, PDPCL30, PDPCL20, PDPCL10, PDPCL5 340°C, 346°C, 354°C, 356°C, 363°C respectively. 100% degradation occur for PCL, PDPCL40, PDPCL30, PDPCL20 and there is 2.4% and 4.7% residue left for PDPCL10 and PDPCL5 at 700°C.

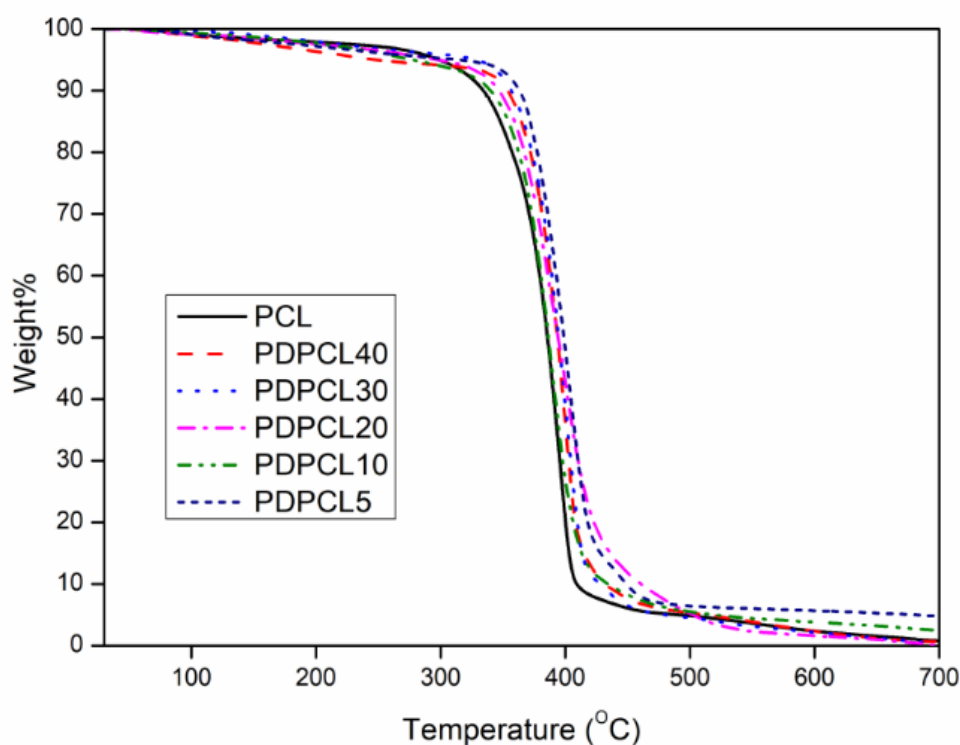


Figure 6.2. TGA curves of PCL and PCL-PDMS-PCL photo-crosslinked films

TGA results show that inclusion of PDMS block in triblock films has small effect on onset temperature (Temperature at which 5% weight loss occurred) of the samples. Indeed, a slight decrease in the onset temperature is observed for copolymer films while comparing with PCL

homopolymer film. This result is unexpected since inclusion of PDMS and increased crosslink density are enhancing the other thermal stability parameter as seen in decomposition temperature and residue content. A similar observation is reported by *Bouakaz et al.* where decrease in onset temperature of PCL/cloisite30B/cloisite15A/graphene nanocomposites is due to the catalytic effect induced through organic modifier degradation[28].

6.3 Differential Scanning Calorimetry (DSC)

6.3.1 Non-Isothermal

A non-isothermal DSC thermogram of pure PCL and PCL-PDMS-PCL triblock copolymeric films of varying PCL chain length is shown in Figure 6.3. Crystal melting temperature (T_{cm}), enthalpy change (ΔH_m) and degree of crystallinity X_c (%) are measured from the endothermic melting peak of the first cycle. The degree of crystallinity X_c (%) is calculated with equation (6.1) given below:

$$X_c (\%) = \frac{\Delta H_m}{\Delta H_m^0} \times 100 \quad (6.1)$$

where ΔH_m is enthalpy of crystal melting peak for that particular sample and ΔH_m^0 is the enthalpy of fusion of 100% crystalline PCL (139.5 J g^{-1}). [12] The degree of crystallinity, crystal melting temperature range (T_{cm}) and crystallization temperature (T_c) range are tabulated in Table 6.1. T_{cm} range shifted to lower temperature gradually with decreasing PCL chain length in copolymer. T_{cm} for PCL, 40-40, 30-30, 20-20 and 10-10 are observed at 53.5, 52.2, 49.7, 43.5 and 33°C, respectively. The shortest PCL chain length sample of 5-5 showed no T_{cm} . With the decreasing PCL chain length, the degree of crystallinity also decreases from 37% to 2.9%, supported by similar trend obtained in XRD.

T_c for PCL, 40-40, 30-30 and 20-20 are observed at 30.8, 26.3, 21.1 and 0.5 °C, respectively. For 10-10 and 5-5, no crystallization peak is observed in thermogram. T_c is shifting to lower degrees with decrease in PCL chain length. The absence of crystallization peak in 10-10 and 5-5 samples inferred that very less PCL content resulted in no formation of crystal and it is further not useful for study of isothermal crystallization and shape memory properties.

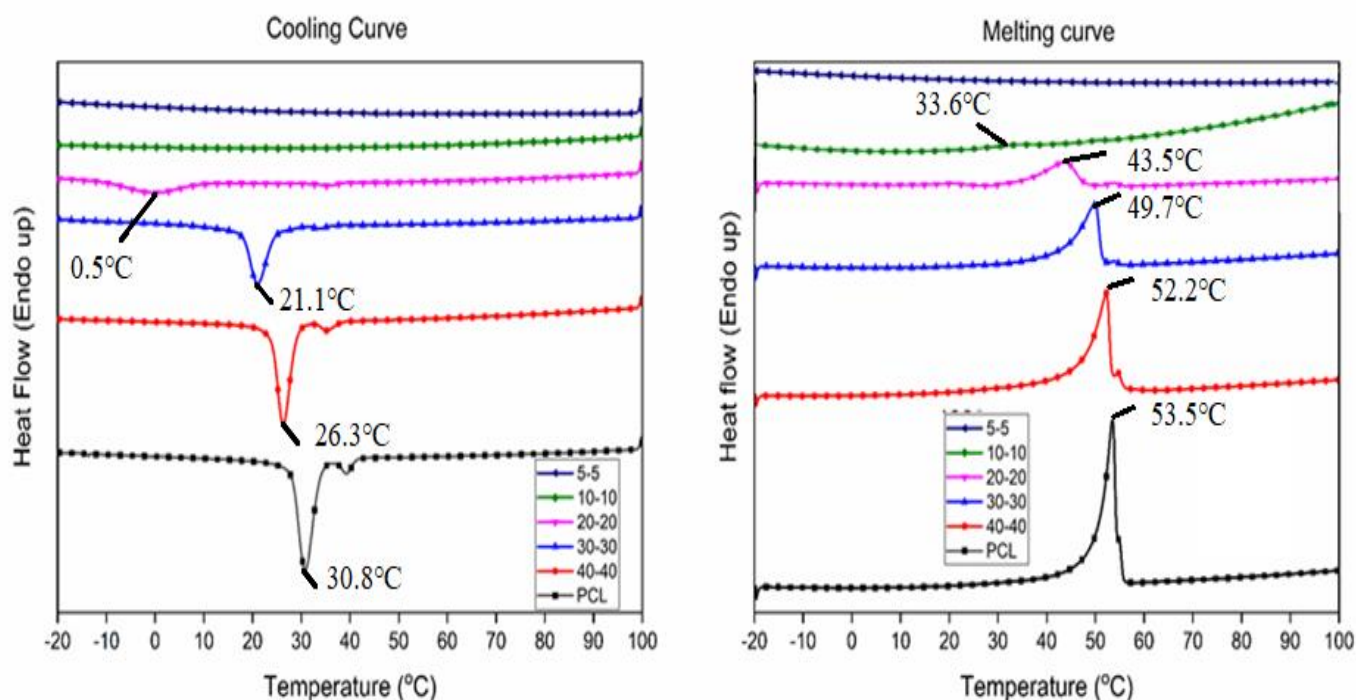


Figure 6.3. DSC thermograms of PCL and PCL-PDMS-PCL triblock copolymer films

Yilgor *et al.*[10] synthesized PCL-PDMS-PCL triblock copolymer with different M_n of PDMS block reported XRD crystallinity from 37% to 65% with increasing PCL content which is supported by DSC results from 34% to 67% on the basis of PCL content. Azemar *et al.*[14] reported crystallinity varying from 60% to 16% with decreasing PCL molecular weight and content in triblock copolymer with PDMS. In case of PCL homopolymer of molecular weight 3000 and 9000 g/mol, the percentage crystallinity is 60 to 54.4 % which is higher than PCL crystallinity reported in this study. This may be due to difference in initiator from ethylene glycol to butan-1-ol and use of different solvents, THF and petroleum ether, for precipitation. Schoener *et al.*[12] reported DSC crystallinity for PCL-PDMS-PCL with

M_n 3000 g/mol of PDMS block and PCL chain length varying from 50-50 to 20-20 is 36% to 17% and T_{cm} 51°C to 34°C. Poojari *et al.*[11] reported 54% to 45% crystallinity by DSC on the basis of PCL content with T_{cm} 55°C to 35°C. These significant variations in T_{cm} of triblock copolymeric films help to develop products for biomedical and packaging applications.

6.3.2 Isothermal

During the formation of the crystalline phase, the isothermal crystallization exothermic curves of PCL and PCL-PDMS-PCL triblock polymer are recorded. The following equation (6.2) is used to calculate relative crystallinity (X_t) at different crystallization times.

$$X_t = \frac{Q_t}{Q_\infty} = \frac{\int_{t_0}^t \left(\frac{dH}{dt}\right) dt}{\int_{t_0}^{\infty} \left(\frac{dH}{dt}\right) dt} \quad (6.2)$$

where Q_t is the enthalpy released at time t and Q_∞ is the enthalpy liberated at infinite time, respectively; t_0 represents the time when the sample enters isothermal state, and dH/dt is the heat flow rate. Figure 6.4 represents the plots of relative crystallinity X_t versus time t for PCL and PCL-PDMS-PCL triblock copolymeric films. Since crystallization temperature for 10-10 and 5-5 film samples does not observe, isothermal crystallization kinetics was carried out for 20-20, 30-30 and 40-40 samples along with PCL. All the crystallization isotherms have typical sigmoid curves, as shown in Figure 6.4. With rising crystallization temperature T_c , these isotherms move to the right along the time axis. The slope of isotherms reduces with increasing T_c , representing successively slower crystallization rates, as can be seen in every individual graph. In comparison to PCL isotherms, copolymers with decreasing PCL chain length are plotted at lower degrees of temperature as per their respective non-isothermal crystallization temperature range.

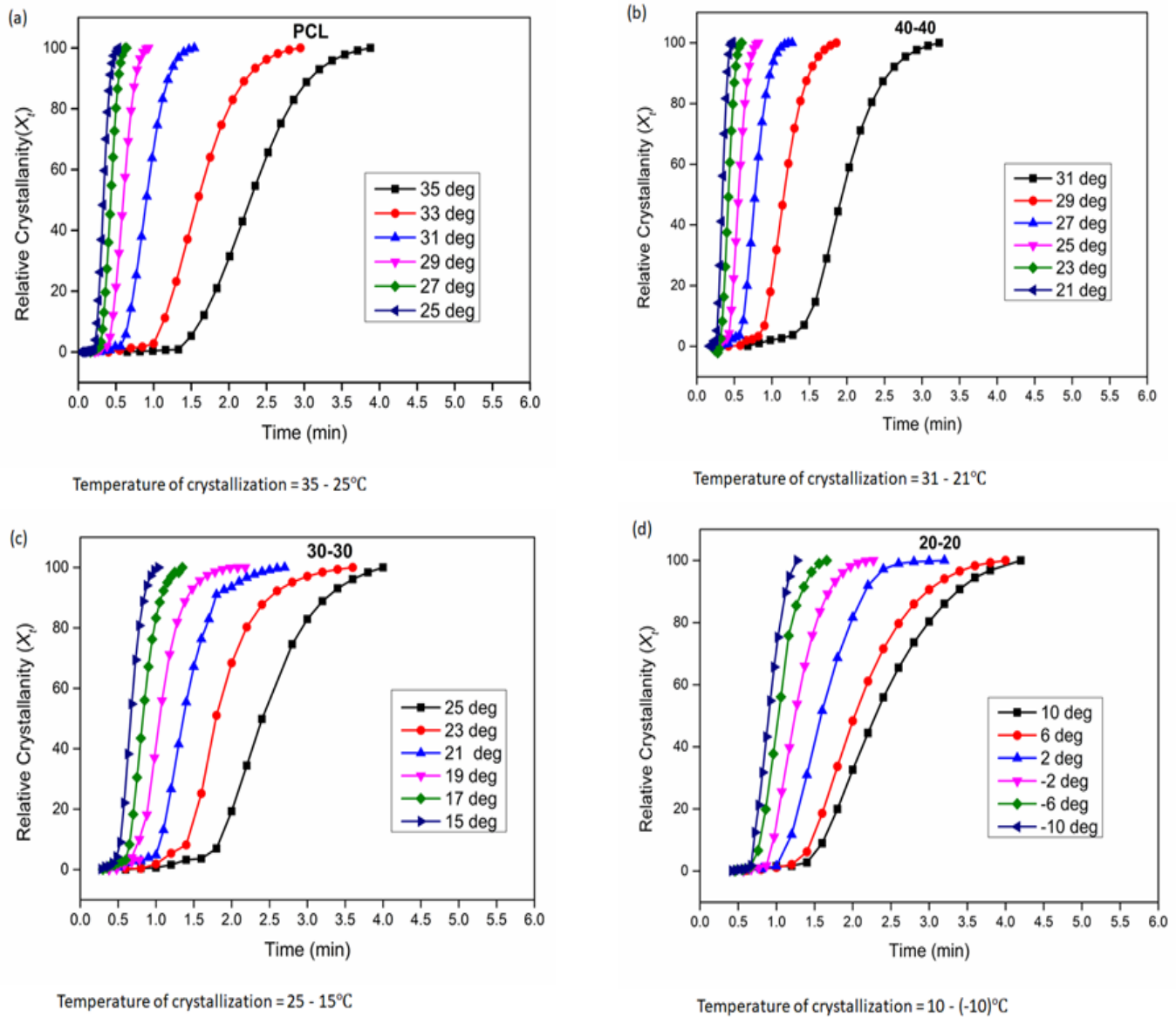


Figure 6.4. Plot of relative crystallinity for (a) PCL, (b) 40-40, (c) 30-30 and (d) 20-20 PCL-PDMS-PCL triblock copolymer films

There is a modest rise in crystallinity with time after most of the crystallization has occurred, which is attributed to the occurrence of secondary crystallization. The time dependency is investigated under the assumption of two crystallization processes, primary and secondary. Time required to achieve 50% crystallinity from these curved is defined as crystallization half-time $t_{1/2}$, which is used to describe the overall rate of crystallization. Higher value of $t_{1/2}$ represents the lower rate of crystallization. Plots of the obtained $t_{1/2}$ values against T_c for pure PCL and PCL-PDMS-PCL copolymers are shown in Figure 6.5. There is no significant

change observed in overall crystallization for different samples as each one is examined at its own crystallization temperature range, as seen in Figure 6.5. The $t_{1/2}$ values are summarized in Table 6.2 of 2.2, 1.95, 2.4 and 2.5 mins for PCL, 40-40, 30-30 and 20-20, respectively. Ninago *et al.* have studied that branches of poly(2- hydroxyethylmethacrylate) (PHEMA) hinder the formation of PCL crystallites by increasing final crystallization time in case of PCL/PHEMA graft copolymer.[151] In a study by Nie *et al.*[254] on tetraethyl orthosilicate and PCL blends, the rate of crystallization decreases with decrease in ratio of PCL.

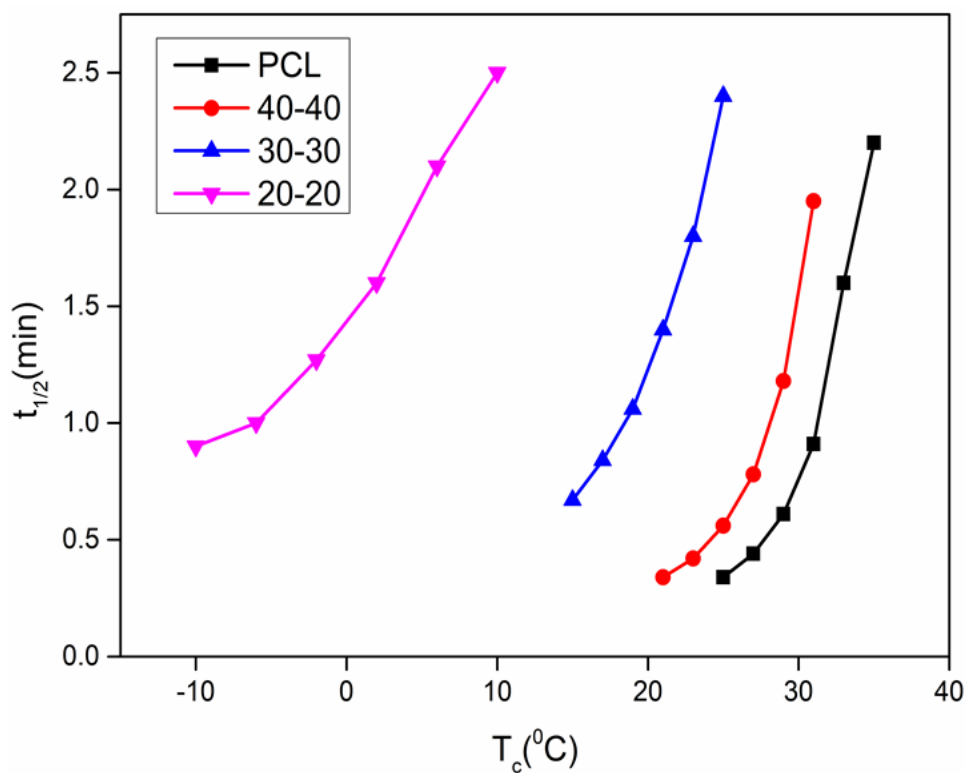


Figure 6.5. Plot of crystallization half-time $t_{1/2}$ against crystallization temperature T_c for PCL and PCL-PDMS-PCL triblock copolymeric films

The Avrami equation (6.3), as given below, is used to analyze the isothermal crystallization kinetics of various PCL-PDMS-PCL copolymeric films:

$$1 - X_t = \exp(-Z_t t^n) \quad (6.3)$$

where X_t is the relative crystallinity, Z_t is the overall kinetic rate constant including the nucleation and growth parameters, t is the time, and n is the Avrami index, which depends on

the nucleation and growth mechanism of the crystals. Taking double logarithmic of equation (6.3), it can be rewritten as equation (6.4):

$$\log[-\ln(1 - X_t)] = \log Z_t + n \log t \quad (6.4)$$

The plot of $\log[-\ln(1 - X_t)]$ against $\log t$ should be a straight line with slope n and intercept $\log Z_t$ if Avrami equation is applicable to explain the crystallization behavior of PCL in the copolymers. Avrami equation is advised to fit in initial experimental data of conversion to minimize the error and maximize R^2 value.

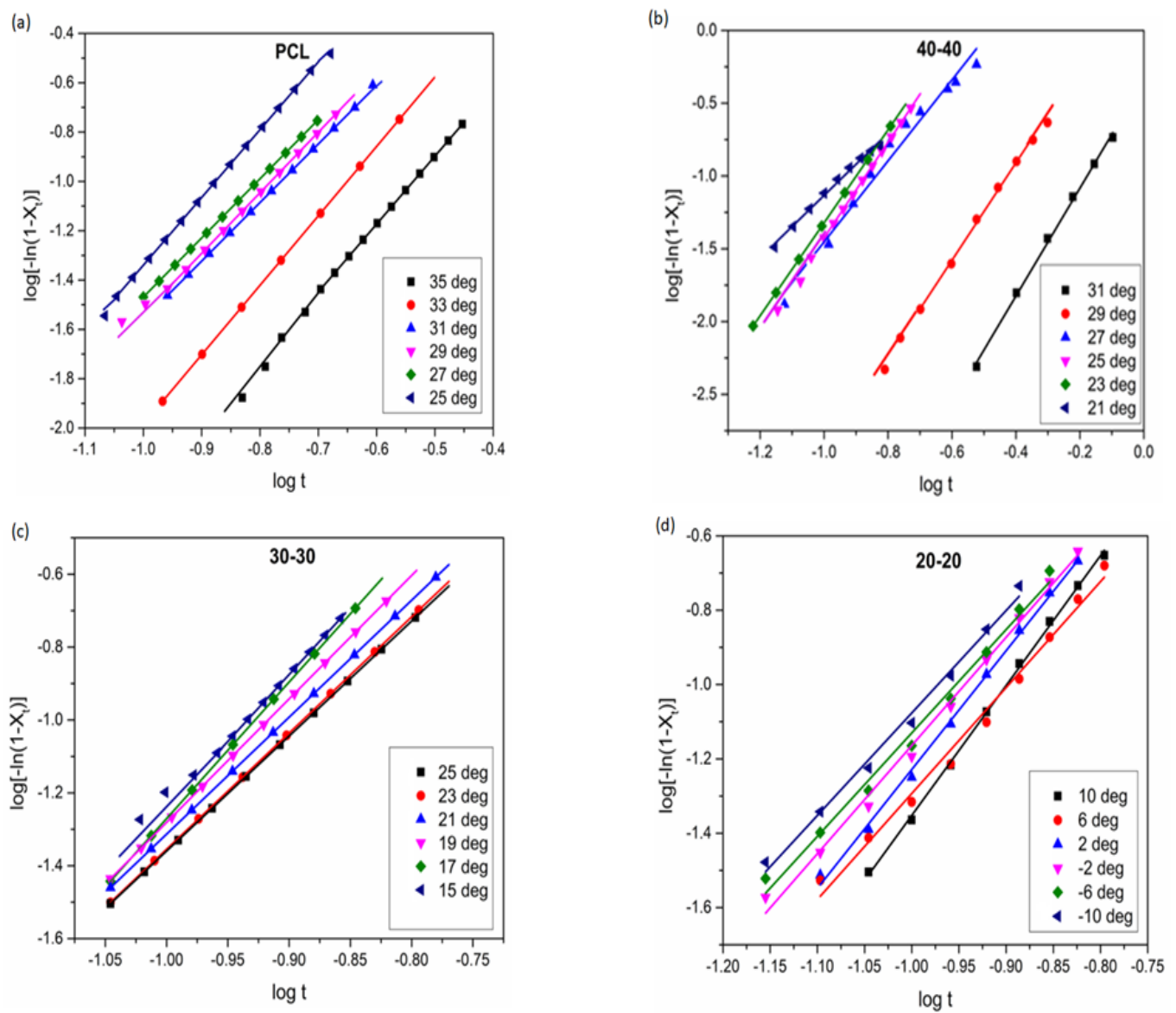


Figure 6.6. Isothermal crystallization tests and Avrami fit for (a) PCL, (b) 40-40, (c) 30-30 and (d) 20-20

Figure 6.6 shows plots of $\log[-\ln(1 - X_t)]$ against $\log t$ for triblock copolymer and PCL as a general guideline Avrami equation is only valid at low conversion (up to 20%). Accordingly, good linear relation is obtained for experimental data for the initial part of the conversion. The values of Z_t and n at low conversion of crystallization at different T_c are obtained by using the experimental data summarized in Table 6.1. The Avrami index n for PCL is around 2.6 and increases significantly for copolymers. The values of Avrami exponent n change from 2.6 to 3.4 for copolymers, indicating that the nucleation mechanism of the PCL crystallization changed significantly. The shift in n value suggests that crystal growth for PCL is two-dimensional, whereas growth mechanism of crystal of PCL in the copolymers tends to be three-dimensional and the nucleation process is heterogeneous under the experimental condition.[144, 254] Table 6.1 shows the enthalpy of crystallization (ΔH_c) decrease with decrease in the PCL chain length in copolymers which indicates that the crystallinity of PCL in the copolymers decreases. This observation is also quite evident in non-isothermal cooling curves and reported by different researchers that decrease in PCL chain length, or molecular weight decreases the crystallinity, enthalpy of melting and enthalpy of crystallization.[11, 12] Decrease in crystallinity is not only due to decreasing PCL length but increase in M_n of PDMS block has the same effect due to hindrance or interference effect generated by increasing PDMS chain length as per the study of Zhang *et al.*[13]

Table 6.1 Avrami equation's isothermal crystallization parameter at various T_{cm}

Samples	T_c ($^{\circ}\text{C}$)	T'_{cm} ($^{\circ}\text{C}$)	$t_{1/2}$	ΔH_c (J/g)	Z_t (min^{-1})	N	Avg. n
PCL	35	54.63	2.2	37.58	9.28×10^{-1}	2.4	2.6
	33	54.22	1.6	42.53	8.13×10^{-1}	2.37	
	31	53.95	0.91	43.26	9.17×10^{-1}	2.45	

	29	53.68	0.61	45.65	1.86	2.75	
	27	53.43	0.44	46.85	8.3×10^{-1}	2.82	
	25	53.23	0.34	45.46	7.5×10^{-1}	2.75	
40-40	31	52.88	1.95	35.77	3.42×10^{-1}	3.70	3.1
	29	52.55	1.18	35.59	4.29×10^{-1}	3.34	
	27	52.29	0.78	37.75	1.40	2.78	
	25	51.98	0.56	38.73	1.86	3.29	
	23	51.71	0.42	38.49	1.87	3.19	
	21	51.41	0.34	41.01	1.00	2.14	
30-30	25	49.91	2.4	28.91	2.42	3.66	3.4
	23	49.56	1.8	29.80	2.47	3.75	
	21	49.22	1.4	28.75	2.10	3.38	
	19	48.89	1.06	27.31	1.89	3.20	
	17	48.6	0.84	27.60	1.83	3.19	
	15	48.38	0.67	29.44	1.79	3.15	
20-20	10	44.67	2.5	25.75	1.74	2.95	3.00
	6	44.29	2.1	25.62	1.96	3.19	
	2	43.95	1.6	24.07	2.14	3.49	
	-2	43.70	1.27	21.57	1.55	2.85	
	-6	43.33	1	18.60	1.65	2.78	
	-10	43.17	0.9	14.98	1.68	2.76	

Further, the stability parameter (ϕ) is calculated. T_{cm}^0 values are plotted against T_{cm} for PCL and copolymers as shown in Figure 6.7 in the range of exothermic crystallization temperature. The Hoffman-Weeks equation (6.5) is used to fit the experimental data as given below:

$$T'_{cm} = \phi T_c + (1-\phi) T^0_{cm} \quad (6.5)$$

Where T^0_{cm} is equilibrium crystal melting temperature and ϕ is a stability parameter related to morphological factors concerning the perfection and size of crystals. The values of T^0_{cm} are obtained by the extrapolation of the least-squares fit lines of the experimental data to intersect the line of $T^0_c = T_{cm}$, as shown in Figure 6.7. In equation 6.5, ϕ can be assumed in the range of 0 and 1. $\phi = 0$ signifies $T'_{cm} = T^0_c$, while $\phi = 1$ means $T'_{cm} = T_c$. As a result, the crystals are most stable for $\phi = 0$ and fundamentally unstable for $\phi = 1$. The values of ϕ are determined by slope of these fit lines. T^0_c for PCL and copolymeric films are summarized in Table 6.1. When PCL is copolymerized with PDMS, the depression of crystal melting points and T^0_{cm} is observed with decrease in PCL chain length. From equation 6.5, it can also be found that the ϕ values of the PCL-PDMS-PCL copolymers are lower than that of PCL and decrease as the chain length of PCL in the copolymer decreases indicating that the stability of the crystals for PCL in the copolymer increases. This is attributed to confined micro-phase separation due to presence of PDMS blocks in between the PCL chains, as seen in optical microscope.

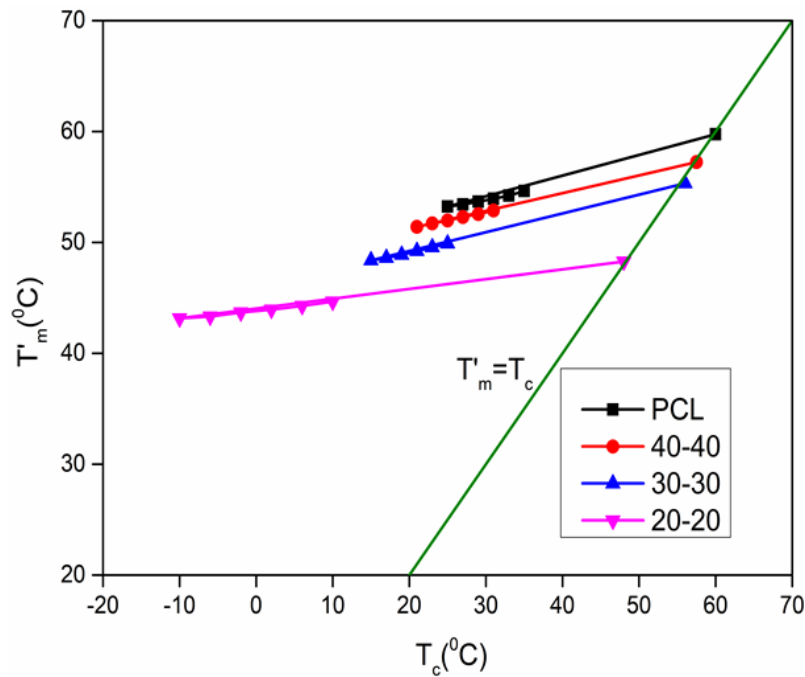


Figure 6.7. Plots of T'_{cm} versus T_c for PCL and PCL-PDMS-PCL triblock copolymeric films

The Lauritzen-Hoffman crystallization kinetic model is applied on experimental data to analyze the growth rate of the spherulites. According to the LH crystallization model, the relation between growth rate G , T_c and the undercooling that is $\Delta T = T_m^0 - T_c$ can be expressed as below equation (6.6):

$$G = G_0 \exp \left(\frac{U^*}{R(T_c - T_\infty)} \right) \exp \left(- \frac{K_g}{T_c (\Delta T) f} \right) \quad (6.6)$$

where G^0 is a pre-exponential factor, R is the gas constant, U^* is the activation energy for the transit of the macromolecules chain into the molten mass, typically given by a universal value of 6280 J/mol. $T_\infty = T_g - 30$ is a hypothetical temperature below which any viscous flow stops, where T_g is the glass-transition temperature of individual composition. f is a correction factor for the decrease in fusion enthalpy with T_c , $f = \frac{2 T_c}{(T_c + T_m^0)}$. Equation (6.6) can be further written by taking log on both sides as equation (6.7):

$$\ln G + \frac{U^*}{R(T_c - T_\infty)} = \ln G_0 - \frac{K_g}{T_c (\Delta T) f} \quad (6.7)$$

Nucleation parameter K_g can be defined as equation (6.8) as follows:

$$K_g = \frac{Z T_{cm}^0 \sigma \sigma_e b_0}{k_B \Delta H_m^0} \quad (6.8)$$

Where $Z = 4$ for regimes I and III, and $Z = 2$ for regime II, due to small degree of supercoiling, regime I has been considered for calculation. σ is lateral surface free energy and σ_e is the fold surface free energy and $\sigma = 0.1 * b_0 * \Delta H_f$ where b_0 is the distance between two adjacent fold planes, $b_0 = 4.38 \times 10^{-10}$ m [254], k_B the Boltzmann constant, ΔH_m^0 is the enthalpy of fusion of 100% crystalline PCL (139.5 J g⁻¹).

Table 6.2 Equilibrium crystal melting temperature T_{cm}^0 , stability parameter ϕ , nucleation parameter K_g , pre-exponential factor G_0 and fold surface free energy σ_e values for PCL and PCL-PDMS-PCL triblock copolymeric films.

Samples	T_{cm}^0 (°C)	ϕ	K_g (k ²)	G_0	σ_e (J/m ²)
PCL	59.8	0.21	6.53×10^4	5.61×10^4	3.56×10^{-3}
40-40	58.0	0.18	6.8×10^4	1.14×10^5	3.67×10^{-3}
30-30	55.3	0.15	7.39×10^4	3.81×10^5	4.05×10^{-3}
20-20	48.3	0.09	8.92×10^4	5.68×10^5	4.98×10^{-3}

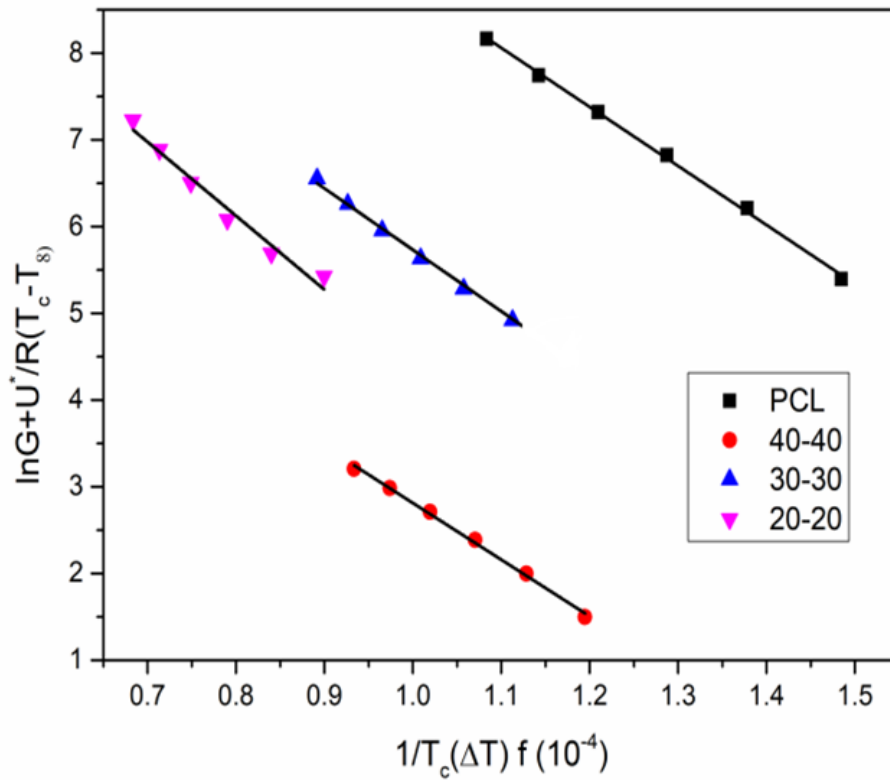


Figure 6.8. Plot of $\ln G + U^*/R (T_c - T_\infty)$ against $1/T_c(\Delta T) f$ for PCL and PCL-PDMS-PCL triblock copolymeric films

According to equation 6.7, the plots of $\ln G + U^*/R (T_c - T_\infty)$ against $1/T_c(\Delta T) f$ for PCL and PCL-PDMS-PCL triblock copolymeric films are in Figure 6.8. The experimental data fit into the straight lines very well. The slopes and intercepts of those lines are used to compute the nucleation parameter K_g (energy barrier for the crystallization process), as well as the pre-exponential factor G_0 , as shown in Table 6.2. For PCL, G_0 is $5.61 \times 10^4 \text{ (min}^{-1}\text{)}$ PCL-PDMS-PCL triblock copolymers exhibited G_0 values 10-fold and K_g values are 1.3-fold to PCL. With decrease in PCL chain length G_0 and K_g values increase. Here, small degrees of supercooling play a major role in nucleation factors. With decrease in PCL chain length, the supercooling range for crystallization shifted to lower temperature gradually and increased the nucleation factor effectively. In case of polyethylene terephthalate (PET) isothermal crystallization kinetics, Lu *et al.* [255] reported that at a small degree of supercooling regime I kinetic is operative and primary nucleation as surface nucleation completed rapidly over the surface and dominated by secondary nucleation for crystal growth. Ninago *et al.* [151] are reported increase in K_g and G_0 of 2 fold and 51 fold respectively for PCL-g-HEMA copolymer than pure PCL, indicating decrease in overall mobility of PCL chains due to major confinement, which reduces their final crystallization capacity. The fold surface energy calculated by equation 6.8 listed in Table 6.2 shows considerable increase in fold surface free energy, which indicates inclusion of PDMS block increases the energy barrier, which hinders the growth of PCL crystallite. Cesur *et al.* studied isothermal crystallization kinetics of PCL composites with oleic acid, zinc oxide, and glycerol monooleate and reported that small amount of filler expedites nucleation and crystal growth, but higher amount creates hindrance and slows down the crystal growth. [144, 145]

6.4 Conclusion

With inclusion of PDMS block, microphase separated crystals are formed as observed via optical microscope. The thermal analysis demonstrated that with decrease in PCL chain length the percentage crystallinity, crystal melting temperature and crystallization temperature decreases from 41.9 to 23.8%, 53.5 to 43.5°C and 30.8 to 0.5°C, respectively. The effect of PCL chain length on the crystallization kinetics has been studied for pure PCL and triblock copolymers of chain length 40-40, 30-30, 20-20 with the help of Avrami and Lauritzen-Hoffman model. The Avrami analysis indicated that primary crystallization is followed by secondary crystallization for pure PCL while three-dimensional spherical growth occurs in copolymers. The stability of crystal perfection (0.21-0.09) increases with inclusion of PDMS block. The energy barrier is increased with increasing content of PDMS and affects the growth rate of crystal.

Chapter 7

Shape memory properties of PCL-PDMS-PCL triblock copolymer films

Overview

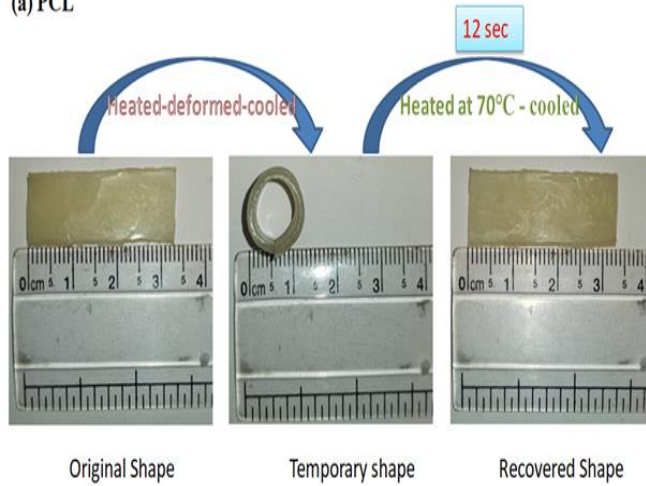
The semi-crystalline nature of PCL embraces shape memory properties of this copolymer. The shape memory properties are evaluated in this chapter via two modes: qualitatively and quantitatively both. In qualitative mode the rectangular shape and cross shape samples have been prepared and converted to ring and cube respectively as temporary shape and checked for shape recovery at elevated temperature. While in quantitative mode the samples have been quantified for shape fixity and shape recovery ratio. It is observed that shape fixity increases with increase in PCL content in copolymers and % crystallinity and shape recovery ratio increase with decrease in molecular weight though difference is not much significant.

7.1 Qualitative Analysis of Shape Memory Properties

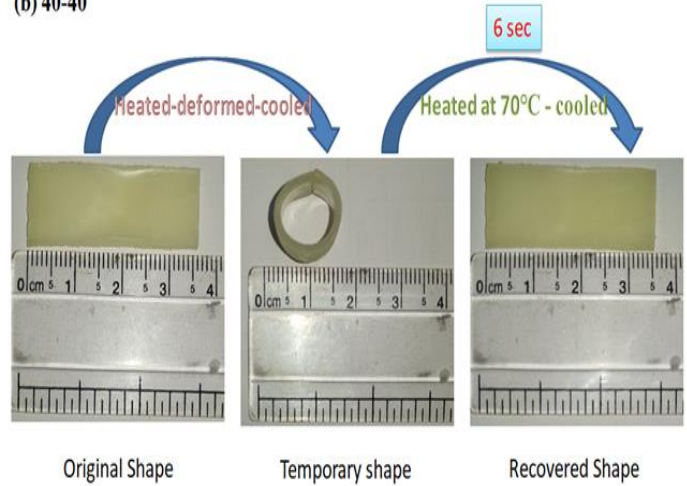
The crystallization temperature (T_c) and crystal melting temperature (T_{cm}) are prominent to determine shape memory behaviour of PCL and its copolymers. At T_c temporary shape is fixed and to recover permanent shape, sample is heated to T_{cm} . The presence of crosslinks in structures restrict the sliding of chain over one another and improves the shape recovery by entropy elasticity.[256] A visual demonstration of shape memory behaviours of PCL and PCL-PDMS-PCL copolymers is performed for better understanding as shown in Figure 7.1 (a), (b), (c), (d) for sample size ~ 40 mm (length) \times ~ 10 mm (width) \times ~ 1 mm (thickness) and in Figure 7.2 (a), (b), (c), (d) for cross shaped sample to be converted into cube shape of ~ 10 mm (side) \times ~ 1 mm (thickness). The original shapes are deformed at 70°C to temporary shape and fix them at their crystallization temperature in cold water bath while deformation

force applied. Temporary shape reheated at 70°C in hot water bath for shape recovery. The time required to recover its shape is 12 sec, 6 sec, 5 sec and 4 sec for PCL, 40-40, 30-30 and 20-20 (Irrespective to original and temporary shape), respectively including manual error. This difference is attributed to varying percentage crystallinity and time required to cover the temperature difference from T_c to T_{cm} . The images shown in Figure 7.1 and 7.2, represents that shape fixity and shape recovery is almost 100% in all four samples. As the PCL chain reduced the cooling temperature is reduced to sustain the temporary shape. 10-10 and 5-5 samples do not exhibit any shape memory properties due to negligible crystallinity as observed in XRD and DSC results in Chapter 4 and 6, respectively. The sample size ~40 mm (length) \times ~10 mm (width) \times ~0.5 mm (thickness) also tested to understand the effect of thickness on shape memory behaviour for rectangular to ring shape. It has been observed that the time required to recover its shape is 3.50sec, 2.75 sec, 2.5 sec and 2.0 sec for PCL, 40-40, 30-30 and 20-20, respectively including manual error. With decrease in thickness of samples, the rate of heat transfer increases, crystals melt faster due to which less time required for shape recovery.

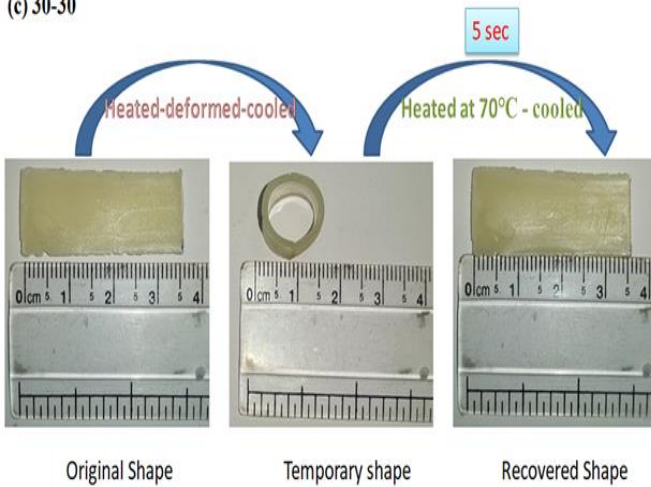
(a) PCL



(b) 40-40



(c) 30-30



(d) 20-20

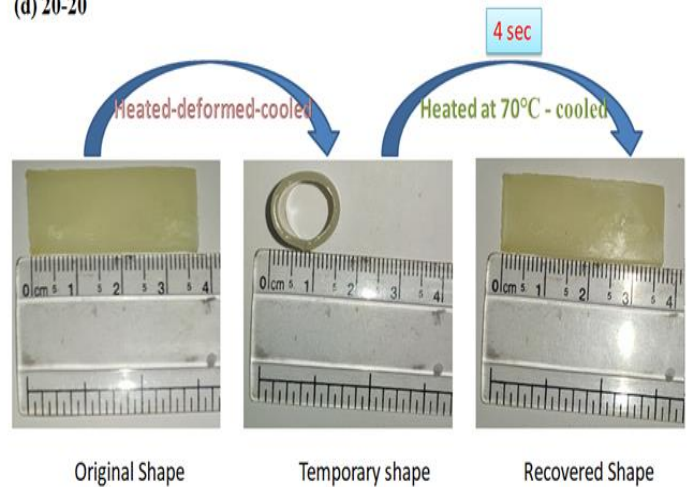
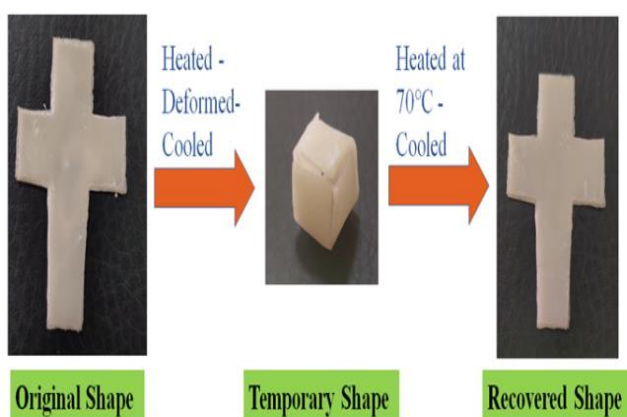


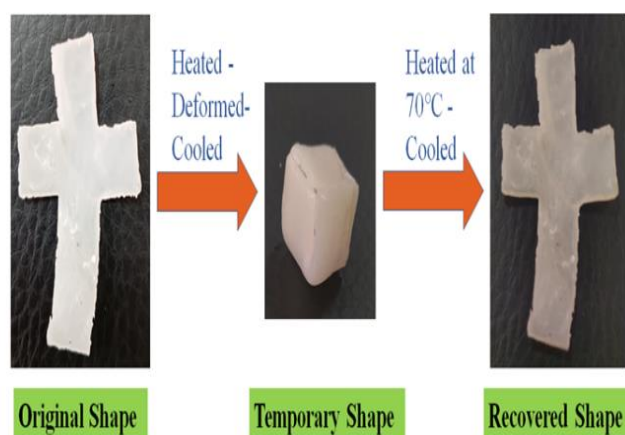
Figure 7.1. Shape memory behaviour of from rectangular to ring with recovery time of

PCL(a), 40-40(b), 30-30(c), 20-20(d)

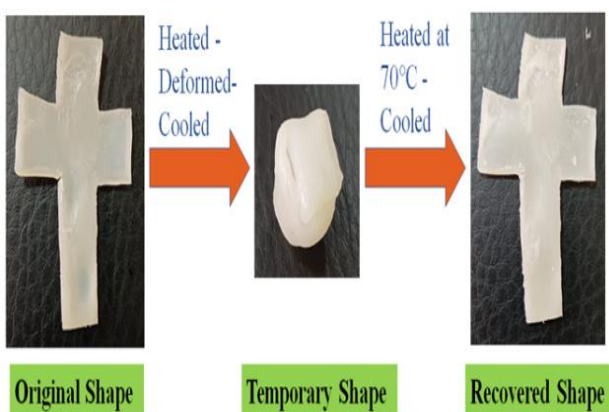
a. PCL



b. 40-40



c. 30-30



d. 20-20

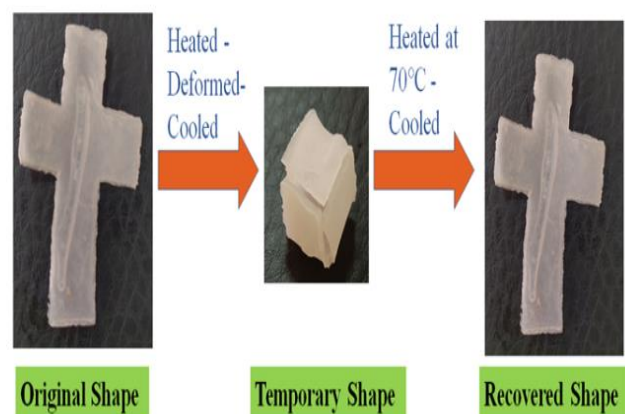


Figure 7.2. Shape memory behaviour from cross-shaped to cube with recovery time of PCL(a), 40-40(b), 30-30(c), 20-20(d)

7.2 Quantitative Analysis of Shape Memory Properties

Shape fixity and shape recovery ratio of each sample for four cycles are calculated by equation 3.2 and 3.3 and presented in Table 7.1. All the samples show effective recovery of rectangular shapes irrespective of their dimension (change in thickness). The shape fixity increases with increase in PCL content in copolymers and percentage crystallinity. There is increase in shape recovery ratio with decrease in molecular weight though difference is not much significant. Shape fixity is almost similar for each cycle for various samples because percentage crystallinity is same at different cycle for that sample. Shape recovery decreased

with each cycle and most significantly from cycle 1 to cycle 2 because original cast film chains had to be extensively realigned after becoming distorted. Shape memory behavior is reported by Schoener *et al.* for PCL-PDMS-PCL triblock copolymers.[12] They have stated that 17% crystallinity (by DSC) is not enough to possess shape memory behavior, whereas in this study, it has been found that 20-20 samples with crystallinity of 17.9% (by DSC) and 23.8% (by XRD) showed shape memory behavior. Here, along with crystallinity, T_{cm} (i. e. 43.5°C) also plays a significant role which is well above ambient temperature after fixing the temporary shape in cold bath and keeping it fixed below T_{cm} .

Table 7.1. Thermomechanical cycles of shape memory properties for PCL-PDMS-PCL triblock copolymers.

Samples	Cycle	Shape Fixity	Shape recovery
PCL	1 st	99.6 ± 0.3	96.8 ± 0.6
	2 nd	99.6 ± 0.5	96.5 ± 0.4
	3 rd	99.5 ± 0.6	97.0 ± 0.3
	4 th	99.3 ± 0.4	97.0 ± 0.7
40-40	1 st	99.3 ± 0.5	96.5 ± 0.7
	2 nd	99.3 ± 0.3	96.1 ± 0.6
	3 rd	99.3 ± 0.7	96.6 ± 0.4
	4 th	99.3 ± 0.6	96.7 ± 0.3
30-30	1 st	99.1 ± 0.4	97.2 ± 0.5
	2 nd	98.9 ± 0.2	97.0 ± 0.3
	3 rd	98.9 ± 0.5	97.5 ± 0.8
	4 th	98.8 ± 0.4	97.5 ± 0.7
20-20	1 st	98.3 ± 0.6	97.3 ± 0.6
	2 nd	98.1 ± 0.5	97.0 ± 0.2
	3 rd	98.2 ± 0.7	97.2 ± 0.5
	4 th	98.0 ± 0.6	97.1 ± 0.5

7.3 Correlation of isothermal crystallization kinetics and shape memory properties

As discussed in chapter 6, the increased crystal perfection stability with inclusion of PDMS helps to fix the temporary shape even with low percentage crystallinity. The shape fixity ratio decreases with decreasing crystallinity and increasing fold surface energy as it hinders the growth of PCL crystallite. Higher fold surface energy requires more time to generate full crystal of PCL segment (as seen in optical images), which ultimately affects the fixity to temporary shape and needs more time to fix the secondary shape. There is only a 1.4-fold change in fold surface free energy σ_e from PCL to copolymers which is reflected in the shape fixity ratio decreasing from 99.6 to 98.3. The increased pre-exponential factor, nucleation value and energy barrier hinder PCL crystal growth which results in faster recovery when T_{cm} is provided for shape recovery of samples. Here, along with crystallinity the crosslink points formed due to photocrosslinking are also an important factor for shape recovery even when the percentage crystallinity is less as seen in the case of 20-20. Tian *et al.* have presented the shape memory behavior of PCL homopolymers with molecular weights of 4000, 6000, 8000 and 10,000 and they have found that with increase in molecular weight, shape fixity increases due to higher crystallization during elongation.[162]

7.4 Conclusion

Photocrosslinked films of PCL and PCL-PDMS-PCL triblock copolymers exhibit excellent shape memory properties. The shape fixity increases with increase in PCL content in copolymers and percentage crystallinity, while shape recovery is almost similar for PCL, 40-40, 30-30 and 20-20. The shape fixity is almost same for each cycle though shape recovery decreases with each cycle due to rearrangement of crystals of PCL segment while melting and cooling. Crystal perfection stability, nucleation parameter, energy barrier and crosslink points affect the shape memory properties of triblock copolymeric films.

Chapter 8

Biodegradation behaviour of PCL-PDMS-PCL triblock copolymer films

Overview

This chapter give a brief about soil burial degradation behaviour of PCL-PDMS-PCL triblock films with different PCL chain length. The samples have been buried for 180 days and checked for morphological properties by digital camera, Optical Microscope (OM) and Scanning Electron Microscope (SEM), whereas, degradation kinetics studied by weight loss during regular intervals. PCL is following second order of degradation kinetics while with inclusion of PDMS it becomes first order degradation kinetics. With decrease in PCL chain length degradation rate has been decreased. The structural changes and percentage crystallinity is also evaluated and mechanism of soil burial degradation has been proposed.

8.1 Morphological Changes

8.1.1 Macroscopic view

Figure 8.1 shows the macroscopic pictures of samples obtained by digital camera (Zeiss 13 megapixels). Initially, the surface of the PCL is smooth. After 80 days flakes are observed on the surface of the film. The disintegration is started and in 180 days film breakdown. The PCL surface looks flake-like and starts disintegrating after 80 days. The cracks become quite visible and major breakdown of film happened. 40-40 is disintegrated after 80 days and cracks are observed and films are breakdown in 180 days. With decrease in PCL chain length of films, the visibility of flakes has reduced and films appeared smoother. 30-30 and 20-20 show small disintegration at 180 days. There is no cracks and flake formation happened for 10-10 and 5-5 though change in color is observed. The films appeared very patchy. The dimensional stability of the films is maintained. With decrease in PCL chain length the

surface erosion and disintegration are delayed significantly in triblock copolymer films. In current study, the crosslink density increases with lower molecular weight of copolymer or lower PCL chain length, which enhances the degradation stability.

The composite of PCL with organic clays showed increase biodegradation time in simulated soil because clay acts as nucleating agent and increase the crystallinity as studied by Serap Cesur [48]. Azemar *et al.* [257] and Kai *et al.* [258] have studied the hydrolytic and buffer solution degradation of PCL-PDMS-PCL triblock copolymers. They depict that hydrophobic nature of PDMS increases the degradation time and helps to tune the degradation of copolymer as per application requirement. Beltran *et al.* [259] degraded PCL/PDMS scaffold under buffer solution (Non-accelerated degradation) and 1M NaOH solution (accelerated degradation) and found that inclusion of PDMS enhanced the degradation.































Sample/ Days	PCL	40-40	30-30	20-20	10-10	5-5
0 days						
40 days						
80 days						
120 days						
180 days						

Figure 8.1. Macroscopic view of PCL and PCL-PDMS-PCL triblock copolymer films at different intervals

8.1.2 Microscopic view

The films are observed under optical microscope with resolution of 40x. The pictures are taken with Moticam Pro 285A camera. And the photos of samples are shown in Figure 8.2. It can be seen by optical microscope that there is development of cracks on the film surface with time. At initial period the surface is smooth and deposition of soil is negligible due to which images are much clear and brighter. As the time increases the cracks developed, in these cracks soil get deposited and cannot be removed by washing, due to which clarity of images get diminished and surface looks darker. With the time cracks become more visible and upper surface looks flaky. In case of 10-10 and 5-5, very less amount of microcracks become visible and these cracks sustain throughout the 180 days. The soil particles are easily visible inside the cracks of these two films.




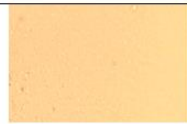
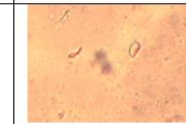
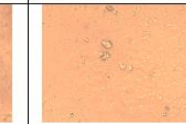

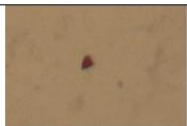


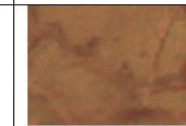
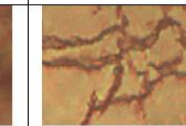




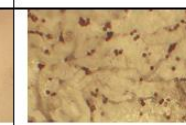
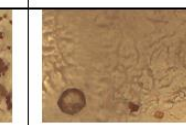



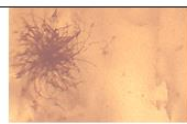
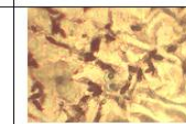
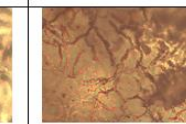




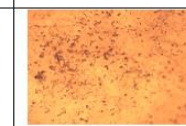

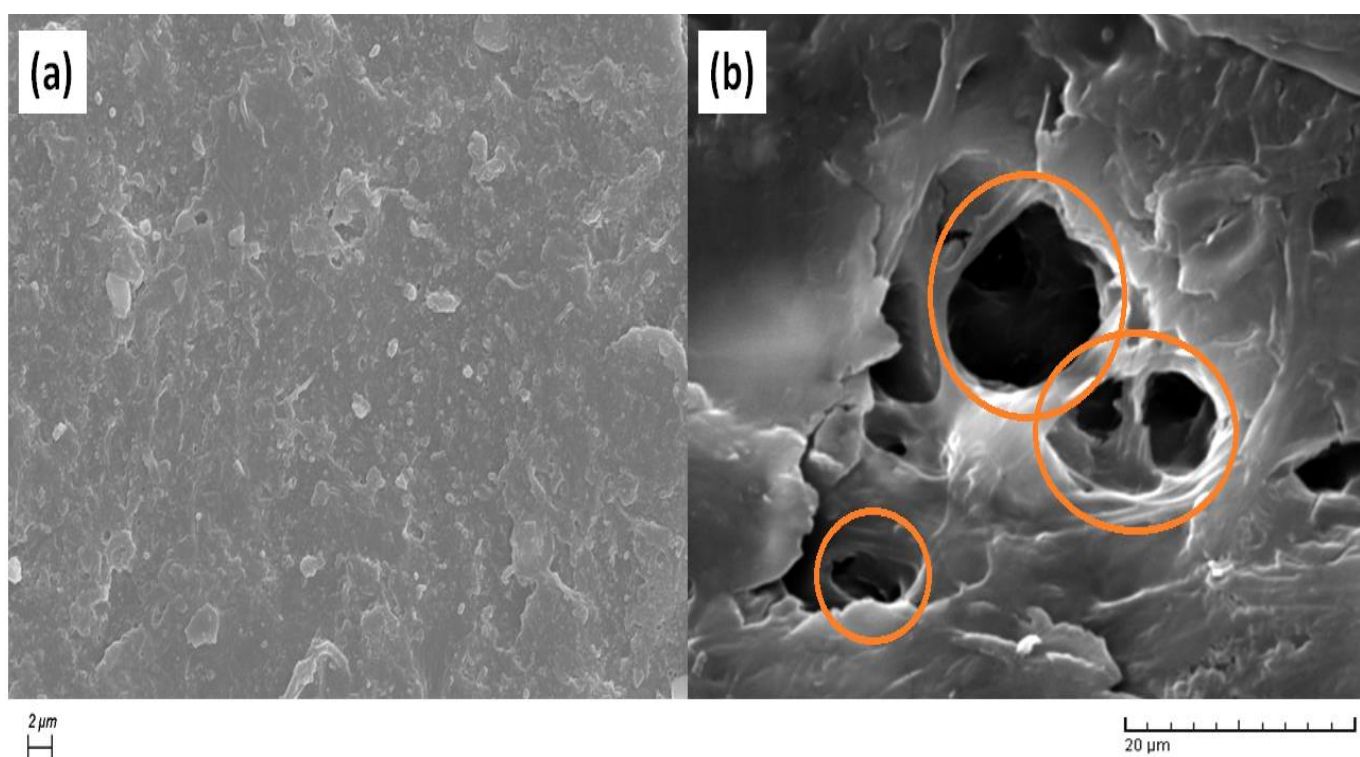
Sample / Days	PCL	40-40	30-30	20-20	10-10	5-5
0 days						
40 days						
80 days						
120 days						
180 days						

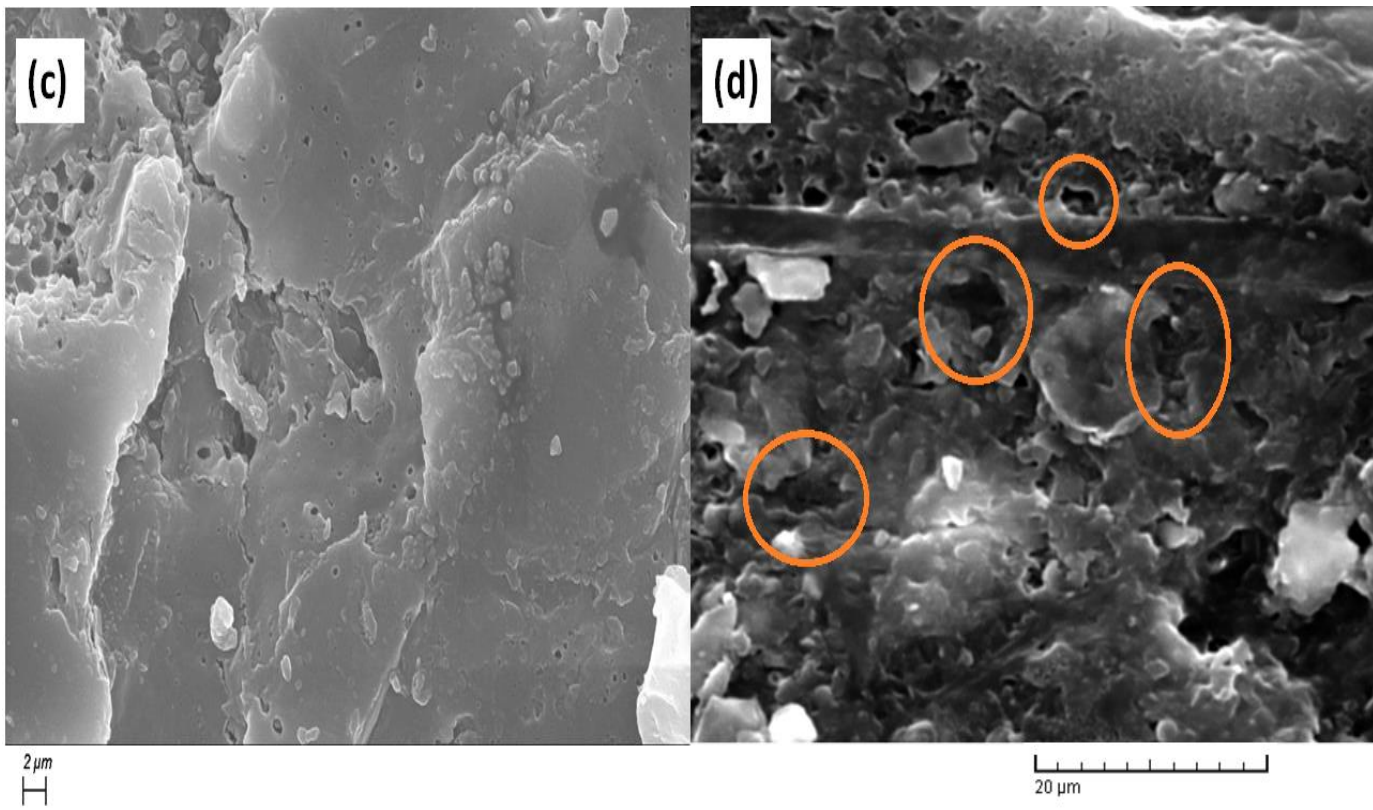
Figure 8.2. Microscopic view by optical microscope of PCL and PCL-PDMS-PCL triblock copolymer films

The SEM images have been taken at 0 days and 180 days to observe the morphological changes at micro level as shown in Figure 8.3. These images show different kind of surface changes on the basis of composition. The surface of PCL is eroded much more than samples with PDMS. This is supported with weight loss data shown in Figure 8.4. In case of PCL, 40-40, 30-30, 20-20 the surface become rougher and holes are quite visible after degradation. The diameter of holes is calculated with the help of ImageJ software developed by National Institute of Health, Maryland, USA. It is observed that hole diameter decreases with decrease in PCL chain length (Table 8.1). The distribution of size of holes becomes uniform with decrease in PCL chain length. In case of 10-10 and 5-5 no holes are observed after 180 days of degradation in SEM images, although significant cracks are visible in both the cases. For 40-40, 30-30 and 20-20, the surface becomes rougher than without degradation. Though, 10-10 and 5-5 do not show significant change on surface. Li *et al.* reported that enzymatic degradation of PCL/silica nanocomposite become more than neat PCL and surface become more rough in case of nanocomposite [260].

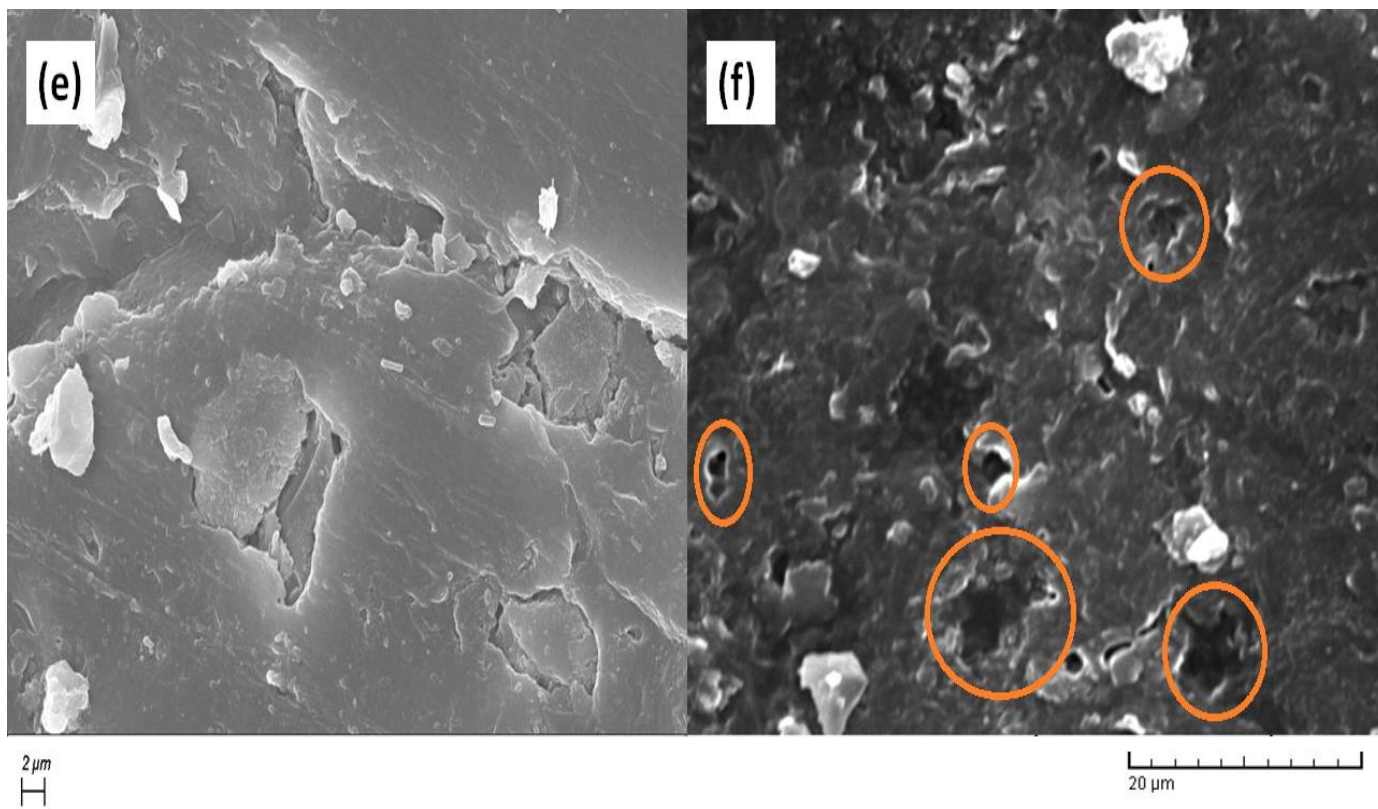
PCL



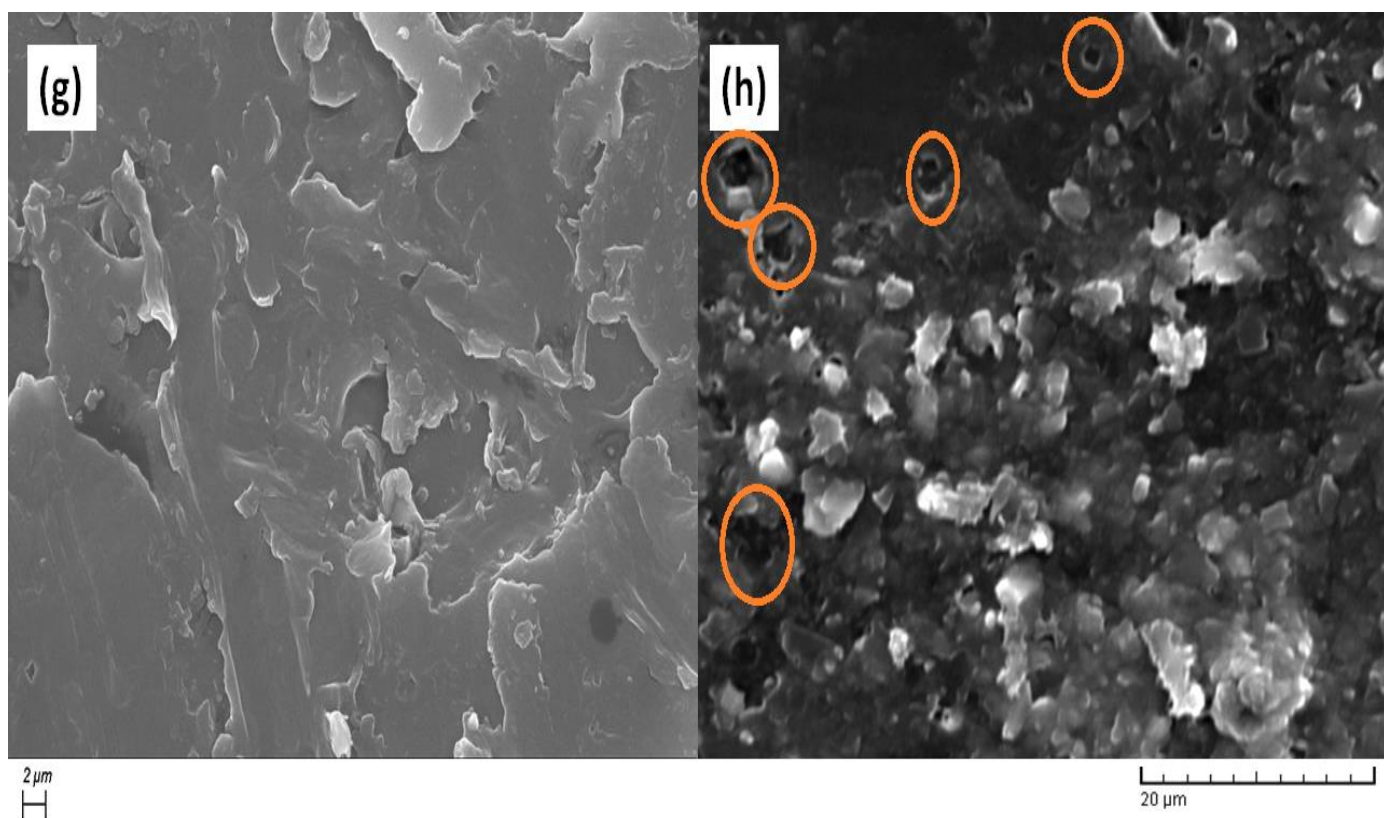
40-40



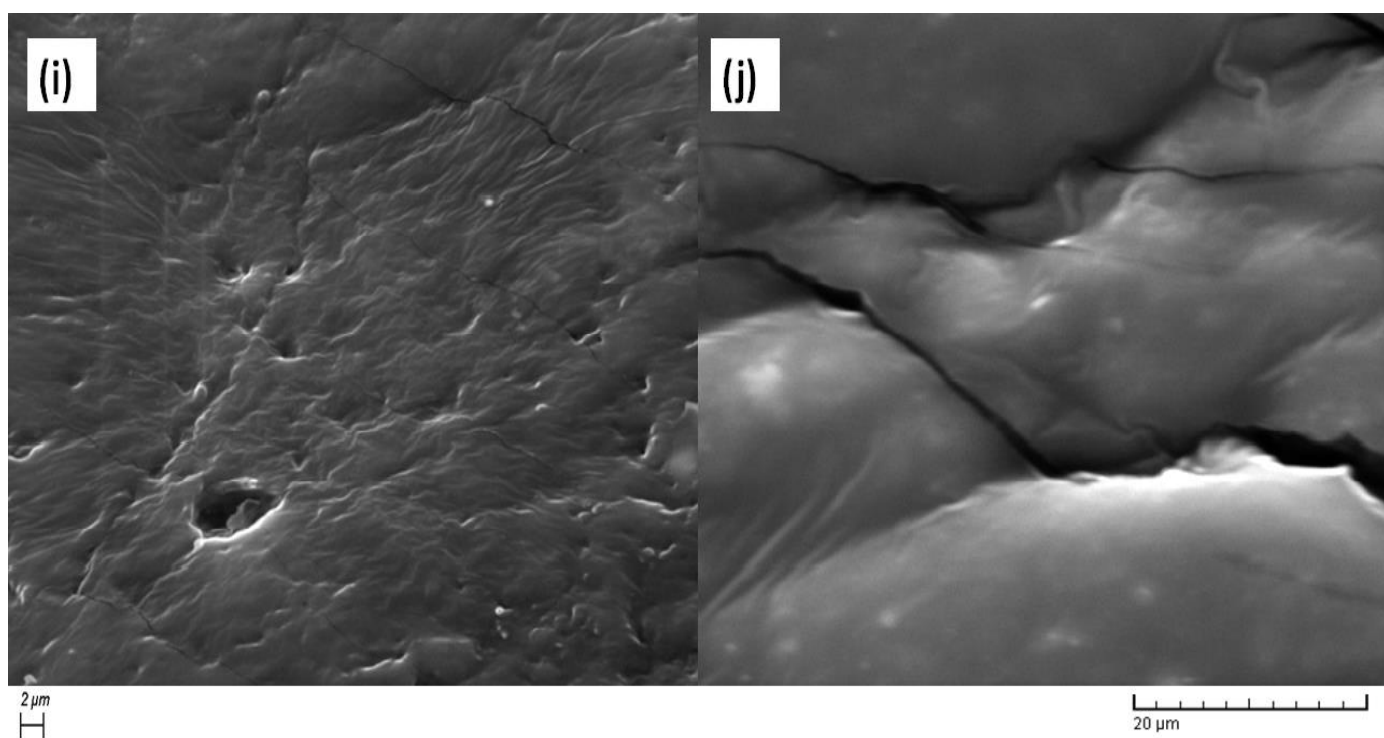
30-30



20-20



10-10



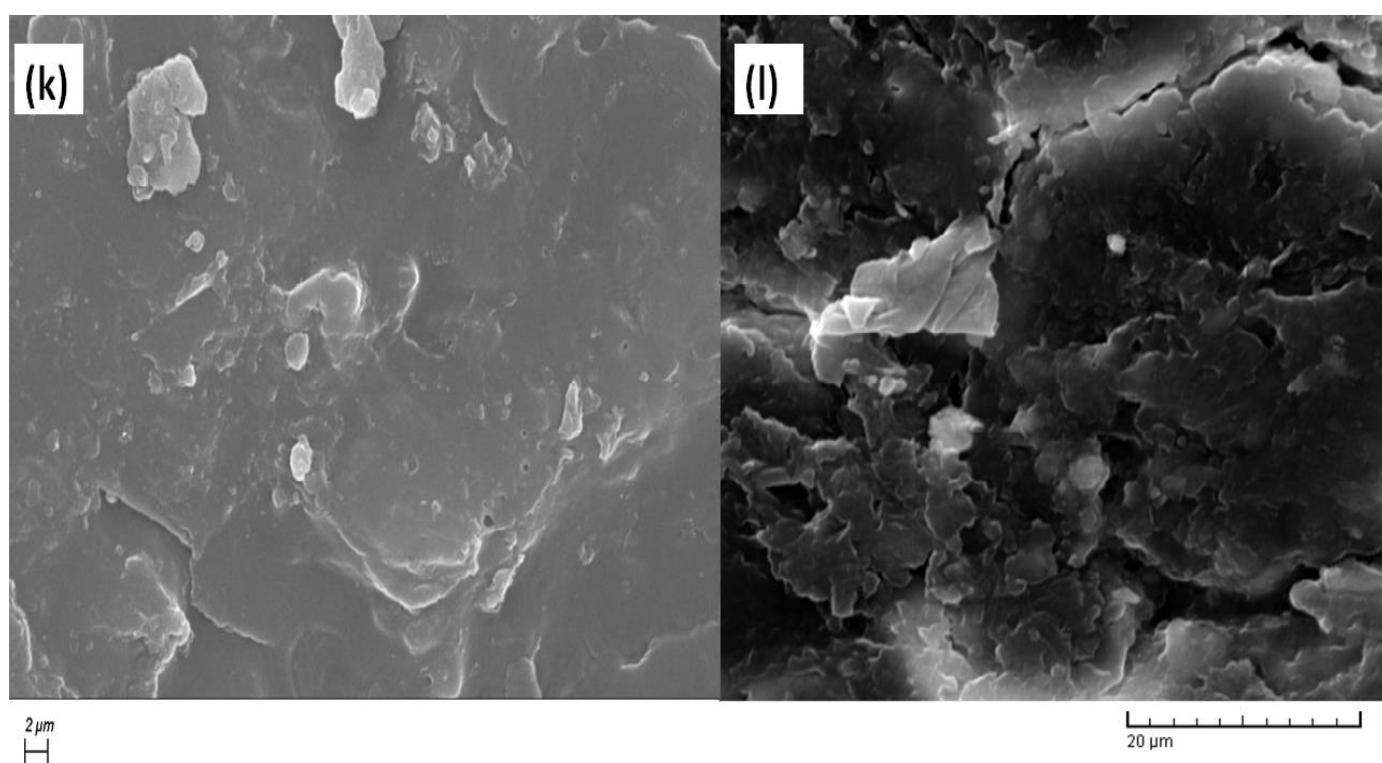


Figure 8.3. SEM images of PCL and PCL-PDMS-PCL triblock copolymer films before degradation and after 180 days of degradation. PCL (a) before soil burial, #PCL (b) after 180 days of soil burial, 40-40 (c) before soil burial, 40-40 (d) after 180 days soil burial, 30-30 (e) before soil burial, 30-30 (f) after 180 days soil burial, 20-20 (g) before soil burial, 20-20 (h) after 180 days soil burial, 10-10 (i) before soil burial, 10-10 (j) after 180 days soil burial, 5-5 (k) before soil burial, 5-5 (l) after 180 days soil burial

8.2 Macrolevel changes

8.2.1 Weight loss in soil burial

The photo crosslinked shape memory PCL-PDMS-PCL copolymer films are soil buried for 180 days and analyzed at time interval of twenty days for percentage weight loss (equation 3.8) as shown in Figure 8.4. The results clearly indicate that pristine PCL films have higher weight loss in comparison to PCL-PDMS-PCL copolymer films. In twenty days, the PCL weight loss is 13.8% whereas for 40-40, 30-30, 20-20, 10-10, 5-5 weight loss is 5.6%, 5.3%,

5.1%, 4.8% and 3.0% respectively. The rate of weight loss for PCL is low for initial 80 days then there is significant increase and 56.3% weight loss is observed. After 180 days the copolymer films show almost linear rate of change in weight loss. With the decrease in PCL chain length the percentage weight loss decreases as can be seen in Figure 8.4. Singh *et al.* have reported compost degradation rate of PCL and its composite with modified nanoclays. The weight loss for pristine PCL is almost 45% in 60 days while there is increase in weight loss for composite systems [261]. Park *et al.* reported a sharp decrease in degradation of poly(ethylene-co-vinyl alcohol)-graft polycaprolactone that is almost 1.2% in 75 days whereas 80% for PCL [44].

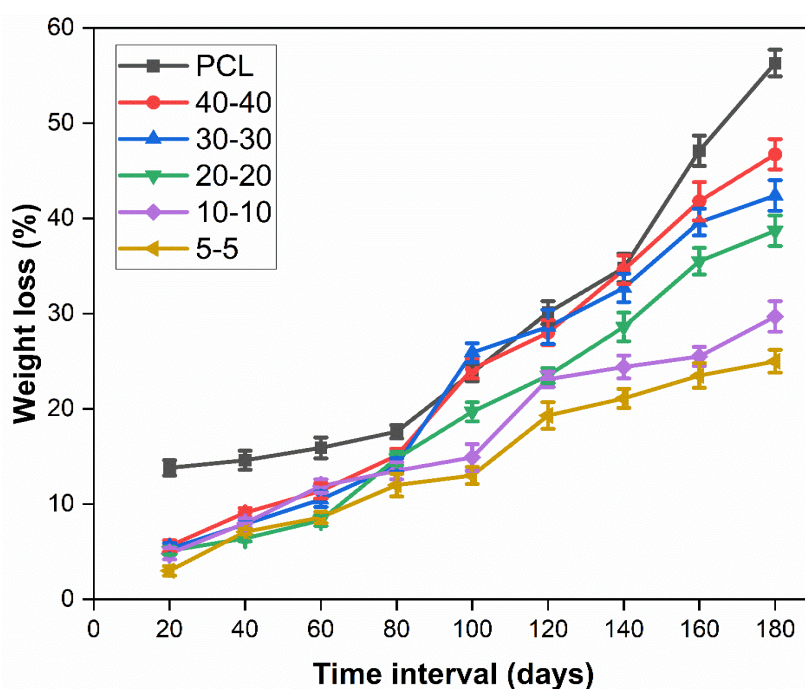


Figure 8.4. Percentage weight loss of PCL-PDMS copolymer films with time in soil burial

8.2.2 Thermal Properties

The TGA thermograms of PCL and PCL-PDMS-PCL triblock films are shown in Figure 8.5. First there is decrease due to water evaporation, then the organic functional group degrade between 250°C and 450°C. The thermal degradation of PCL under inert atmosphere, such as nitrogen, occurs through the rupturing of the polyester chains via the ester pyrolysis reaction with the release of carboxylic acid groups, water and carbon dioxide gas. When two pyrolysis

reactions occur with the ester functions along the chain during thermal degradation of PCL under inert atmosphere, the 5-hexenoic is most probably formed [112]. The Inclusion of PDMS chain increased the degradation temperature and improved the thermal degradation behaviour of copolymer.

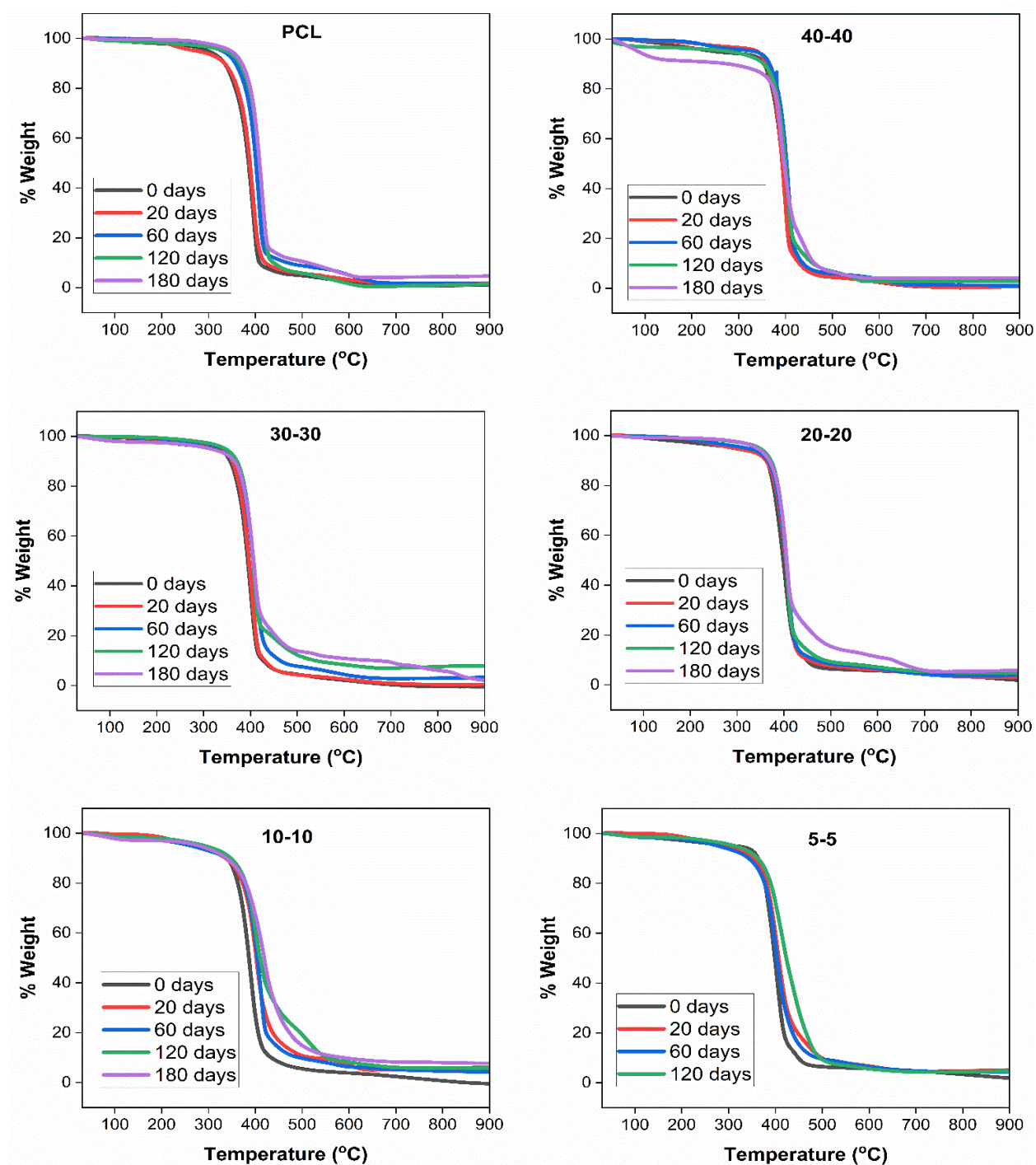


Figure 8.5. TGA curves of a pure PCL and PCL-PDMS-PCL triblock copolymer films at different degradation time

Table 8.1 represents the degradation of PCL and PCL-PDMS-PCL triblock films degradation temperature at 50% degradation by weight. Before degradation it shows an increasing trend of temperature at 50% weight loss with inclusion of PDMS. While, in particular composition it has been observed that with increase in time of soil burial the temperature increases. The amorphous part degrades first in case of PCL and crystalline part later, so there is a significant difference in degradation temperature. In case of tri-blocks inclusion of PDMS increase the temperature stability, but here completely amorphous PDMS does not degrade due to hydrophobicity and non-biodegradability. With increase in soil burial time the amorphous part of PCL degrades first then, crystalline while PDMS part kept intact, which increase the difference in temperature stability after degradation of 180 days.

Table 8.1. TGA data from Figure 8.5 and degradation analysis by SEM images of after degradation with hole diameter calculation

Sample	T _{50%} (°C)					Hole diameter calculated from SEM Images after degradation (in µm)
	0 Days	20 days	60 Days	120 days	180 days	After 180 days
PCL	385.6	388.3	401.2	408.8	409.0	10-16
40-40	393.4	392.9	402.4	399.7	396.9	4-10
30-30	394.5	396.9	405.8	405.9	406.5	3-7
20-20	395.7	401.7	404.1	405.1	405.8	2-5
10-10	396.4	402.8	404.6	409.9	418.8	No holes observed
5-5	398.7	406.7	408.1	423.2	434.8	No holes observed

Degradation of soil buried specimens are examined for crystal melting temperature and crystallization temperature with differential scanning calorimetry (DSC) for regular time interval as shown in Table 8.2. Before soil burial, samples have been tested for all these parameters to be consider as a reference mentioned as zero days. There is a continuous increase in crystal melting temperature for all the polymeric films while the crystallization

temperature is keep decreasing except 5-5. There is an interesting observation that 5-5 does not exhibit T_{cm} and T_c initially, though after 20 days of soil burial T_{cm} and T_c are observed in each time interval.

8.3 Structural changes

The structural analysis of triblock copolymer films was carried out by Fourier Transform Infrared spectroscopy for before degradation and after 180 days degradation as shown in Figure 8.6. The PCL characteristic bands are recorded at 2943 cm^{-1} for asymmetric $-\text{CH}_2$ stretching, 2865 cm^{-1} for symmetric $-\text{CH}_2$ stretching, 1725 cm^{-1} for $\text{C}=\text{O}$ carbonyl stretching, 1294 cm^{-1} for $\text{C}-\text{O}$ and $\text{C}-\text{C}$ stretching, 1239 cm^{-1} for asymmetric $\text{C}-\text{O}-\text{C}$ stretching and 1169 cm^{-1} for symmetric $\text{C}-\text{O}-\text{C}$ stretching for fresh sample. After degradation of 180 days the peaks intensity get diminished shows degradation up to molecular level. There is an additional peak in degraded sample at 800 cm^{-1} due to deposited and non-removable soil content. For PCL-PDMS-PCL copolymer films additional peaks are observed at 800 cm^{-1} for Si-C (methyl of PDMS), a weak band around 3300 cm^{-1} assigned to amino end groups, a very sharp peak for $-\text{CH}_3$ stretching at 1259 cm^{-1} and doublet at 1090 and 1018 cm^{-1} assigned to Si-O-Si stretching. A non-hydrogen bonded $\text{C}=\text{O}$ peak at 1723 cm^{-1} is observed due to ester group in PCL and there is slight shift observed in $-\text{CH}_2$ stretching at 2961 cm^{-1} in case of triblock copolymer than pure PCL due to additional $-\text{CH}_2$ chain of PDMS. Hydrogen bonded $\text{C}=\text{O}$ stretching peak at 1649 cm^{-1} of amide I and $\text{H}-\text{N}-\text{C}=\text{O}$ stretching peak at 1531 cm^{-1} of amide II are observed. Similarly, Meikail *et al.* have reported secondary amide and protonated amine stretching at 1648 cm^{-1} and 1555 cm^{-1} [245]. Poojari *et al.* reported absorption band at 1100 cm^{-1} for Si-O-Si and at 1260 cm^{-1} for Si- CH_3 bonds of PDMS [11]. Azemar *et al.* have reported peaks at 800 cm^{-1} for Si- CH_3 bonds and 1097 cm^{-1} for Si-O bond of PDMS while peaks at 2943 cm^{-1} for methylene and at 1725 cm^{-1} for ester of PCL [4, 14]. Chan *et al.* have synthesized poly(PCL/PDMS) urethane and reported similar peaks [246]. In

triblock copolymers, 40-40, 30-30, 20-20 and 10-10, the intensity of peaks increases with increasing PDMS content for samples before degradation. After degradation the intensity of peaks reduces for respective sample accordingly. Peaks at 1649 cm^{-1} associated with hydrogen bonded C=O and at 1259 cm^{-1} associated with Si-CH₃ bonds almost vanished. In case of 5-5 of highest PDMS content the intensity of peaks increased could be due to very less degradation and deposited soil content over the period. Cesur *et al.* have reported that there is no qualitative difference in PCL composite films after degradation, though there is quantitative difference observed. It was seen that first amorphous region degraded followed by crystalline region [47, 48].

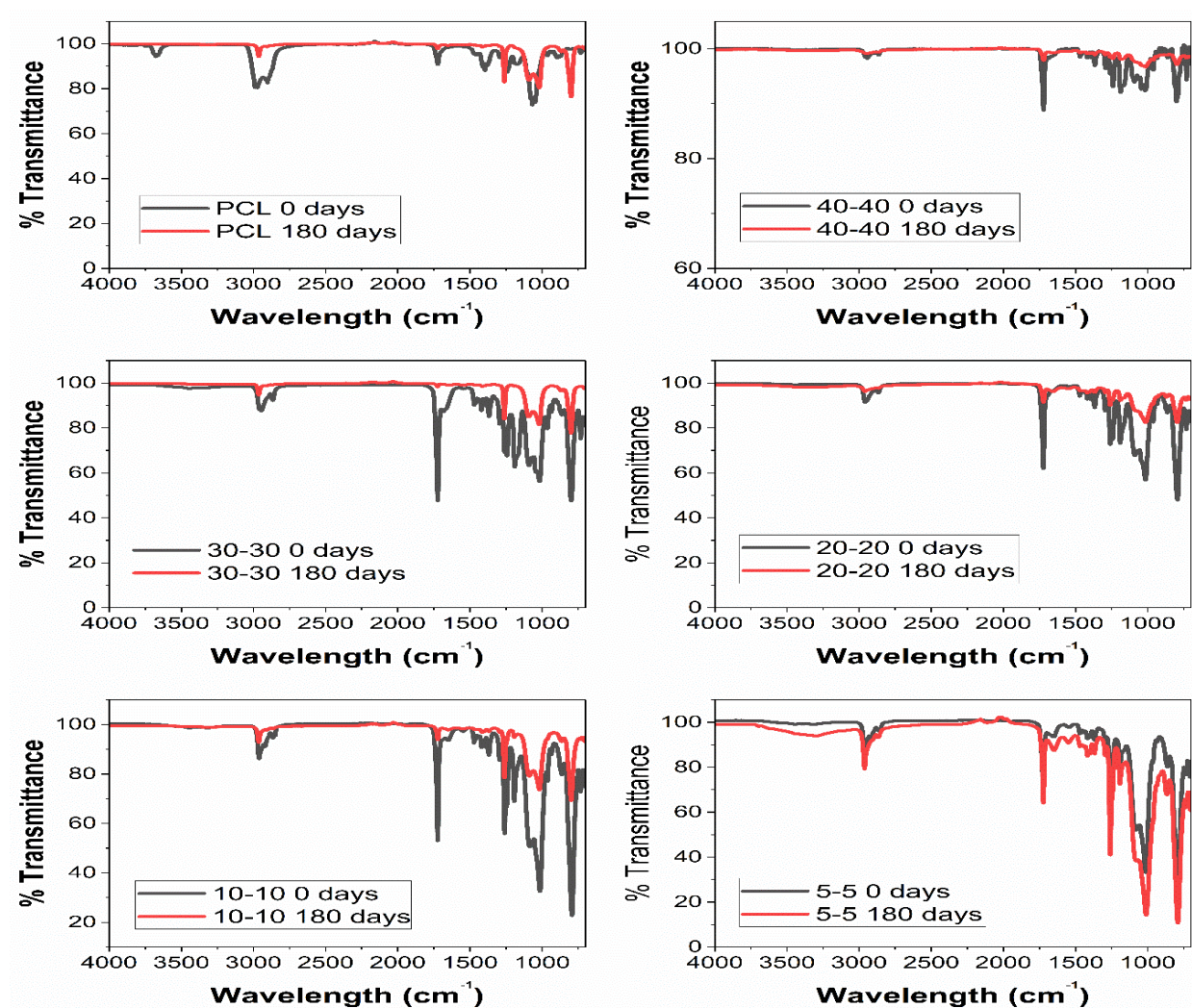


Figure 8.6. FTIR of PCL and PCL-PDMS-PCL triblock films before degradation and after degradation of 180 days

Degradation of soil buried specimens are examined for crystal melting temperature and crystallization temperature with differential scanning calorimetry (DSC) for regular time interval as shown in Table 8.2. Before soil burial, samples have been tested for all these parameters to be considered as a reference mentioned as zero days. There is a continuous increase in crystal melting temperature for all the polymeric films while the crystallization temperature is keep decreasing except 5-5. There is an interesting observation that 5-5 does not exhibit T_{cm} and T_c initially, though after 20 days of soil burial T_{cm} and T_c are observed in each time interval.

Table 8.2. Percentage crystallinity, crystal melting point and crystallization temperature of PCL and PCL-PDMS-PCL triblock copolymer films at before degradation and different time of interval of degradation

Sample/ Days	PCL		40-40		30-30		20-20		10-10		5-5	
	T_{cm}	T_c	T_{cm}	T_c	T_{cm}	T_c	T_{cm}	T_c	T_{cm}	T_c	T_{cm}	T_c
0 days	53.5	30.8	52.2	26.3	49.7	21.1	43.5	0.5	33.6	nil	nil	nil
40 days	53.1	27.7	52.5	24.7	50.0	21.4	46.7	10.1	47.8	20.2		
80 days	53.7	27.0	52.2	23.7	49.9	21.4	46.8	9.6, 28.9	35.8, 52.2	19.3	47.1	19.4
120 days	53.5	27.8	53.2	25.2	49.8	19.5	47.3	8.9	49.7	15.5	46.8	19.2
180 days	54.1	27.3	53.5	25.0	51.2	19.5	46.8	7.53	48.2	16.2	46.8	37.1

The percentage crystallinity of PCL, 40-40, 30-30, 20-20, 10-10 and 5-5 before degradation are 45.8, 37.3, 31.6, 17.9, 1.9 and nil, respectively as shown in Figure 8.7. In 40 days, there is significant increase in percentage crystallinity due to initial degradation of amorphous region of PCL and causes surface erosion as seen in Figure 8.1 & 8.2. After 40 days there is decrease in percentage crystallinity indicates chain fragmentation of crystalline region of PCL. 5-5 doesn't have crystallinity before degradation, though after 20 days of soil burial

percentage crystallinity is observed in each time interval. Ma *et al.* analyzed the biodegradation of different molecular weight PCL films by *Candida antarctica* lipase for 20 hours and reported that crystallinity decreased in initial 8 hour which indicate simultaneous degradation of both crystalline and amorphous region though in 8 to 20 hour the reduction in crystallinity is not in a regular pattern and not much significant [262].

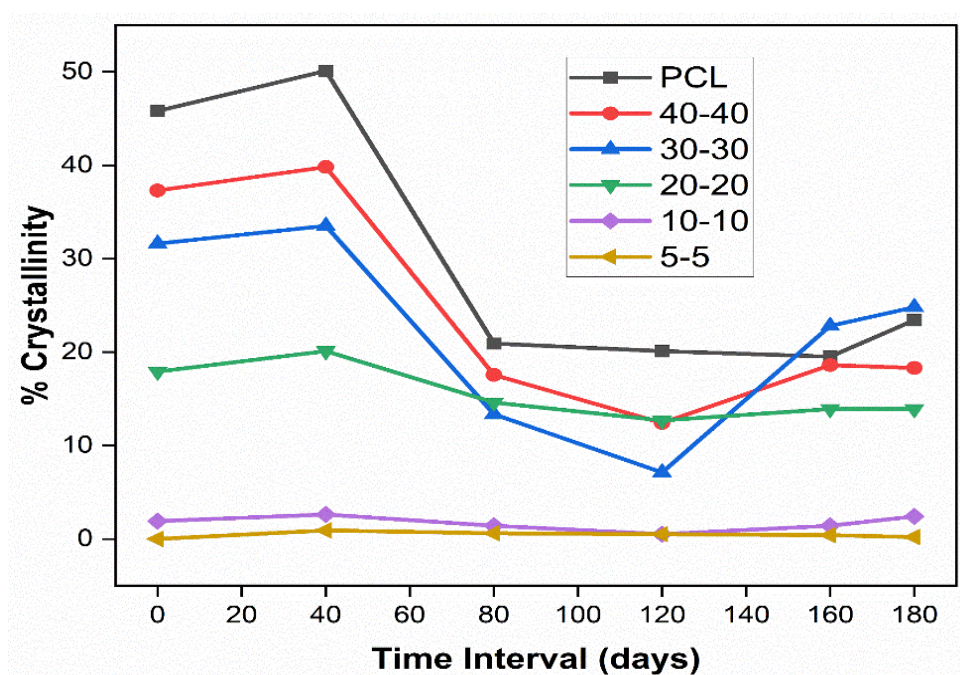


Figure 8.7. DSC percentage crystallinity of PCL and PCL-PDMS-PCL triblock films before degradation and degradation at different time of interval

8.3 Mechanism of degradation

The degradation mechanism of PCL-PDMS-PCL triblock photo-crosslinked copolymer films is proposed as shown in Figure 8.8. The surface erosion takes place initially due to degradation of amorphous region of PCL content. It reduces the smoothness and lusture of film. The presence of PDMS is somehow protecting the PCL content to degrade rapidly due to slow biodegradable behavior in presence of moisture. Further, soil microorganism and moisture attack on crystalline part of PCL content and causes chain scission and degradation of macromolecules. This resulted in cracks formation and breakage of films gradually. As the PCL chain length decreases and crosslink density increases, the rate of degradation of films

become low. So, inclusion of the PDMS and change in crosslink density are the key factors to tune the degradation rate of PCL copolymer for different application.

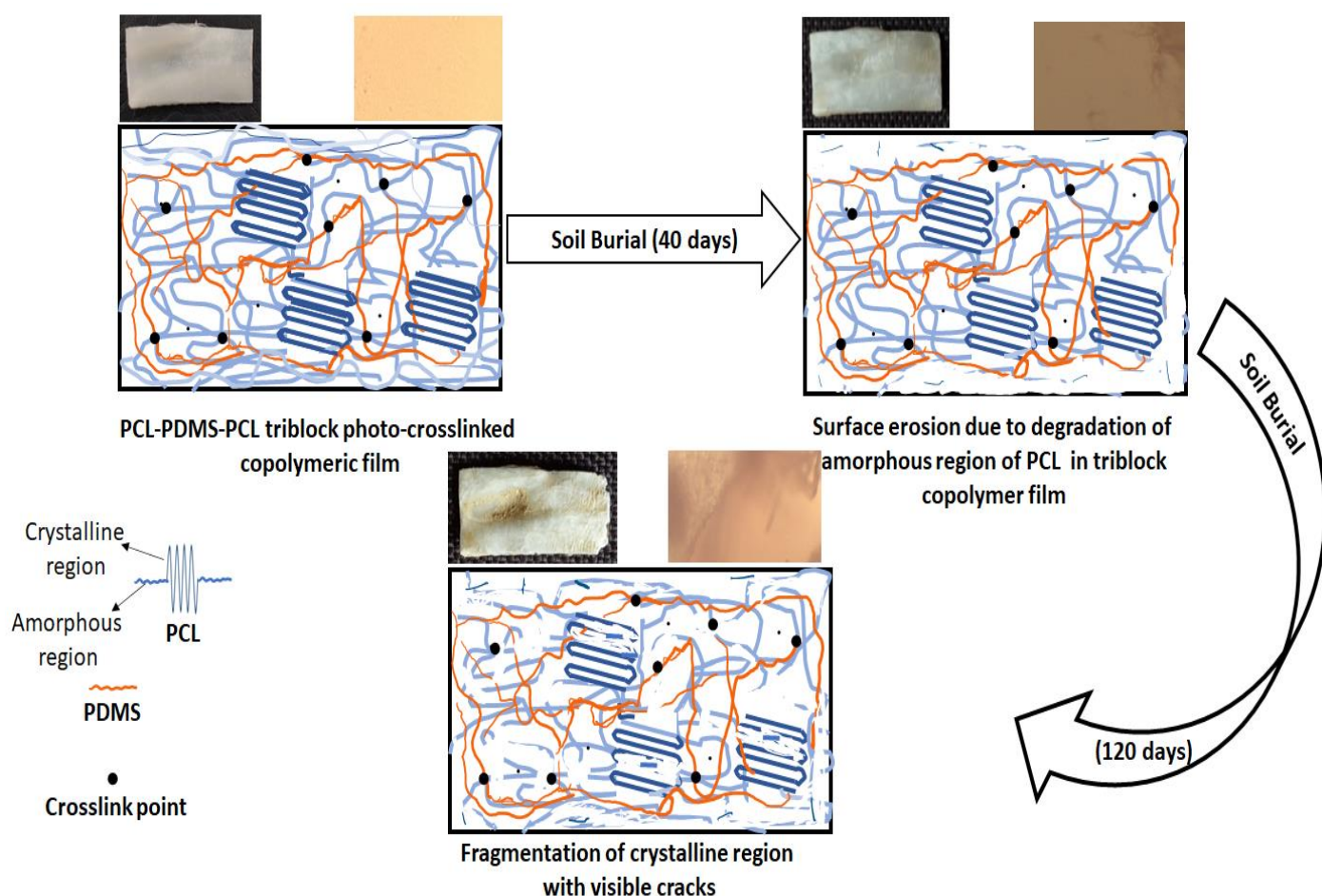


Figure 8.8. Mechanism of degradation of PCL-PDMS-PCL photo-crosslinked triblock copolymer films

8.5 Conclusion

In this study, PCL-PDMS-PCL triblock copolymer films with different PCL chain length are evaluated for their degradation behavior in soil burial. The morphological changes observed with digital camera, optical microscope, and SEM, indicates that surface erosion takes place initially and gradually cracks become visible and film break due to chain scission and C-O bond cleavage. The macrolevel changes analyzed with thermal degradation of samples in different interval. The degradation temperature keeps increasing for fifty percent weight loss for each sample at different time interval of soil burial. The degradation temperature becomes

high with reduction in PCL chain length and increase in crosslink density. The crystal melting temperature keep increasing and crystallization temperature decrease continuously with soil burial time interval, though 5-5 does not follow the trend due to very low PCL content. The structural changes shows that PCL content is majorly degrade after 180 days of soil burial. The percentage crystallinity increased slightly after 40 days due to degradation of amorphous region of PCL content, further it decreases continuously due to attack on crystalline part as well as on amorphous part of PCL. The varying PCL length, inclusion of PDMS content and varying crosslink density become the influencing factor of degradation behavior of PCL-PDMS-PCL triblock photo-crosslinked copolymer films. For different application, requirement of slow degradation can be achieved by addition of PDMS and increase in crosslink density.

Chapter 9

Conclusion and Future Scope

9.1 Conclusion and future scope of the research work

The PCL-PDMS-PCL triblock photocrosslinked films are synthesised via ring opening polymerisation. The PCL chain length varying from 40-40 to 5-5 while keeping the PDMS content constant in copolymer composition. The molecular structure is determined by FTIR and NMR techniques. The molecular weight obtained is in the range of 11640 g/mol to 3641 g/mol and percentage crystallinity from nil to 41.9%.

The viscoelastic properties are evaluated above crystal melting temperature. It has been found that at 80°C, the viscoelastic properties of triblock films are dependent on molecular weight and crosslink density. The LVER range obtained is up to 1% shear strain for all samples. In Frequency sweep, the storage modulus is increasing with decrease in molecular weight. There is decrease in loss factor and more solid like behaviour as the PCL length get decrease and crosslink density increases. Creep recovery and structure recovery are increasing with decrease in PCL chain length. The tensile strength, elongation and storage modulus at ambient condition is decreasing with decrease in PCL chain length. This study helps to analyse the behaviour of films while going under stretching or stress for shape memory application.

The range of crystallization temperature is obtained by non-isothermal DSC thermogram, which was further used to evaluate isothermal crystallization kinetics. The isothermal study is carried out with Avrami and Lauritzen-Hoffman model. The Avrami analysis helps to quantify the crystal growth of PCL and PCL-PDMS-PCL triblock copolymers. It concludes

that crystal growth for PCL is two-dimensional, whereas growth mechanism of crystal of PCL in the copolymers tends to be three-dimensional. With the inclusion of PDMS, stability of the crystals for PCL in the copolymer increases due to micro-phase separation which further helps to fix the temporary shape in shape memory application. The energy barrier is increased with increasing content of PDMS and affects the growth rate of crystal. The shape fixity ratio decreases with decreasing crystallinity and increasing fold surface energy as it hinders the growth of PCL crystallite. Higher fold surface energy requires more time to generate full crystal of PCL segment, which ultimately affects the fixity to temporary shape and needs more time to fix the secondary shape.

Soil burial degradation decreases with inclusion of PDMS and amorphous part of PCL get degraded first followed by crystalline part. The shape memory properties are dependent on the semicrystalline structure of PCL, still with inclusion of PDMS the crystal perfection stability increases which keep intact the shape memory behaviour including shape fixity and shape recovery.

The widens application of shape memory PCL-PDMS-PCL triblock copolymers are ended in landfill which make it obvious to study about soil burial degradation behaviour. This study tells that degradation behaviour of triblock can be tuned with PCL chain length. As the PCL length is getting decreases the degradation rate is getting decreased. The amorphous part of PCL is get attacked by microorganism first then its crystalline part. Still, PCL and PDMS both are biocompatible, so they are not going to affect the environment and soil negatively.

From the attained results of the produced polymers in this work, it is apparent that mechanical properties need to be improved to broaden the application area. The incorporation of filler, and preparing a composite will certainly enhance the mechanical properties. Here the filler should be either natural or biocompatible so that, soil burial degradation behaviour

may not deviate much. Addition of antimicrobial additives will also lead to antimicrobial packaging and coatings applications. The cost analysis is required for the commercialisation of this polymer after final tuning of all the required properties according to application area.

9.2 Future Scope

- To synthesis other copolymers by using different biocompatible comonomers with Polycaprolactone to produce samples with broader range of temperature responsive shape memory behavior and study their properties.
- With increasing environmental concerns, there is a growing demand for sustainable packaging materials. PCL copolymers, being biodegradable and derived from renewable resources, hold great potential for use in sustainable packaging solutions. Future developments may involve optimizing PCL copolymers for specific packaging requirements, improving their barrier properties, and exploring novel processing techniques for large-scale production.
- PCL copolymers are widely used in additive manufacturing or 3D printing due to their low melting point, good mechanical properties, and biodegradability. Future advancements may involve developing new PCL-based filaments or resins with enhanced properties such as improved printability, higher resolution, and better compatibility with various printing techniques.
- Future developments may involve exploring novel coating formulations, optimizing adhesion properties, and improving the durability and performance of PCL based coatings for applications in industries such as automotive, aerospace, and electronics.

Chapter 10

References

-
1. Jullian N, Rubatat L, Gerard P, et al (2011) Structure and rheology of di- and triblock copolymers of polystyrene and poly(n-butyl acrylate). *J Rheol (N Y N Y)* 55:379–400. <https://doi.org/10.1122/1.3544590>
 2. Thunga M (2009) Rheological and mechanical behaviour of block copolymers, multigraft copolymers and block copolymer nanocomposites
 3. Zhang Y, Karasu F, Rocco C, et al (2016) PDMS-based self-replenishing coatings. *Polymer (Guildf)* 107:249–262. <https://doi.org/10.1016/j.polymer.2016.11.026>
 4. Azemar F, Fay F, Réhel K, Linossier I (2015) Development of hybrid antifouling paints. *Prog Org Coatings* 87:10–19. <https://doi.org/10.1016/j.porgcoat.2015.04.007>
 5. Gevaux L, Lejars M, Margaillan A, Bressy C (2018) Water erodible coatings based on a hydrolyzable PDMS/polyester network. *Mater Today Commun* 17:517–526. <https://doi.org/10.1016/j.mtcomm.2018.10.020>
 6. Xue R, Behera P, Xu J, et al (2014) Polydimethylsiloxane core-polycaprolactone shell nanofibers as biocompatible, real-time oxygen sensors. *Sensors Actuators, B Chem* 192:697–707. <https://doi.org/10.1016/j.snb.2013.10.084>
 7. Govedarica MN, Gođevac D, Ostojic S (2011) Synthesis and characterization of novel urethane-siloxane copolymers with a high content of PCL-PDMS-PCL segments. *J Appl Polym Sci* 122:2715–2730. <https://doi.org/10.1002/app>
 8. Gordin C, Rusu M, Delaite C, Salhi S (2009) Crystallinity behaviour in poly (ϵ -caprolactone) -b- Poly (dimethylsiloxane) diblock and triblock copolymers through FTIR and DSC. *Mater Plast* 46:37–46
 9. Ekin A, Webster DC (2006) Synthesis and characterization of novel hydroxyalkyl carbamate

- and dihydroxyalkyl carbamate terminated poly (dimethylsiloxane) oligomers and their block copolymers with poly (ϵ -caprolactone). *Macromolecules* 39:8659–8668.
<https://doi.org/10.1021/ma061629a>
10. Yilgör E, Isik M, Söz CK, Yilgör I (2016) Synthesis and structure-property behavior of polycaprolactone-polydimethylsiloxane-polycaprolactone triblock copolymers. *Polymer (Guildf)* 83:138–153. <https://doi.org/10.1016/j.polymer.2015.12.024>
 11. Poojari Y, Clarson SJ (2009) Lipase catalyzed synthesis of poly(ϵ -Caprolactone)-poly(Dimethylsiloxane)-poly(ϵ -Caprolactone) triblock copolymers. *Silicon* 1:165–172.
<https://doi.org/10.1007/s12633-009-9013-3>
 12. Schoener CA, Weyand CB, Murthy R, Grunlan MA (2010) Shape memory polymers with silicon-containing segments. *J Mater Chem* 20:1787–1793. <https://doi.org/10.1039/b924032b>
 13. Zhang D, Giese ML, Prukop SL, Grunlan MA (2011) Poly (ϵ -caprolactone) -based shape memory polymers with variable polydimethylsiloxane soft segment lengths. *J Polym Sci Part A Polym Chem* 49:754–761. <https://doi.org/10.1002/pola.24488>
 14. Fabrice A, Fabienne F, Karine R, Linossier I (2014) Control of hydration and degradation properties of triblock copolymers polycaprolactone-b-polydimethylsiloxane-b-polycaprolactone. *J Appl Polym Sci* 40431:1–8. <https://doi.org/10.1002/app.40431>
 15. Kelly CA, Murphy SH, Leeke GA, et al (2013) Rheological studies of polycaprolactone in supercritical CO₂. *Eur Polym J* 49:464–470. <https://doi.org/10.1016/j.eurpolymj.2012.11.021>
 16. Sangroniz L, Barbieri F, Cavallo D, et al (2018) Rheology of self-nucleated poly(ϵ -caprolactone) melts
 17. Kotula AP, Migler KB (2018) Evaluating models for polycaprolactone crystallization via simultaneous rheology and Raman spectroscopy. *J Rheol (N Y N Y)* 62:343–356.
<https://doi.org/10.1122/1.5008381>
 18. Chae DW, Nam Y, An SG, et al (2017) Effects of molecular architecture on the rheological

- and physical properties of polycaprolactone. *Korea Aust Rheol J* 29:129–135.
<https://doi.org/10.1007/s13367-017-0014-2>
19. Wietor JL, Van Beek DJM, Peters GW, et al (2011) Effects of branching and crystallization on rheology of polycaprolactone supramolecular polymers with ureidopyrimidinone end groups. *Macromolecules* 44:1211–1219. <https://doi.org/10.1021/ma1026065>
 20. Ginzburg A, Ramakrishnan V, Rongo L, et al (2020) The influence of polypropylene-block/graft-polycaprolactone copolymers on melt rheology, morphology, and dielectric properties of polypropylene/polycarbonate blends. *Rheol Acta* 59:601–619.
<https://doi.org/10.1007/s00397-020-01223-7>
 21. Narayanan G, Chung CC, Aguda R, et al (2016) Correlation of the stoichiometries of poly(ϵ -caprolactone) and α -cyclodextrin pseudorotaxanes with their solution rheology and the molecular orientation, crystallite size, and thermomechanical properties of their nanofibers. *RSC Adv* 6:111326–111336. <https://doi.org/10.1039/c6ra23536k>
 22. Hassan Ajili S, Golshan Ebrahimi N, Ansari M (2008) Rheological study of segmented polyurethane and polycaprolactone blends. *Rheol Acta* 47:81–87.
<https://doi.org/10.1007/s00397-007-0213-8>
 23. Noroozi N, Schafer LL, Savvas GH (2012) Thermorheological Properties of Poly (ϵ -caprolactone)/ Polylactide Blends. *Polym Eng Sci* 52:2348–2359. <https://doi.org/10.1002/pen>
 24. Shin BY, Lee S Il, Shin YS, et al (2004) Rheological, mechanical and biodegradation studies on blends of thermoplastic starch and polycaprolactone. *Polym Eng Sci* 44:1429–1438.
<https://doi.org/10.1002/pen.20139>
 25. Elbadawi M (2019) Rheological and Mechanical Investigation into the Effect of Different Molecular Weight Poly(ethylene glycol)s on Polycaprolactone-Ciprofloxacin Filaments. *ACS Omega* 4:5412–5423. <https://doi.org/10.1021/acsomega.8b03057>
 26. Kim KJ, White JL (2009) Effects of regenerated cellulose and natural fiber on interfacial

- adhesion, rheology and crystallization property in ϵ -polycaprolactone compounds. *Compos Interfaces* 16:619–637. <https://doi.org/10.1163/092764409X12477406858223>
27. Sousa JC, Costa ARM, Lima JC, et al (2020) Polycaprolactone (PCL)/alumina and PCL/niobium pentoxide composites: Rheology, crystallization, and mechanical properties. *Polym Compos* 41:1265–1276. <https://doi.org/10.1002/pc.25452>
 28. Bouakaz BS, Habi A, Grohens Y, Pillin I (2018) Effect of combinations of nanofillers on rheology-structure relations in biodegradable poly(ϵ -caprolactone) nanocomposites. *Appl Clay Sci* 161:35–47. <https://doi.org/10.1016/j.clay.2018.04.006>
 29. Sathya K, Syed S.H. R (2006) Rheological Behavior of Starch–Polycaprolactone (PCL) Nanocomposite Melts Synthesized by Reactive Extrusion. *Polym Eng Sci* 46:650–658. <https://doi.org/10.1002/pen>
 30. Wang Y, Xu C, Wu D, et al (2018) Rheology of the cellulose nanocrystals filled poly(ϵ -caprolactone) biocomposites. *Polymer (Guildf)* 140:167–178. <https://doi.org/10.1016/j.polymer.2018.02.050>
 31. Nie Y, Zhan H, Kou L, Gu Y (2021) Atomistic Insights on the Rheological Property of Polycaprolactone Composites with the Addition of Graphene. *Adv Mater Technol* 2100507:1–9. <https://doi.org/10.1002/admt.202100507>
 32. Vega JF, Fernández-Alcázar J, López J V., et al (2017) Competition between supernucleation and plasticization in the crystallization and rheological behavior of PCL/CNT-based nanocomposites and nanohybrids. *J Polym Sci Part B Polym Phys* 55:1310–1325. <https://doi.org/10.1002/polb.24385>
 33. Salehiyan R, Hyun K (2013) Effect of organoclay on non-linear rheological properties of poly(lactic acid)/poly(caprolactone) blends. *Korean J Chem Eng* 30:1013–1022. <https://doi.org/10.1007/s11814-013-0035-6>
 34. Sebastian JM, Graessley WW, Register RA (2002) Steady-shear rheology of block copolymer

- melts and concentrated solutions: Defect-mediated flow at low stresses in body-centered-cubic systems. *J Rheol (N Y N Y)* 46:863. <https://doi.org/10.1122/1.1475979>
35. Wang X, Dormidontova EE, Lodge TP (2002) The Order - Disorder Transition and the Disordered Micelle Regime for Poly (ethylenepropylene- b -dimethylsiloxane) Spheres. *Macromolecules* 35:9687–9697
 36. He P, Shen W, Yu W, Zhou C (2014) Mesophase Separation and Rheology of Olefin Multiblock Copolymers. *Macromolecules* 47:807–820
 37. Park HE, Dealy JM, Marchand GR, et al (2010) Rheology and Structure of Molten, Olefin Multiblock Copolymers. *Macromolecules* 43:6789–6799. <https://doi.org/10.1021/ma1012122>
 38. Nie Z, Yu W, Zhou C (2016) Nonlinear rheological behavior of multiblock copolymers under large amplitude oscillatory shear large amplitude oscillatory shear. *J Rheol (N Y N Y)* 60:1161–1179. <https://doi.org/10.1122/1.4961483>
 39. Bramfeldt H, Sarazin P, Vermette P (2008) Blends as a strategy towards tailored hydrolytic degradation of poly(ϵ -caprolactone-co-d,l-lactide)-poly(ethylene glycol)-poly(ϵ -caprolactone-co-d,l-lactide) co-polymers. *Polym Degrad Stab* 93:877–882. <https://doi.org/10.1016/j.polymdegradstab.2008.01.023>
 40. Pamuła E, Dobrzyński P, Bero M, Paluszkiwicz C (2005) Hydrolytic degradation of porous scaffolds for tissue engineering from terpolymer of L-lactide, ϵ -caprolactone and glycolide. *J Mol Struct* 744–747:557–562. <https://doi.org/10.1016/j.molstruc.2004.11.016>
 41. Fernández J, Etxeberria A, Sarasua JR (2015) In vitro degradation studies and mechanical behavior of poly(ϵ -caprolactone-co- δ -valerolactone) and poly(ϵ -caprolactone-co-L-lactide) with random and semi-alternating chain microstructures. *Eur Polym J* 71:585–595. <https://doi.org/10.1016/j.eurpolymj.2015.09.001>
 42. Gouda MK, Swellam AE, Omar SH (2012) Biodegradation of Synthetic Polyesters (BTA and PCL) with Natural Flora in Soil Burial and Pure Cultures under Ambient Temperature. *Res J*

43. Rizzarelli P, Cirica M, Pastorelli G, et al (2015) Aliphatic poly(ester amide)s from sebacic acid and aminoalcohols of different chain length: Synthesis, characterization and soil burial degradation. *Polym Degrad Stab* 121:90–99.
<https://doi.org/10.1016/j.polymdegradstab.2015.08.010>
44. Park ES, Kim HS, Kim MN, Yoon JS (2005) Soil burial test for poly(ethylene-co-vinyl alcohol)-graft-polycaprolactone. *J Appl Polym Sci* 96:1064–1071.
<https://doi.org/10.1002/app.21498>
45. Arolkar GA, Jacob SM, Pandiyaraj KN, et al (2016) Effect of TEOS plasma polymerization on corn starch/poly(ϵ -caprolactone) film: Characterization, properties and biodegradation. *RSC Adv* 6:16779–16789. <https://doi.org/10.1039/c5ra23414j>
46. Ludueña LN, Vázquez A, Alvarez VA (2013) Effect of the type of clay organo-modifier on the morphology, thermal/mechanical/impact/barrier properties and biodegradation in soil of polycaprolactone/clay nanocomposites. *J Appl Polym Sci* 128:2648–2657.
<https://doi.org/10.1002/app.38425>
47. Cesur S, Koroğlu C, Yalçın HT (2018) Antimicrobial and biodegradable food packaging applications of polycaprolactone/organo nanoclay/chitosan polymeric composite films. *J Vinyl Addit Technol* 24:376–387. <https://doi.org/10.1002/vnl.21607>
48. Cesur S (2018) The Effects of Additives on the Biodegradation of Polycaprolactone Composites. *J Polym Environ* 26:1425–1444. <https://doi.org/10.1007/s10924-017-1029-y>
49. Chan DS, Fnais N, Ibrahim I, et al (2019) Exploring polycaprolactone in tracheal surgery: A scoping review of in-vivo studies. *Int J Pediatr Otorhinolaryngol* 123:38–42.
<https://doi.org/10.1016/j.ijporl.2019.04.039>
50. Dwivedi R, Kumar S, Pandey R, et al (2020) Polycaprolactone as biomaterial for bone scaffolds: Review of literature. *J Oral Biol Craniofacial Res* 10:381–388.

<https://doi.org/10.1016/j.jobcr.2019.10.003>

51. Janmohammadi M, Nourbakhsh MS (2019) Electrospun polycaprolactone scaffolds for tissue engineering: a review. *Int J Polym Mater Polym Biomater* 68:527–539.
<https://doi.org/10.1080/00914037.2018.1466139>
52. Woodruff MA, Hutmacher DW (2010) The return of a forgotten polymer - Polycaprolactone in the 21st century. *Prog Polym Sci* 35:1217–1256.
<https://doi.org/10.1016/j.progpolymsci.2010.04.002>
53. Guarino V, Gentile G, Sorrentino L, Ambrosio L (2017) Polycaprolactone: Synthesis, Properties, and Applications
54. Labet M, Thielemans W (2009) Synthesis of polycaprolactone: A review. *Chem Soc Rev* 38:3484–3504. <https://doi.org/10.1039/b820162p>
55. Mondal D, Griffith M, Venkatraman SS (2016) Polycaprolactone-based biomaterials for tissue engineering and drug delivery: Current scenario and challenges. *Int J Polym Mater Polym Biomater* 65:255–265. <https://doi.org/10.1080/00914037.2015.1103241>
56. Suwantong O (2016) Biomedical applications of electrospun polycaprolactone fiber mats. *Polym Adv Technol* 27:1264–1273. <https://doi.org/10.1002/pat.3876>
57. Hajiali F, Tajbakhsh S, Shojaei A (2018) Fabrication and Properties of Polycaprolactone Composites Containing Calcium Phosphate-Based Ceramics and Bioactive Glasses in Bone Tissue Engineering: A Review. *Polym Rev* 58:164–207.
<https://doi.org/10.1080/15583724.2017.1332640>
58. Prasad A, Kandasubramanian B (2019) Fused deposition processing polycaprolactone of composites for biomedical applications. *Polym Technol Mater* 58:1365–1398.
<https://doi.org/10.1080/25740881.2018.1563117>
59. Abrisham M, Noroozi M, Panahi-Sarmad M, et al (2020) The role of polycaprolactone-triol (PCL-T) in biomedical applications: A state-of-the-art review. *Eur Polym J* 131:109701.

<https://doi.org/10.1016/j.eurpolymj.2020.109701>

60. Dodero A, Alloisio M, Castellano M, Vicini S (2020) Multilayer Alginate-Polycaprolactone Electrospun Membranes as Skin Wound Patches with Drug Delivery Abilities. *ACS Appl Mater Interfaces* 12:31162–31171. <https://doi.org/10.1021/acsami.0c07352>
61. Mandal P, Shunmugam R (2020) Polycaprolactone: a biodegradable polymer with its application in the field of self-assembly study. *J Macromol Sci Part A Pure Appl Chem* 58:111–129. <https://doi.org/10.1080/10601325.2020.1831392>
62. Dabbaghi A, Ramazani A, Farshchi N, et al (2021) Synthesis, physical and mechanical properties of amphiphilic hydrogels based on polycaprolactone and polyethylene glycol for bioapplications: A review. *J Ind Eng Chem* 101:307–323. <https://doi.org/10.1016/j.jiec.2021.05.051>
63. Raina N, Pahwa R, Khosla JK, et al (2021) Polycaprolactone-based materials in wound healing applications. *Polym Bull online*: <https://doi.org/10.1007/s00289-021-03865-w>
64. Mahmoud Salehi AO, Heidari Keshel S, Sefat F, Tayebi L (2021) Use of polycaprolactone in corneal tissue engineering: A review. *Mater Today Commun* 27:102402. <https://doi.org/10.1016/j.mtcomm.2021.102402>
65. Ilyas RA, Zuhri MYM, Nor M, et al (2022) Natural Fiber-Reinforced Polycaprolactone Green and Hybrid Biocomposites for Various Advanced Applications. *Polymers (Basel)* 14:182–211
66. Bartnikowski M, Dargaville TR, Ivanovski S, Hutmacher DW (2019) Degradation mechanisms of polycaprolactone in the context of chemistry, geometry and environment. *Prog Polym Sci* 96:1–20. <https://doi.org/10.1016/j.progpolymsci.2019.05.004>
67. Tran J, Pesenti T, Cressonnier J, et al (2019) Degradable Copolymer Nanoparticles from Radical Ring-Opening Copolymerization between Cyclic Ketene Acetals and Vinyl Ethers. *Biomacromolecules* 20:305–317. <https://doi.org/10.1021/acs.biomac.8b01500>
68. Liu C, Qin H, Mather PT (2007) Review of progress in shape-memory polymers. *J Mater*

- Chem Chem 17:1543–1558. <https://doi.org/10.1039/b615954k>
69. Han W, Liao X, Yang Q, et al (2017) Crystallization and morphological transition of poly(l-lactide)-poly(ϵ -caprolactone) diblock copolymers with different block length ratios. RSC Adv 7:22515–22523. <https://doi.org/10.1039/c7ra03496b>
 70. Dakshinamoorthy D, Peruch F (2012) Block and random copolymerization of μ -caprolactone, L-, and rac-lactide using titanium complex derived from aminodiol ligand. J Polym Sci Part A Polym Chem 50:2161–2171. <https://doi.org/10.1002/pola.25983>
 71. Yang J, Zhou Q, Shen K, et al (2018) Controlling nanodomain morphology of epoxy thermosets templated by poly(caprolactone)-: Block -poly(dimethylsiloxane)- block - poly(caprolactone) ABA triblock copolymer. RSC Adv 8:3705–3715. <https://doi.org/10.1039/c7ra12826f>
 72. Qindeel M, Ahmed N, Shah KU, et al (2020) New, Environment Friendly Approach for Synthesis of Amphiphilic PCL–PEG–PCL Triblock Copolymer: An Efficient Carrier for Fabrication of Nanomicelles. J Polym Environ 28:1237–1251. <https://doi.org/10.1007/s10924-020-01683-1>
 73. Rani S, Gupta U (2021) Synthesis, Morphology, and Rheological Evaluation of HPMA (N -2-Hydroxypropyl Methacrylamide)-PCL (Polycaprolactone) Conjugates. ACS Omega 6:29788–29803. <https://doi.org/10.1021/acsomega.1c04243>
 74. Li J, Xu H, Hu N, et al (2012) Studies on photoreactive and biodegradable copolymers composed of poly(-caprolactone) and 4-hydroxycinnamic acid. Polym J 44:1123–1130. <https://doi.org/10.1038/pj.2012.85>
 75. Liu MJ, Chen SC, Yang KK, Wang YZ (2015) Biodegradable polylactide based materials with improved crystallinity, mechanical properties and rheological behaviour by introducing a long-chain branched copolymer. RSC Adv 5:42162–42173. <https://doi.org/10.1039/c5ra04742k>
 76. Jiao M, Yang K, Cao J, et al (2014) Designing and characterization of poly(L-Lactide)/poly(ϵ -

- Caprolactone) multiblock copolymers. *J Macromol Sci Part B Phys* 53:191–204.
<https://doi.org/10.1080/00222348.2013.810058>
77. Polo Fonseca L, Bergamo Trinca R, Isabel Felisberti M (2016) Thermo-responsive polyurethane hydrogels based on poly(ethylene glycol) and poly(caprolactone): Physico-chemical and mechanical properties. *J Appl Polym Sci* 133:1–10.
<https://doi.org/10.1002/app.43573>
 78. Fuoco T, Finne-Wistrand A (2019) Enhancing the Properties of Poly(ϵ -caprolactone) by Simple and Effective Random Copolymerization of ϵ -Caprolactone with p-Dioxanone. *Biomacromolecules* 20:3171–3180. <https://doi.org/10.1021/acs.biomac.9b00745>
 79. Yang LQ, Meng S, Liu DH, et al (2014) Potential Biodegradable Implants from ϵ -Caprolactone and D, L-Lactide Copolymers: Synthesis, Properties, and In Vivo Degradation. *Int J Polym Anal Charact* 19:422–440. <https://doi.org/10.1080/1023666X.2014.920069>
 80. Saatchi M, Behl M, Nöchel U, Lendlein A (2015) Copolymer networks from oligo (ϵ -caprolactone) and n-butyl acrylate enable a reversible bidirectional shape-memory effect at human body temperature. *Macromol Rapid Commun* 36:880–884
 81. Bellani CF, Pollet E, Hebraud A, et al (2016) Morphological, thermal, and mechanical properties of poly(ϵ -caprolactone)/poly(ϵ -caprolactone)-grafted-cellulose nanocrystals mats produced by electrospinning. *J Appl Polym Sci* 133:4–11. <https://doi.org/10.1002/app.43445>
 82. Ninago MD, De Freitas AGO, Hanazumi V, et al (2015) Synthesis of Grafted Block Copolymers Based on ϵ -Caprolactone: Influence of Branches on Their Thermal Behavior. *Macromol Chem Phys* 216:2331–2343. <https://doi.org/10.1002/macp.201500248>
 83. Moura I, Nogueira R, Bounor-Legare V, Machado A V. (2014) Effect of PCL and EVA molar mass on the development of sustainable polymers. *Soft Mater* 12:88–97.
<https://doi.org/10.1080/1539445X.2012.756818>
 84. Hedir GG, Bell CA, O'Reilly RK, Dove AP (2015) Functional degradable polymers by radical

- ring-opening copolymerization of MDO and vinyl bromobutanoate: Synthesis, degradability and post-polymerization modification. *Biomacromolecules* 16:2049–2058.
<https://doi.org/10.1021/acs.biomac.5b00476>
85. Dai G, Xie Q, Chen S, et al (2018) Biodegradable poly(ester)-poly(methyl methacrylate) copolymer for marine anti-biofouling. *Prog Org Coatings* 124:55–60.
<https://doi.org/10.1016/j.porgcoat.2018.08.003>
 86. Komatsu S, Asoh TA, Ishihara R, Kikuchi A (2017) Facile preparation of degradable thermoresponsive polymers as biomaterials: Thermoresponsive polymers prepared by radical polymerization degrade to water-soluble oligomers. *Polymer (Guildf)* 130:68–73.
<https://doi.org/10.1016/j.polymer.2017.09.073>
 87. Shi Y, Schmalz H, Agarwal S (2015) Designed enzymatically degradable amphiphilic conetworks by radical ring-opening polymerization. *Polym Chem* 6:6409–6415.
<https://doi.org/10.1039/c5py00962f>
 88. Undin J, Finne-Wistrand A, Albertsson AC (2014) Adjustable degradation properties and biocompatibility of amorphous and functional poly(ester-acrylate)-based materials. *Biomacromolecules* 15:2800–2807. <https://doi.org/10.1021/bm500689g>
 89. Undin J, Finne-Wistrand A, Albertsson AC (2013) Copolymerization of 2-methylene-1,3-dioxepane and glycidyl methacrylate, a well-defined and efficient process for achieving functionalized polyesters for covalent binding of bioactive molecules. *Biomacromolecules* 14:2095–2102. <https://doi.org/10.1021/bm4004783>
 90. El-Naggar ME, shalaby ES, Abd-Al-Aleem AH, et al (2021) Synthesis of environmentally benign antimicrobial dressing nanofibers based on polycaprolactone blended with gold nanoparticles and spearmint oil nanoemulsion. *J Mater Res Technol* 15:3447–3460.
<https://doi.org/10.1016/j.jmrt.2021.09.136>
 91. Bai H, Xiu H, Gao J, et al (2012) Tailoring impact toughness of poly(L-lactide)/poly(ϵ -

- caprolactone) (PLLA/PCL) blends by controlling crystallization of PLLA matrix. *ACS Appl Mater Interfaces* 4:897–905. <https://doi.org/10.1021/am201564f>
92. Hu M, Deng C, Gu X, et al (2020) Manipulating the Strength-Toughness Balance of Poly(l-lactide) (PLLA) via Introducing Ductile Poly(ϵ -caprolactone) (PCL) and Strong Shear Flow. *Ind Eng Chem Res* 59:1000–1009. <https://doi.org/10.1021/acs.iecr.9b05380>
 93. Lv Q, Wu D, Xie H, et al (2016) Crystallization of poly(ϵ -caprolactone) in its immiscible blend with polylactide: Insight into the role of annealing histories. *RSC Adv* 6:37721–37730. <https://doi.org/10.1039/c6ra07752h>
 94. Ostafinska A, Fortelny I, Nevoralova M, et al (2015) Synergistic effects in mechanical properties of PLA/PCL blends with optimized composition, processing, and morphology. *RSC Adv* 5:98971–98982. <https://doi.org/10.1039/c5ra21178f>
 95. Wachirahuttapong S, Thongpin C, Sombatsompop N (2016) Effect of PCL and Compatibility Contents on the Morphology, Crystallization and Mechanical Properties of PLA/PCL Blends. *Energy Procedia* 89:198–206. <https://doi.org/10.1016/j.egypro.2016.05.026>
 96. Chang R, Rohindra D, Lata R, et al (2019) Development of poly(ϵ -caprolactone)/pine resin blends: Study of thermal, mechanical, and antimicrobial properties. *Polym Eng Sci* 59:E32–E41. <https://doi.org/10.1002/pen.24950>
 97. Bou-Francis A, Piercey M, Al-Qatami O, et al (2020) Polycaprolactone blends for fracture fixation in low load-bearing applications. *J Appl Polym Sci* 137:48940. <https://doi.org/10.1002/app.48940>
 98. Wang F, Yang X, Zou Y (2016) Effect of the maleation of lignosulfonate on the mechanical and thermal properties of lignosulfonate/poly(ϵ -caprolactone) blends. *J Appl Polym Sci* 133:1–7. <https://doi.org/10.1002/app.42925>
 99. Zeng A, Wang Y, Li D, et al (2021) Preparation and antibacterial properties of polycaprolactone/quaternized chitosan blends. *Chinese J Chem Eng* 32:462–471.

<https://doi.org/10.1016/j.cjche.2020.10.001>

100. Vergara-Porras B, Gracida-Rodríguez JN, Pérez-Guevara F (2016) Thermal processing influence on mechanical, thermal, and biodegradation behavior in poly(β -hydroxybutyrate)/poly(ϵ -caprolactone) blends: A descriptive model. *J Appl Polym Sci* 133:1–12. <https://doi.org/10.1002/app.43569>
101. Przybysz M, Marć M, Klein M, et al (2018) Structural, mechanical and thermal behavior assessments of PCL/PHB blends reactively compatibilized with organic peroxides. *Polym Test* 67:513–521. <https://doi.org/10.1016/j.polymertesting.2018.03.014>
102. Woodard LN, Grunlan MA (2019) Hydrolytic Degradation of PCL-PLLA Semi-IPNs Exhibiting Rapid, Tunable Degradation. *ACS Biomater Sci Eng* 5:498–508. <https://doi.org/10.1021/acsbiomaterials.8b01135>
103. Díaz E, Puerto I, Sandonis I, Ibañez I (2014) Morphology and Mechanical Properties of PLLA and PCL Scaffolds. *Polym - Plast Technol Eng* 53:150–155. <https://doi.org/10.1080/03602559.2013.843699>
104. Sharma D, Satapathy BK (2019) Performance evaluation of electrospun nanofibrous mats of polylactic acid (PLA)/poly (ϵ -caprolactone) (PCL) blends. *Mater Today Proc* 19:188–195. <https://doi.org/10.1016/j.matpr.2019.06.698>
105. Keridou I, Franco L, Turon P, et al (2018) Scaffolds with Tunable Properties Constituted by Electrospun Nanofibers of Polyglycolide and Poly(ϵ -caprolactone). *Macromol Mater Eng* 303:1–14. <https://doi.org/10.1002/mame.201800100>
106. Katsumata K, Saito T, Yu F, et al (2011) The toughening effect of a small amount of poly(ϵ -caprolactone) on the mechanical properties of the poly(3-hydroxybutyrate-co-3-hydroxyhexanoate)/PCL blend. *Polym J* 43:484–492. <https://doi.org/10.1038/pj.2011.12>
107. Rohindra D, Lata R, Kuboyama K, Ougizawa T (2019) Crystallization behavior in miscible blends of poly(ϵ -caprolactone) and poly(hexylene adipate) with similar thermal properties

- studied by time-resolved Fourier transform infrared spectroscopy. *Polym Cryst* 2:1–8.
<https://doi.org/10.1002/pcr2.10037>
108. Abdelrazek EM, Hezma AM, El-khodary A, Elzayat AM (2016) Spectroscopic studies and thermal properties of PCL/PMMA biopolymer blend. *Egypt J Basic Appl Sci* 3:10–15.
<https://doi.org/10.1016/j.ejbas.2015.06.001>
 109. Pötschke P, Villmow T, Krause B (2013) Melt mixed PCL/MWCNT composites prepared at different rotation speeds: Characterization of rheological, thermal, and electrical properties, molecular weight, MWCNT macrodispersion, and MWCNT length distribution. *Polymer (Guildf)* 54:3071–3078. <https://doi.org/10.1016/j.polymer.2013.04.012>
 110. Dhakal H, Bourmaud A, Berzin F, et al (2018) Mechanical properties of leaf sheath date palm fibre waste biomass reinforced polycaprolactone (PCL) biocomposites. *Ind Crops Prod* 126:394–402. <https://doi.org/10.1016/j.indcrop.2018.10.044>
 111. Leung LH, Naguib HE (2013) Viscoelastic properties of poly(ϵ -caprolactone) - hydroxyapatite micro- and nano-composites. *Polym Adv Technol* 24:144–150.
<https://doi.org/10.1002/pat.3061>
 112. Mdletshe TS, Mishra SB, Mishra AK (2015) Studies on the effect of silicon carbide nanoparticles on the thermal, mechanical, and biodegradation properties of poly(caprolactone). *J Appl Polym Sci* 132:1–9. <https://doi.org/10.1002/app.42145>
 113. Wu Q, Ma N, Liu T, Koranteng E (2019) Properties of Compatible Soy Protein Isolate / Polycaprolactone Composite with Special Interface Structure. *Polym Compos* 40:E383–E391.
<https://doi.org/10.1002/pc.24694>
 114. Lee KS, Chang YW (2013) Thermal, mechanical, and rheological properties of poly(ϵ -caprolactone)/halloysite nanotube nanocomposites. *J Appl Polym Sci* 128:2807–2816.
<https://doi.org/10.1002/app.38457>
 115. Reul LTA, Pereira CAB, Sousa FM, et al (2019) Polycaprolactone/babassu compounds:

- Rheological, thermal, and morphological characteristics. *Polym Compos* 40:E540–E549.
<https://doi.org/10.1002/pc.24861>
116. Wu CS, Liao HT (2012) Polycaprolactone-based green renewable ecocomposites made from rice straw fiber: Characterization and assessment of mechanical and thermal properties. *Ind Eng Chem Res* 51:3329–3337. <https://doi.org/10.1021/ie202002p>
 117. Weng F, Zhang P, Koranteng E, et al (2021) Effects of shell powder size and content on the properties of polycaprolactone composites. *J Appl Polym Sci* 138:1–11.
<https://doi.org/10.1002/app.51264>
 118. Liu J, Roque R, Barbosa GF, Malavolta AT (2021) Compression stiffness evaluation of polycaprolactone-amorphous calcium phosphate 3D-designed scaffolds oriented by finite element analysis. *J Appl Polym Sci* 138:1–9. <https://doi.org/10.1002/app.51245>
 119. Merino D, Alvarez VA (2020) Thermal degradation of poly (ϵ -caprolactone) nanocomposites with soy lecithin-modified bentonite fillers. *Thermochim Acta* 689:178638.
<https://doi.org/10.1016/j.addma.2020.101070>
 120. Rešček A, Ščetar M, Hrnjak-Murgić Z, et al (2016) Polyethylene/Polycaprolactone Nanocomposite Films for Food Packaging Modified with Magnetite and Casein: Oxygen Barrier, Mechanical, and Thermal Properties. *Polym - Plast Technol Eng* 55:1450–1459.
<https://doi.org/10.1080/03602559.2016.1163606>
 121. Jafari H, Shahrousvand M, Kaffashi B (2020) Preparation and characterization of reinforced poly (ϵ -caprolactone) nanocomposites by cellulose nanowhiskers. *Polym Compos* 41:624–632.
<https://doi.org/10.1002/pc.25393>
 122. Saravanamoorthy S, Chandra Bose A, Velmathi S (2015) Facile fabrication of polycaprolactone/h-MoO₃ nanocomposites and their structural, optical and electrical properties. *RSC Adv* 5:99074–99083. <https://doi.org/10.1039/c5ra17733b>
 123. Bicy K, Geethamma VG, Kalarikkal N, et al (2018) Poly(ϵ -caprolactone)/Functionalized-

- Carbon Nanotube Electrospun Nanocomposites: Crystallization and Thermal Properties. *Macromol Symp* 381:1–6. <https://doi.org/10.1002/masy.201800140>
124. Xie M miao, Wang B bin, Zhang P (2019) The effect of crystallization behavior on high conductivity, enhanced mechanism and thermal stability of poly(ϵ -caprolactone)/multi-walled carbon nanotube composites. *J Dispers Sci Technol* 40:94–102. <https://doi.org/10.1080/01932691.2018.1464470>
 125. Singh J, Pandey PM, Kaur T, Singh N (2021) A comparative analysis of solvent cast 3D printed carbonyl iron powder reinforced polycaprolactone polymeric stents for intravascular applications. *J Biomed Mater Res - Part B Appl Biomater* 109:1344–1359. <https://doi.org/10.1002/jbm.b.34795>
 126. Fadaie M, Mirzaei E, Geramizadeh B, Asvar Z (2018) Incorporation of nanofibrillated chitosan into electrospun PCL nanofibers makes scaffolds with enhanced mechanical and biological properties. *Carbohydr Polym* 199:628–640. <https://doi.org/10.1016/j.carbpol.2018.07.061>
 127. Victor, H. Antolí'n-Cero'n Sergio, Go' mez-Salazar Martin R, Soto V, Luna-Ba'rcenas G, et al (2012) Comparative Study of the Thermal and Mechanical Properties of Nanocomposites Prepared by In Situ Polymerization of ϵ -Caprolactone and Functionalized Carbon Nanotubes. *Polym Compos* 33:5563–572. <https://doi.org/10.1002/pc>
 128. Wang Y, Li T, Ma P, et al (2018) Graphene-assisted fabrication of poly(ϵ -caprolactone)-based nanocomposites with high mechanical properties and self-healing functionality. *New J Chem* 42:10348–10356. <https://doi.org/10.1039/c8nj01278d>
 129. Cheng Z, Xiuwen W, Guopu C, et al (2018) AuNPs-PCL nanocomposite accelerated abdominal wound healing through photothermal effect and improving cell adhesion. *J Biomater Sci Polym Ed* 29:2035–2049. <https://doi.org/10.1080/09205063.2018.1526460>
 130. Inukai S, Kurokawa N, Hotta A (2020) Mechanical properties of poly(ϵ -caprolactone)

- composites with electrospun cellulose nanofibers surface modified by 3-aminopropyltriethoxysilane. *J Appl Polym Sci* 137:1–10. <https://doi.org/10.1002/app.48599>
131. Zaman HU, Beg MDH (2015) Improvement of physico-mechanical, thermomechanical, thermal and degradation properties of PCL/gelatin biocomposites: Effect of gamma radiation. *Radiat Phys Chem* 109:73–82. <https://doi.org/10.1016/j.radphyschem.2014.12.011>
 132. Kumar D, Babu G, Krishnan S (2019) Study on mechanical & thermal properties of PCL blended graphene biocomposites. *Polimeros* 29:1–9. <https://doi.org/10.1590/0104-1428.05318>
 133. Lozano-Sánchez LM, Bagudanch I, Sustaita AO, et al (2018) Single-point incremental forming of two biocompatible polymers: An insight into their thermal and structural properties. *Polymers (Basel)* 10:. <https://doi.org/10.3390/polym10040391>
 134. Iroh JO (1999) *Polymer data handbook*
 135. Wurm A, Zhuravlev E, Eckstein K, et al (2012) Crystallization and homogeneous nucleation kinetics of poly(ϵ -caprolactone) (PCL) with different molar masses. *Macromolecules* 45:3816–3828. <https://doi.org/10.1021/ma300363b>
 136. Jiang Y, Fang L, Kratz K, Lendlein A (2014) Crystallization behavior of copolyesterurethanes containing different weight contents of crystallizable poly(ϵ -caprolactone) segments. *Macromol Symp* 345:59–65. <https://doi.org/10.1002/masy.201400138>
 137. Shen H, Quintard G, Chen J, Taha M (2015) Synthesis and thermomechanical properties of allyl-functionalized polycaprolactone urethane-co-2-hydroxyethyl methacrylate networks. *J Appl Polym Sci* 132:1–10. <https://doi.org/10.1002/APP.41295>
 138. Shen H, Chen J, Taha M (2014) Cross-linking and damping properties of poly(caprolactone-co-glycidyl methacrylate). *Polym J* 46:598–608. <https://doi.org/10.1038/pj.2014.29>
 139. Abdolmohammadi S, Siyamak S, Ibrahim NA, et al (2012) Enhancement of Mechanical and Thermal Properties of Polycaprolactone/Chitosan Blend by Calcium Carbonate Nanoparticles. *Int J Mol Sci* 13:4508–4522. <https://doi.org/10.3390/ijms13044508>

140. Bing Z, Zai-Zai T, Jie H, et al (2013) Isothermal crystallization kinetics of multi-walled carbon nanotubes-graft-poly(ϵ -caprolactone) with high grafting degrees. *CrystEngComm* 15:7824–7832. <https://doi.org/10.1039/c3ce40606g>
141. Liu L, Zhang Y, Li C, et al (2020) Facile preparation PCL/ modified nano ZnO organic-inorganic composite and its application in antibacterial materials. *J Polym Res* 27:78. <https://doi.org/10.1007/s10965-020-02046-z>
142. Seyrek ME, Okur M, Saraçoğlu N (2021) Improvement of mechanical, thermal and antimicrobial properties of organically modified montmorillonite loaded polycaprolactone for food packaging. *J Vinyl Addit Technol* 27:894–908. <https://doi.org/10.1002/vnl.21860>
143. Schäfer H, Reul LTA, Souza FM, et al (2021) Crystallization behavior of polycaprolactone/babassu compounds. *J Therm Anal Calorim* 143:2963–2972. <https://doi.org/10.1007/s10973-020-09433-0>
144. Cesur S, Alp B, Küçüköksel Y, et al (2015) Crystallization kinetics and affecting parameters on polycaprolactone composites with inorganic and organic additives. *J Vinyl Addit Technol* 21:174–182. <https://doi.org/10.1002/vnl.21399>
145. Alp B, Cesur S (2013) Isothermal crystallization kinetics and mechanical properties of polycaprolactone composites with zinc oxide, oleic acid, and glycerol monooleate. *J Appl Polym Sci* 130:1259–1275. <https://doi.org/10.1002/app.39217>
146. Mahalakshmi S, Parthasarathy V, Tung KL, et al (2019) Non-isothermal Crystallization and Degradation Kinetics of Fe₃O₄ –Thymolblue Functionalized Poly(ϵ -caprolactone). *J Polym Environ* 0:0. <https://doi.org/10.1007/s10924-019-01401-6>
147. Kratochvíl J, Rotrekl J, Kaprálková L, et al (2013) Epoxy/poly(ϵ -caprolactone) nanocomposites: Effect of transformations of structure on crystallization. *J Appl Polym Sci* 130:3197–3204. <https://doi.org/10.1002/app.39536>
148. Liang JZ, Zhou L, Tang CY, Tsui CP (2013) Crystallization properties of polycaprolactone

- composites filled with nanometer calcium carbonate. *J Appl Polym Sci* 128:2940–2944.
<https://doi.org/10.1002/app.38359>
149. Yang B, Zhang X, Wang C, et al (2019) Effect of polyvinyl acetals on non-isothermal crystallization behaviour and mechanical properties of poly(ϵ -caprolactone). *RSC Adv* 9:36815–36824. <https://doi.org/10.1039/c9ra08133j>
 150. Harmansyah F, Woo EM, Lee LT, Chien HR (2014) Distorted ring-banded spherulites in poly(l-lactic acid)/poly(ϵ -caprolactone) blends. *RSC Adv* 4:49006–49015.
<https://doi.org/10.1039/c4ra08658a>
 151. Ninago MD, Redondo FL, Freites AGO De, et al (2019) Effects of Branches on the Isothermal Crystallization of Copolymers Based on Poly (ϵ -caprolactone). *Macromol Symp* 383:1700082. <https://doi.org/10.1002/masy.201700082>
 152. Rizzuto M, Mugica A, Zubitur M, et al (2016) Plasticization and anti-plasticization effects caused by poly(lactide-ran-caprolactone) addition to double crystalline poly(l-lactide)/poly(ϵ -caprolactone) blends. *CrystEngComm* 18:2014–2023. <https://doi.org/10.1039/c5ce02559a>
 153. Lanfranconi M, Alvarez VA, Ludueña LN (2016) Isothermal crystallization of polycaprolactone/modified clay biodegradable nanocomposites. *J Therm Anal Calorim* 126:1273–1280. <https://doi.org/10.1007/s10973-016-5734-x>
 154. Wu C-M, Huang C-W (2011) Melting and Crystallization Behavior of Copolymer From Cyclic Butylene Terephthalate and Polycaprolactone. *Polym Eng Sci* 51:1004–1013.
<https://doi.org/10.1002/pen>
 155. Palacios JK, Mugica A, Zubitur M, et al (2016) Sequential crystallization and morphology of triple crystalline biodegradable PEO-b-PCL-b-PLLA triblock terpolymers. *RSC Adv* 6:4739–4750. <https://doi.org/10.1039/c5ra25812j>
 156. Bai Y, Zhang X, Wang Q (2014) Shape memory property of microcrystalline cellulose – poly (ϵ -caprolactone) polymer network with broad transition temperature. *J Mater Sci* 49:2252–

2262. <https://doi.org/10.1007/s10853-013-7920-6>
157. Raana S, Mahyar A-A, Massoumi B, et al (2017) Conductive and Biodegradable Scaffolds Based On Five-Arm and Functionalized Star-Like Polyaniline-Polycaprolactone Copolymer with D- Glucose Core Raana. *New J Chem* 41:6371–6384.
<https://doi.org/10.1039/C7NJ01063J>
158. Yin G, Chen G, Zhou Z, Li Q (2015) Modification of PEG-b-PCL block copolymer with high melting temperature by the enhancement of POSS crystal and ordered phase structure. *RSC Adv* 5:33356–33363. <https://doi.org/10.1039/c5ra01971k>
159. Luo S, Peng X, Chen Y, et al (2015) Synthesis, characterization, and crystallization of biodegradable poly(ϵ -caprolactone)-poly(L-lactide) diblock copolymers. *E-Polymers* 15:15–23. <https://doi.org/10.1515/epoly-2014-0155>
160. Jing X, Mi HY, Huang HX, Turng LS (2016) Shape memory thermoplastic polyurethane (TPU)/poly(ϵ -caprolactone) (PCL) blends as self-knotting sutures. *J Mech Behav Biomed Mater* 64:94–103. <https://doi.org/10.1016/j.jmbbm.2016.07.023>
161. Sethuraman V, Makornkaewkeyoon K, Khalf A, Madihally S V. (2013) Influence of scaffold forming techniques on stress relaxation behavior of polycaprolactone scaffolds. *J Appl Polym Sci* 130:4237–4244. <https://doi.org/10.1002/app.39599>
162. Tian G, Zhu G, Ren T, et al (2019) The effects of PCL diol molecular weight on properties of shape memory poly(ϵ -caprolactone) networks. *J Appl Polym Sci* 136:1–8.
<https://doi.org/10.1002/app.47055>
163. Liang JZ, Duan DR, Tang CY, et al (2013) Flexural properties of Poly-L-Lactide and polycaprolactone shape memory composites filled with nanometer calcium carbonate. *J Macromol Sci Part B Phys* 52:964–972. <https://doi.org/10.1080/00222348.2012.746572>
164. Jahangiri M, Kalajahi AE, Rezaei M, Bagheri M (2019) Shape memory hydroxypropyl cellulose-g-poly (ϵ -caprolactone) networks with controlled drug release capabilities. *J Polym*

Res 26:. <https://doi.org/10.1007/s10965-019-1798-1>

165. Bai Y, Jiang C, Wang Q, Wang T (2013) Multi-shape-memory property study of novel poly (ϵ -caprolactone)/ ethyl cellulose polymer networks. *Macromol Chem Phys* 214:2465–2472
166. Zhou Y, Zhou, D, Cao P, et al (2021) 4D Printing of Shape Memory Vascular Stent Based on β CD-g-Polycaprolactone. *Macromol Rapid Commun* 42:1–9.
<https://doi.org/10.1002/marc.202100176>
167. Iregui Á, Otaegi I, Arandia I, et al (2020) Fully Reversible Spherulitic Morphology in Cationically Photopolymerized DGEBA/PCL Shape-Memory Blends. *Macromolecules* 53:1368–1379. <https://doi.org/10.1021/acs.macromol.9b02474>
168. Liu W, Zhang R, Huang M, et al (2016) Design and structural study of a triple-shape memory PCL/PVC blend. *Polymer (Guildf)* 104:115–122.
<https://doi.org/10.1016/j.polymer.2016.09.079>
169. Lai S, Wang X (2017) Shape memory properties of olefin block copolymer (OBC)/ poly (E - caprolactone) (PCL) blends. *J Appl Polym Sci* 134:45475. <https://doi.org/10.1002/app.45475>
170. Chen WC, Lai SM, Chang MY, Liao ZC (2014) Preparation and properties of natural rubber (NR)/polycaprolactone (PCL) bio-based shape memory polymer blends. *J Macromol Sci Part B Phys* 53:645–661. <https://doi.org/10.1080/00222348.2013.860304>
171. Tian G, Zhu G, Xu S, Ren T (2019) A novel shape memory poly(ϵ -caprolactone)/hydroxyapatite nanoparticle networks for potential biomedical applications. *J Solid State Chem* 272:78–86. <https://doi.org/10.1016/j.jssc.2019.01.029>
172. Ishii S, Uto K, Niiyama E, et al (2016) Hybridizing Poly(ϵ -caprolactone) and Plasmonic Titanium Nitride Nanoparticles for Broadband Photoresponsive Shape Memory Films. *Appl Mater Interfaces* 8:5634–5640. <https://doi.org/10.1021/acsami.5b12658>
173. Wang W, Liu D, Lu L, et al (2016) The improvement of the shape memory function of poly(ϵ -caprolactone)/nano-crystalline cellulose nanocomposites via recrystallization under a high-

- pressure environment. *J Mater Chem A* 4:5984–5992. <https://doi.org/10.1039/c6ta00930a>
174. Lu H, Gou J (2012) Fabrication and electroactive responsive behavior of shape-memory nanocomposite incorporated with self-assembled multiwalled carbon nanotube nanopaper. *Polym Adv Technol* 23:1529–1535. <https://doi.org/10.1002/pat.2074>
 175. Yang P, Zhu G, Shen X, et al (2016) Poly(ϵ -caprolactone)-based shape memory polymers crosslinked by polyhedral oligomeric silsesquioxane. *RSC Adv* 6:90212–90219. <https://doi.org/10.1039/C6RA20431G>
 176. Qu M, Wang H, Chen Q, et al (2022) A thermally-electrically double-responsive polycaprolactone – thermoplastic polyurethane/multi-walled carbon nanotube fiber assisted with highly effective shape memory and strain sensing performance. *Chem Eng J* 427:131648. <https://doi.org/10.1016/j.cej.2021.131648>
 177. Banerjee A, Chatterjee K, Madras G (2015) Enzymatic degradation of polycaprolactone-gelatin blend. *Mater Res Express* 2:45303. <https://doi.org/10.1088/2053-1591/2/4/045303>
 178. Feng S, Yue Y, Chen J, et al (2020) Biodegradation mechanism of polycaprolactone by a novel esterase MGS0156: A QM/MM approach. *Environ Sci Process Impacts* 22:2332–2344. <https://doi.org/10.1039/d0em00340a>
 179. Almeida BC, Figueiredo P, Carvalho ATP (2019) Polycaprolactone Enzymatic Hydrolysis: A Mechanistic Study. *ACS Omega* 4:6769–6774. <https://doi.org/10.1021/acsomega.9b00345>
 180. Woodard LN, Page VM, Kmetz KT, Grunlan MA (2016) PCL–PLLA Semi-IPN Shape Memory Polymers (SMPs): Degradation and Mechanical Properties. *Macromol Rapid Commun* 37:1972–1977. <https://doi.org/10.1002/marc.201600414>
 181. Yang Y, Michalczyk C, Singer F, et al (2015) In vitro study of polycaprolactone/bioactive glass composite coatings on corrosion and bioactivity of pure Mg. *Appl Surf Sci* 355:832–841. <https://doi.org/10.1016/j.apsusc.2015.07.053>
 182. Tsujimoto T, Takayama T, Uyama H (2015) Biodegradable Shape Memory Polymeric

- Material from Epoxidized Soybean Oil and Polycaprolactone. *Polymers (Basel)* 7:2165–2174.
<https://doi.org/10.3390/polym7101506>
183. Kim JJ, Singh RK, Seo SJ, et al (2014) Magnetic scaffolds of polycaprolactone with functionalized magnetite nanoparticles: Physicochemical, mechanical, and biological properties effective for bone regeneration. *RSC Adv* 4:17325–17336.
<https://doi.org/10.1039/c4ra00040d>
 184. Badrossamay MR, McIlwee HA, Goss JA, Parker KK (2010) Nanofiber assembly by rotary jet-spinning. *Nano Lett* 10:2257–2261. <https://doi.org/10.1021/nl101355x>
 185. Sadeghianmaryan A, Yazdanpanah Z, Soltani YA, et al (2020) Curcumin-loaded electrospun polycaprolactone/montmorillonite nanocomposite: wound dressing application with anti-bacterial and low cell toxicity properties. *J Biomater Sci Polym Ed* 31:169–187.
<https://doi.org/10.1080/09205063.2019.1680928>
 186. Mi HY, Jing X, Napiwocki BN, et al (2017) Biocompatible, degradable thermoplastic polyurethane based on polycaprolactone-block -polytetrahydrofuran- block -polycaprolactone copolymers for soft tissue engineering. *J Mater Chem B* 5:4137–4151.
<https://doi.org/10.1039/c7tb00419b>
 187. Zhao N, Lv Z, Ma J, et al (2019) Fabrication of hydrophilic small diameter vascular foam scaffolds of poly(ϵ -caprolactone)/polylactic blend by sodium hydroxide solution. *Eur Polym J* 110:31–40. <https://doi.org/10.1016/j.eurpolymj.2018.11.011>
 188. Świątek M, Brož A, Tarasiuk J, et al (2019) Carbon nanotube/iron oxide hybrid particles and their PCL-based 3D composites for potential bone regeneration. *Mater Sci Eng C* 104:109913.
<https://doi.org/10.1016/j.msec.2019.109913>
 189. Collignon A, Wauquier F, Lesieur J, et al (2019) Bioactive Glass / Polycaprolactone Hybrid with a Dual Cortical / Trabecular Structure for Bone Regeneration. *ACS Appl Bio Mater* 2:3473–3483. <https://doi.org/10.1021/acsbm.9b00407>

190. Choi E, Jin S, Shim J, Yun W (2019) Fabrication and characterization of 3D – printed biocomposite scaffolds based on PCL and silanated silica particles for bone tissue regeneration. *Chem Eng J* 360:519–530. <https://doi.org/10.1016/j.cej.2018.11.176>
191. Siqueira IAWB, Koba N, Moura D, et al (2017) Porous membranes of the polycaprolactone (PCL) containing calcium silicate fibers for guided bone regeneration. *Mater Lett* 206:210–213. <https://doi.org/10.1016/j.matlet.2017.07.011>
192. Fereshteh Z, Fathi M, Bagri A, Boccaccini AR (2016) Preparation and characterization of aligned porous PCL/zein scaffolds as drug delivery systems via improved unidirectional freeze-drying method. *Mater Sci Eng C* 68:613–622. <https://doi.org/10.1016/j.msec.2016.06.009>
193. Dash TK, Konkimalla VB (2012) Polymeric Modification and Its Implication in Drug Delivery: Poly- ϵ - caprolactone (PCL) as a Model Polymer. *Mol Pharm* 9:2365–2379
194. Chandrasiri I, Abebe DG, Loku Yaddehige M, et al (2020) Self-Assembling PCL–PAMAM Linear Dendritic Block Copolymers (LDBC)s for Bioimaging and Phototherapeutic Applications. *ACS Appl Bio Mater*. <https://doi.org/10.1021/acsabm.0c00432>
195. Yeroslavsky G, Umezawa M, Okubo K, et al (2020) Stabilization of indocyanine green dye in polymeric micelles for NIR-II fluorescence imaging and cancer treatment. *Biomater Sci* 8:2245–2254. <https://doi.org/10.1039/c9bm02010a>
196. Wu S, Su F, Magee HY, et al (2019) CRGD functionalized 2,1,3-benzothiadiazole (BTD)-containing two-photon absorbing red-emitter-conjugated amphiphilic poly(ethylene glycol)-: Block -poly(ϵ -caprolactone) for targeted bioimaging. *RSC Adv* 9:34235–34243. <https://doi.org/10.1039/c9ra06694b>
197. Molina BG, Cianga L, Bendrea AD, et al (2019) An amphiphilic, heterografted polythiophene copolymer containing biocompatible/biodegradable side chains for use as an (electro)active surface in biomedical applications. *Polym Chem* 10:5010–5022.

<https://doi.org/10.1039/c9py00926d>

198. Dong X, Wei C, Lu L, et al (2016) Fluorescent nanogel based on four-arm PEG-PCL copolymer with porphyrin core for bioimaging. *Mater Sci Eng C* 61:214–219.
<https://doi.org/10.1016/j.msec.2015.12.037>
199. Huang S, Liu S, Wang K, et al (2015) Highly fluorescent and bioresorbable polymeric nanoparticles with enhanced photostability for cell imaging. *Nanoscale* 7:889–895.
<https://doi.org/10.1039/c4nr05576d>
200. Yang C, Huang S, Wang X, Wang M (2016) Theranostic unimolecular micelles of highly fluorescent conjugated polymer bottlebrushes for far red/near infrared bioimaging and efficient anticancer drug delivery. *Polym Chem* 7:7455–7468. <https://doi.org/10.1039/c6py01838f>
201. Ruan Z, Liu L, Fu L, et al (2016) An amphiphilic block copolymer conjugated with carborane and a NIR fluorescent probe for potential imaging-guided BNCT therapy. *Polym Chem* 7:4411–4418. <https://doi.org/10.1039/c6py00799f>
202. Tabesh E, Kharaziha M, Mahmoudi M, et al (2019) Biological and corrosion evaluation of Laponite®: Poly(caprolactone) nanocomposite coating for biomedical applications. *Colloids Surfaces A Physicochem Eng Asp* 583:123945. <https://doi.org/10.1016/j.colsurfa.2019.123945>
203. Jokar M, Darvishi S, Torkaman R, et al (2016) Corrosion and bioactivity evaluation of nanocomposite PCL-forsterite coating applied on 316L stainless steel. *Surf Coatings Technol* 307:324–331. <https://doi.org/10.1016/j.surfcoat.2016.08.094>
204. Mojarad Shafiee B, Torkaman R, Mahmoudi M, et al (2019) An improvement in corrosion resistance of 316L AISI coated using PCL-gelatin composite by dip-coating method. *Prog Org Coatings* 130:200–205. <https://doi.org/10.1016/j.porgcoat.2019.01.057>
205. Capellato P, Silva G, Popat K, et al (2020) Cell investigation of Adult Human dermal fibroblasts on PCL nanofibers/TiO₂ nanotubes Ti-30Ta alloy for biomedical application. *Artif Organs* Early view: <https://doi.org/10.1111/aor.13713>

206. Bakhsheshi-Rad HR, Hamzah E, Shuang CP, Berto F (2020) Preparation of poly(ϵ -caprolactone)-hydroxyapatite composite coating for improvement of corrosion performance of biodegradable magnesium. *Mater Des Process Commun* early view: <https://doi.org/10.1002/mdp2.170>
207. Palanisamy MS, Kulandaivelu R, Nellaiappan SNTS (2020) Improving the corrosion resistance and bioactivity of magnesium by a carbonate conversion-polycaprolactone duplex coating approach. *New J Chem* 44:4772–4785. <https://doi.org/10.1039/c9nj06030h>
208. Kim J, Mousa HM, Park CH, Kim CS (2017) Enhanced corrosion resistance and biocompatibility of AZ31 Mg alloy using PCL/ZnO NPs via electrospinning. *Appl Surf Sci* 396:249–258. <https://doi.org/10.1016/j.apsusc.2016.10.092>
209. Bakhsheshi-Rad HR, Ismail AF, Aziz M, et al (2019) Antibacterial activity and corrosion resistance of Ta₂O₅ thin film and electrospun PCL/MgO-Ag nanofiber coatings on biodegradable Mg alloy implants. *Ceram Int* 45:11883–11892. <https://doi.org/10.1016/j.ceramint.2019.03.071>
210. Huang W, Mei D, Zhang J, et al (2021) Improved corrosion resistance and cytocompatibility of Mg–Zn–Y–Nd alloy by the electrografted polycaprolactone coating. *Colloids Surfaces A Physicochem Eng Asp* 629:127471. <https://doi.org/10.1016/j.colsurfa.2021.127471>
211. Sangroniz A, Sangroniz L, Hamzehlou S, et al (2020) Lactide-caprolactone copolymers with tuneable barrier properties for packaging applications. *Polymer (Guildf)* 122681. <https://doi.org/10.1016/j.polymer.2020.122681>
212. Ahmed J, Mulla M, Jacob H, et al (2019) Polylactide/poly(ϵ -caprolactone)/zinc oxide/clove essential oil composite antimicrobial films for scrambled egg packaging. *Food Packag Shelf Life* 21:100355. <https://doi.org/10.1016/j.fpsl.2019.100355>
213. Milovanovic S, Hollermann G, Errenst C, et al (2018) Supercritical CO₂ impregnation of PLA/PCL films with natural substances for bacterial growth control in food packaging. *Food*

- Res Int 107:486–495. <https://doi.org/10.1016/j.foodres.2018.02.065>
214. Qin Y, Liu D, Wu Y, et al (2015) Effect of PLA/PCL/cinnamaldehyde antimicrobial packaging on physicochemical and microbial quality of button mushroom (*Agaricus bisporus*). *Postharvest Biol Technol* 99:73–79. <https://doi.org/10.1016/j.postharvbio.2014.07.018>
 215. Correa JP, Molina V, Sanchez M, et al (2017) Improving ham shelf life with a polyhydroxybutyrate/polycaprolactone biodegradable film activated with nisin. *Food Packag Shelf Life* 11:31–39. <https://doi.org/10.1016/j.fpsl.2016.11.004>
 216. Hadj-Hamou AS, Yahiaoui F (2019) Performances of PCL/PVC/Organoclay Nanobioblends Films for Packaging Applications. *Macromol Symp* 386:1–8. <https://doi.org/10.1002/masy.201800239>
 217. Alix S, Mahieu A, Terrie C, et al (2013) Active pseudo-multilayered films from polycaprolactone and starch based matrix for food-packaging applications. *Eur Polym J* 49:1234–1242. <https://doi.org/10.1016/j.eurpolymj.2013.03.016>
 218. Ortega-Toro R, Contreras J, Talens P, Chiralt. A (2015) Physical and structural properties and thermal behaviour of starch-poly(ϵ -caprolactone) blend films for food packaging. *Food Packag Shelf Life* 5:10–20. <https://doi.org/10.1016/j.fpsl.2015.04.001>
 219. Khalid S, Yu L, Feng M, et al (2018) Development and characterization of biodegradable antimicrobial packaging films based on polycaprolactone, starch and pomegranate rind hybrids. *Food Packag Shelf Life* 18:71–79. <https://doi.org/10.1016/j.fpsl.2018.08.008>
 220. Wang K, Lim PN, Tong SY, Thian ES (2019) Development of grapefruit seed extract-loaded poly(ϵ -caprolactone)/chitosan films for antimicrobial food packaging. *Food Packag Shelf Life* 22:100396. <https://doi.org/10.1016/j.fpsl.2019.100396>
 221. Jeong S, Lee HG, Cho CH, Yoo SR (2020) Characterization of multi-functional, biodegradable sodium metabisulfite-incorporated films based on polycaprolactone for active food packaging applications. *Food Packag Shelf Life* 25:100512. <https://doi.org/10.1016/j.fpsl.2020.100512>

222. Benhacine F, Ouargli A, Hadj-Hamou AS (2019) Preparation and Characterization of Novel Food Packaging Materials Based on Biodegradable PCL/Ag-Kaolinite Nanocomposites with Controlled Release Properties. *Polym Technol Mater* 58:328–340.
<https://doi.org/10.1080/03602559.2018.1471714>
223. Xie J, Hung YC (2018) UV-A activated TiO₂ embedded biodegradable polymer film for antimicrobial food packaging application. *Lwt-Food Sci Technol* 96:307–314.
<https://doi.org/10.1016/j.lwt.2018.05.050>
224. Cai Y, Guan J, Wang W, et al (2021) pH and light-responsive polycaprolactone/curcumin@zif-8 composite films with enhanced antibacterial activity. *J Food Sci* 86:3550–3562. <https://doi.org/10.1111/1750-3841.15839>
225. Angelica D, Alberto J, Costa V, et al (2019) A novel nanocomposite for food packaging developed by electrospinning and electrospraying. *Food Packag Shelf Life* 20:100314.
<https://doi.org/10.1016/j.fpsl.2019.100314>
226. Hasanpour Ardekani-Zadeh A, Hosseini SF (2019) Electrospun essential oil-doped chitosan/poly(ϵ -caprolactone) hybrid nanofibrous mats for antimicrobial food biopackaging exploits. *Carbohydr Polym* 223:115108. <https://doi.org/10.1016/j.carbpol.2019.115108>
227. Mathiazhagan S, Periasamy V, Vadivel A (2021) Ecofriendly antimicrobial *Acalypha indica* leaf extract immobilized polycaprolactone nanofibrous mat for food package applications. *J Food Process Preserv* 45:1–12. <https://doi.org/10.1111/jfpp.15302>
228. Lin W, Ni Y, Pang J (2020) Size effect-inspired fabrication of konjac glucomannan/polycaprolactone fiber films for antibacterial food packaging. *Int J Biol Macromol* 149:853–860. <https://doi.org/10.1016/j.ijbiomac.2020.01.242>
229. Sugane K, Yoshioka Y, Shimasaki T, et al (2018) Self-healing 8-armed star-shaped ϵ -caprolactone oligomers dually crosslinked by the Diels-Alder and urethanization reactions. *Polymer (Guildf)* 144:92–102. <https://doi.org/10.1016/j.polymer.2018.04.045>

230. Rodriguez ED, Luo X, Mather PT (2011) Linear / Network Poly (ϵ -caprolactone) Blends Exhibiting Shape Memory Assisted Self-Healing (SMASH). ACS Appl Mater Interfaces 3:152–161
231. Lai SM, Liu JL, Huang YH (2020) Preparation of Self-healing Natural Rubber/Polycaprolactone (NR/PCL) Blends. J Macromol Sci Part B Phys. <https://doi.org/10.1080/00222348.2020.1757218>
232. Xu X, Fan P, Ren J, et al (2018) Self-healing thermoplastic polyurethane (TPU)/polycaprolactone (PCL) /multi-wall carbon nanotubes (MWCNTs) blend as shape-memory composites. Compos Sci Technol 168:255–262. <https://doi.org/10.1016/j.compscitech.2018.10.003>
233. Lutz A, Berg O Van Den, Damme J Van, et al (2015) A Shape-Recovery Polymer Coating for the Corrosion Protection of Metallic Surfaces. ACS Appl Mater Interfaces 7:175–183. <https://doi.org/10.1021/am505621x>
234. Huang Y, Deng L, Ju P, et al (2018) Applications of Polymer , Composite , and Coating Materials Triple-action self-healing protective coatings based on shape memory polymer (SMP) containing dual-function microspheres Triple-action self-healing protective coatings based on shape memory pol. ACS Appl Mater Interfaces 10:23369–23379. <https://doi.org/10.1021/acsami.8b06985>
235. Rajitha K, Mohana KN (2020) Application of modified graphene oxide – Polycaprolactone nanocomposite coating for corrosion control of mild steel in saline medium. Mater Chem Phys 241:122050. <https://doi.org/10.1016/j.matchemphys.2019.122050>
236. Ai X, Xie Q, Ma C, Zhang G (2020) Fouling Release Coating Consisting of Hyperbranched Poly(ϵ -caprolactone)/Siloxane Elastomer. ACS Appl Polym Mater 2:1429–1437. <https://doi.org/10.1021/acsapm.9b01056>
237. Ding Z, Li J, Xin W, et al (2019) Progress in Organic Coatings Low gloss waterborne

- polyurethane coatings with anti-dripping and flame retardancy via montmorillonite nanosheets. *Prog Org Coatings* 136:105273. <https://doi.org/10.1016/j.porgcoat.2019.105273>
238. Arya RK, Kaur J, Chandra A, et al (2021) Designing of biodegradable polycaprolactone: Binary and ternary coatings to minimize the defects and cost of solvent(s). *J Appl Polym Sci* 138:1–15. <https://doi.org/10.1002/app.50888>
 239. Akat H (2021) Thiol – ended polycaprolactone : Synthesis , preparation and use in Pb (II) and Cd (II) removal from water samples. *Mater Today Commun* 29:102908
 240. Reshmi CR, Sundaran SP, Juraij A, Athiyanathil S (2016) RSC Advances Fabrication of superhydrophobic polycaprolactone / beeswax electrospun separation †. *RSC Adv* 7:2092–2102. <https://doi.org/10.1039/C6RA26123J>
 241. He N, Li L, Chen J, et al (2021) Extraordinary Superhydrophobic Polycaprolactone-Based Composite Membrane with an Alternated Micro-Nano Hierarchical Structure as an Eco-friendly Oil/Water Separator. *ACS Appl Mater Interfaces* 13:24117–24129. <https://doi.org/10.1021/acsami.1c03019>
 242. Zhang X, Zhao J (2019) Biomimetic preparation of a polycaprolactone membrane with a hierarchical structure as a highly efficient oil – water separator. *J Mater Chem A* 7:24532–24542. <https://doi.org/10.1039/c9ta08660a>
 243. Eksiler K, Andou Y, Nakayama N, et al (2017) Design of biodegradable PCL/PI films as a joining tape for grafting plant. *Environ Technol (United Kingdom)* 38:2362–2372. <https://doi.org/10.1080/09593330.2016.1261186>
 244. Chen F, Xu L, Tian Y, et al (2021) Electrospun Polycaprolactone Nano fiber Composites with Embedded Carbon Nanotubes/Nanoparticles for Photothermal Absorption. *ACS Appl Nano Mater* 4:5230–5239. <https://doi.org/10.1021/acsanm.1c00623>
 245. Meikhail MS, Abdelghany AM, Awad WM (2018) Role of CdSe quantum dots in the structure and antibacterial activity of chitosan / poly ε -caprolactone thin films. *Egypt J Basic Appl Sci*

- 5:138–144. <https://doi.org/10.1016/j.ejbas.2018.05.003>
246. Chan BQY, Liow SS, Loh XJ (2016) Organic-inorganic shape memory thermoplastic polyurethane based on polycaprolactone and polydimethylsiloxane. *RSC Adv* 6:34946–34954. <https://doi.org/10.1039/c6ra04041a>
 247. Yadav R, Purwar R (2021) Influence of metal oxide nanoparticles on morphological, structural, rheological and conductive properties of mulberry silk fibroin nanocomposite solutions. *Polym Test* 93:106916. <https://doi.org/10.1016/j.polymertesting.2020.106916>
 248. Sachan R, Purwar R (2021) Water based quad acrylic copolymer / cloisite 30B nanocomposite heat resistant adhesive : thermal and rheological properties. *J Adhes Sci Technol* 1–16. <https://doi.org/10.1080/01694243.2021.1979760>
 249. Winter HH, Chambon F (1986) Analysis of Linear Viscoelasticity of a Crosslinking Polymer at the Gel Point. *J Rheol (N Y N Y)* 30:367–382. <https://doi.org/10.1122/1.549853>
 250. Xie J, Jin YC (2016) Parameter determination for the cross rheology equation and its application to modeling non-Newtonian flows using the WC-MPS method. *Eng Appl Comput Fluid Mech* 10:111–129. <https://doi.org/10.1080/19942060.2015.1104267>
 251. Daver F, Kajtaz M, Brandt M, Shanks RA (2016) Creep and recovery behaviour of polyolefin-rubber nanocomposites developed for additive manufacturing. *Polymers (Basel)* 8:. <https://doi.org/10.3390/polym8120437>
 252. Tweedie CA, Van Vliet KJ (2006) Contact creep compliance of viscoelastic materials via nanoindentation. *J Mater Res* 21:1576–1589. <https://doi.org/10.1557/jmr.2006.0197>
 253. Dogan M, Kayacier A, Toker ÖS, et al (2013) Steady, Dynamic, Creep, and Recovery Analysis of Ice Cream Mixes Added with Different Concentrations of Xanthan Gum. *Food Bioprocess Technol* 6:1420–1433. <https://doi.org/10.1007/s11947-012-0872-z>
 254. Nie K, Zheng S, Lu F, Zhu Q (2005) Inorganic-organic hybrids involving poly(ϵ -caprolactone) and silica network: Hydrogen-bonding interactions and isothermal crystallization kinetics. *J*

- Polym Sci Part B Polym Phys 43:2594–2603. <https://doi.org/10.1002/polb.20491>
255. Lu XF, Hay JN (2001) Isothermal crystallization kinetics and melting behaviour of poly(ethylene terephthalate). *Polymer (Guildf)* 42:9423–9431. [https://doi.org/10.1016/S0032-3861\(01\)00502-X](https://doi.org/10.1016/S0032-3861(01)00502-X)
 256. Deshmukh P, Yoon H, Cho S, et al (2017) Impact of poly(ϵ -caprolactone) architecture on the thermomechanical and shape memory properties. *J Polym Sci Part A Polym Chem* 55:3424–3433. <https://doi.org/10.1002/pola.28721>
 257. Azemar F, Fay F, Réhel K, Linossier I (2014) Control of hydration and degradation properties of triblock copolymers polycaprolactone-b-polydimethylsiloxane-b-polycaprolactone. *J Appl Polym Sci* 131:1–8. <https://doi.org/10.1002/app.40431>
 258. Kai D, Prabhakaran MP, Chan BQY, et al (2016) Elastic poly(ϵ -caprolactone)-polydimethylsiloxane copolymer fibers with shape memory effect for bone tissue engineering. *Biomed Mater* 11:. <https://doi.org/10.1088/1748-6041/11/1/015007>
 259. Beltran FO, Houk CJ, Grunlan MA (2021) Bioactive Siloxane-Containing Shape-Memory Polymer (SMP) Scaffolds with Tunable Degradation Rates. *ACS Biomater Sci Eng* 7:1631–1639. <https://doi.org/10.1021/acsbiomaterials.1c00113>
 260. Barkoula NM, Alcock B, Cabrera NO, Peijs T (2008) Rheology, Mechanical Properties, and Biodegradation of Poly(ϵ -caprolactone)/Silica Nanocomposites. *Polym Polym Compos* 16:101–113. <https://doi.org/10.1002/pc>
 261. Singh NK, Purkayastha B Das, Roy JK, et al (2010) Nanoparticle-induced controlled biodegradation and its mechanism in poly(ϵ -caprolactone). *ACS Appl Mater Interfaces* 2:69–81. <https://doi.org/10.1021/am900584r>
 262. Ma Q, Shi K, Su T, Wang Z (2020) Biodegradation of Polycaprolactone (PCL) with Different Molecular Weights by *Candida antarctica* Lipase. *J Polym Environ* 28:2947–2955. <https://doi.org/10.1007/s10924-020-01826-4>

Publications from the research work

1. **Radha Sachan**, Sudhir G. Warkar and Roli Purwar (2022), An overview on synthesis, properties and applications of polycaprolactone copolymers, blends & composites, Polymer-Plastics Technology and Materials, 62(3), 327-358, DOI: 10.1080/25740881.2022.2113890
2. **Radha Sachan**, Sudhir G. Warkar and Roli Purwar (2022), Photocrosslinked Poly(ϵ -caprolactone) – Polydimethylsiloxane – Poly(ϵ -caprolactone) Triblock Copolymeric Films: Structural, Thermal and Shape Memory Properties, ChemistrySelect 7 (33), e202201340, DOI: 10.1002/slct.202201340
3. **Radha Sachan** and Roli Purwar (2023), Soil burial degradation studies of photocrosslinked PCL-PDMS-PCL triblock copolymer films, Polymer Engineering & Science 63(12), 4107-4117, DOI:10.1002/pen.26511
4. **Radha Sachan** and Roli Purwar (2024), Effect of PCL Chain Length on Rheological and Mechanical Properties of PCL-PDMS-PCL Triblock Copolymer Films, Journal of Applied Polymer Science (Accepted)

Book chapter

1. Roli Purwar and **Radha Sachan** (2020), Thermoresponsive shape memory polymers for smart textiles, Advances in functional and protective textiles, 1st edition, Edited by Shahid ul-Islam and Bhupendra Singh Butola, Elsevier Publications, ISBN: 978-0-12-822676-6.

Conference Publications

1. **Radha Sachan** (Oral presentation), Isothermal Crystallization Kinetics of Thermoresponsive Shape Memory PCL-PDMS-PCL Triblock Copolymers,

International Conference on Polymer Science and Technology SPSI-MACRO 2023, 10-13 Dec. 2023, IIT Guwahati, India.

2. **Radha Sachan**, Roli Purwar and Sudhir G. Warkar, (Oral presentation), Structural and thermal properties of photocrosslinked poly(ϵ -caprolactone) – polydimethylsiloxane- poly(ϵ -caprolactone) triblock copolymeric films, International Conference on Sustainability in Chemical Processes through Digitalization, Artificial Intelligence and Green Chemistry, CHEMCON-2022, 27-30 Dec. 2022, Kanpur, Uttar Pradesh, India.
3. **Radha Sachan** and Roli Purwar Poster presentation, Studies on high heat resistant acrylic adhesive, International Conference on Polymer Science and Technology SPSIMACRO 2018, 19-22 Dec. 2018, IISER Pune, India.
4. **Radha Sachan** and Roli Purwar Poster presentation, Silica modified candelilla wax/PU coating for hydrophobic textile, Textile Summit 2018, 17 Nov. 2018, TAI Delhi, India.

Other publications during research tenure

Research Articles

1. Mohit Yadav, Ritwik Shekhar, Versha Joshi, Roli Purwar, **Radha Sachan** (2024), Studies on semi-batch emulsion polymerization: Role of surfactant, Journal of Surface Science and Technology Vol 38(3-4), 1-16, DOI: 10.18311/jsst/2019/23508
2. **Radha Sachan** and Roli Purwar (2021), Silica Modified candelilla wax/thermoplastic polyurethane blend coatings for hydrophobic textiles, The Journal of The Textiles Institute, 113 (7), 1302-1308, DOI: 10.1080/00405000.2021.1926128
3. **Radha Sachan** and Roli Purwar (2021), Water based quad acrylic copolymer/cloisite 30B nanocomposite heat resistant adhesive: thermal and rheological properties,

Journal of Adhesion Science and Technology, 36 (14), 1541-1556, DOI:
10.1080/01694243.2021.1979760

Book chapter

1. Kartik Jindal, Chaitnaya Chibber, **Radha Sachan** and Roli Purwar (2022), Antimicrobial adhesive using Arnebia Nobilis into silicone acrylate blend for potential wound care application, Lecture Notes in Mechanical Engineering. ISSN: 2195-4356. DOI: 10.1007/978-981-16-9523-0_10

Curriculum Vitae

RADHA SACHAN



Mobile: +91 8588825567

E-Mail: radha.s@hbtu.ac.in

Kanpur, Uttar Pradesh, India

Orchid ID: 0009-0009-1530-4422

Google Scholar: <https://scholar.google.com/citations?user=K45BBLkAAAAJ&hl=en>

Research Gate: <https://www.researchgate.net/profile/Radha-Sachan-2>

Professional Synopsis

A dynamic professional with more than one year of academic experience and almost seven years of industrial experience in Product & Process Improvement, Quality Assurance and Technical Services/Marketing.

Academic/Organisational Experience

Jun'22-Present: Assistant Professor (Chemical Technology-Paint Technology) –
Harcourt Butler Technical University, Kanpur

Dec'15-Jul'16: Technical Sales Manager - Delta Specialties, Delhi.

Apr'14- June'15: Technical Services Manager - Afcona Additives Pvt. Ltd.,

Apr'12- March'14: Sr. Chemist-Technical Services Lab - Afcona Additives Pvt. Ltd.,
Delhi. **Mar'11- August'11: Process member - Product Application Center** - Srisol India
Pvt. Ltd., Noida.

Jul'09-Feb'11: Executive- Quality Analysis - BASF Coatings India Pvt. Ltd., Mangalore

Jul'08-Jul'09: Graduate Engineer Trainee - BASF Coatings India Pvt. Ltd., Mangalore

June'07-July'07(5 weeks): Summer Intern - AKZONOBEL Coatings India Pvt. Ltd.,
Bangalore as Trainee for internship in Marine Coating department.

Scholastics

- Ph.D. from DTU Delhi (Former DCE)
- M.Tech. (Polymer Technology) from DTU Delhi (Former DCE) in 2018 (**Gold Medallist**)

- Executive Management Programme from Shailesh J. Mehta IIT Bombay, with specialisation in Marketing and HRM, Project work: B2B marketing strategy 2013-14
- B.Tech. (Chemical Technology-Paint Technology) from H.B.T.I. Kanpur in 2008

M.Tech.

1. Minor Project

Silica modified candelilla wax/thermoplastic polyurethane based hydrophobic coating for textiles (Duration: 1 year)

Guide: Dr. Roli Purwar and Dr. Deenan Santhiya, DTU, Delhi

2. Major Project

Studies on high heat resistant acrylic adhesive (Duration: 1 year)

Guide: Dr. Roli Purwar and Dr. Deenan Santhiya, DTU, Delhi

B.Tech.

Project: UV Curable Powder Coatings (Duration: 1 year)

Guide: Dr. Pramod Kr. Kamani, HBTI, Kanpur

Membership in Research Organizations and Professional Bodies

1. Life Member of Indian Institute of Chemical Engineers (IChE)
2. Life member of Paint and Coating Technologists' Association (PACT)

Achievements

1. Represented HBTU Kanpur and PACT in **Paint India 2024**.
2. Session Chair in International Conference **CHEM-TECHNOVA 2024** (21th -23rd March 2024) organized by HBTU Kanpur
3. Invited lecture on **Polymeric Adhesive** in “Executive Training Program on Polymer Engineering” (12th – 24th June 2023) organized by IOCL, India and Dept. of Plastic Technology, HBTU Kanpur.
4. **Commendable Research Award** in recognition for the research during the year 2022 (06th April 2023) by Delhi Technological University, Delhi.

5. **Convenor** of **9th PACT Vision Seminar** on “ Advanced in Frontiers of Paint & Printing Ink Technology” (18-19 March 23) organized by Dept. of Paint Technology, HBTU Kanpur.
6. **Chair the Session** in International Conference **CHEMCON-2022** (27th – 30th December 2022) organized by IChE and HBTU, Kanpur
7. **TEQIP-III fellowship** for Ph.D. during (August’18 to September’21).
8. **Gold medalist** in **M.Tech.- Polymer Technology** from DTU, Delhi
9. Qualified **GATE 2017** In Engineering Sciences (XE) with score **424**.
10. Represented Delta Specialties in **Paint India 2016**.
11. Invited lecture on “**Slip and Leveling Additives**” in ISSPA 2015- Ghaziabad.
12. Represented Afcona Additives India in **China Coat 2013** and **Paint India 2012**.